Universitat Autònoma de Barcelona

Nuevas Estrategias para el Diseño de Sistemas Chipless-RFID y Aplicaciones

Tesis Doctoral

Autor:
Cristian Herrojo Prieto

Director:
Prof. Ferran Martín Antolín

Programa de Doctorado en Ingeniería Electrónica y de Telecomunicación

Universitat Autònoma de Barcelona

Departamento de Ingeniería Electrónica

cimitec

Bellaterra (Cerdanyola del Vallès), 22 de marzo de 2018

Capítulo 6

Conclusiones y Líneas Futuras

Conclusiones

Esta tesis se ha centrado en el diseño e implementación de nuevos sistemas Chipless-RFID. La mayor parte del trabajo realizado se ha focalizado en implementar etiquetas sin chip capaces de incrementar la capacidad de información respecto al estado del arte de la tecnología. Al mismo tiempo, se ha realizado un gran esfuerzo para que dichas etiquetas fuesen competitivas en términos de capacidad de programación, información y coste, con relación a las dos tecnologías de identificación automática que lideran el mercado: códigos de barras ópticos y RFID con chip. Además, se ha demostrado que los sistemas implementados en esta tesis pueden tener cabida en diferentes aplicaciones, especialmente en seguridad documental para dificultar el fraude o copia de documentos (certificados, actas notariales, recetas médicas, exámenes, etc.).

El contenido de esta tesis se ha dividido en cinco capítulos (excluyendo el capítulo de conclusiones y líneas futuras). Una vez se ha expuesto la motivación y objetivos generales en el **Capítulo 1**, los aspectos más relevantes discutidos en cada capítulo se muestran a continuación:

En el **Capítulo 2** se han introducido las ventajas e inconvenientes de las dos tecnologías de identificación automática con más peso en el mercado: (i) códigos de barras ópticos y (ii) RFID, llegando a la conclusión de que el único motivo por el que los sistemas RFID sólo han reemplazado a los códigos de barras ópticos de forma parcial es el coste del circuito integrado de aplicación específica que llevan integrado. Posteriormente, se ha realizado una introducción al estado del arte de sistemas Chipless-RFID basados tanto en el dominio del tiempo como de la frecuencia, y los diferentes mecanismos de codificación empleados. Por último, se han definido las principales figuras de mérito, que se han utilizado como criterio para comparar diferentes etiquetas y mecanismos de codificación.

En el **Capítulo 3** se han analizado las propiedades de simetría de líneas de transmisión acopladas a resonadores eléctricamente pequeños y simétricos como mecanismo de codificación de etiquetas Chipless-RFID. El análisis de dicha estrategia de codificación es especialmente interesante en etiquetas basadas en el

dominio de la frecuencia, concretamente, etiquetas basadas en una línea de transmisión acoplada a múltiples resonadores, ya que los estados lógicos '0' y '1' se pueden conseguir con la apropiada orientación de las partículas resonantes con respecto a la línea *host*. Además, se han estudiado diferentes estructuras resonantes eléctricamente pequeñas que se pueden encontrar en la literatura, siendo el S-SRR la más pequeña en términos eléctricos. De este modo, es posible conseguir etiquetas Chipless-RFID más compactas que proporcionen una densidad de bits por unidad de superficie mayor. Es importante destacar que, a pesar de que el S-SRR es una partícula cuasi-simétrica, se ha demostrado que es posible maximizar y minimizar su acoplo a la línea de transmisión y conseguir los estados lógicos '0' y '1', respectivamente, con la apropiada orientación de la partícula.

En el **Capítulo 4**, en primer lugar, se han diseñado e implementado etiquetas de 10 bits en un ancho de banda de 1 GHz, concretamente de 2 a 3 GHz (banda *S*), basadas en una línea de transmisión CPW cargada con múltiples resonadores S-SRR, donde cada uno de los resonadores ha proporcionado un bit de información. Los estados lógicos '0' y '1' se han conseguido mediante la ausencia o presencia, respectivamente, de un cero de transmisión a la frecuencia de resonancia fundamental del resonador. Posteriormente, se han diseñado e implementado etiquetas Chipless-RFID multi-estado basadas en resonadores S-SRR para aumentar significativamente la capacidad de información de las etiquetas anteriores. Concretamente, se ha comprobado el funcionamiento de etiquetas donde los elementos resonantes que la forman pueden proporcionar hasta cuatro estados lógicos, consiguiendo etiquetas con una DPF y DPS de 18 bits/GHz y 2.19 bits/cm^2, respectivamente. Dichos estados lógicos se han determinado por el nivel de atenuación de las bandas de rechazo introducidas por cada uno de los elementos resonantes, los cuales se han controlado con el nivel de acoplamiento magnético entre el resonador y la línea de transmisión CPW mediante rotación. Esta funcionalidad multi-estado no tiene sentido en una aplicación donde la detección del código identificativo sea en campo lejano. Por este motivo, se ha diseñado e implementado una configuración diferente donde la línea de transmisión (lector) y la etiqueta están grabadas en sustratos diferentes y la comunicación entre ellos es en campo cercano. Con esta estrategia se ha conseguido una DPF y DPS de 16 bits/GHz y 2.37 bits/cm^2, respectivamente. Aunque con este sistema se ha logrado una de las mejores DPF que se pueden encontrar en la literatura, a la vez que una DPS por encima de la media, es realmente complicado aumentar el número de estados lógicos por resonador más allá de cuatro. Además, en términos de ancho de banda, las etiquetas basadas en el dominio de la frecuencia no son eficientes, ya que, cuanto mayor es el número de bits, mayor es el ancho de banda y más complejo es el sistema lector.

En el **Capítulo 5** se ha diseñado e implementado (en tecnología CPW y *microstrip*) un sistema Chipless-RFID completamente novedoso que puede solventar las limitaciones de la estrategia propuesta en el **Capítulo 4,** y puede competir en términos de capacidad de información con las etiquetas RFID con chip. Dicho sistema está basado en el dominio del tiempo, donde las etiquetas están formadas por resonadores idénticos grabados en posiciones predefinidas y equidistantes, y su lectura se realiza secuencialmente y en campo cercano. De este modo, la señal de interrogación es simplemente una señal harmónica sintonizada a la frecuencia de resonancia fundamental de los resonadores que forman la etiqueta. Con esta estrategia se ha conseguido una densidad de bits por unidad de superficie

cercana a 9 bits/cm^2, superando ampliamente la capacidad de información de cualquier sistema que se pueda encontrar en la literatura. Tal capacidad de información se consigue a expensas de perder rango de lectura. Sin embargo, esto no es un problema en aplicaciones de seguridad documental. De hecho, es un valor añadido con el propósito de ofrecer mayores niveles de confianza respecto a espionaje y "escuchas". Además, se ha demostrado su capacidad de reprogramación, la posibilidad de leer las etiquetas con independencia de su orientación con respecto al sistema lector, e incluso, la posibilidad de implantarse sobre papel (incluido papel ordinario) y utilizando tintas conductoras. Este último aspecto es especialmente importante si se quiere reducir el coste de la etiqueta por debajo del céntimo de euro.

En términos generales se puede concluir que los objetivos propuestos en esta tesis se han cumplido, aportando diferentes soluciones al diseño de etiquetas Chipless-RFID, tanto en el dominio de la frecuencia como del tiempo. Dichas soluciones se han publicado en diferentes revistas especializadas y congresos internacionales.

Líneas Futuras

Los resultados obtenidos animan y abren la posibilidad de explorar o profundizar, en un futuro cercano, diferentes líneas de investigación que han surgido en el desarrollo de esta tesis. Principalmente, dichas líneas de investigación están relacionadas con el sistema Chipless-RFID implementado en tecnología *microstrip* presentado en el **Capítulo 5**, el cual está basado en el dominio del tiempo, y la lectura de los bits de información es secuencial y en campo cercano. En primer lugar, se pretende optimizar la partícula resonante que forma la etiqueta para poder implementar etiquetas de 96 bits en el borde largo de un documento de tamaño DIN A4. Además, se plantea la opción de usar dos filas de resonadores para doblar la capacidad, o incluso, usar otro tipo de configuraciones de cabezal lector/etiqueta para reducir el tamaño, y a su vez, incrementar la capacidad de información.

Otra opción que se plantea consiste en implementar etiquetas Chipless-RFID utilizando tintas orgánicas con base acuosa, por lo tanto, más ecológicas comparado con las tintas conductoras convencionales, las cuales utilizan metales y disolventes que suelen ser menos ecológicos. En términos de coste, puede ser una implementación más económica, ya que los metales como el cobre o la plata son más caros que un compuesto orgánico sintetizado.

Por otra parte, se pretende usar la misma estrategia como *encoder* para determinar la posición absoluta/relativa de ascensores y elevadores. Típicamente, esta función la realizan los *encoders* ópticos, los cuales ofrecen una muy buena resolución y precisión. No obstante, su funcionamiento se degrada significativamente en entornos donde se acumula suciedad (polvo, grasa, etcétera), como sucede en el hueco de un ascensor. Una posible solución puede ser utilizar *encoders* de microondas, los cuales, en principio, parecen ser más robustos frente a condiciones de suciedad extrema.

En principio, la posición del ascensor a lo largo de todo su recorrido se puede determinar de dos maneras diferentes: (i) grabando los elementos resonantes en la

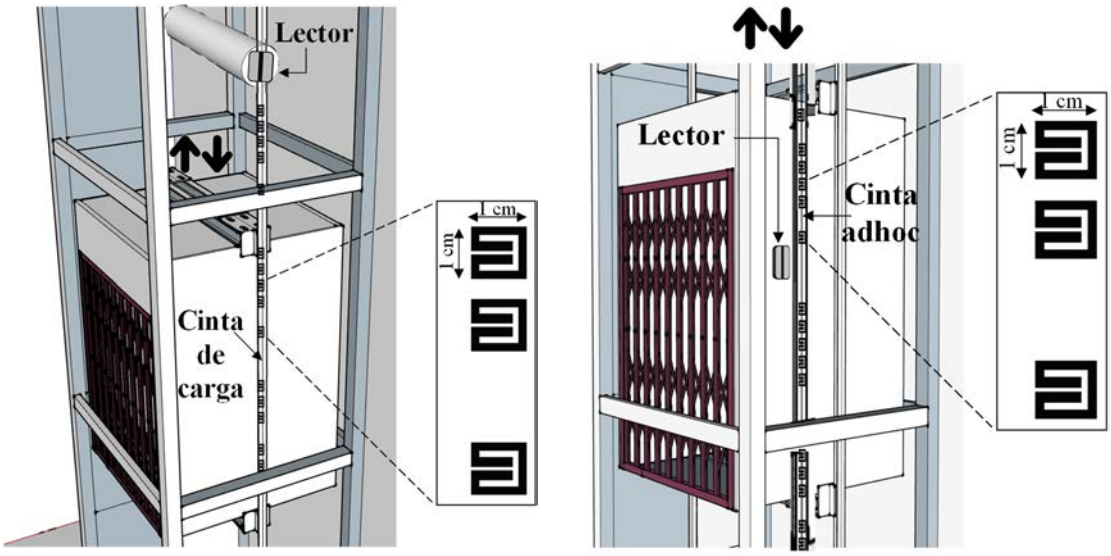

(a) (b)

Figura 6.1. Esquema de funcionamiento del sistema para la medida de la posición precisa de la cabina del ascensor. (a) Resonadores grabados sobre la cinta de carga y (b) resonadores grabados sobre una cinta *adhoc* fija, ubicada en el hueco del ascensor.

cinta de carga del ascensor o (ii) grabando los elementos resonantes en una cinta *adhoc*. En ambos casos, la cinta tendrá que estar suficientemente cerca del cabezal lector como para que el código se pueda detectar correctamente. La primera opción [ver Figura 6.1(a)] parece ser la más idónea e interesante, ya que el código se graba en un elemento que forma parte del ascensor. Sin embargo, primeramente, hay que analizar los materiales que componen la cinta de carga, y comprobar si puede actuar como dieléctrico. Si finalmente no fuese posible la implementación de los elementos resonantes en dicha cinta de carga, se puede plantear la segunda opción mencionada anteriormente como alternativa [ver Figura 6.1(b)]. Concretamente, la idea consiste en añadir una cinta vertical *adhoc* fija en el hueco del ascensor, a lo largo de todo el mismo, y muy cerca de la cabina del ascensor. Sobre ésta se dispone el cabezal del lector, el cual se mueve de forma solidaria con la cabina, estando el cabezal de lector muy cerca de la cinta *adhoc*. En este segundo caso, es el lector el elemento móvil, mientras que la cinta con los resonadores grabados es fija, al contrario que en el caso anterior.

Este sistema presenta varios retos, entre ellos, aumentar la distancia de lectura entre el cabezal lector y el *encoder*, ya que vibraciones significativas de la cinta de carga o, alternativamente, la cinta *adhoc*, pueden provocar errores a la hora de determinar la posición del ascensor. Para tal propósito, se pretende aumentar el tamaño de los elementos resonantes, aunque este aspecto conlleve a una resolución menor, y utilizar sustratos con permitividades bajas en el lector para que las líneas de campo electromagnético no estén tan concentradas en el dieléctrico.

Referencias

[1] O. Rance, E. Perret, R. Siragusa, and P. Lemaître-Auger, *RCS Synthesis for Chipless RFID: Theory and Design*. Elsevier, 2017.

[2] E. Perret, *Radio Frequency Identification and Sensors: From RFID to Chipless RFID*. John Wiley & Sons, Inc.,Hoboken, NJ, USA, 2014.

[3] A. Vena, E. Perret, and S. Tedjini, *Chipless RFID Based on RF Encoding Particle : Realization, Coding and Reading System*. ISTE Press - Elsevier, 2016.

[4] N. C. Karmakar, E. M. Amin, and J. K. Saha, *Chipless RFID Sensors*. John Wiley & Sons, Inc,Hoboken, NJ, USA, 2016.

[5] N. C. Karmakar, *Handbook of Smart Antennas for RFID Systems*. John Wiley & Sons, Inc.,Hoboken, NJ, USA, 2010.

[6] R. Rezaiesarlak and M. Manteghi, *Chipless RFID: Design Procedure and Detection Techniques*. Springer, 2015.

[7] K. Finkenzeller, *RFID Handbook : Fundamentals and Applications in Contactless Smart Cards, Radio Frequency Identification and Near-Field Communication*. Wiley-Blackwell, 2010.

[8] N. C. Karmakar, P. Kalansuriya, R. E. Azim, and R. Koswatta, *Chipless Radio Frequency Identification Reader Signal Processing*. John Wiley & Sons, Inc.,Hoboken, NJ, 2016.

[9] V. D. Hunt, A. Puglia, and M. Puglia, *RFID : A Guide to Radio Frequency Identification*. Wiley-Interscience, 2007.

[10] N. C. Karmakar, M. Zomorrodi, and C. Divarathne, *Advanced Chipless RFID*. John Wiley & Sons, Inc.,Hoboken, NJ, USA, 2016.

[11] S. Preradovic and N. Karmakar, *Multiresonator-Based Chipless RFID: Barcode of the Future*. Springer,New York, USA, 2012.

[12] N. C. Karmakar, E. M. Amin, and J. K. Saha, *Chipless RFID Reader Architecture*. John Wiley & Sons, Inc,Hoboken, NJ, USA, 2013.

[13] M. Schussler, C. Mandel, M. Maasch, A. Giere, and R. Jakoby, "Phase modulation scheme for chipless RFID- and wireless sensor tags," in *2009 Asia*

Pacific Microwave Conference, Dec. 2009, pp. 229–232.

[14] P. A. Nysen, H. Skeie, and D. Armstrong, "System for interrogating a passive transponder carrying phase-encoded information." Google Patents, 1988.

[15] C. S. Hartmann, "A global SAW ID tag with large data capacity," in *Proceedings 2002 IEEE Ultrasonics Symposium*, Oct. 2002, vol. 1, pp. 65–69.

[16] N. Saldanha and D. C. Malocha, "Design parameters for SAW multi-tone frequency coded reflectors," in *Proceedings IEEE Ultrasonics Symposium*, Oct. 2007, pp. 2087–2090.

[17] S. Härmä, V. P. Plessky, C. S. Hartmann, and W. Steichen, "Z-path SAW RFID tag," *IEEE Trans. Ultrason. Ferroelectr. Freq. Control*, vol. 55, no. 1, pp. 208–212, Feb. 2008.

[18] T. Han, W. Wang, H. Wu, and Y. Shui, "Reflection and scattering characteristics of reflectors in SAW tags," *IEEE Trans. Ultrason. Ferroelectr. Freq. Control*, vol. 55, no. 6, pp. 1387–1390, Jun. 2008.

[19] S. Härmä, V. P. Plessky, X. Li, and P. Hartogh, "Feasibility of ultra-wideband SAW RFID tags meeting FCC rules," *IEEE Trans. Ultrason. Ferroelectr. Freq. Control*, vol. 56, no. 4, pp. 812–820, Apr. 2009.

[20] C. Hartmann, P. Hartmann, P. Brown, J. Bellamy, L. Claiborne, and W. Bonner, "Anti-collision methods for Global SAW RFID Tag systems," in *Proceedings IEEE Ultrasonics Symposium*, Aug. 2004, vol. 2, pp. 805–808.

[21] L. Zhang, S. Rodriguez, H. Tenhunen, and L.-R. Zheng, "An innovative fully printable RFID technology based on high speed time-domain reflections," in *Conference on High Density Microsystem Design and Packaging and Component Failure Analysis, 2006. HDP'06.*, Jun. 2006, pp. 166–170.

[22] L. Zheng, S. Rodriguez, L. Zhang, B. Shao, and L.-R. Zheng, "Design and implementation of a fully reconfigurable chipless RFID tag using Inkjet printing technology," in *2008 IEEE International Symposium on Circuits and Systems*, May 2008, pp. 1524–1527.

[23] B. Shao, Q. Chen, Y. Amin, D. S. Mendoza, R. Liu, and L. R. Zheng, "An ultra-low-cost RFID tag with 1.67 Gbps data rate by ink-jet printing on paper substrate," in *2010 IEEE Asian Solid-State Circuits Conference, A-SSCC 2010*, Nov. 2010.

[24] A. Chamarti and K. Varahramyan, "Transmission delay line based ID generation circuit for RFID applications," *IEEE Microw. Compon. Lett.*, vol. 16, no. 11, pp. 588–590, Oct. 2006.

[25] J. Vemagiri, A. Chamarti, M. Agarwal, and K. Varahramyan, "Transmission line delay-based radio frequency identification (RFID) tag," *Microw. Opt. Technol. Lett.*, vol. 49, no. 8, pp. 1900–1904, Aug. 2007.

[26] F. J. Herraiz-Martínez, F. Paredes, G. Zamora, F. Martín, and J. Bonache, "Printed magnetoinductive-wave (MIW) delay lines for chipless RFID applications," *IEEE Trans. Antennas Propag.*, vol. 60, no. 11, pp. 5075–5082, Jul. 2012.

[27] M. Forouzandeh and N. C. Karmakar, "Chipless RFID tags and sensors: a review on time-domain techniques," *Wirel. Power Transf.*, vol. 2, no. 2, pp. 62–77, Oct. 2015.

[28] S. Gupta, B. Nikfal, and C. Caloz, "Chipless RFID system based on group delay engineered dispersive delay structures," *IEEE Antennas Wirel. Propag. Lett.*, vol. 10, no. 2, pp. 1366–1368, Dec. 2011.

[29] E. Shamonina, V. A. Kalinin, K. H. Ringhofer, and L. Solymar, "Magneto-inductive waveguide," *Electron. Lett.*, vol. 38, no. 8, p. 371, Apr. 2002.

[30] S. Gupta, B. Nikfal, and C. Caloz, "RFID system based on pulse-position modulation using group delay engineered microwave C-sections," in *2010 Asia-Pacific Microwave Conference*, Dec. 2010, pp. 203–206.

[31] E. G. Cristal, "Analysis and exact synthesis of cascaded commensurate transmission-line C-Section all-pass networks," *IEEE Trans. Microw. Theory Tech.*, vol. 14, no. 6, pp. 285–291, Jun. 1966.

[32] R. Nair, E. Perret, and S. Tedjini, "Temporal multi-frequency encoding technique for chipless RFID applications," in *IEEE MTT-S International Microwave Symposium Digest*, Jun. 2012, pp. 1–3.

[33] R. S. Nair, E. Perret, and S. Tedjini, "Group delay modulation for pulse position coding based on periodically coupled C-sections," in *Annals of Telecommunications*, Aug. 2013, vol. 68, no. 7–8, pp. 447–457.

[34] R. Nair, E. Perret, and S. Tedjini, "Chipless RFID based on group delay encoding," in *2011 IEEE International Conference on RFID-Technologies and Applications*, Sep. 2011, vol. 1, pp. 214–218.

[35] C. Mandel, M. Schussler, M. Maasch, and R. Jakoby, "A novel passive phase modulator based on LH delay lines for chipless microwave RFID applications," in *2009 IEEE MTT-S International Microwave Workshop on Wireless Sensing, Local Positioning, and RFID*, Sep. 2009, pp. 1–4.

[36] M. Schüßler, C. Damm, M. Maasch, and R. Jakoby, "Performance evaluation of left-handed delay lines for RFID backscatter applications," in *IEEE MTT-S International Microwave Symposium Digest*, Jun. 2008, pp. 177–180.

[37] S. Preradovic, I. Balbin, N. C. Karmakar, and G. Swiegers, "A novel chipless RFID system based on planar multiresonators for barcode replacement," in *2008 IEEE International Conference on RFID*, Apr. 2008, pp. 289–296.

[38] I. Jalaly and I. D. Robertson, "Capacitively-tuned split microstrip resonators for RFID barcodes," in *2005 European Microwave Conference*, Oct. 2005, vol. 2, pp. 1161–1164.

[39] S. Preradovic and N. Karmakar, "Chipless RFID: Bar code of the future," *IEEE Microw. Mag.*, vol. 11, no. 7, pp. 87–97, Dec. 2010.

[40] I. Jalaly and I. D. Robertson, "RF barcodes using multiple frequency bands," in *IEEE MTT-S International Microwave Symposium Digest*, Jun. 2005, pp. 139–142.

[41] S. Preradovic, I. Balbin, N. Karmakar, and G. F. Swiegers, "Multiresonator-based chipless RFID system for low-cost item tracking," *IEEE Trans. Microw. Theory Tech.*, vol. 57, no. 5, pp. 1411–1419, Apr. 2009.

[42] S. Preradovic and N. Karmakar, "Multiresonator based chipless RFID tag and dedicated RFID reader," in *2010 IEEE MTT-S International Microwave Symposium*, May 2010, pp. 1520–1523.

[43] S. Preradovic and N. Karmakar, "4th generation multiresonator-based chipless RFID tag utilizing spiral EBGs," in *2010 European Microwave*

Conference, Sep. 2010, pp. 1746–1749.

[44] S. Preradovic, S. Roy, and N. Karmakar, "Fully printable multi-bit chipless RFID transponder on flexible laminate," in *2009 Asia Pacific Microwave Conference*, Dec. 2009, pp. 2371–2374.

[45] S. Preradovic and N. Karmakar, "Design of chipless RFID tag for operation on flexible laminates," *IEEE Antennas Wirel. Propag. Lett.*, vol. 9, pp. 207–210, Mar. 2010.

[46] I. Balbin and N. C. Karmakar, "Phase-encoded chipless RFID transponder for large scale low cost applications," *IEEE Microw. Compon. Lett.*, vol. 19, no. 8, pp. 509–511, Jul. 2009.

[47] C. M. Nijas *et al.*, "Chipless RFID tag using multiple microstrip open stub resonators," *IEEE Trans. Antennas Propag.*, vol. 60, no. 9, pp. 4429–4432, Jul. 2012.

[48] S. Bhuiyan, A. K. M. Azad, and N. Karmakar, "Dual-band modified complementary split ring resonator (MCSRR) based multi-resonator circuit for chipless RFID Tag," in *IEEE 8th International Conference on Intelligent Sensors, Sensor Networks*, Apr. 2013, pp. 277–281.

[49] A. Vena, E. Perret, and S. Tedjini, "A fully printable Chipless RFID tag with detuning correction technique," *IEEE Microw. Compon. Lett.*, vol. 22, no. 4, pp. 209–211, Mar. 2012.

[50] H. S. Jang, W. G. Lim, K. S. Oh, S. M. Moon, and J. W. Yu, "Design of low-cost chipless system using printable chipless tag with electromagnetic code," *IEEE Microw. Compon. Lett.*, vol. 20, no. 11, pp. 640–642, Sep. 2010.

[51] J. McVay, A. Hoorfar, and N. Engheta, "Space-filling curve RFID tags," in *2006 IEEE Radio and Wireless Symposium*, Oct. 2006, pp. 199–202.

[52] D. Girbau, J. Lorenzo, A. Lazaro, C. Ferrater, and R. Villarino, "Frequency-coded chipless RFID tag based on dual-band resonators," *IEEE Antennas Wirel. Propag. Lett.*, vol. 11, no. 4, pp. 126–128, Jan. 2012.

[53] R. Rezaiesarlak and M. Manteghi, "Complex-natural-resonance-based design of chipless RFID tag for high-density data," *IEEE Trans. Antennas Propag.*, vol. 62, no. 2, pp. 898–904, Nov. 2014.

[54] C. M. Nijas, S. Suseela, U. Deepak, P. Wahid, and P. Mohanan, "Low cost chipless tag with multi-bit encoding technique," in *IEEE MTT-S International Microwave and RF Conference*, Dec. 2013, pp. 1–4.

[55] J. Machac and M. Polivka, "Influence of mutual coupling on performance of small scatterers for chipless RFID tags," in *2014 24th International Conference Radioelektronika, RADIOELEKTRONIKA*, Apr. 2014.

[56] M. Svanda, J. Machac, M. Polivka, and J. Havlicek, "A comparison of two ways to reducing the mutual coupling of chipless RFID tag scatterers," in *2016 21st International Conference on Microwave, Radar and Wireless Communications, MIKON 2016*, May 2016, pp. 2–5.

[57] A. Vena, E. Perret, and S. Tedjini, "High-capacity chipless RFID tag insensitive to the polarization," *IEEE Trans. Antennas Propag.*, vol. 60, no. 10, pp. 4509–4515, Jul. 2012.

[58] A. Vena, E. Perret, and S. Tedjini, "Design of compact and auto-compensated single-layer chipless RFID tag," *IEEE Trans. Microw. Theory*

Tech., vol. 60, no. 9, pp. 2913–2924, Jul. 2012.

[59] M. Khaliel, A. El-Awamry, A. Fawky, M. El-Hadidy, and T. Kaiser, "A novel co/cross-polarizing chipless RFID tags for high coding capacity and robust detection," in *2015 IEEE International Symposium on Antennas and Propagation & USNC/URSI National Radio Science Meeting*, Jul. 2015, pp. 159–160.

[60] O. Rance, R. Siragusa, P. Lemaitre-Auger, and E. Perret, "Toward RCS magnitude level coding for chipless RFID," *IEEE Trans. Microw. Theory Tech.*, vol. 64, no. 7, pp. 2315–2325, May 2016.

[61] Y. Ni, X. Huang, Y. Lv, and C. Cheng, "Hybrid coding chipless tag based on impedance loading," *IET Microwaves, Antennas Propag.*, vol. 11, no. 10, pp. 1325–1331, Aug. 2017.

[62] O. Rance, R. Siragusa, P. Lemaitre-Auger, and E. Perret, "RCS magnitude coding for chipless RFID based on depolarizing tag," in *2015 IEEE MTT-S International Microwave Symposium*, May 2015, pp. 2–5.

[63] A. Vena, A. A. Babar, L. Sydanheimo, M. M. Tentzeris, and L. Ukkonen, "A novel near-transparent ask-reconfigurable inkjet-printed chipless RFID tag," *IEEE Antennas Wirel. Propag. Lett.*, vol. 12, pp. 753–756, Jun. 2013.

[64] A. Vena, E. Perret, and S. Tedjini, "Chipless RFID tag using hybrid coding technique," *IEEE Trans. Microw. Theory Tech.*, vol. 59, no. 12, pp. 3356–3364, Nov. 2011.

[65] M. S. Bhuiyan and N. Karmakar, "A spectrally efficient chipless RFID tag based on split-wheel resonator," in *2014 International Workshop on Antenna Technology: Small Antennas, Novel EM Structures and Materials, and Applications, iWAT 2014*, Mar. 2014, pp. 11–14.

[66] A. El-Awamry, M. Khaliel, A. Fawky, M. El-Hadidy, and T. Kaiser, "Novel notch modulation algorithm for enhancing the chipless RFID tags coding capacity," in *2015 IEEE International Conference on RFID*, Apr. 2015, pp. 25–31.

[67] A. Vena, E. Perret, and S. Tedjini, "RFID chipless tag based on multiple phase shifters," in *IEEE MTT-S International Microwave Symposium Digest*, Jun. 2011, pp. 3–6.

[68] A. Islam and N. Karmakar, "Compact printable chipless RFID tags using polarization diversity," in *2012 9th European Radar Conference*, Nov. 2012, pp. 912–915.

[69] M. M. Khan, F. A. Tahir, M. F. Farooqui, A. Shamim, and H. M. Cheema, "3.56-bits/cm compact inkjet printed and application specific Chipless RFID tag," *IEEE Antennas Wirel. Propag. Lett.*, vol. 15, pp. 1109–1112, Oct. 2016.

[70] M. A. Islam and N. Karmakar, "A novel compact printable dual-polarized chipless RFID system," *IEEE Trans. Microw. Theory Tech.*, vol. 60, no. 7, pp. 2142–2151, May 2012.

[71] C. Feng, W. Zhang, L. Li, L. Han, X. Chen, and R. Ma, "Angle-based chipless RFID tag with high capacity and insensitivity to polarization," *IEEE Trans. Antennas Propag.*, vol. 63, no. 4, pp. 1789–1797, Jan. 2015.

[72] A. Vena, E. Perret, and S. Tedjini, "A compact chipless RFID tag using polarization diversity for encoding and sensing," in *2012 IEEE International Conference on RFID, RFID 2012*, Apr. 2012, pp. 191–197.

[73] S. Genovesi, F. Costa, and A. Monorchio, "Chipless RFID tag exploiting multifrequency delta-phase quantization encoding," *IEEE Antennas Wirel. Propag. Lett.*, vol. 15, pp. 738–741, Aug. 2016.

[74] F. Martín, *Artificial Transmission Lines for RF and Microwave Applications*. John Wiley & Sons, Inc,Hoboken, NJ, 2015.

[75] J.-S. Hong and M. J. Lancaster, "Couplings of microstrip square open-loop resonators for cross-coupled planar microwave filters," *IEEE Trans. Microw. Theory Tech.*, vol. 44, no. 11, pp. 2099–2109, Nov. 1996.

[76] J. B. Pendry, A. J. Holden, D. J. Robbins, and W. J. Stewart, "Magnetism from conductors and enhanced nonlinear phenomena," *IEEE Trans. Microw. Theory Tech.*, vol. 47, no. 11, pp. 2075–2084, Nov. 1999.

[77] D. Schurig, J. J. Mock, and D. R. Smith, "Electric-field-coupled resonators for negative permittivity metamaterials," *Appl. Phys. Lett.*, vol. 88, no. 4, pp. 1–3, Jan. 2006.

[78] J. Naqui and F. Martín, "Some Applications of Metamaterial Resonators Based on Symmetry Properties," *Comput. Mater. Contin.*, vol. 39, no. 3, pp. 267–288, 2014.

[79] H. Chen *et al.*, "Left-handed materials composed of only S-shaped resonators," *Phys. Rev. E - Stat. Nonlinear, Soft Matter Phys.*, vol. 70, pp. 1–4, Jan. 2004.

[80] H. S. Chen, L. X. Ran, J. T. Huangfu, X. M. Zhang, and K. S. Chen, "Magnetic properties of s-shaped split-ring resonators," *Prog. Electromagn. Res.*, vol. 51, pp. 231–247, Jan. 2005.

[81] J. Naqui, J. Coromina, A. K. Horestani, C. Fumeaux, and F. Martín, "Angular displacement and velocity sensors based on coplanar waveguides (CPWs) loaded with s-shaped split ring resonators (S-SRR)," *Sensors*, vol. 15, no. 5, pp. 9628–9650, Apr. 2015.

[82] S. Preradovic and N. Karmakar, "Chipless RFID for intelligent traffic information system," in *2011 IEEE International Symposium on Antennas and Propagation*, Jul. 2011.

[83] J. Naqui, *Symmetry Properties in Transmission Lines Loaded with Electrically Small Resonators*. Springer, 2016.

[84] J. Naqui and F. Martín, "Transmission lines loaded with bisymmetric resonators and their application to angular displacement and velocity sensors," *IEEE Trans. Microw. Theory Tech.*, vol. 61, no. 12, pp. 4700–4713, Oct. 2013.

[85] J. Naqui, M. Durán-Sindreu, and F. Martín, "Alignment and position sensors based on split ring resonators," *Sensors*, vol. 12, no. 9, pp. 11790–11797, Aug. 2012.

[86] L. Su, J. Naqui, J. Mata-Contreras, and F. Martin, "Cascaded splitter/combiner microstrip sections loaded with complementary split ring resonators (CSRRs): Modeling, analysis and applications," in *2016 IEEE MTT-S International Microwave Symposium*, May 2016, pp. 1–4.

[87] J. Naqui *et al.*, "Transmission lines loaded with pairs of stepped impedance resonators: modeling and application to differential permittivity measurements," *IEEE Trans. Microw. Theory Tech.*, vol. 64, no. 11, pp. 3864–3877, Oct. 2016.

[88] D. M. Pozar, *Microwave Engineering*, 4th Editio. Wiley,New York, 2012.

[89] R. Mongia and R. Mongia, *RF and Microwave Coupled-Line Circuits*. Artech House, 2007.

[90] J. Naqui, M. Durán-Sindreu, and F. Martín, "Selective mode suppression in coplanar waveguides using metamaterial resonators," *Appl. Phys. A Mater. Sci. Process.*, vol. 109, no. 4, pp. 1053–1058, Nov. 2012.

[91] J. Naqui, M. Durán-Sindreu, and F. Martin, "Strategies for the implementation of sensors and RF barcodes based on transmission lines loaded with symmetric resonators," in *2013 Conference Proceedings: 21st International Conference on Applied Electromagnetics and Communications*, Oct. 2013.

[92] F. Aznar *et al.*, "Characterization of miniaturized metamaterial resonators coupled to planar transmission lines through parameter extraction," *J. Appl. Phys.*, vol. 104, no. 11, pp. 1–8, Oct. 2008.

[93] J. Naqui and F. Martin, "Application of broadside-coupled split ring resonator (BC-SRR) loaded transmission lines to the design of rotary encoders for space applications," in *2016 IEEE MTT-S International Microwave Symposium*, May 2016, pp. 1–4.

[94] R. Marqués, F. Medina, and R. Rafii-El-Idrissi, "Role of bianisotropy in negative permeability and left-handed metamaterials," *Phys. Rev. B - Condens. Matter Mater. Phys.*, vol. 65, no. 14, pp. 1–6, Apr. 2002.

Artículos de la Tesis

Artículos Fundamentales de la tesis

EPJ16: C. Herrojo, J. Naqui, F. Paredes, and F. Martín, "Spectral signature barcodes based on s-shaped split ring resonators (S-SRRs)," *EPJ Appl. Metamat.*, vol. 3, pp. 1-6, Apr. 2016.

TMTT16: C. Herrojo, F. Paredes, J. Mata-Contreras, S. Zuffanelli, and F. Martín, "Multistate multiresonator spectral signature barcodes implemented by means of s-shaped split ring resonators (S-SRRs)," *IEEE Trans. Microw. Theory Tech.*, vol. 65, no. 7, pp. 2341-2352, Jul. 2017.

SENSORS17: C. Herrojo, J. Mata-Contreras, F. Paredes and, F. Martín, "Microwave encoders for chipless RFID and angular velocity sensors based on s-shaped split ring resonators," *IEEE Sensors J.*, vol. 17, no. 15, pp. 4805-4813, Aug. 2017.

MISM17: C. Herrojo, J. Mata-Contreras, F. Paredes, A. Núñez, E. Ramon, and F. Martín, "Near-field chipless-RFID tags with sequential bit reading implemented in plastic substrates," *J. Magn. Magn. Mater.*, Oct. 2017.

EPJ17: C. Herrojo, J. Mata-Contreras, F. Paredes, and F. Martín, "High data density and capacity in chipless radiofrequency identification (chipless-RFID) tags based on double-chains of S-shaped split ring resonators (S-SRRs)," *EPJ Appl. Metamat.*, vol. 4, pp. 1-8, Oct. 2017.

TMTT17: C. Herrojo, J. Mata-Contreras, A. Núñez, F. Paredes, E. Ramon, and F. Martín, "Near-field chipless-RFID system with high data capacity for security and authentication applications," *IEEE Trans. Microw. Theory Tech.*, vol. 65, no. 12, pp. 5298-5308, Dec. 2017.

MWCL18: C. Herrojo, J. Mata-Contreras, F. Paredes, A. Núñez, E. Ramon and F. Martín, "Near-field chipless-RFID system with erasable/programmable 40-bit tags inkjet printed on paper substrates," *IEEE Microw. Compon. Lett.*, vol. 28, no. 3, pp. 272-274, Mar 2018.

Artículos No Fundamentales de la tesis*

IMS16(c): C. Herrojo, J. Naqui, F. Paredes, and F. Martín, "Spectral signature barcodes implemented by multi-state multi-resonator circuits for chipless RFID tags," in *2016 IEEE MTT-S International Microwave Symposium*, San Francisco, CA, May 2016, pp. 1-4.

IMS17(c): C. Herrojo, J. Mata-Contreras, F. Paredes, and F. Martín, "Near-field chipless RFID encoders with sequential bit reading and high data capacity," in 2017 *IEEE MTT-S International Microwave Symposium*, Honololu, HI, Jun. 2017, pp. 1564-1567.

EuMC18(c): C. Herrojo, M. Moras, F. Paredes, J. Mata-Contreras, A. Núñez, E. Ramon, and F. Martín, "Erasable/programmable chipless-RFID tags with orientation-independent sequential bit reading," in *European Microwave Conference*, Madrid, Spain, Sep. 2018. Enviado.

TECH18: C. Herrojo, M.Moras, F. Paredes, J. Mata-Contreras, A. Núñez, E. Ramon, and F. Martín, "Very low-cost 80-bit chipless-RFID tags inkjet printed on ordinary paper," *Technologies*. Enviado.

MAG18: C. Herrojo, M. Moras, F. Paredes, A. Núñez, J. Mata-Contreras, E. Ramon, and F. Martín, "Time-domain signature Chipless-RFID tags: near-field chipless-RFID systems with high data capacity," *IEEE Microw. Mag.* Enviado.

SENSORS18: F. Paredes, C. Herrojo, M. Moras, J. Mata-Contreras, A. Núñez, E. Ramon, and F. Martín, "Near-field chipless-RFID sensing and identification system with switching reading," *Sensors*. Enviado.

A continuación, se muestran otras contribuciones a congresos, en calidad de **invitado**, que no se han adjuntado en esta tesis, pero que forman parte de ella:

IWMD15(c): C. Herrojo, J. Naqui, and F. Martín, "S-shaped split ring resonators (S-SRRs) for the design of spectral signature barcodes", in *International Workshop on Metamaterials-by-Design, Theory, Methods, and Applications to Communications and Sensing*, Paris, France, 3-4 Dec. 2015. Invited.

PIERS17(c): C. Herrojo, J. Mata-Contreras, F. Paredes, and F. Martín, "Near-field chipless RFID tags for identification and authentication applications", in

* Los artículos de congresos(c) no pueden formar parte fundamental de la tesis por compendio de publicaciones, tal y como dice la normativa del doctorado en Ingeniería Electrónica y de Telecomunicación de la Universitat Autònoma de Barcelona. Sin embargo, en esta tesis se han incluido como complementación. Asimismo, incluidos en la lista, artículos pendientes de aceptación.

Progress in Electromagnetic Research Symposium, St Petersburg, Russia, May 2017. Invited.

MAGMA17[c]: C. Herrojo, J. Mata-Contreras, F. Paredes, A. Núñez, E. Ramon, and F. Martín, "Near-field chipless-RFID tags with sequential bit reading implemented in plastic substrates", in *Moscow International Symposium on Magnetism*, Moscow, Russia, Jul. 2017. Invited.

META17[c]: C. Herrojo, J. Mata-Contreras, F. Paredes and F. Martín, "Chipless RFID tags based on metamaterial concepts," in *2017 11th International Congress on Engineered Materials Platforms for Novel Wave Phenomena (Metamaterials)*, Marseille, France, Aug. 2017, pp. 139-141. Invited.

IWMD17[c]: F. Martín, C. Herrojo, P. Vélez, L. Su, J. Mata-Contreras, and F. Paredes, "Application of metamaterial concepts to sensors and chipless RFID," in *Journal of Physics: Conference Series*, Madrid, Spain, Dec. 2017. Invited.

SPIE18[c]: C. Herrojo, J. Mata-Contreras, A. Núñez, F. Paredes, E. Ramon, and F. Martín, "Application of metamaterial concepts to chipless RFID," in *SPIE Photonics Europe*, Strasbourg, France, Apr. 2018. Invited.

Artículos Fundamentales de la Tesis

Artículo EPJ16

Spectral Signature Barcodes Based on S-Shaped Split Ring Resonators (S-SRRs)

C. Herrojo, J. Naqui, F. Paredes and F. Martín

EPJ Appl. Metamat. 2016, **3**, 1

DOI: 10.1051/epjam/2016002

EPJ Applied Metamaterials

Available online at:
http://epjam.edp-open.org

RESEARCH ARTICLE OPEN ACCESS

Spectral signature barcodes based on S-shaped Split Ring Resonators (S-SRRs)

Cristian Herrojo*, Jordi Naqui, Ferran Paredes, and Ferran Martín

CIMITEC, Departament d'Enginyeria Electrònica, Universitat Autònoma de Barcelona, 08193 Bellaterra, Spain

Received 26 February 2016 / Accepted 26 April 2016

Abstract – In this paper, it is shown that S-shaped split ring resonators (S-SRRs) are useful particles for the implementation of spectral signature (i.e., a class of radiofrequency) barcodes based on coplanar waveguide (CPW) transmission lines loaded with such resonant elements. By virtue of its S shape, these resonators are electrically small. Hence S-SRRs are of interest for the miniaturization of the barcodes, since multiple resonators, each tuned at a different frequency, are used for encoding purposes. In particular, a 10-bit barcode occupying 1 GHz spectral bandwidth centered at 2.5 GHz, with dimensions of 9 cm^2, is presented in this paper.

Key words: Split ring resonators (SRRs), Radiofrequency barcodes, Chipless RFID.

1 Introduction

Metamaterial transmission lines can be implemented by loading a host line with electrically small resonant elements, such as split ring resonators (SRRs) [1], or complementary split ring resonators (CSRRs) [2], among others. Many microwave devices based on these artificial lines have been designed on the basis of the further controllability, as compared to ordinary lines, of line impedance and dispersion [3], achieved by virtue of the loading elements (which provide more degrees of freedom for device design). The key aspect in these designs is thus impedance and dispersion engineering. However, in other applications, the resonance phenomenon is the key aspect. In this case, where the functionality is based on particle resonance (rather than on impedance and dispersion engineering), the lines are usually referred to as transmission lines with metamaterial loading [3]. These structures have been applied to the design of planar bandstop and notch filters [4, 5], multiband printed dipole and monopole antennas [6–8], common-mode suppressed differential lines and filters [9, 10], microwave sensors [11–18], and radiofrequency barcodes [19–21], among others.

In this work, radiofrequency barcodes implemented by means of S-shaped SRRs (S-SRRs), previously used for the implementation of metamaterials [22–24], are presented in a journal paper for the first time. S-SRRs are electrically smaller than electric-LC resonators (ELC) and even smaller than split ring resonators (SRRs) [15]. Thus, high miniaturization levels can be obtained by using S-SRRs, with direct impact on the achievable number of bits per cm^2, superior in S-SRR-based barcodes.

S-SRRs have been successfully applied to the design of microwave filters [25] and sensors [26] as well. Coupled to CPW transmission lines, S-SRRs generate notches (transmission zeros) in the transmission coefficient at their resonance frequency. However, through a proper orientation, line to resonator coupling can be prevented, and hence the presence or absence of the transmission zero can be controlled, and this is used for encoding, as will be later shown.

2 Topology and working principle

The typical topology of this particle is depicted in Figure 1. This particle cannot be excited by means of an uniform time-varying magnetic field applied in the direction orthogonal to the plane of the particle, contrary to SRRs [1, 27], but it can be driven by means of counter magnetic fields, as depicted in the figure, and similar to the excitation of electric LC (ELC) resonant particles [28]. According to this, it follows that by etching these S-SRRs on the back substrate side of a coplanar waveguide (CPW), the fundamental resonance can be

*e-mail: cristian.herrojo@uab.cat

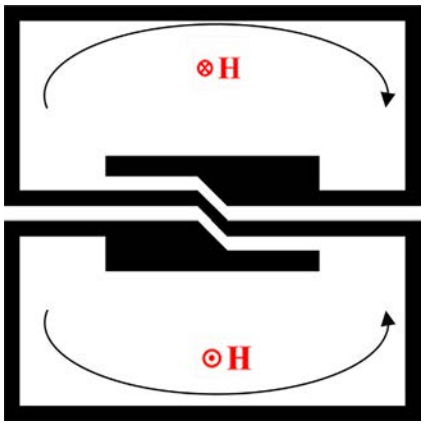

Figure 1. Typical topology of an S-SRR and indication of the driving mechanism by means of counter-magnetic fields.

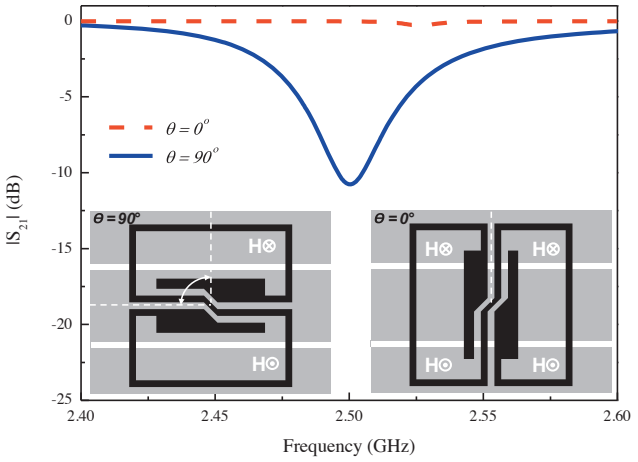

Figure 2. Response of the CPW loaded with a single S-SRR for the two considered states: "1" (90°) and "0" (0°).

excited as long as each loop of the particle lies on bottom of one of the slots of the CPW, as indicated in Figure 2. However, by rotating the particle 90° (0° orientation in Figure 2), no significant excitation is expected since there is not a net magnetic field in each loop, able to induce a current. According to this, S-SRRs are useful for the implementation of multi-resonator [19, 20] spectral signature barcodes for chipless RFID, where each resonator corresponds to a bit and the "0" or "1" logic states are simply set by the orientation of the S-SRRs.

3 Circuit model and design

The typical topology (including relevant dimensions) and circuit model of a CPW loaded with a square S-SRR, etched on the back substrate side, are depicted in Figure 3 [26]. The line is modeled by the inductance L and the capacitance C, the S-SRR is described by the capacitance C_s and by the inductance of each loop, L_s. Finally, the coupling between the line and the resonator is accounted for by the mutual inductance $2M$. Note that this model is formally identical to the one describing a SRR-loaded CPW transmission line [1, 3]. As discussed in [26], the mutual coupling depends on the relative orientation between the line and the resonator, it being maximum for the 90° orientation, i.e., the one indicated in Figure 3a. In the circuit of Figure 3b, losses have been excluded. This circuit can be transformed to the one indicated in Figure 3c, where the reactive elements of both models are related by [3]:

$$L_s' = \frac{M^2}{2L_s} \tag{1}$$

$$C_s' = \frac{4L_s^2 C_s}{M^2} \tag{2}$$

$$L' = L - L_s' \tag{3}$$

and the notch (angular) frequency is given by

$$\omega_0 = \frac{1}{\sqrt{2L_s C_s}} = \frac{1}{\sqrt{L_s' C_s'}} \tag{4}$$

This model has been validated by parameter extraction, following the procedure reported in [29]. Figure 4 shows the frequency response of a particular S-SRR-loaded CPW, where both the lossless electromagnetic (inferred from

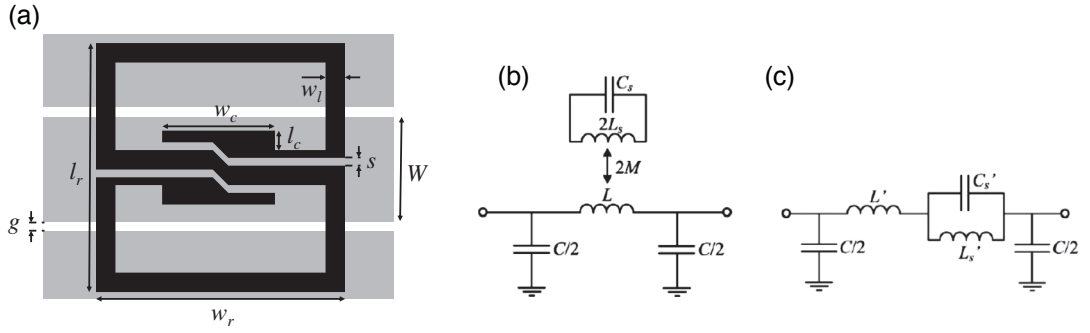

Figure 3. Topology of a S-SRR-loaded CPW (a), lumped element equivalent circuit model (b), and transformed model (c).

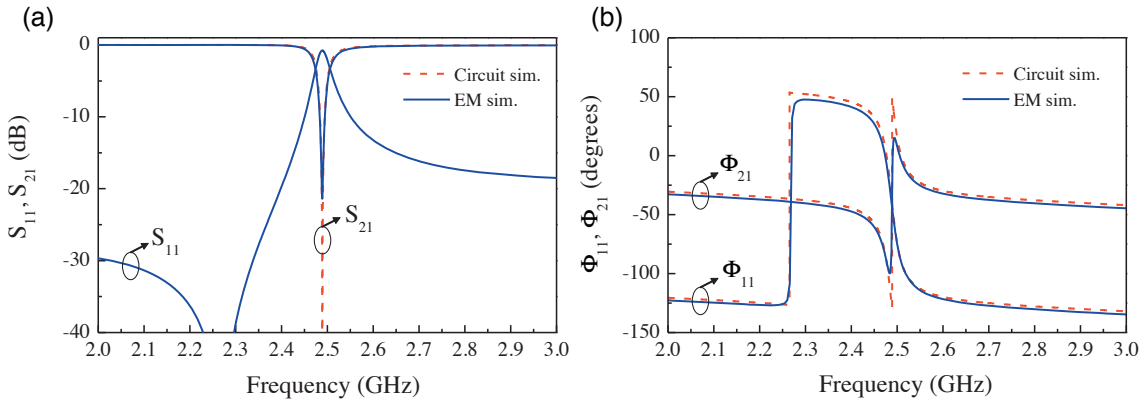

Figure 4. Frequency response of a CPW loaded with a square S-SRR. (a) Magnitude response; (b) phase response. Dimensions are: $l_r = w_r = 5.6$ mm, $w_l = s = 0.2$ mm, $w_c = 2.87$ mm, and $l_c = 0.47$ mm. Line dimensions are: $W = 2.1$ mm, $g = 0.2$ mm corresponding to a 50 Ω transmission line. The extracted element values are: $C = 0.92$ pF, $L' = 1.69$ nH, $C_s' = 58.6$ pF, and $L_s' = 69.8$ pH.

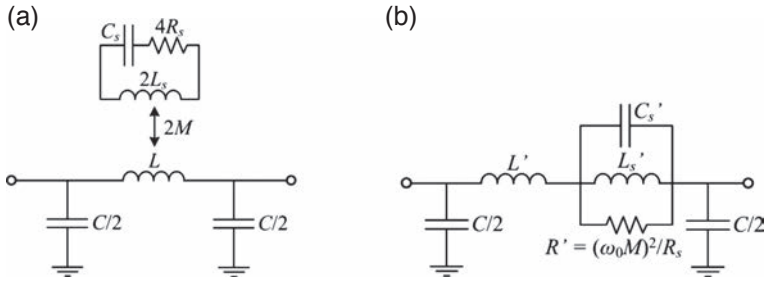

Figure 5. Lossy equivalent circuit model of an S-SRR-loaded CPW. (a) Simplified model and (b) equivalent transformed model.

Keysight Momentum) and circuit simulations are compared. The considered substrate is *Rogers RO4003C* with dielectric constant $\varepsilon_r = 3.55$ and thickness $h = 0.81$ mm (dimensions as well as circuit element values are indicated in the caption). As can be appreciated, there is very good agreement between the circuit and electromagnetic simulations in the frequency range of interest, pointing out the validity of the lumped element equivalent circuit model.

For design purposes, there are two important parameters: the notch depth, and the −3 dB notch bandwidth. In order to accommodate the largest number of bits in a given spectral bandwidth, it is convenient to reduce the notch bandwidth of each individual resonator as much as possible, but, due to losses, this affects the notch depth, reducing its magnitude and consequently jeopardizing the correct reading of the written code. Therefore, a tradeoff results. To gain insight into this important aspect, let us now consider the presence of losses in the circuit models (Figure 5). The notch magnitude in the circuit of Figure 5b can be expressed as [26]:

$$|S_{21}|(\mathrm{dB}) = 20\log_{10}\left|\frac{1}{Z_s\left(\frac{Y_p^2 Z_0}{2}+\frac{1}{2Z_0}\right)+Y_p(Z_s+Z_0)+1}\right| \tag{5}$$

where Z_s is the impedance of the series branch, Y_p is the admittance of the shunt branch, and Z_0 is the port impedance. The previous expression, evaluated at resonance, can be written as:

$$|S_{21}|(\mathrm{dB}) = 20\log_{10}\left|\frac{1}{\left(Z_{L'}+\frac{\omega_0^2 M^2}{R_s}\right)\left(\frac{Y_p^2 Z_0}{2}+\frac{1}{2Z_0}\right)+Y_p\left(Z_{L'}+\frac{\omega_0^2 M^2}{R_s}+Z_0\right)+1}\right| \tag{6}$$

where $Z_{L'}$ is the impedance of the line inductance. To the light of equation (6), M tends to increase the notch depth, whereas an increase in R_s reduces the magnitude of the notch, as expected. Nevertheless, R_s is not a design parameter, contrary to M, which depends on S-SRR orientation and also on substrate thickness. Note that, according to expressions (1) and (2), if M increases, L_s' also increases, whereas C_s' decreases, thereby enhancing the bandwidth (related to the ratio L_s'/C_s').

By considering the substrate permittivity and thickness indicated before ($\varepsilon_r = 3.55$, and $h = 0.81$ mm) and a loss tangent of $\tan\delta = 0.0021$, we have obtained the frequency response of the S-SRR-loaded CPW of Figure 2, inferred from electromagnetic simulation with losses (the conductivity of copper for the metallic layers has been assumed). Then we have repeated these electromagnetic simulations by considering different substrate thicknesses, in order to infer the effect of M on bandwidth and notch depth. The results are depicted

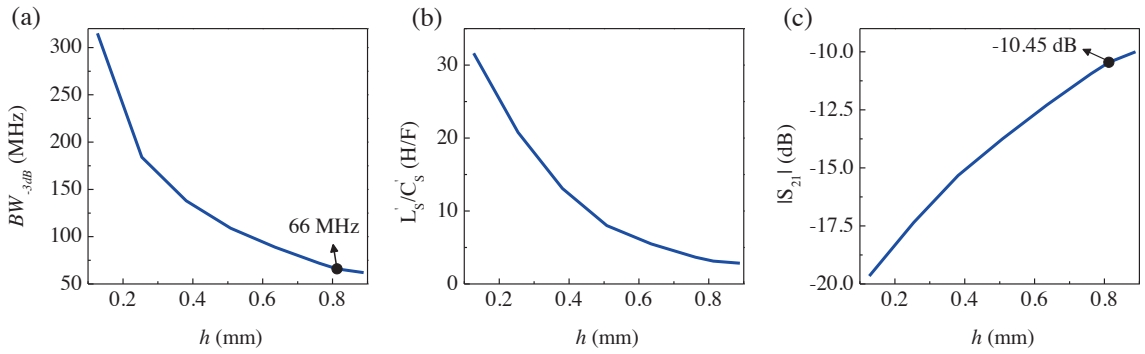

Figure 6. Dependence of the notch bandwidth (a), L_s'/C_s' (b), and notch depth (c) with substrate thickness.

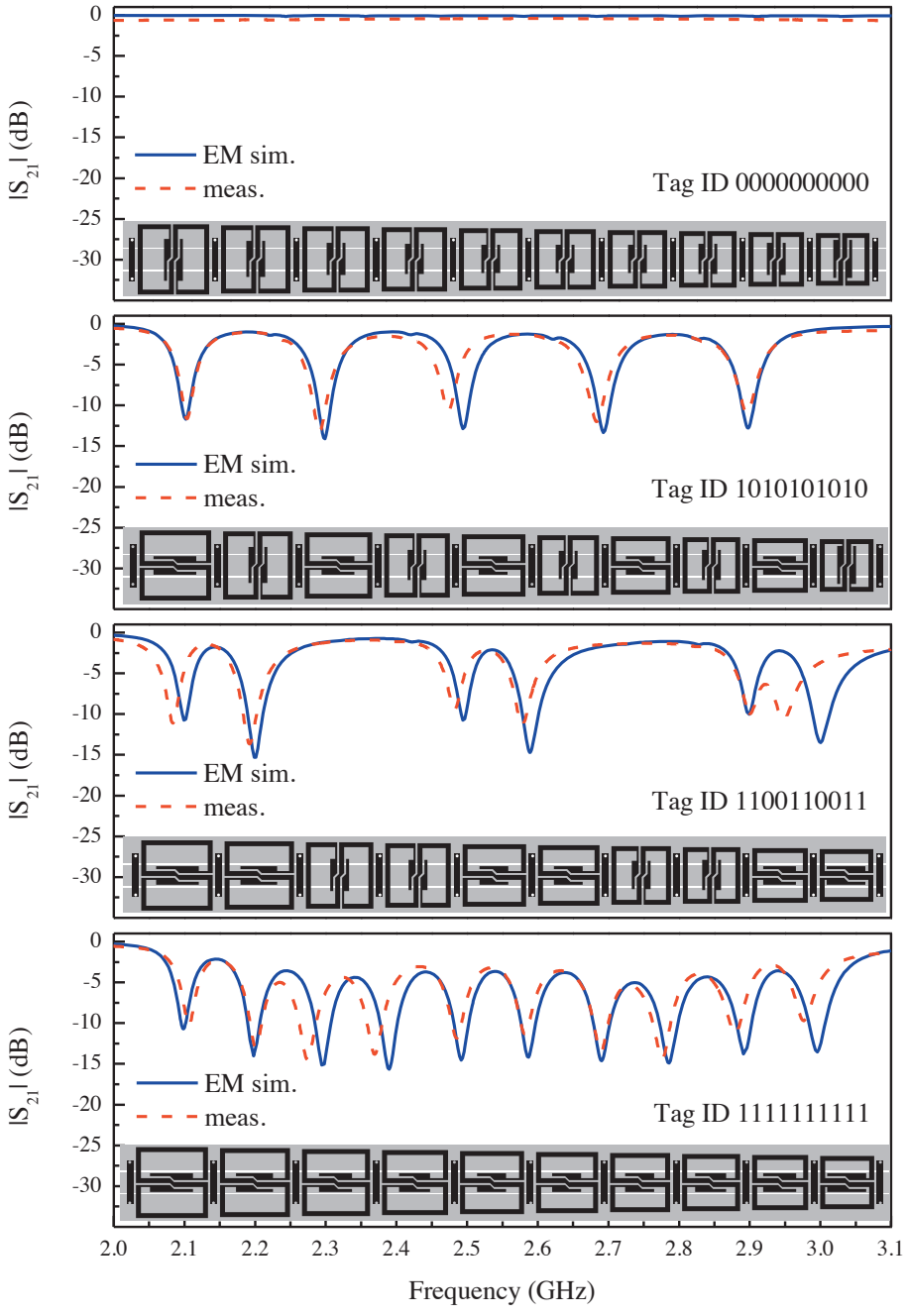

Figure 7. Simulated and measured transmission coefficient of the corresponding indicated codes.

in Figure 6, where we have also included the dependence of L_s'/C_s' on substrate thickness. In order to accommodate 10 bits (and hence 10 resonators) in a 1 GHz spectral bandwidth between 2 GHz and 3 GHz, it is necessary to limit the resonator bandwidths to less than 100 MHz. In view of Figure 6, for the thickness of $h = 0.81$ mm, the notch depth is found to be larger than 10 dB, which is a reasonable value to adequately read the "1" logic states, whereas this thickness clearly gives a bandwidth much smaller than 100 MHz. Therefore, this has been the considered thickness value, which corresponds to a commercially available microwave substrate. From the considered resonator (with a frequency of 2.5 GHz), the other resonant elements have been obtained by merely scaling the length of the loops.

4 Results

The topology of the S-SRR with reference frequency has been determined with a relatively small value of L_s and large value of C_s (significant L_s'/C_s' ratio) in order to achieve a notch depth of at least 10 dB. The dimensions are $l_r = w_r = 6.4$ mm, $w_l = 0.5$ mm, $s = 0.2$ mm, $w_c = 2.9$ mm, and $l_c = 0.5$ mm. After scaling, in order to generate notch frequencies equally distributed within the bandwidth 2–3 GHz, we have implemented several codes by loading the CPW with such resonant elements, where the "1" and "0' logic states have been simply achieved by properly orienting the S-SRRs. The four considered codes and the corresponding frequency responses (inferred from lossy electromagnetic simulations and measurements) are depicted in Figure 7. Note that the ground plane regions of the CPW are connected by means of backside strips and vias in order to avoid the generation of the parasitic slot mode. The measured responses have been achieved by means of the *Agilent N5221A* vector network analyzer. According to Figure 7, there is good agreement between the electromagnetic simulation and measurement, and the different code responses reveal that a threshold of 5 dB suffices to distinguish between the "0" and "1" logic states. The area of the codes is as small as 9 cm^2. Moreover, the fact that by rotating the S-SRR the coupling can be controlled opens the possibility of increasing the number of states per resonator, and thus increase the information density per GHz (work is in progress).

5 Conclusions

In summary, novel spectral signature barcodes implemented by loading a CPW with S-SRRs have been proposed. On the basis of the lumped element equivalent circuit model, which has been validated through parameter extraction, we have analyzed the effects of line to resonator coupling and losses on the response of the S-SRR loaded CPW. Particularly, it has been found that by increasing the mutual coupling, the notch magnitude of the structure is enhanced but at the expense of a broader bandwidth. Hence, it has been concluded that a tradeoff for design purposes is necessary, and with this in mind we have designed the S-SRRs in order to accommodate 10 notches (corresponding to 10 bits) in a 1 GHz spectral bandwidth between 2 GHz and 3 GHz. The resulting codes, smaller than 9 cm^2, exhibit responses that can be easily read, with equidistant notches for the extreme case where all the bits are set to the "1" state.

Acknowledgements. This work was supported by MINECO-Spain (projects TEC2013-40600-R and RTC-2014-2550-7 ChiplessRFID), by Generalitat de Catalunya (project 2014SGR-157), by Institució Catalana de Recerca i Estudis Avançats (who awarded Ferran Martín), and by FEDER funds. Cristian Herrojo has been granted by MINECO with the grant number BES-2014-068164.

References

1. F. Martín, F. Falcone, J. Bonache, R. Marqués, M. Sorolla, Split ring resonator based left handed coplanar waveguide, Appl. Phys. Lett. 83 (2003) 4652–4654.
2. F. Falcone, T. Lopetegi, J.D. Baena, R. Marqués, F. Martín, M. Sorolla, Effective negative-epsilon stop-band microstrip lines based on complementary split ring resonators, IEEE Microw. Wirel. Compon. Lett. 14 (2004) 280–282.
3. F. Martín, Artificial Transmission Lines for RF and Microwave Applications, John Wiley, Hoboken, NJ, 2015.
4. F. Martín, F. Falcone, J. Bonache, R. Marqués, M. Sorolla, Miniaturized CPW stop band filters based on multiple tuned split ring resonators, IEEE Microw. Wirel. Compon. Lett. 13 (2003) 511–513.
5. J. García-García, J. Bonache, I. Gil, F. Martín, R. Marqués, F. Falcone, T. Lopetegi, M.A.G. Laso, M. Sorolla, Comparison of electromagnetic bandgap and split rings resonator microstrip lines as stop band structures, Microw. Opt. Technol. Lett. 44 (2005) 376–379.
6. F.J. Herraiz-Martínez, L.E. García-Muñoz, D. González-Ovejero, V. González-Posadas, D. Segovia-Vargas, Dual-frequency printed dipole loaded with split ring resonators, IEEE Antennas Wirel. Propag. Lett. 8 (2009) 137–140.
7. F.J. Herraiz-Martínez, G. Zamora, F. Paredes, F. Martín, J. Bonache, Multiband printed monopole antennas loaded with open complementary split ring resonators for PANs and WLANs, IEEE Antennas Wirel. Propag. Lett. 10 (2011) 1528–1531.
8. F.J. Herraiz-Martínez, F. Paredes, G. Zamora, F. Martín, J. Bonache, Dual-band printed dipole antenna loaded with open complementary split-ring resonators (OCSRRs) for wireless applications, Microw. Opt. Technol. Lett. 54 (2012) 1014–1017.
9. J. Naqui, A. Fernández-Prieto, M. Durán-Sindreu, F. Mesa, J. Martel, F. Medina, F. Martín, Common mode suppression in microstrip differential lines by means of complementary split ring resonators: theory and applications, IEEE Trans. Microwave Theor. Tech. 60 (2012) 3023–3034.
10. P. Vélez, J. Naqui, A. Fernández-Prieto, M. Durán-Sindreu, J. Bonache, J. Martel, F. Medina, F. Martín, Differential bandpass filter with common mode suppression based on open split ring resonators and open complementary split ring resonators, IEEE Microw. Wirel. Compon. Lett. 23 (1) (2013) 22–24.
11. M. Puentes, C. Weiss, M. Schüßler, R. Jakoby, Sensor array based on split ring resonators for analysis of organic tissues, IEEE MTT-S International Microwave Symposium Digest, Baltimore, MD, USA, 2011, pp. 5–10.

12. J. Naqui, M. Durán-Sindreu, F. Martín, Novel sensors based on the symmetry properties of Split Ring Resonators (SRRs), Sensors 11 (2011) 7545–7553.
13. M.S. Boybay, O.M. Ramahi, Material characterization using complementary split-ring resonators, IEEE Trans. Instrum. Meas. 61 (2012) 3039–3046.
14. J. Naqui, M. Durán-Sindreu, F. Martín, Alignment and position sensors based on split ring resonators, Sensors 12 (2012) 11790–11797.
15. J. Naqui, F. Martín, Transmission lines loaded with bisymmetric resonators and their application to angular displacement and velocity sensors, IEEE Trans. Microwave Theor. Tech. 61 (2013) 4700–4713.
16. A. Abduljabar, D. Rowe, A. Porch, D. Barrow, Novel microwave microfluidic sensor using a microstrip split-ring resonator, IEEE Trans. Microwave Theor. Tech. 62 (2014) 679–688.
17. A. Ebrahimi, W. Withayachumnankul, S. Al-Sarawi, D. Abbott, High-sensitivity metamaterial-inspired sensor for microfluidic dielectric characterization, IEEE Sens. J. 14 (2014) 1345–1351.
18. A. Ebrahimi, W. Withayachumnankul, S.F. Al-Sarawi, D. Abbott, Metamaterial-inspired rotation sensor with wide dynamic range, IEEE Sens. J. 14 (2014) 2609–2614.
19. S. Preradovic, N.C. Karmakar, Chipless RFID: bar code of the future, IEEE Microw. Mag. 11 (2010) 87–97.
20. S. Preradovic, I. Balbin, N.C. Karmakar, G.F. Swiegers, Multiresonator-based chipless RFID system for low-cost item tracking, IEEE Trans. Microwave Theor. Tech. 57 (2009) 1411–1419.
21. J. Naqui, M. Durán-Sindreu, F. Martín, On the symmetry properties of coplanar waveguides loaded with symmetric resonators: analysis and potential applications, IEEE MTT-S Int. Microwave Symp. Dig, Montreal (Canada), 2012.
22. H. Chen, L. Ran, J. Huangfu, X. Zhang, K. Chen, T.M. Grzegorczyk, J.A. Kong, Left-handed materials composed of only S-shaped resonators, Phys. Rev. E 70 (2004) 057605.
23. H. Chen, L. Ran, J. Huangfu, X. Zhang, K. Chen, T.M. Grzegorczyk, J.A. Kong, Negative refraction of a combined double S-shaped metamaterial, Appl. Phys. Lett. 86 (2005) 151909.
24. H. Chen, L.X. Ran, J.T. Huang-Fu, X.-M. Zhang, K.-S. Cheng, T.M. Grzegorczyk, J.A. Kong, Magnetic properties of S-shaped split ring resonators, Progress Electromagn. Res. 51 (2005) 231–247.
25. A.K. Horestani, M. Durán-Sindreu, J. Naqui, C. Fumeaux, F. Martín, Compact coplanar waveguide band-pass filter based on coupled S-shaped split ring resonators, Microw. Opt. Technol. Lett. 57 (2015) 1113–1116.
26. J. Naqui, J. Coromina, A. Karami-Horestani, C. Fumeaux, F. Martín, Angular displacement and velocity sensors based on coplanar waveguides (CPWs) loaded with S-shaped split ring resonator (S-SRR), Sensors 15 (2015) 9628–9650.
27. J.B. Pendry, A.J. Holden, D.J. Robbins, W.J. Stewart, Magnetism from conductors and enhanced nonlinear phenomena, IEEE Trans. Microwave Theor. Tech. 47 (1999) 2075–2084.
28. D. Schurig, J.J. Mock, D.R. Smith, Electric-field-coupled resonators for negative permittivity metamaterials, Appl. Phys. Lett. 88 (2006) 041109.
29. F. Aznar, M. Gil, J. Bonache, J.D. Baena, L. Jelinek, R. Marqués, F. Martín, Characterization of miniaturized metamaterial resonators coupled to planar transmission lines, J. Appl. Phys. 104 (2008) 114501-1-8.

Cite this article as: Herrojo C, Naqui J, Paredes F & Martín F: Spectral signature barcodes based on S-shaped Split Ring Resonators (S-64 SRRs). EPJ Appl. Metamat. 2016, **3**, 1.

Artículo TMTT16

Multistate Multiresonator Spectral Signature Barcodes Implemented by Means of S-Shaped Split Ring Resonators (S-SRRs)

C. Herrojo, F. Paredes, J. Mata-Contreras, S. Zuffanelli and F. Martín

Multistate Multiresonator Spectral Signature Barcodes Implemented by Means of S-Shaped Split Ring Resonators (S-SRRs)

Cristian Herrojo, *Graduate Student Member, IEEE*, Ferran Paredes, *Associate Member, IEEE*, Javier Mata-Contreras, Simone Zuffanelli, *Member, IEEE*, and Ferran Martín, *Fellow, IEEE*

***Abstract*— Spectral signature barcodes functional at the *S* frequency band are presented in this paper. The barcodes are implemented by loading a coplanar waveguide transmission line by means of multiple S-shaped split ring resonators (S-SRRs), each one tuned to a different frequency. The main particularity of this paper is the fact that more than two logic states (i.e., three or four, depending on the implementation) are assigned to each resonant element. By this means, the total number of bits of the barcode (for a given number of resonators) is increased, as compared with previous approaches based on two logic states per resonator. This multistate functionality is achieved by rotating the S-SRRs. Such rotation modulates the line-to-resonator coupling intensity, and consequently the notch depth at the S-SRR fundamental resonance. Therefore, by considering three or four fixed rotation angles (or orientations) between the line axis and the S-SRR (for the tri- and four-state multiresonator barcodes, respectively), intermediate levels between the maximum and minimum attenuation are achieved. This multistate strategy only exploits a single frequency per resonant element (the fundamental one). Therefore, the data capacity per bandwidth are improved as compared with two-state-based barcodes or to multistate barcodes that use two frequencies per resonant element. As illustrative examples, two different four-state multiresonator barcodes with eight S-SRRs (providing $4^8 = 65.536$ different codes, or 16 bits) and with nine S-SRRs (equivalent to 18 bits), occupying a spectral bandwidth of 1 GHz and less than 6.75 and 8.2 cm^2, respectively, are designed, fabricated, and characterized.**

***Index Terms*— Coplanar waveguide (CPW) technology, S-shaped split ring resonators (S-SRRs), spectral signature barcodes.**

I. Introduction

In RADIO frequency identification (RFID) systems, objects or items are equipped with tags, which communicate wirelessly with the interrogator or reader [1], [2]. RFID tags are typically composed of a compact antenna and an application specific integrated circuit that contains the ID code of the object or item. In UHF-RFID, read distances of various meters are usual, and line-of-sight for tag reading is not necessary. However, the presence of the microchip increases fabrication costs of the tag, and this limits the penetration of this technology in certain market segments [3].

To alleviate this problem, chipless tags have been proposed [3]–[5]. In chipless RFID, the tags are equipped with planar passive encoders, which can be implemented by means of low-cost mass production fabrication techniques, including subtractive (etching) or printed (e.g., screen printing) techniques. However, such encoders represent a penalty in terms of tag size and data storage capacity. Although planar encoders cannot compete with microchips in these aspects (size and information capacity), their low cost fully justifies the research activity toward optimizing dimensions and number of bits.

This paper is focused on multiresonator transmission line-based encoders, where a transmission line is loaded with multiple resonant elements (each tuned to a different frequency) [3], [6]–[8]. The tag code is inferred from the spectral signature of the loaded lines, given by a number of attenuation peaks (or notches) in the frequency response. The logic states "0" or "1" are determined by the absence or presence, respectively, of a notch at the resonance frequency of the resonators representing each bit of information. Such spectral signature barcodes, as they are usually designated, work in the frequency domain. Multiresonator encoders based on the measurement of the radar cross section have been also reported [9]–[14].

Other chipless tags use reflectors in a transmission line [15]–[19], and tag ID is obtained from the reflected pulses of a pulsed input signal. The spectral bandwidth is small, but the data storage capability is also small as compared with frequency domain-based tags.

In order to decrease tag size and enhance the data storage capability (or number of bits) per frequency unit (a figure of merit) in multiresonator spectral signature barcodes, a multistate approach was proposed in [20]. Three logic states, rather than two, were assigned to each resonant element, an S-shaped split ring resonator (S-SRR) [21]–[23], thereby increasing the data capacity per resonant element. The use of S-SRRs is justified by their small electrical size, and by the fact that the logic states are simply achieved by properly orienting the resonator with regard to the line, as will be later discussed (S-SRR rotation was the principle for the

Manuscript received October 4, 2016; revised December 22, 2016, February 7, 2017, and February 13, 2017; accepted February 15, 2017. Date of publication March 14, 2017; date of current version June 29, 2017. This work was supported in part by MINECO, Spain, under Project TEC2013-40600-R and Project RTC-2014-2550-7, in part by the Generalitat de Catalunya under Project 2014SGR-157, in part by the Institució Catalana de Recerca i Estudis Avançats (who awarded F. Martín), and in part by FEDER funds. The work of C. Herrojo was supported by MINECO through FPI under Grant BES-2014-068164.

The authors are with GEMMA/CIMITEC, Department d'Enginyeria Electrònica, Universitat Autònoma de Barcelona, 08193 Bellaterra, Spain (e-mail: ferran.martin@uab.es).

Color versions of one or more of the figures in this paper are available online at http://ieeexplore.ieee.org.

Digital Object Identifier 10.1109/TMTT.2017.2672547

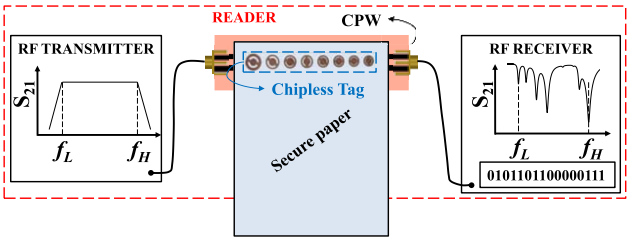

Fig. 1. Sketch of the chipless RFID system based on inductive coupling between the active part of the reader (CPW) and the tag (set of resonant elements). Note that the tag may be integrated within the tagged item (e.g., secure paper).

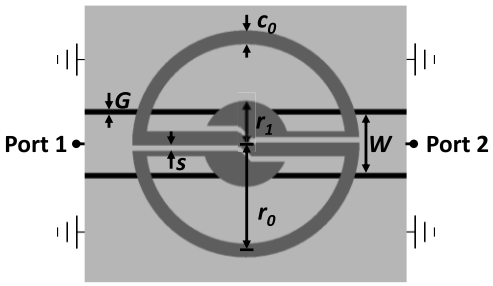

Fig. 2. Typical topology of an S-SRR-loaded CPW and relevant dimensions. The S-SRR is etched in the back substrate side.

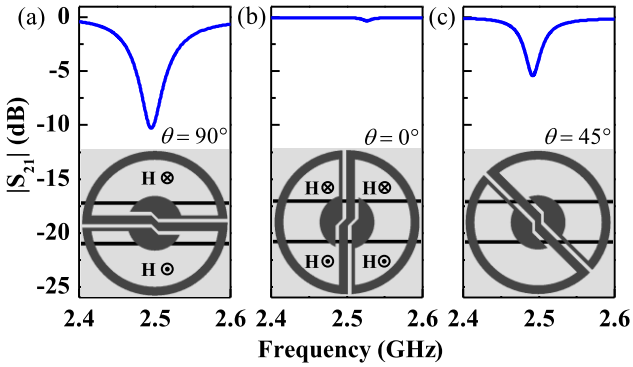

Fig. 3. Frequency responses for three different orientations between the S-SRR and the line to illustrate the working principle of the multiresonator tags with more than two states per resonant element. (a) Maximum coupling. (b) Minimum coupling. (c) Intermediate coupling.

implementation of angular displacement and velocity sensors, reported in [24]).

In this paper (an expanded version of [20]), we extend the number of states per resonator to four, by properly designing the S-SRRs and the host line, a coplanar waveguide (CPW). Moreover, we propose two different types of barcodes, one with the S-SRRs etched in the back substrate side of the CPW, and the other one with the S-SRRs etched in a different substrate. In the latter case, the one of interest in this paper, the tag is simply the set of resonant elements etched, or printed, on the corresponding substrate. This substrate is different than the one where the transmission line is fabricated. The line can be considered to be part of the reader. Tag reading requires proximity and proper alignment between the line and resonant elements, and such reading is related to inductive coupling. In other words, we propose novel near-field chipless RFID tags that do not require antennas, since the communication between the tag (set of resonators) and the reader (line) is by proximity. Such limitations (proximity and adequate orientation between tag and reader) are, however, compensated by two important aspects: 1) tag size (since antennas are not required) and 2) data capacity per spectral bandwidth, due to the fact that up to four states per resonant element can be considered, as will be demonstrated in Section III-C (note that losses in the wireless link prevent the application of these multistate multiresonator barcodes in far-field chipless RFID). In certain applications, such as security and authentication, tag size and number of bits are the main concerns. Optimization of these aspects at the expense of a reading system that ensures proximity and correct orientation between tag and reader (e.g., through a guiding system) can be accepted (see in Fig. 1 a scheme of the proposed system).

This paper is organized as follows. In Section II, the working principle of these S-SRR-based multistate multiresonator barcodes is presented, and the design requirements for the resonant elements and the CPW host line are discussed by considering both the tristate and four-state spectral signature barcodes. Section III is focused on the design examples. One example is an *S*-band encoder based on ten tristate resonators occupying an area of 860 mm^2 and 1-GHz spectral bandwidth, already presented in [20] but included here for completeness. Then, a pair of encoders implemented by means of eight and nine four-state S-SRRs, providing 16 and 18 bits, respectively, also occupying 1-GHz spectral bandwidth and an area of 675 and 820 mm^2, are reported. In the encoder with 18 bits, the S-SRRs and CPW are etched in the same substrate, and such encoder has been designed as a first step toward the 16-bit encoder with S-SRR etched on a separate substrate (the encoder of interest in this paper for the reasons explained before). In Section IV, the 16-bit encoder based on eight four-state S-SRRs is compared with other frequency domain encoders. Finally, the main conclusions are highlighted in Section V.

II. Working Principle, Design Requirements, and Modeling

Coupling modulation between the host line and the resonant elements by rotation is the working principle of the proposed multistate multiresonator encoders [25], [26]. This principle was also applied to the design of angular displacement and velocity sensors [24], [27]–[30]. The key point is that for certain planar resonators, such as the S-SRR (see Fig. 2), their proximity to a host line, in our case a CPW transmission line, does not guarantee the appearance of line-to-resonator coupling. Fig. 3 shows three different orientations of the S-SRR with regard to the CPW axis (the S-SRR is etched in the back substrate side). With the S-SRR orientation corresponding to Fig. 3(a), the magnetic field generated by the line is counter directional in each S-SRR semiloop, and the particle is excited. Consequently, a transmission zero at the fundamental S-SRR resonance is generated. The reason is that the currents at both halves (semiloops) of the particle flow in opposite directions (clockwise and counterclockwise) at that frequency. Conversely, for an orientation angle of 90° [Fig. 3(b)], the net magnetic field in each resonator half (semiloop) is negligible. Consequently, line-to-resonator

coupling is very small, and signal attenuation at resonance is insignificant. By rotating the particle [Fig. 3(c)], the coupling level and hence the notch depth can be modulated. Consequently, three, or more, logic states per resonant element can be obtained by considering different angles between the S-SRR and the line.

It is worth to note that this functionality (coupling modulation) can be achieved with other resonant particles, in particular, with the electric *LC* (ELC) resonator [31]. Indeed, the ELC resonator is a bisymmetric particle, exhibiting a magnetic wall and an electric wall (both orthogonally oriented) at the fundamental resonance. When the magnetic wall of the ELC is aligned with the symmetry plane of the CPW transmission line, line-to-resonator coupling is maximized. However, by rotating the particle 90°, the electric wall of the ELC aligns with the symmetry plane of the line, and this prevents the appearance of coupling [28]. For different orientations, the coupling level and notch depth at resonance can be tailored to some extent, and the behavior is very similar to the one achievable with S-SRRs. However, the ELC is electrically much larger than the S-SRR, and for this main reason, this particle (ELC) is discarded in this paper. The fact that the notch frequency does not experience a significant variation with the rotation angle is an important concern (if this is the case, overlapping with the resonance frequency of adjacent resonators is avoided). In this regard, S-SRRs are useful particles, since their resonance frequency is quite invariant with the rotation angle [24]. Therefore, S-SRRs are suitable particles for the implementation of multiresonator barcodes.

Let us now discuss the specific topology of the S-SRR (Fig. 2). The circular shape is explained by the fact that this shape tends to linearize the response (notch depth in dB) with the rotation angle (we have thus considered in this application the notch depth in dB, since roughly a linear dependence of the notch variation with the rotation angle is achieved). Note that the width of the loops is relatively wide, and the particle is terminated with semicircular patches (see central region). This topology results in relatively small S-SRR inductance and large S-SRR capacitance, and this is necessary to achieve significant notch depth for the maximum coupling state (90° rotation). Such notch depth should be large enough in order to be able to discriminate the intermediate states. Note, however, that by increasing the notch depth, the bandwidth per resonant element is also increased (because C_s/L_s increases). Therefore, a tradeoff is necessary. The S-SRR of Fig. 2 has been designed with an eye toward providing at least 10-dB attenuation (for the state corresponding to maximum coupling, i.e., with 90° orientation) and a maximum bandwidth (at half maximum) of 50 MHz. Such resonant particle has been designed to resonate at 2.5 GHz, and it is the reference S-SRR for the tristate ten-resonator barcode first presented in [20], where resonance frequencies are separated by 100 MHz within the *S* frequency band (the spectral bandwidth covers the range 2–3 GHz).

Fig. 4 shows the lossy simulation response of the structure of Fig. 2 for rotation angles of 45° and 90°, corresponding to the intermediate state and maximum coupling state, respectively (the substrate is *Rogers RO4003C* with

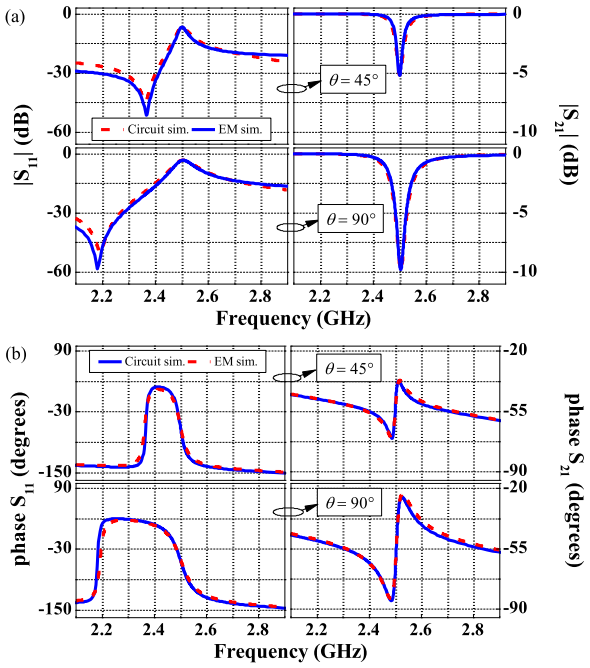

Fig. 4. Frequency response (including electromagnetic simulation and circuit simulation) of the CPW loaded with an S-SRR of Fig. 2 for different S-SRR angles. (a) Magnitude and (b) phase of the reflection (S_{11}) and transmission (S_{21}) coefficients. The electromagnetic simulations have been obtained with *Keysight Momentum*. S-SRR dimensions (in reference to Fig. 2) are $r_1 = 1.3$ mm, $r_0 = 3.4$ mm, $s = 0.2$ mm, and $c_0 = 0.5$ mm. Line dimensions are $W = 2.1$ mm and $G = 0.2$ mm corresponding to a 50 Ω transmission line.

thickness $h = 0.81$ mm, dielectric constant $\varepsilon_r = 3.55$, and $\tan\delta = 0.0021$). These responses are appropriate to clearly discriminate the intermediate state, with a notch depth of roughly 5 dB, in contrast to the maximum attenuation of approximately 10 dB achieved by 90° S-SRR rotation. Note that the notch frequency for the 45° and 90° orientations scarcely varies.

The equivalent circuit model of the S-SRR-loaded CPW is shown in Fig. 5(a) [24]. In this circuit, L and C are the inductance and capacitance, respectively, of the line, the S-SRR is accounted by the capacitance C_s and by the inductance of each loop, L_s, and the mutual inductance $2M$ describes the coupling between the line and the resonator. Contrary to previous works, we include in this model the losses of the S-SRR through the resistance R_s. The reason is that the notch depth (a relevant parameter) is related to losses. As discussed before, the mutual coupling depends on the relative orientation between the line and the resonator. Therefore, M is actually an angle-dependent parameter, or $M = M(\theta)$. The circuit of Fig. 5(a) can be transformed to the one indicated in Fig. 5(b), where the reactive elements of both models are related by [24]

$$L_s' = \frac{M^2}{2L_s} \tag{1}$$

$$C_s' = \frac{4L_s^2 C_s}{M^2} \tag{2}$$

$$L' = L - L_s' \tag{3}$$

$$R_s' = \frac{M^2}{2L_s C_s R_s}. \tag{4}$$

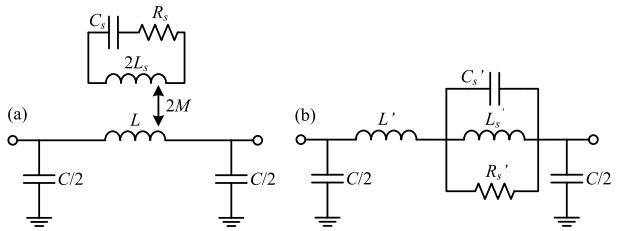

Fig. 5. Equivalent circuit model, including losses in the S-SRR, of (a) S-SRR-loaded CPW transmission line and (b) transformed model.

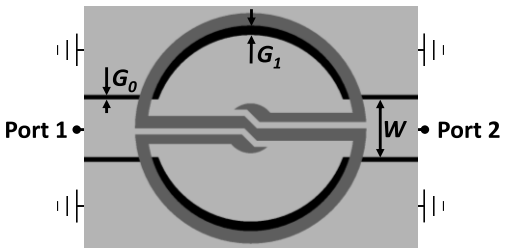

Fig. 6. Topology of a CPW transmission line section loaded with an S-SRR (etched in the back substrate side) corresponding to the reference resonant element of the four-state multiresonator barcode, and relevant dimensions of the circularly shaped CPW: $W = 1.85$ mm, $G_0 = 0.15$ mm, and $G_1 = 0.31$ mm corresponding to a 50 Ω transmission line.

TABLE I
EXTRACTED ELEMENT VALUES OF THE CIRCUIT OF FIG. 5(b) FOR THE TRISTATE S-SRR

θ (degrees)	L'_s (nH)	C'_s (pF)	R'_s (Ω)	L' (nH)	C (pF)
45	0.04	103	63.8	2.34	1.36
90	0.11	36.5	165	2.28	1.34

TABLE II
ELEMENT VALUES OF THE CIRCUIT OF FIG. 5(a) FOR THE TRISTATE S-SRR

θ (degrees)	L_s (nH)	C_s (pF)	R_s (Ω)	L (nH)	M (nH)
45	10.0	0.20	3.05	2.38	0.44
90	10.0	0.20	3.31	2.39	0.74

We have extracted the parameters of the circuit of Fig. 5(b) from the electromagnetic responses corresponding to the 45° and 90° S-SRR orientations (see Table I). The method, reported in [32], is essentially based on the magnitude and phase response at certain frequencies, rather than on curve fitting. The circuit responses are also included in Fig. 4, and it can be appreciated that the agreement between electromagnetic and circuit simulation is good.

We have estimated the inductance of the S-SRR, L_s, by eliminating the central semicircular patches and by obtaining the reactance of the resulting structure, after connecting a differential port to the resulting terminals [28]. From the value of this inductance, i.e., $L_s = 10$ nH, we have then inferred the mutual inductance and the capacitance of the S-SRR. These S-SRR elements and the additional elements of the circuit of Fig. 5(a), inferred by inverting (1)–(4), are given in Table II. It can be seen that M is significantly larger for the 90° orientation, as expected. The other reactive parameters do not experience significant variations for both orientations, which is coherent with the proposed model, where the single angle-dependent parameter is the mutual coupling. The unloaded quality factor has been found to be 103 and 95 for the 45° and 90° orientations, respectively.

Let us now consider the requirements for the four-state multiresonator barcodes. In this case, further notch depth (and hence coupling) for the maximum coupling state (90°) is necessary, since two intermediate states are considered. To enhance the coupling, the transverse dimensions of the line in the region where the S-SRR are present can be reshaped, resulting in a nonuniform transmission line. Specifically, the CPW transmission line is designed with circular and wider slots above the position of the S-SRRs (see the reference resonator/CPW in Fig. 6). By this means, the magnetic field lines generated by the CPW efficiently penetrate the area delimited by the semicircular halves of the S-SRR, enhancing the line-to-resonator coupling.

The S-SRR and the circularly shaped CPW of Fig. 6 have been designed, so that for the state corresponding to maximum coupling, at least 15 dB of attenuation and less than 125 MHz bandwidth in the resulting notch are obtained. Such resonant particle has been designed to resonate at 2.5 GHz, and it is the reference S-SRR for the four-state nine-resonator (nine instead of ten because the deeper the notch, the wider the bandwidth) barcode with S-SRRs and CPW etched in the same substrate. In these barcodes, to be presented later, resonance frequencies are separated by 125 MHz within the S frequency band (the spectral bandwidth covers the range 2–3 GHz).

Fig. 7 shows the lossy simulated response of the structure of Fig. 6 for the orientations of 25°, 50°, and 90°, corresponding to the three considered states with significant coupling level (these values provide roughly equidistant notch depths). The substrate is *Rogers RO4003C* with thickness $h = 508$ μm, dielectric constant $\varepsilon_r = 3.55$, and $\tan\delta = 0.0021$ (narrower than the one considered in the tristate multiresonator barcode, in order to enhance the line-to-resonator coupling). These responses are appropriate to discriminate the two intermediate states, corresponding to the angles of 25° and 50° (note that the notch frequency is roughly the same in all the cases). We have extracted the parameters of the circuit of Fig. 5(b) from the electromagnetic responses corresponding to the 25°, 50°, and 90° S-SRR orientations (see Table III). The circuit responses, also included in Fig. 7, are in good agreement with the electromagnetic simulations. Except M, the circuit elements of the circuit of Fig. 5(a), given in Table IV, are roughly invariant under rotation. By contrast, M exhibits roughly a linear dependence with θ, which is reasonable on account of the shape of the resonator and the line [28] (the variation is roughly linear if the resonator is circular, and this linearity is enforced if the CPW is circularly shaped as well).

Let us now focus on the relation between the geometry of the S-SRRs and the circuit model parameters. Obtaining analytical expressions is cumbersome on account of the complex geometry of the resonant particles and the presence of the CPW. Therefore, a parametric analysis has been carried out.

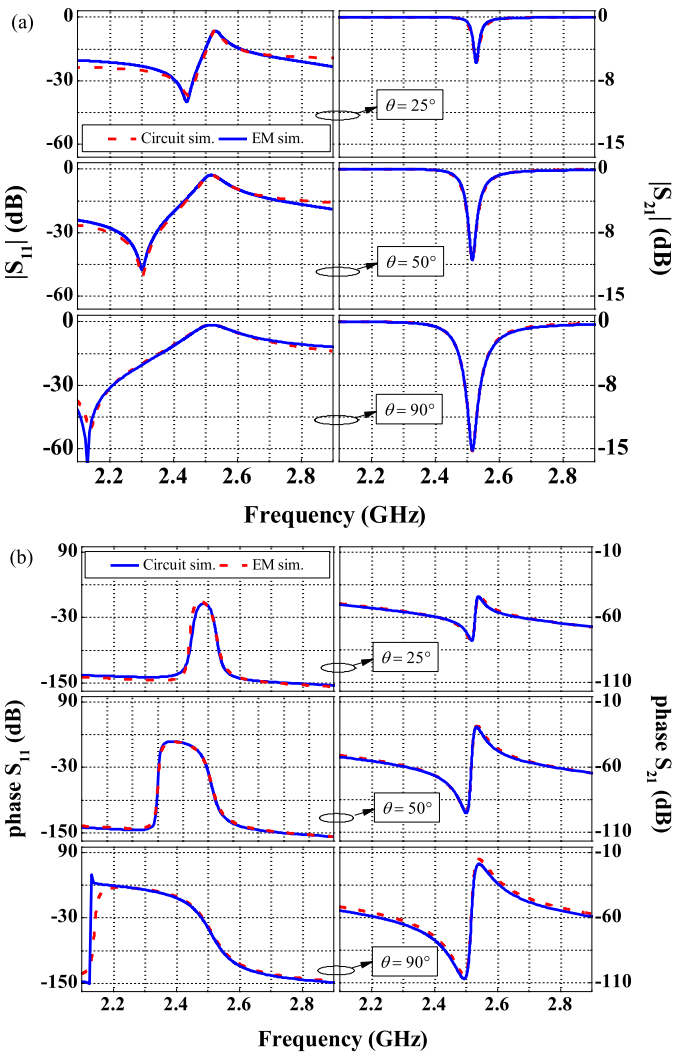

Fig. 7. Frequency response (including electromagnetic simulation and circuit simulation) of the S-SRR-loaded CPW of Fig. 6 for different angular orientations. (a) Magnitude and (b) phase of the reflection (S_{11}) and transmission (S_{21}) coefficients. The electromagnetic simulations have been carried out with *Keysight Momentum*. S-SRR dimensions (in reference to Fig. 6) are $r_1 = 0.8$ mm, $r_0 = 3.5$ mm, $s = 0.2$ mm, and $c_0 = 0.4$ mm. Line dimensions are $W = 1.85$ mm, $G_0 = 0.15$ mm, and $G_1 = 0.31$ mm corresponding to a 50 Ω transmission line.

It has been done by considering the structure of Fig. 2, with dimensions indicated in Fig. 4, and by varying either c_0 or r_1 with regard to the values of Fig. 4. The orientation providing maximum attenuation (i.e., 90°) has been considered. The parameters of both circuit models [Fig. 5(a) and (b)] for different values of c_0 are given in Tables V and VI, whereas the effects of varying r_1 are summarized in Tables VII and VIII.

Essentially, the width of the loop, c_0, affects the inductance, L_s, and resistance, R_s, of the particle, whereas the radius of the central patches, r_1, has influence on the value of the capacitance, C_s, and resistance, R_s, as well. It is interesting to note that the notch depth (also included in the tables) is scarcely dependent on r_1, but it varies significantly with c_0. Therefore, according to this paper, it follows that the width of the loops is a fundamental design parameter. For design purposes, a tradeoff is necessary since, due to the limited

TABLE III

EXTRACTED ELEMENT VALUES OF THE CIRCUIT OF FIG. 5(b) FOR THE FOUR-STATE S-SRR

θ (degrees)	L'_s (nH)	C'_s (pF)	R'_s (Ω)	L' (nH)	C (pF)
25	0.03	135	60.9	2.46	1.59
50	0.08	47.3	175	2.45	1.57
90	0.18	22.3	356	2.35	1.51

TABLE IV

ELEMENT VALUES OF THE CIRCUIT OF FIG. 5(a) FOR THE FOUR-STATE S-SRR

θ (degrees)	L_s (nH)	C_s (pF)	R_s (Ω)	L (nH)	M (nH)
25	11.3	0.18	2.73	2.49	0.41
50	11.3	0.18	2.71	2.54	0.69
90	11.3	0.18	2.83	2.83	1.00

Q-factor of the S-SRRs, it is not possible to achieve narrowband responses with deep notches. Necessarily, enhancing the notch depth means to widen the bandwidth. So the design process consists of varying c_0 until a reasonable notch depth and bandwidth is achieved. Then, the S-SRR resonance frequency can be adjusted by the patch capacitance (through r_1) and also by the length of the loops. The length of the loops has mainly influence on L_s and R_s. In general, small loops are convenient to reduce R_s and to achieve small particle size, but the limit is dictated by the required value of L_s (or frequency).

III. DESIGN EXAMPLES AND POTENTIAL APPLICATIONS

Both tri- and four-state multiresonator encoders are presented in this section on the basis of the reference S-SRRs and lines introduced in Section II, where the S-SRRs are etched in the back substrate side of the CPW transmission line. In addition, we present the design of a four-state S-SRR-based encoder implemented by etching the S-SRRs and the CPW transmission line in different substrates. Such encoders are of particular interest for certain applications where tag size and number of bits can be optimized (thanks to the use of multistate resonators) at the expense of sacrificing long range reading (e.g., security, authentication, and so on). Such encoders are those of interest in this paper, since it is in these encoders where the use of multistate resonators is fully justified. In far-field chipless RFID, it is not realistic to distinguish between the different states mainly due to losses in the wireless link between the reader and the tags. By contrast, in this near-field-based chipless RFID system, the CPW (which is part of the reader) must be in contact and conveniently aligned with the S-SRRs (the tag) and antennas are avoided in both the reader and the tag. This allows us to clearly discern between the four states, as will be later shown. Obviously, the alignment and proximity (contact) between the tag and the CPW transmission line for reading requires a guiding system, but this is not necessarily an issue in certain applications such as those indicated earlier.

TABLE V
EXTRACTED ELEMENT VALUES OF THE CIRCUIT OF FIG. 5(b) FOR DIFFERENT VALUES OF c_0

c_0	L'_s (pH)	C'_s (pF)	R'_s (Ω)	L' (nH)	C (pF)	S_{21} (dB)
0.2	91.0	50.9	135	2.34	1.26	-8.01
0.3	101	43.3	150	2.31	1.28	-8.73
0.4	105	39.8	161	2.33	1.32	-9.25
0.5	110	36.5	165	2.28	1.34	-9.49
0.6	114	34.1	167	2.29	1.36	-9.64
0.7	118	32.2	174	2.29	1.37	-9.98
0.8	119	31.4	176	2.28	1.39	-10.01

TABLE VI
ELEMENT VALUES OF THE CIRCUIT OF FIG. 5(a) FOR DIFFERENT VALUES OF c_0

c_0	L_s (nH)	C_s (pF)	R_s (Ω)	L (nH)	M (nH)
0.2	12.4	0.19	3.67	2.43	0.75
0.3	11.4	0.19	3.54	2.41	0.76
0.4	10.6	0.20	3.33	2.43	0.75
0.5	10.0	0.20	3.31	2.39	0.74
0.6	9.32	0.20	3.26	2.40	0.74
0.7	9.06	0.21	3.18	2.41	0.73
0.8	8.62	0.22	3.1	2.40	0.72

TABLE VII
EXTRACTED ELEMENT VALUES OF THE CIRCUIT OF FIG. 5(b) FOR DIFFERENT VALUES OF r_1

r_1	L'_s (pH)	C'_s (pF)	R'_s (Ω)	L' (nH)	C (pF)	S_{21} (dB)
0.7	104	31.3	166	2.28	1.35	-9.82
0.8	105	32.2	167	2.29	1.36	-9.85
0.9	107	32.7	168	2.29	1.35	-9.85
1.0	106	34.2	169	2.30	1.35	-9.82
1.1	111	33.9	170	2.29	1.34	-9.75
1.2	109	35.5	168	2.30	1.34	-9.65
1.3	110	36.5	165	2.28	1.34	-9.49

TABLE VIII
ELEMENT VALUES OF THE CIRCUIT OF FIG. 5(a) FOR DIFFERENT VALUES OF r_1

r_1	L_s (nH)	C_s (pF)	R_s (Ω)	L (nH)	M (nH)
0.7	10.0	0.16	3.91	2.38	0.72
0.8	10.0	0.17	3.74	2.39	0.72
0.9	10.0	0.17	3.64	2.40	0.73
1.0	10.0	0.18	3.46	2.41	0.73
1.1	10.0	0.19	3.52	2.40	0.74
1.2	10.0	0.19	3.36	2.41	0.74
1.3	10.0	0.20	3.31	2.39	0.74

A. Tristate Ten-Resonator Encoder

The implementation of the tristate ten-resonator barcode has been done by scaling up or down the circumference perimeter of the S-SRR of Fig. 2, keeping unaltered the other dimensions. Such lengths have been calculated with the objective of achieving equidistant resonance frequencies (separated 100 MHz) between 2.1 and 3 GHz. The layouts and simulated frequency responses (S_{21}) of four encoders with the indicated (arbitrary) codes are shown in Fig. 8. We have used "X" to designate the intermediate state (45°). As can be seen, the difference in attenuation level for states "X" and "1" is significant, independently of the state of the neighbor S-SRRs.

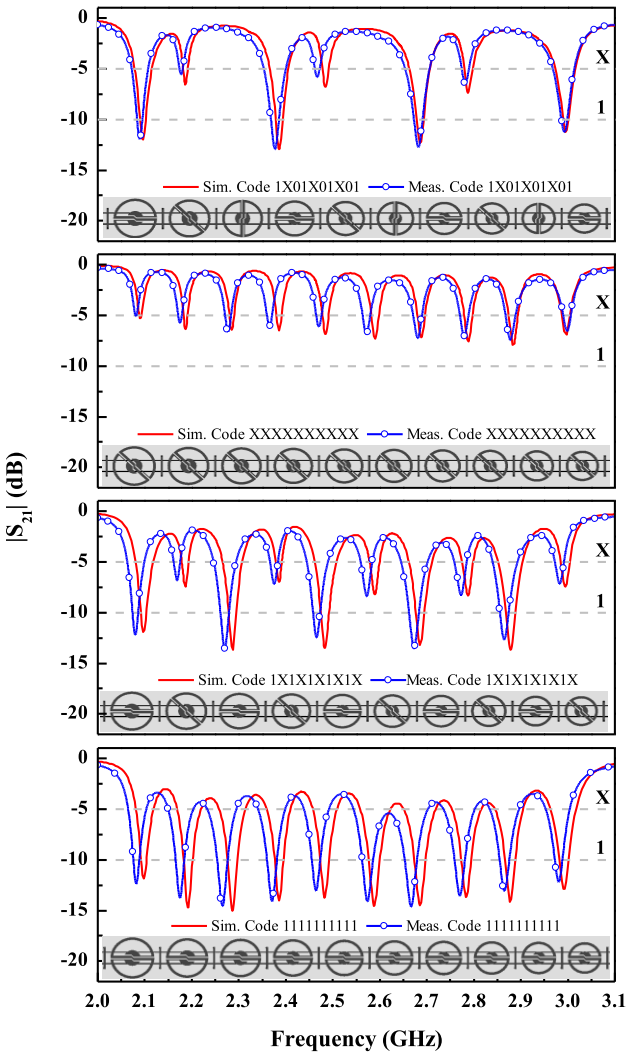

Fig. 8. Layout and frequency responses of the tristate ten-resonator spectral signature barcodes with the indicated codes. The dots in the measured responses do not correspond to data points (1.600), but are used to better discern them from the simulated responses.

The encoders of Fig. 8 have been fabricated through photomask etching. The measured responses are also shown in Fig. 8. Note that by situating the thresholds at −5 and −10 dB, the three different states can be perfectly discerned (between 0 dB and the threshold level named X, the data reads as 0, between the level corresponding to the label X and 1, the data reads as X, and for notches deeper than the level of 1, the data reads as 1). Nevertheless, the notch level is unavoidably somehow influenced by the effects of the neighbor S-SRRs. For that main reason the notch depth is not identical for a given state, but the achieved results allow us to discern between the different states. With these encoders $3^{10} = 59.049$ different codes can be generated (i.e., corresponding to more

than 15 bits, or $2^{15} = 32.768$ states). Area is small (i.e., 95 mm × 9 mm), and the information density per frequency (DPF), given by the number of bits per unit frequency is above 15 bits/GHz.

B. Four-State Nine-Resonator Encoder

For the implementation of the four-state nine-resonator encoder from the reference structure of Fig. 6 (with S-SRR and CPW etched in the same substrate), we have increased or decreased the capacitance of the reference S-SRR in a tuning process focused on obtaining equidistant frequencies in the interval 2–3 GHz. The layouts and frequency responses of four encoders are shown in Fig. 9 (the corresponding codes are indicated in Fig. 9). The intermediate states are designated in this case by "01" and "10" for the 25° and 50° orientations, respectively, whereas the states "00" and "11" correspond to unrotated and maximally rotated (90°) S-SRRs, respectively. The fabricated encoders exhibit the responses also shown in Fig. 9. With these encoders, $4^9 = 2^{18} = 262.144$ different combinations can be generated, corresponding to 18 bits. This number of combinations is substantially superior than the one of the previous tristate-based encoders, and size is smaller, i.e., (91 mm × 9 mm), since nine resonant elements, rather than ten, have been used.

The previous four-state (and tristate) S-SRR-based encoders, with the resonant elements etched in the back substrate side of the CPW transmission line, can be considered as preliminary prototypes of the S-SRR-based encoder of interest in this paper, to be discussed next.

C. Four-State Eight-Resonator Encoder With S-SRRs and CPW Etched in Different Substrates

Typically, multiresonator barcodes (with two states per resonant element) have been equipped with cross polarized transmitter (TX) and receiver (RX) antennas (usually monopole antennas), in order to wirelessly communicate with the reader [6]–[8]. These chipless tags are thus composed by the S-SRRs and the CPW transmission line (the encoder), plus the TX and RX antennas, and the communication with the reader is via far field.

A different configuration for multistate multiresonator encoders consists of implementing the CPW transmission line and the S-SRRs in a different substrate, as anticipated before. This makes sense if the CPW transmission line is considered to be part of the reader, while the spectral signature barcode is composed only by the set of S-SRRs, etched, or printed, on a different substrate (Fig. 1). The communication between the tag (set of S-SRRs) and the reader (CPW and the necessary electronics) is near-field in this case, and it is based on the inductive coupling between the CPW transmission line and the S-SRRs. Rather than contactless, the reader (CPW) and the tag (S-SRRs) must be in contact and aligned within this approach, but this is not an issue in certain applications, such as security, authentication, and so on. Particularly, an application that can be envisaged is secure paper. The idea behind such application is that the paper is encoded with an S-SRR-based spectral signature (rather than with optical barcodes, easy to copy), buried on it. The code, i.e., the set of S-SRRs, can be printed

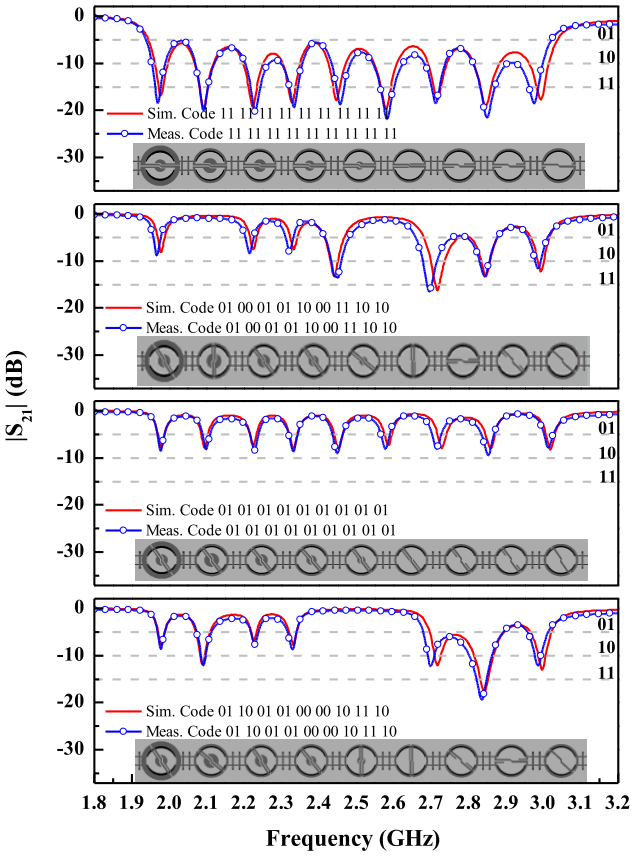

Fig. 9. Layout and frequency responses of the four-state nine-resonator spectral signature barcodes with the indicated codes. Between 0 dB and the threshold level named 01, the data reads as 00, between the level corresponding to the label 01 and 10, the data reads as 01, between 10 and 11, it reads as 10, and for notches deeper than the level of 11, the data reads as 11.

on a flexible substrate or, even, directly on the final (paper) product. In order to perform identification, a robust guiding channel for the paper is necessary to guarantee the contact and alignment between the tag (S-SRRs) and the active part of the reader (CPW). Lateral misalignment between tag and CPW should be less than 0.3 mm, as demonstrated later. Note that in this application, a wireless link between the tag and the reader does not represent an added value. Moreover, losses in the wireless link, may limit the readability of the tag, especially if four-state S-SRR-based tags are considered, as mentioned before. Nevertheless, tag size and information capacity per GHz are the key aspects, and for that reason the four-state S-SRR-based encoders are the preferred solution in this application (secure paper).

As a proof-of-concept, we have implemented spectral signature barcodes by etching eight S-SRRs on the commercial *Rogers RO4003C* substrate, with thickness $h = 203$ μm, dielectric constant $\varepsilon_r = 3.55$, and loss tangent $\tan\delta = 0.0021$, whereas the CPW transmission line has been implemented on the *Rogers RO4003C* substrate, with thickness $h = 508$ μm and same dielectric constant and loss tangent. In this proof-of-concept demonstrator, we have chosen a narrow substrate for S-SRR etching, similar to the typical flexible substrate required in a real application. The 3-D views of the CPW and S-SRR (isolated) are depicted in Fig. 10. The tag is

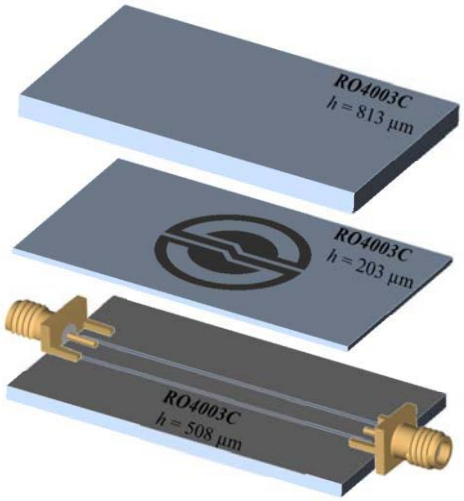

Fig. 10. Topology of the reference S-SRR of the four-state multiresonator barcode separated from the CPW transmission line, and relevant dimensions (values before scaling): $r_1 = 1.5$ mm, $r_0 = 2.4$ mm, $s = 0.2$ mm, and $c_0 = 0.4$ mm. Line dimensions are $W = 1$ mm and $G = 0.2$ mm corresponding to a 50 Ω transmission line.

put on top of the CPW transmission line, with the S-SRRs etched on the substrate side opposite to the one in contact with the CPW of the reader. In addition, we have considered a top dielectric slab (a commercial 0.81 mm thick *RO4003C* substrate with identical dielectric constant and loss tangent) in order to make pressure and thus minimize the effects of the air gap [33] as much as possible. The presence of this substrate has been taken into account in the design of the S-SRRs and tags. Note that in this case, the CPW transmission line is uniform (contrary to the previous four-state multiresonator encoder). The reason is that since the S-SRRs are separated from the CPW transmission line by a very narrow substrate, the coupling level between line and resonant elements is high, and it is not necessary in this case to circularly shape the transverse dimensions of the line in the regions where the S-SRRs are present. It is worth mentioning that in our in-house measurement system (see Fig. 11), rather than a guiding channel for the tag, it has been positioned on top of the CPW and aligned to it by means of references (holes) drilled on the CPW and tag. Then, pressure to minimize the air gap has been done manually. The reader is the CPW connected to the two-port network analyzer.

The dimensions of the reference resonator (with fundamental resonance frequency at 2.5 GHz) are indicated in the caption of Fig. 10, where the particle is depicted. The layouts and simulated frequency responses of four encoders are depicted in Fig. 12 (the codes are indicated in the figure). The intermediate states, designated by "01" and "10", are obtained by rotating the S-SRR 55° and 70°, respectively (providing equidistant notch depths) for rotation corresponding to the largest S-SRR can be appreciated in Fig. 13, where the notch depth as a function of the rotation angle is depicted (note that for the smallest S-SRR, the curve, also included, is roughly the same).

Due to the effects of the air gap (obviously not present in the simulation, but not completely suppressed in measurement), the measured responses have been found to shift 20% upwards

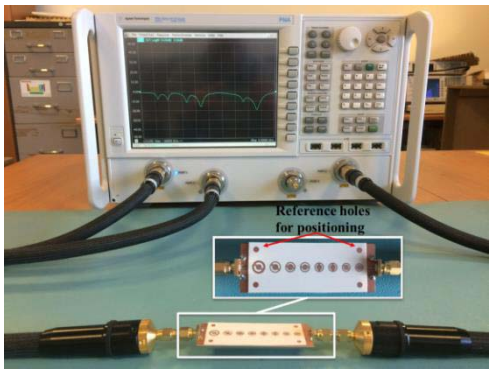

Fig. 11. Photograph of the experimental setup.

(overall shift in the response). For this reason, we have scaled 20% up the dimensions of the S-SRRs and we have repeated the fabrication of the encoders. These new fabricated encoders exhibit the measured responses also shown in Fig. 12, and their size is 75 mm × 9 mm.

The agreement between the measured responses of the different codes and those inferred from electromagnetic simulation is reasonably good, although the notch depths and resonance frequencies slightly change in some cases. The reason is the lack of an automatic and robust system in our in-house experimental setup to accurately align and pressure the tags over the CPW and thus minimize the effects of misalignment and air gap. Nevertheless, these results demonstrate that the implementation and reading of four-state multiresonator spectral signature barcodes, implemented in a different substrate than the host CPW line, is possible. Moreover, these results point out the possibility of implementing spectral signature-based chipless RFID systems with small tag size and significant number of bits. This has been achieved by avoiding the use of antennas and by considering multiple states per resonant element, thanks to the near-field reading (through inductive coupling) of the tags.

An important aspect affecting the bit error rate is the effect of lateral and vertical displacement (air gap) between the tag (S-SRRs) and the CPW transmission line. Thus, we have studied through electromagnetic simulation such effects on the variation of the notch depth and resonance frequencies. We have defined tolerance windows for both the notch depth and frequency. Specifically, since the distance between thresholds (notch depth) is 5 dB, the tolerance windows for the notch depth are considered to cover that range (i.e., 2.5 dB up and down). For the notch frequency, the windows are 142 MHz wide (71 MHz up and down) since this is the distance between adjacent resonance frequencies. In order to estimate the achievable tolerances in lateral and vertical displacement, we have considered the extreme cases of the largest (i.e., the lowest notch frequency) and smallest (the highest frequency) S-SRRs.

The variations of the notch depth and frequency with lateral displacement for states "01", "10" and "11" are depicted in Fig. 14 (note that state "00" is not relevant since the S-SRR is not excited regardless of the lateral or vertical displacement). With these results, we conclude that the maximum tolerance for lateral displacement is dictated by the frequency variation

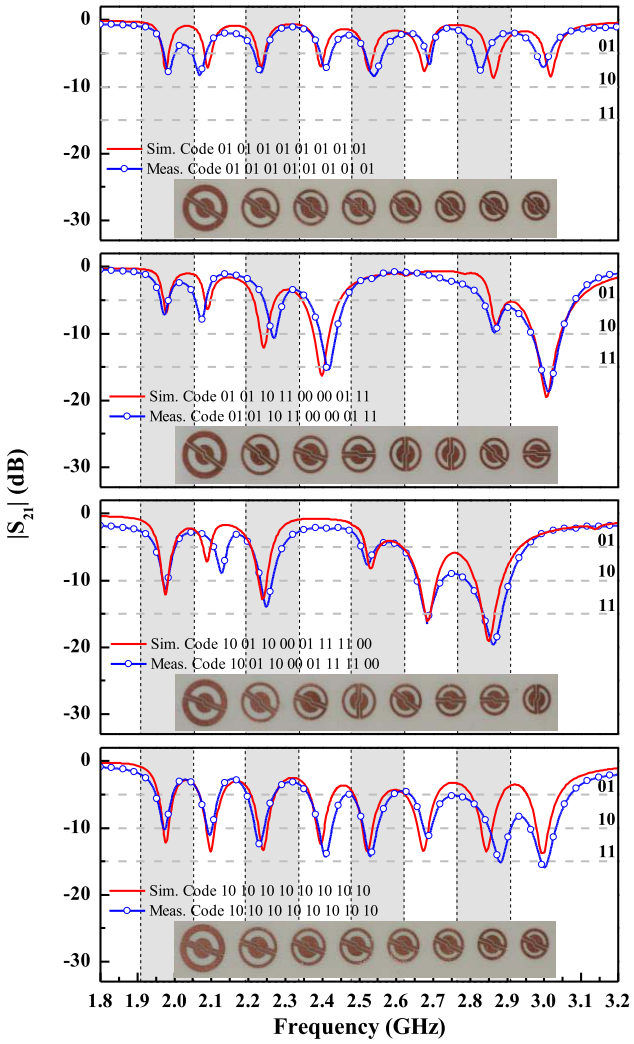

Fig. 12. Photograph and frequency responses of the four-state eight-resonator spectral signature barcodes with the indicated codes. In this case, the dimensions of the different S-SRRs have been obtained from the dimensions of the reference one by modifying the perimeter of the circular loop, as in the case of the tristate ten-resonator barcodes of Section III-A. Note also that these photographs correspond actually to the barcodes after scaling, as mentioned in the text.

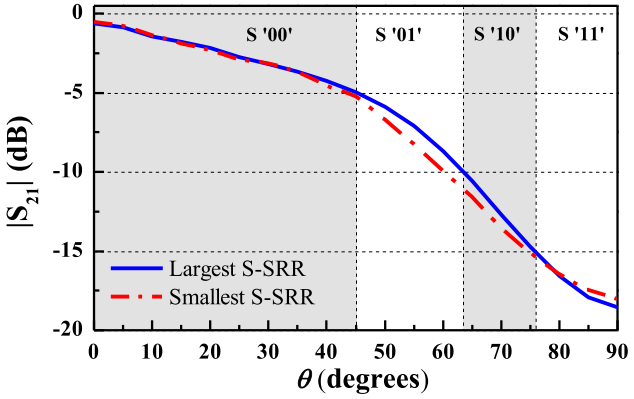

Fig. 13. Notch depth variation with the rotation angle for the extreme S-SRRs of the considered four-state eight-resonators tags.

of state "11" of the smallest S-SRR, and it is 0.3 mm. For which concern the air gap (vertical displacement), its effects on notch variation in the considered range are negligible, but not on frequency variation (see Fig. 15). In this case, the tolerance

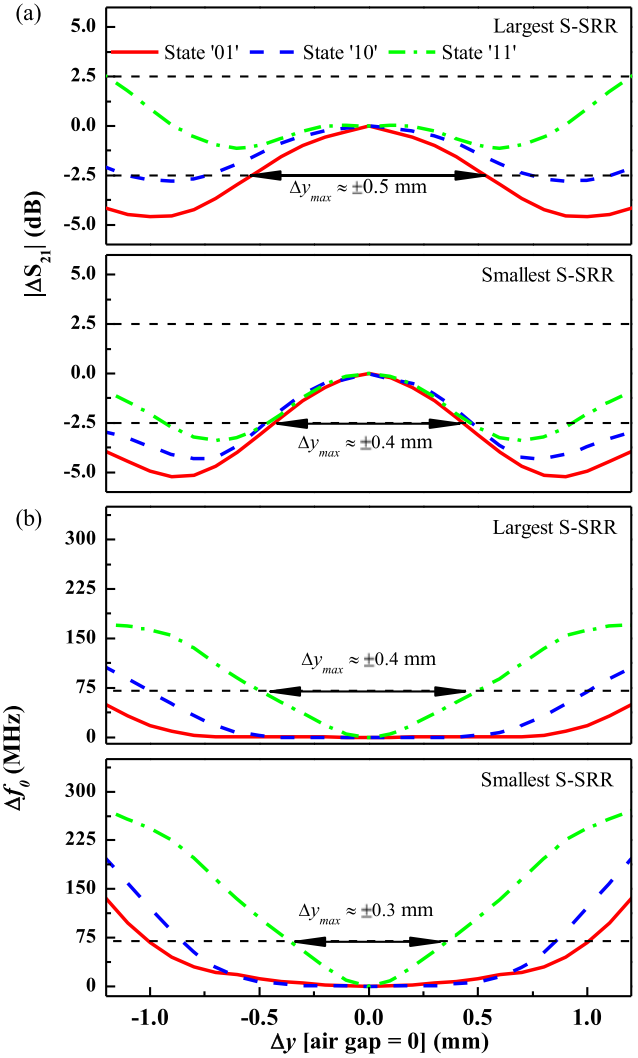

Fig. 14. (a) Effects of lateral displacement on the notch depth and (b) frequency for the extreme S-SRRs of Fig. 11 (before scaling).

is 4.5 μm, and this limit is dictated by the smallest S-SRR as well.

According to these results, the effects of vertical displacement are more critical. However, the idea in a real scenario is to make the measurement by contacting the CPW and tag under certain controllable pressure (i.e., by means of a mechanical system that displaces horizontally the tag until the position of the CPW, and then vertically to ensure contact and minimize the air gap, not completely unavoidable). Obviously, this is not the case in our in-house set-up where, rather than a real guiding system, the tag is positioned and aligned on top of the CPW by means of references in both elements. With a reliable and robust guiding system (from a mechanical viewpoint) such value seems to be reasonable. For which concern lateral displacement (misalignment), in a hypothetical commercial system based on this approach, it seems reasonable to constrict the misalignment in less than 0.3 mm [less favorable case according to Fig. 14(b)]. Alternatively, it is possible to further separate the resonance frequencies, but at the expense of a smaller number of bits per bandwidth. To further support the previous analysis, we report in Fig. 16 the responses of the tag with all resonators rotated 90°, for different values of

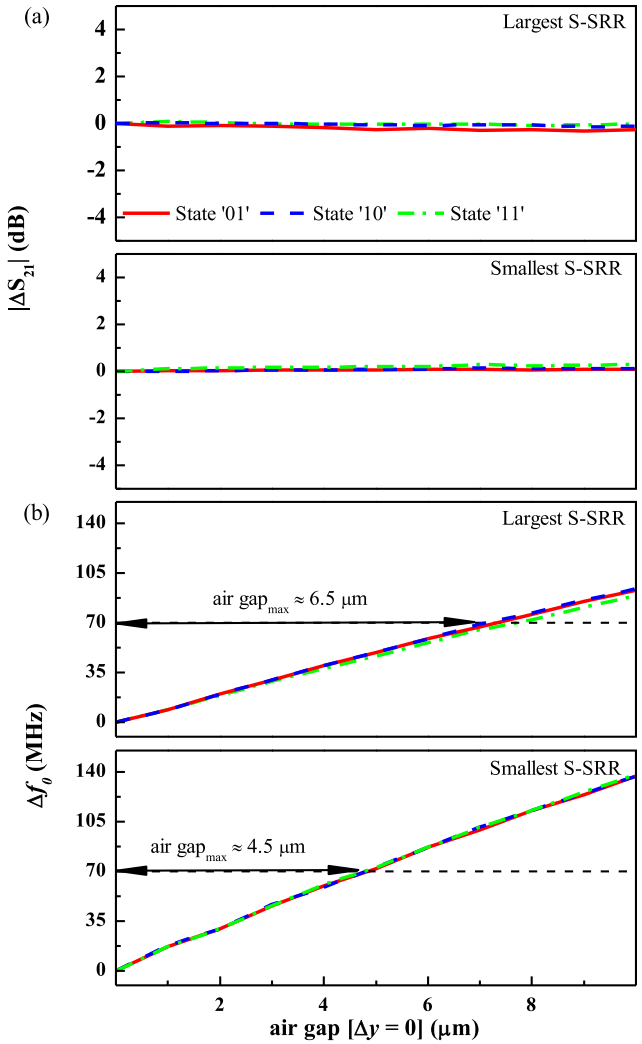

Fig. 15. (a) Effects of vertical displacement (air gap) on the notch depth and (b) frequency for the extreme S-SRRs of Fig. 11 (before scaling).

the lateral displacement and gap distance. Erroneous readings are visible and correspond to misalignments or air gaps beyond the tolerance values.

For the implementation of these tags in a polymer or paper, redesign S-SRRs taking into account the parameters of the substrate under consideration (thickness, dielectric constant and loss tangent) is necessary. The conductance of the conductive inks and the achievable thickness of the metallic films are additional important parameters that must be considered. For which concerns cost in a real scenario, industrial processes such as screen printing are preferred over inkjet (in spite that throughput has been recently improved), especially if many tags must be fabricated. This requires personalized masks for each code, which increases costs, but such costs may be affordable in applications where many replicas (typically hundreds or thousands) of the same code must be used (e.g., in corporate documents, identifying a person or a company).

IV. Comparison to Other Frequency-Domain Chipless Tags

We have compared our near-field-based chipless tags with other frequency domain chipless tags in terms of the used frequency range, number of bits, area, information DPF, and

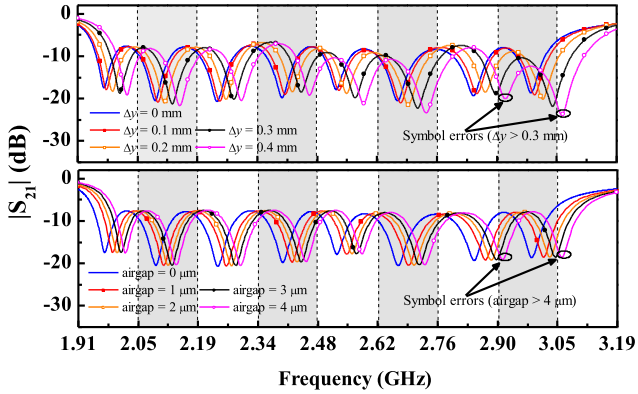

Fig. 16. Simulated responses of the four-state eight-resonators tag with all S-SRRs rotated 90° (all bits set to logic level "1") for different values of lateral displacement and air-gap separation.

TABLE IX
Comparison of Frequency-Domain Chipless Tags

Ref.	Frequency range (GHz)	Number of bits	Tag area (cm^2)	DPF (bit/GHz)	DPS (bit/ cm^2)
[6]	3.1 - 7	35	57.2	8.97	0.61
[9]	0.7 - 0.9	5	50.1	25.0	0.10
[10]	5 - 6	5	6.48	11.1	0.77
[12]	2 - 4	20	17.5	10.0	1.14
[13]	2 - 5.5	9	3.00	2.57	3.00
[14]	3.1 - 10.6	19	9.00	2.53	2.11
[34]	2 - 5	9	7.20	3.00	1.25
[35]	3 - 10	28.5	8.00	4.07	3.56
[36]	3.2 - 9.6	64	10.9	10.0	5.88
[37]	3.1 - 10.6	24	5.76	3.20	4.17
[38]	1.9 - 3.1	20	17.5	16.7	1.14
[39]	2.5 - 7.5	22.9	8.00	4.58	2.86
Present work	**2 - 3**	**16**	**6.75**	**16.0**	**2.37**

information density per surface (DPS). The results are shown in Table IX. The relevant parameters (or figures of merit) of these tags are those of the last two columns. In this regard, it is remarkable the work [9], where a huge DPF is obtained, but at the expense of a very large area (or low DPS). In [38], the DPF is comparable to the one reported in this paper, but the DPS is roughly half the one achieved by us. It is also worth mentioning the work carried out in [36], where the authors achieve simultaneously good DPF and DPS. In our case, the DPF is substantially improved as compared with [36], but the DPS is not as good as in [36]. In summary, as compared with other frequency domain chipless tags, shown in Table IX, our proposal represents a very good balance between the achievable number of bits per bandwidth and per area unit.

V. Conclusion

In conclusion, multistate (up to four states) multiresonator spectral signature barcodes implemented by loading a host CPW transmission line with S-SRRs have been designed, fabricated, and characterized for the first time. The different states have been achieved by rotating the S-SRRs. This rotation (orientation) modulates the coupling level between the line

and the resonators, thus varying the attenuation level in the transmission coefficient at the fundamental frequency of the considered resonator. After designing and implementing a three-state and a four-state multiresonator encoders (using ten and nine S-SRRs, respectively) with the S-SRRs etched in the back substrate side of the CPW, we have implemented a four-state eight-resonator encoder where the S-SRRs have been etched in a different substrate. This has opened a new paradigm in spectral signature-based chipless RFID, where the tag is simply the set of S-SRRs etched (or printed) in the considered substrate (it can be a flexible substrate or even paper, in a real scenario), the CPW transmission line is an essential part (active part) of the reader, and the communication between the tag and the reader is by inductive coupling. This requires good alignment and contact between the tag and the reader, but this is possible in certain applications, especially those related to security and authentication, as has been discussed in the paper. By this means, antennas are avoided, with direct impact on tag size. In addition, it has been experimentally demonstrated that by means of this approach, the four states can be discriminated. The proof-of-concept has been implemented by considering a narrow commercial microwave substrate with moderate dielectric constant (3.55) for the S-SRRs, i.e., conditions similar to those of flexible substrates. Work is in progress toward the implementation of multistate multiresonator encoders in such substrates by means of printed techniques.

REFERENCES

[1] K. Finkenzeller, *RFID Handbook: Radio-Frequency Identification Fundamentals and Applications*, 2nd ed. New York, NY, USA: Wiley, 2004.

[2] V. D. Hunt, A. Puglia, and M. Puglia, *RFID: A Guide to Radio Frequency Identification*. New York, NY, USA: Wiley, 2007.

[3] S. Preradovic and N. C. Karmakar, "Chipless RFID: Bar code of the future," *IEEE Microw. Mag.*, vol. 11, no. 7, pp. 87–97, Dec. 2010.

[4] E. Perret, *Radio Frequency Identification and Sensors: From RFID to Chipless RFID*. New York, NY, USA: Wiley, 2014.

[5] R. Rezaiesarlak and M. Manteghi, *Chipless RFID: Design Procedure and Detection Techniques*. New York, NY, USA: Springer Int., 2015.

[6] I. Preradovic, I. Balbin, N. C. Karmakar, and G. F. Swiegers, "Multiresonator-based chipless RFID system for low-cost item tracking," *IEEE Trans. Microw. Theory Techn.*, vol. 57, no. 5, pp. 1411–1419, May 2009.

[7] S. Preradovic and N. C. Karmakar, "Design of chipless RFID tag for operation on flexible laminates," *IEEE Antennas Wireless Propag. Lett.*, vol. 9, pp. 207–210, 2010.

[8] S. Preradovic and N. C. Karmakar, *Multiresonator-Based Chipless RFID: Barcode of the Future*. New York, NY, USA: Springer-Verlag, 2012.

[9] J. McVay, A. Hoorfar, and N. Engheta, "Space-filling curve RFID tags," in *Proc. IEEE Radio Wireless Symp.*, Oct. 2006, pp. 199–202.

[10] I. Jalaly and I. D. Robertson, "Capacitively-tuned split microstrip resonators for RFID barcodes," in *Proc. Eur. Microw. Conf.*, vol. 2. Oct. 2005, pp. 4–7.

[11] H.-S. Jang, W.-G. Lim, K.-S. Oh, S.-M. Moon, and J.-W. Yu, "Design of low-cost chipless system using printable chipless tag with electromagnetic code," *IEEE Microw. Wireless Compon. Lett.*, vol. 20, no. 11, pp. 640–642, Nov. 2010.

[12] A. Vena, E. Perret, and S. Tedjini, "A fully printable chipless RFID tag with detuning correction technique," *IEEE Microw. Wireless Compon. Lett.*, vol. 22, no. 4, pp. 209–211, Apr. 2012.

[13] A. Vena, E. Perret, and S. Tedjini, "Design of compact and auto-compensated single-layer chipless RFID tag," *IEEE Trans. Microw. Theory Techn.*, vol. 60, no. 9, pp. 2913–2924, Sep. 2012.

[14] A. Vena, E. Perret, and S. Tedjini, "High-capacity chipless RFID tag insensitive to the polarization," *IEEE Trans. Antennas Propag.*, vol. 60, no. 10, pp. 4509–4515, Oct. 2012.

[15] C. S. Hartmann, "A global SAW ID tag with large data capacity," in *Proc. IEEE Ultrason. Symp.*, vol. 1. Oct. 2002, pp. 65–69.

[16] A. Chamarti and K. Varahramyan, "Transmission delay line based ID generation circuit for RFID applications," *IEEE Microw. Wireless Compon. Lett.*, vol. 16, no. 11, pp. 588–590, Nov. 2006.

[17] M. Schüßler, C. Damm, and R. Jakoby, "Periodically LC loaded lines for RFID backscatter applications," in *Proc. Metamater. Conf.*, Oct. 2007, pp. 103–106.

[18] M. Schüßler, C. Damm, M. Maasch, and R. Jakoby, "Performance evaluation of left-handed delay lines for RFID backscatter applications," in *IEEE MTT-S Int. Microw. Symp. Dig.*, Jun. 2008, pp. 177–180.

[19] F. J. Herraiz-Martinez, F. Paredes, G. Z. Gonzalez, F. Martin, and J. Bonache, "Printed magnetoinductive-wave (MIW) delay lines for chipless RFID applications," *IEEE Trans. Antennas Propag.*, vol. 60, no. 11, pp. 5075–5082, Nov. 2012.

[20] C. Herrojo, J. Naqui, F. Paredes, and F. Martín, "Spectral signature barcodes implemented by multi-state multi-resonator circuits for chipless RFID tags," in *IEEE MTT-S Int. Microw. Symp. Dig.*, May 2016, pp. 1–4.

[21] H. Chen *et al.*, "Left-handed materials composed of only S-shaped resonators," *Phys. Rev. E, Stat. Phys. Plasmas Fluids Relat. Interdiscip. Top.*, vol. 70, no. 5, pp. 057605-1–057605-4, Nov. 2004.

[22] H. Chen *et al.*, "Negative refraction of a combined double S-shaped metamaterial," *Appl. Phys. Lett.*, vol. 86, no. 15, p. 151909, 2005.

[23] H. Chen *et al.*, "Magnetic properties of S-shaped split-ring resonators," *Prog. Electromagn. Res.*, vol. 51, pp. 231–247, 2005, doi: 10.2528/PIER04051201.

[24] J. Naqui, J. Coromina, A. Karami-Horestani, C. Fumeaux, and F. Martín, "Angular displacement and velocity sensors based on coplanar waveguides (CPWs) loaded with S-shaped split ring resonators (S-SRR)," *Sensors*, vol. 15, no. 5, pp. 9628–9650, 2015.

[25] F. Martín, *Artificial Transmission Lines for RF and Microwave Applications*. Hoboken, NJ, USA: Wiley, 2015.

[26] J. Naqui, *Symmetry Properties in Transmission Lines Loaded With Electrically Small Resonators: Circuit Modeling and Applications*. New York, NY, USA: Springer Int., 2016.

[27] J. Naqui, M. Durán-Sindreu, and F. Martín, "Novel sensors based on the symmetry properties of split ring resonators (SRRs)," *Sensors*, vol. 11, no. 8, pp. 7545–7553, 2011.

[28] J. Naqui and F. Martin, "Transmission lines loaded with bisymmetric resonators and their application to angular displacement and velocity sensors," *IEEE Trans. Microw. Theory Techn.*, vol. 61, no. 12, pp. 4700–4713, Dec. 2013.

[29] A. K. Horestani, D. Abbott, and C. Fumeaux, "Rotation sensor based on horn-shaped split ring resonator," *IEEE Sensors J.*, vol. 13, no. 8, pp. 3014–3015, Aug. 2013.

[30] J. Naqui and F. Martín,, "Angular displacement and velocity sensors based on electric-LC (ELC) loaded microstrip lines," *IEEE Sensors J.*, vol. 14, no. 4, pp. 939–940, Apr. 2014.

[31] D. Schurig, J. J. Mock, and D. R. Smith, "Electric-field-coupled resonators for negative permittivity metamaterials," *Appl. Phys. Lett.*, vol. 88, no. 4, p. 041109, 2006.

[32] F. Aznar *et al.*, "Characterization of miniaturized metamaterial resonators coupled to planar transmission lines through parameter extraction," *J. Appl. Phys.*, vol. 104, pp. 114501-1–114501-8, Dec. 2008.

[33] C.-L. Yang, C. Lee, K. Chen, and K.-Z. Chen, "Noncontact measurement of complex permittivity and thickness by using planar resonators," *IEEE Trans. Microw. Theory Techn.*, vol. 64, no. 1, pp. 247–257, Jan. 2016.

[34] O. Rance, R. Siragusa, P. Lemaître-Auger, and E. Perret, "Toward RCS magnitude level coding for chipless RFID," *IEEE Trans. Microw. Theory Techn.*, vol. 64, no. 7, pp. 2315–2325, Jul. 2016.

[35] M. M. Khan, F. A. Tahir, M. F. Farooqui, A. Shamim, and H. M. Cheema, "3.56-bits/cm^2 compact inkjet printed and application specific chipless RFID tag," *IEEE Antennas Wireless Propag. Lett.*, vol. 15, pp. 1109–1112, 2016.

[36] M. A. Islam and N. C. Karmakar, "A novel compact printable dual-polarized chipless RFID system," *IEEE Trans. Microw. Theory Techn.*, vol. 60, no. 7, pp. 2142–2151, Jul. 2012.

[37] R. Rezaiesarlak and M. Manteghi, "Complex-natural-resonance-based design of chipless RFID tag for high-density data," *IEEE Trans. Antennas Propag.*, vol. 62, no. 2, pp. 898–904, Feb. 2014.

[38] M. Svanda, J. Machac, M. Polivka, and J. Havlicek, "A comparison of two ways to reducing the mutual coupling of chipless RFID tag scatterers," in *Proc. 21st Int. Conf. Microw., Radar Wireless Commun. (MIKON)*, May 2016, pp. 1–4.

[39] A. Vena, E. Perret, and S. Tedjini, "Chipless RFID tag using hybrid coding technique," *IEEE Trans. Microw. Theory Techn.*, vol. 59, no. 12, pp. 3356–3364, Dec. 2011.

Cristian Herrojo (GS'16) was born in Badalona, Spain, in 1983. He received the Telecommunications Technical Engineering degree (with a specialization in electronic systems) and Telecommunications Engineering degree from the Universitat Autònoma de Barcelona, Barcelona (UAB), Spain, in 2010 and 2012, respectively, where he is currently pursuing the Ph.D. degree with a focus on the design of RF/microwave resonant structures applied to RFID tags without chip.

Ferran Paredes (A'15) was born in Badalona, Spain, in 1983. He received the Telecommunications Engineering Diploma degree in electronics, Telecommunications Engineering degree, and Ph.D. degree in electronics engineering from the Universitat Autònoma de Barcelona, Bellaterra, Spain, in 2004, 2006, and 2012, respectively.

From 2006 to 2008, he was an Assistant Professor with the Universitat Autònoma de Barcelona, where he is currently a Research Assistant. His current research interests include metamaterial concepts, passive microwaves devices, antennas, and RFID.

Javier Mata-Contreras was born in Málaga, Spain, in 1976. He received the Ingeniería de Telecomunicación and Ph.D. degrees from the Universidad de Málaga (UMA), Málaga, in 2000 and 2010, respectively. His Ph.D. thesis focused on distributed amplifiers and mixers with transmission lines based on metamaterials.

In 2000, he joined the Department of Ingeniería de Comunicaciones, UMA, as an Assistant Professor. He is currently with CIMITEC, Universitat Autònoma de Barcelona, Bellaterra, Spain, as a Visiting Professor. His current research interests include active and passive microwave devices and active distributed circuits based on metamaterials.

Simone Zuffanelli (GS'14–M'15) was born in Prato, Italy, in 1983. He received the Electronics Engineering Diploma degree from the Università Degli Studi di Firenze, Firenze, Italy, in 2008, and the master's degree in microelectronics and nanoelectronics engineering from the Universitat Autònoma de Barcelona, Bellaterra, Spain, in 2011.

He was involved in electronic design in the context of European projects Persona and NOMS. He is currently a Researcher with the Universitat Autònoma de Barcelona, where he is involved in the field of metamaterial inspired antennas and RFID tags.

Ferran Martín (M'04–SM'08–F'12) was born in Barakaldo, Spain, in 1965. He received the B.S. degree in physics and Ph.D. degree from the Universitat Autònoma de Barcelona (UAB), Barcelona, Spain, in 1988 and 1992, respectively.

From 1994 to 2006, he was an Associate Professor of electronics with the Departament d'Enginyeria Electrònica, UAB, where he has been a Full Professor of electronics since 2007. He is currently the Head of the Microwave Engineering Metamaterials and Antennas Group (GEMMA Group), UAB, where he is also the Director of CIMITEC, a research center on metamaterials supported by TECNIO (Generalitat de Catalunya). He has authored or coauthored over 500 technical conference papers, letters, journal papers, and book chapters. He co-authored *Metamaterials with Negative Parameters: Theory, Design and Microwave Applications* (Wiley, 2008), and authored *Artificial Transmission Lines for RF and Microwave Applications* (Wiley, 2015), and he has generated 16 Ph.Ds. He holds several patents on metamaterials and has headed several development contracts. His current research interests include the modeling and simulation of electron devices for high-frequency applications, millimetre-wave and terahertz generation systems, application of electromagnetic bandgaps to microwave and millimeter-wave circuits, and metamaterials and their application to the miniaturization and optimization of microwave circuits and antennas.

Prof. Martín is a member of the IEEE Microwave Theory and Techniques Society, the Editorial Board of *IET Microwaves, Antennas and Propagation* and *International Journal of RF and the Microwave Computer-Aided Engineering,* and the Technical Committees of the European Microwave Conference and the International Congress on Advanced Electromagnetic Materials in Microwaves and Optics (Metamaterials). He has been a Fellow of the IET since 2016. He was a recipient of the 2006 Duran Farell Prize for Technological Research, the Parc de Recerca UAB-Santander Technology Transfer Chair, and the two ICREA ACADEMIA Awards in 2008 and 2013. He is currently a Reviewer for the IEEE TRANSACTIONS ON MICROWAVE THEORY AND TECHNIQUES, IEEE MICROWAVE AND WIRELESS COMPONENTS LETTERS, and many other journals. He has organized several international events related to metamaterials, including workshops at the IEEE MTT-S International Microwave Symposium in 2005 and 2007, the European Microwave Conference in 2009, and the Fifth International Congress on Advanced Electromagnetic Materials in Microwaves and Optics (Metamaterials 2011), where he was the Chair of the Local Organizing Committee. He was a Guest Editor of three special issues on metamaterials in three international journals.

Artículo SENSORS17

Microwave Encoders for Chipless RFID and Angular Velocity Sensors Based on S-Shaped Split Ring Resonators

C. Herrojo, J. Mata-Contreras, F. Paredes and F. Martín

Microwave Encoders for Chipless RFID and Angular Velocity Sensors Based on S-Shaped Split Ring Resonators

Cristian Herrojo, *Student Member, IEEE*, Javier Mata-Contreras, Ferran Paredes, *Member, IEEE*, and Ferran Martín, *Fellow, IEEE*

***Abstract*— In this paper, it is demonstrated that a chain of S-shaped split ring resonators (S-SRRs) etched on a dielectric substrate can modulate the amplitude of a carrier signal injected to a transmission line (a coplanar waveguide (CPW). To this end, the S-SRR chain must be transversally displaced above the CPW, in close proximity to it. By this means, the transmission coefficient of the line is modulated by the time-varying electromagnetic (inductive) coupling between the line and the S-SRRs of the chain, related to their relative motion. Based on this principle, two different applications can be envisaged: 1) angular velocity sensors and 2) near-field chipless radiofrequency identification (chipless-RFID) tags. In the former application, the S-SRR chain is circularly shaped and the S-SRRs are distributed uniformly along the perimeter of the rotor, at equidistant positions. By this means, the amplitude-modulated signal generated by rotor motion exhibits envelope peaks, whose distance is related to the angular velocity of the rotor. In the use of S-SRRs as microwave encoders for chipless RFID tags, not all the S-SRRs of the chain are present. Their presence or absence at the predefined (equidistant) positions is related to the logic state "1" or "0." Tag reading is sequential, and it is achieved through tag motion (at constant velocity) above the reader, a CPW transmission line fed by a carrier signal. The ID code is contained in the envelope function of the resulting amplitude modulated signal, which can be obtained by means of an envelope detector. With the proposed approach, a high number of pulses in angular velocity sensors can be achieved (with direct impact on angle resolution and sensitivity to changes in instantaneous rotation speed). Moreover, chipless-RFID tags with unprecedented number of bits can be obtained. The proposed angular velocity sensors can be useful in space environments, whereas the chipless-RFID systems based on the proposed tags are useful in applications where reading range can be sacrificed in favor of high data capacity (large number of bits), e.g., security and authentication.**

***Index Terms*— Angular velocity sensors, chipless RFID, coplanar waveguide, s-shaped split ring resonators (S-SRRs).**

Manuscript received April 7, 2017; revised May 29, 2017; accepted June 9, 2017. Date of publication June 15, 2017; date of current version July 10, 2017. This work was supported in part by MINECO-Spain under Project TEC2013-40600-R and Project RTC-2014-2550-7, in part by Generalitat de Catalunya under Project 2014SGR-157, ICREA, and in part by FEDER funds. The work of C. Herrojo was supported by MINECO through FPI under Grant BES-2014-068164. The associate editor coordinating the review of this paper and approving it for publication was Dr. Francis P. Hindle. *(Corresponding author: Cristian Herrojo.)*

The authors are with GEMMA/CIMITEC, Departament d'Enginyeria Electrònica, Universitat Autònoma de Barcelona, 08193 Bellaterra, Spain (e-mail: ferran.martin@uab.es).

Digital Object Identifier 10.1109/JSEN.2017.2715982

I. Introduction

TRANSMISSION lines loaded with electrically small resonators have been used in many different microwave applications [1], [2]. In particular, it has been demonstrated that split ring resonator (SRR) loaded lines [3] and complementary split ring resonator (CSRR) loaded lines [4], [5] are useful for the implementation of one dimensional (1D) metamaterials. By combining SRRs with shunt inductors and CSRRs with series capacitors, left-handed lines exhibiting antiparallel phase and group velocities within a certain frequency band have been reported [3], [5]. The controllability of the dispersion relation and characteristic impedance in these artificial lines has opened the door to the design of microwave devices with superior performance or with novel functionalities, on the basis of impedance and dispersion engineering [1], [2].

In other applications, where a transmission line is simply loaded with resonant elements (SRR, CSRR, or other electrically small resonators), the resonance phenomenon, rather than dispersion and impedance engineering, is exploited [1]. Such resonator-loaded lines exhibit stopband functionality useful in many different microwave applications, such as blocking spurious signals in microwave circuits [6], multiband dipole and monopole antennas based on the concept of trap antennas [7], [8], microwave sensors [9] and chipless-RFID tags [10].

Concerning sensors implemented by means of resonator loaded lines, various approaches have been presented. Most of such sensors are based on the variation of resonance frequency caused by the variable to be measured (measurand) [11]–[17]. Other sensors implemented by means of resonator loaded lines are based on symmetry properties, including coupling modulation sensors [9], [18]–[24] and sensors based on frequency splitting [25]–[28]. In coupling modulation sensors, a transmission line is symmetrically loaded with a symmetric resonator. The key aspect for sensing purposes is that the resonant element exhibits a symmetry plane acting as electric wall (at the fundamental resonance, the one of interest), provided the transmission line exhibits a magnetic wall at its axial symmetry plane (as occurs in most usual transmission lines, such as microstrip, CPW, etc.). If symmetry is preserved, the resonator is not excited due to perfect cancellation of electric and magnetic fields on the resonator area. However,

if symmetry is broken, e.g., by the effects of a spatial variable, or by an asymmetric dielectric load, then the resonator is excited and a notch in the transmission coefficient appears. Moreover, the magnitude (depth) of such notch is related to the level of asymmetry, and can be used as output variable in these coupling modulation sensors. In frequency splitting sensors, a transmission line is symmetrically loaded with a pair of identical (but not necessarily symmetric) resonant elements. Under these conditions, the structure exhibits a single transmission zero (notch) in the vicinity of the fundamental resonance frequency of the loading elements. Conversely, when symmetry is broken, frequency splitting appears, and the separation between the two notches gives a measure of the level of asymmetry. Both, coupling modulation and frequency splitting sensors are robust in front of cross sensitivities caused by environmental factors such as temperature and moisture drifts. The reason is that symmetry is invariant under changing ambient conditions.

There is another type of sensors where the transmission coefficient of a transmission line is modulated by the effects of a movable resonant element, or set of resonant elements, in close proximity to the line. In [22], angular velocity sensors based on electric LC (ELC) resonators were reported. In that work, the transmission line is a CPW and the ELC resonator is axial to the rotor. Since the ELC resonator is a bisymmetric resonator exhibiting orthogonal electric and magnetic walls at the fundamental resonance, by rotating the ELC resonator in close proximity to the CPW transmission line, line-to-resonator coupling is modulated and, consequently, the transmission coefficient varies between a maximum and a minimum value twice per cycle. By injecting a harmonic signal (carrier) tuned to the resonance frequency of the ELC resonators, the amplitude is modulated at the output, and the distance between adjacent maxima, or minima, in the envelope function corresponds to half the period of the rotor. Variations of the angular velocity sensor proposed in [22] can be found in [23] and [24].

In the previous angular velocity sensors, also useful as angular displacement sensors, two pulses per cycle are generated. This prevents from the measurement of instantaneous angular velocities that can vary during a cycle. To solve this problem, the edge configuration was presented in [29], where the rotor was equipped with a circular chain of SRRs etched along its external perimeter. By situating the stator, a CPW transmission line, just below the SRR chain, the transmission coefficient of the line is modulated at the rhythm of the SRRs passing on top of the CPW axis. Since the number of SRRs of the chain can be made very large (300 in [29]), it follows that the number of pulses of the resulting envelope function is also large. Therefore, the measurement of quasi-instantaneous angular velocities is possible. In a recent work [30], an angular velocity sensor exhibiting 1200 pulses per cycle, based on a double chain of SRRs and with optimized carrier frequency, was reported.

Concerning chipless-RFID tags, there are three main approaches for their implementation: (i) time domain based tags, (ii) frequency domain based tags and (iii) hybrid tags. Time domain based tags are realized by loading a transmission line with scatterers, and the interrogation signal is a pulse injected to it [31]–[40]. The ID code is inferred from the echoes of that signal. In frequency domain based tags, a transmission line is loaded with as many resonators (each tuned to a different frequency) as number of bits (retransmission based tags) [41], [42]. An alternative are the backscattered based tags [43]–[49]. The interrogation signal in both cases is a multi-frequency signal that must be swept across the spectral bandwidth occupied by the resonant elements. The ID code is obtained from the singularities present in the amplitude (notches), phase or time delay response. The number of bits in retransmission based tags has been increased by using resonators able to provide more than two states. Such states are obtained from the relative orientation between the resonator and the line [10], [50], [51], providing different notch depth. However, by this means, the number of bits achievable is still far from those of chipped RFID tags. Hybrid tags [52]–[56] are multi-domain tags where more than one domain (e.g. time, frequency, phase, polarization, etc.) are used simultaneously in order to achieve more than one bit of information per resonant element. Examples of hybrid tags include encoders based on frequency position and polarization diversity [54], and encoders where frequency domain is combined with phase deviation [53], among others.

In this paper, chains of S-SRRs are used as microwave encoders for two different applications: angular velocity measurements and near-field chipless RFID tags. The principle, identical in both applications, is explained in Section II. Section III is focused on the design of the S-SRR chain and the S-SRR-loaded line, necessary for tag reading and for the measurement of angular velocities. The validation of the two considered applications is reported in Section IV. In Section V, the use of S-SRRs as resonant elements is justified. Finally, the main conclusions are highlighted in Section VI.

II. Physical Principle

The principle of the proposed devices, first reported in [29], is the modulation of the transmission coefficient of a transmission line produced by the motion of a chain of resonant elements in close proximity to the line. The proximity is necessary since the above-cited modulation in the transmission coefficient is achieved by the time-varying electromagnetic coupling between the line and the resonant elements. As the resonator chain moves with regard to the line, such coupling varies and, consequently, the transmission coefficient, whose magnitude decreases with the coupling level, also varies.

For angular velocity measurements, the chain must be circularly-shaped and located in the external perimeter of the rotor. In this application the resonant elements must be equidistant and distributed uniformly along the rotor perimeter. If a transmission line (active part of the stator) is located in close proximity to the chain, and it is fed by a harmonic signal tuned to a certain frequency close to the resonance frequency of the resonators, rotor motion is expected to modulate the amplitude of the signal at the output port of the line (due to the modulation of the transmission coefficient). Obviously, the time distance between adjacent peaks (or valleys) in the envelope function is intimately related to the rotation speed,

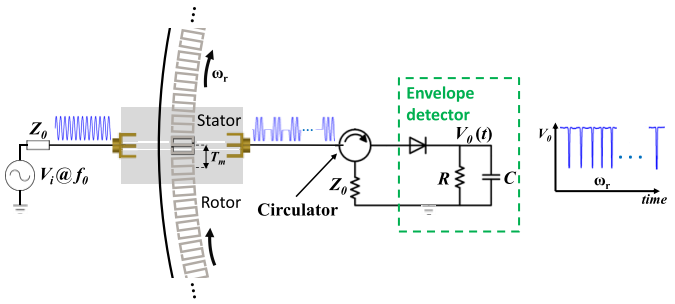

Fig. 1. Illustration of the working principle for angular velocity measurements based on the amplitude modulation of a harmonic signal produced by rotor motion.

and hence such angular velocity can be inferred from the envelope function. Such function can be obtained by means of an isolator and an envelope detector (composed of a Schottky diode and a low pass filter). The isolator can be implemented by means of a circulator and it is necessary to protect the transmission line against mismatching reflections from the diode (a highly nonlinear device). The working principle for this application is illustrated in Fig. 1. In [29] and [30], angular velocity sensors based on this principle and implemented by means of split ring resonators (SRRs) were considered. In this paper, we use S-shaped SRRs (S-SRRs), which are electrically small and are useful not only for angular velocity measurement, but also for the implementation of chipless RFID tags with high data density (advantages and disadvantages of S-SRRs as compared to SRRs are pointed out in the discussion).

For chipless RFID systems, the tags are a set of aligned resonant elements printed on a dielectric substrate (typically a flexible substrate, including organic substrates, such as paper, plastics, or liquid crystal polymers). However, the resonators are not necessarily uniformly distributed. For this application, equidistant positions for the resonant elements of the tag, each one representing a bit of information, are predefined. The logic state '1' is associated to the presence of resonant element, whereas the absence of resonator at the predefined positions corresponds to the logic '0' state. Tag reading proceeds similarly to the measurement of angular velocities (see Fig. 2). The tag must be displaced on top of a transmission line fed by a harmonic signal (tuned to a frequency close to the resonance frequency of the tag resonators). By this means, the amplitude of the feeding signal is modulated, and the ID code of the tag is contained in the envelope function of the amplitude modulated signal present at the output port of the transmission line. The necessary stages to obtain such envelope function are identical to those needed in angular velocity measurements (specified in the previous paragraph).

III. Design of the S-SRR Chain and S-SRR-Loaded CPW Transmission Line

In this paper, the resonant elements of the chain (for both the rotor and the chipless tags) are S-shaped split ring resonators (S-SRRs) [57]–[59]. The transmission line, acting as stator (for angular velocity measurements) or as active part of the reader (for chipless RFID systems), is a coplanar

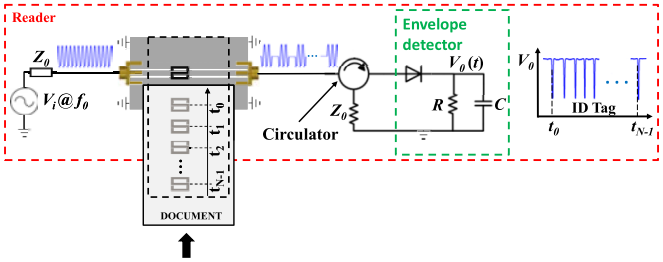

Fig. 2. Illustration of the working principle for tag reading in a chipless RFID system based on near-field coupling and sequential bit reading.

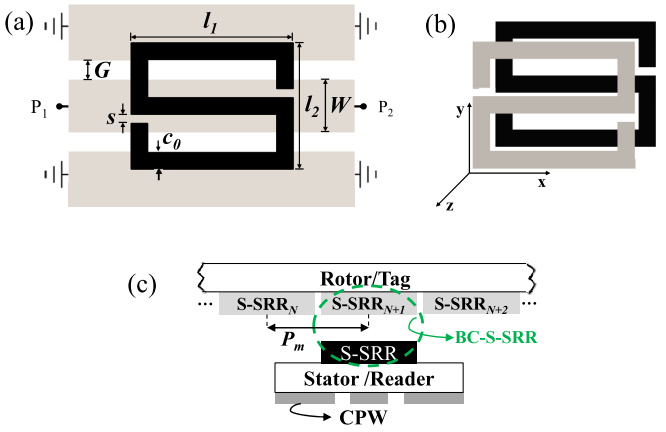

Fig. 3. Square S-shaped SRR coupled to a CPW transmission line (a) 3D view of the broadside coupled S-SRR (BC-S-SRR) (b), and cross sectional view of the stator/reader and rotor/tag (c).

waveguide (CPW) transmission line. S-SRRs are electrically small particles that can be excited by the counter magnetic field lines generated in the slots of the CPW transmission line when such particles are aligned and oriented as depicted in Fig. 3(a). For chipless RFID tags, the small electrical size of S-SRRs provides a small size for the tag. For angular velocity measurements, a large number of pulses (a figure of merit) in a certain rotor perimeter can be achieved if the particles occupy a small size. For these two reasons, S-SRRs are the resonators considered in this paper. Note that in [29] and [30] rectangular shaped SRRs were used for angular velocity measurements (the stator was a CPW transmission line, as well). With the considered shape factor of the resonant elements, the distance between adjacent resonant elements was very small, and a large number of pulses was achieved.

For both applications (angular velocity sensors and chipless RFID tags), a small distance between adjacent predefined resonator positions (either with or without S-SRRs) is very convenient. Such small separation favors compact size in chipless tags and large number of resonators (and hence pulses) in rotors. However, by tiny spacing adjacent resonators, inter-resonator coupling and simultaneous coupling between the line and several S-SRRs of the chain are favored. These effects should be avoided in order to prevent the appearance of multiple transmission zeros located at positions difficult to predict a priori. The solution to these limiting aspects related to small inter-resonator separation is to etch an identical S-SRR in the back substrate side of the CPW transmission

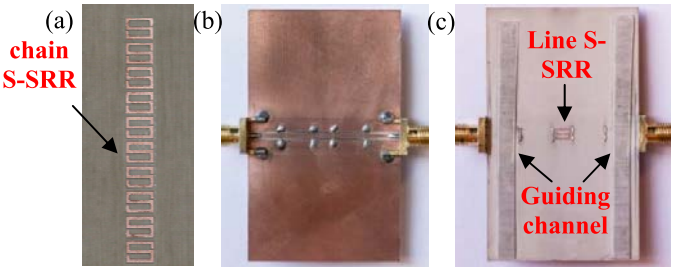

Fig. 4. Photograph of the fabricated 10-S-SRR chain (a) and top (b) and bottom (c) views of the S-SRR-loaded CPW transmission line. Dimensions are, in ref. to Fig. 2(a) and Fig. 2(b), (in mm) $W = 1.2$ and $G = 0.48$, $l_1 = 3.8$, $l_2 = 2.96$, $c_0 = 0.4$, $s = 0.2$, and $P_m = 3.5$. CPW transmission line and tag are separated by a 0.25 mm air gap.

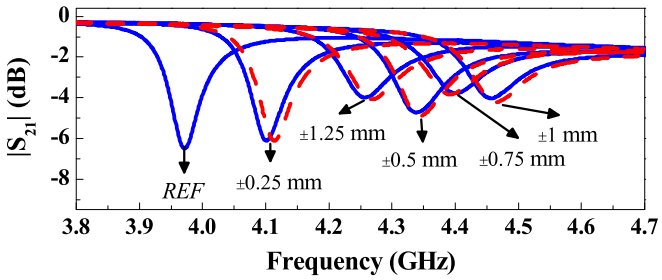

Fig. 5. Measured frequency response of the S-SRR-chain/CPW for different relative positions of the S-SRR chain in the vicinity of the reference position.

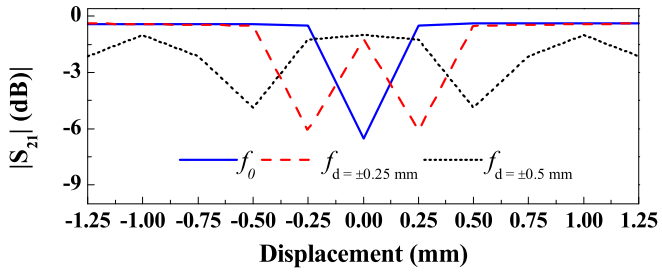

Fig. 6. Measured attenuation as a function of the relative displacement between the line and the chain at the indicated frequencies.

line, but oppositely oriented [see Fig. 3(b)]. When the relative position between the S-SRR of the line and the S-SRR chain corresponds to a perfectly aligned (vertically) pair of S-SRRs (the one of the line with one of the S-SRRs of the chain), both vertically aligned S-SRRs can be seen as a single resonant element (broad-side coupled S-SRR or BC-S-SRR). Since the fundamental resonance frequency of the BC-S-SRR, f_0, is smaller than the one of the individual (uncoupled) resonators, it follows that by setting the frequency of the feeding signal (carrier frequency, f_c) of the CPW transmission line (necessary for tag reading or for angular velocity measurements, as mentioned before) to $f_c = f_0$, or close to it, then the above cited cross couplings are avoided. Such strategy was pointed out in [29] in reference to angular velocity measurements based on pairs of SRRs. The cross sectional view of the S-SRR chain and the S-SRR-loaded CPW, separated by the air gap, can be seen in Fig. 3(c).

The considered substrate for the implementation of the S-SRR chains is the *Rogers RO4003C* with thickness $h = 203\ \mu$m and dielectric constant $\varepsilon_r = 3.55$. Since this substrate is very narrow, and hence flexible, it has been attached to a rigid substrate *FR4* (with thickness $h = 1.6$ mm and dielectric constant $\varepsilon_r = 4.7$). By these means, mechanical stability, necessary for tag reading and angular velocity measurements, is ensured. The CPW transmission line and the S-SRR of the reader/stator have been etched on opposite sides of a *Rogers RO3010* substrate with thickness $h = 635\ \mu$m and dielectric constant $\varepsilon_r = 10.2$. The size of the S-SRRs has been optimized in order to obtain a resonance frequency for the broadside coupled counterpart (BC-S-SRR) of $f_0 = 4$ GHz. For characterization purposes, we have fabricated a linear chain of 10 S-SRRs [see Fig. 4(a)]. The top and bottom views of the S-SRR-loaded CPW transmission line can be seen in Figs. 4(b) and (c), respectively. Note that a guiding channel has been added to the bottom side of the CPW in order to guide, with the necessary alignment, the S-SRR chain over the S-SRR of the line. We have measured the response of the structure for different positions of the S-SRR chain in the vicinity of the reference position (corresponding to a perfect alignment between the S-SRR of the line and one of the S-SRRs of the chain). The results are depicted in Fig. 5. When the tag is not situated in the reference position, the attenuation at f_0 severely decreases. This can be appreciated in Fig. 6, where attenuation at different frequencies, as a function of the relative displacement between the line and the chain, is also depicted. It can be appreciated that for frequencies larger than f_0 (i.e., $f_{d=\pm 0.25mm}$ and $f_{d=\pm 0.5mm}$, corresponding to the notch frequencies for the indicated relative displacements), two attenuation peaks per chain period, rather than one, appear. The reason is that for carrier frequencies slightly larger than f_0 there are two equivalent positions (one for positive displacement and the other one for negative displacement) where the transmission coefficient is a minimum. In practice, it is difficult to perfectly set the carrier frequency to $f_c = f_0$. The reason is that it is not easy to accurately control the air gap separation between the line and the S-SRR chain. Therefore, a convenient strategy is to set f_c above f_0, accepting that two attenuation peaks (rather than one) per chain S-SRR cross above the S-SRR of the line will appear. Through this approach, some tolerance in the air gap can be assumed. Note that by increasing the air gap distance, the effect is an overall shift of the responses to larger frequencies, as illustrated in Fig. 7. If the carrier frequency is chosen as $f_c = f_0$, and the gap increases, it may give rise to reading errors or false angular velocity measurements.

IV. Applications

In this section, specific S-SRR chains with identical S-SRRs as those considered in the previous section and etched in the same substrate are used for two different applications: chipless RFID systems and angular velocity measurements. For angular velocity measurements, the chain must be circularly shaped along the perimeter of the rotor, and the S-SRRs must be located at periodic positions. Since the number of resonant elements along the perimeter of the rotor is known, it follows that the angular velocity is given by the time distance between adjacent peaks in the envelope function (T_m), provided a single notch per S-SRR cross, above the S-SRR of the line,

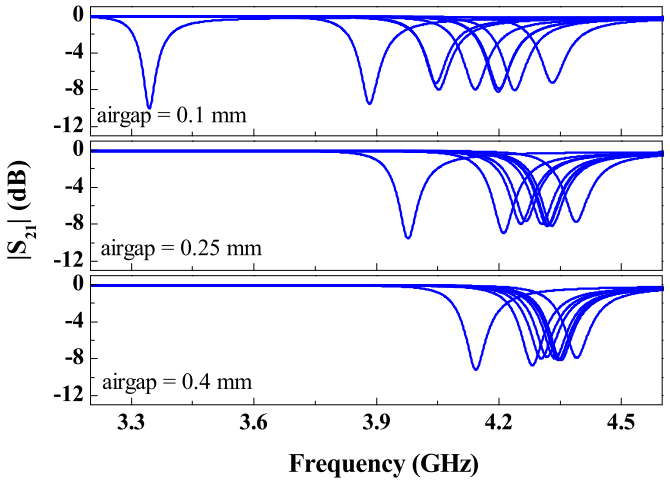

Fig. 7. Transmission coefficient, inferred from electromagnetic simulation using *Keysight Momentum*, for different relative displacements between the S-SRR chain and the CPW, parameterized by the air gap separation.

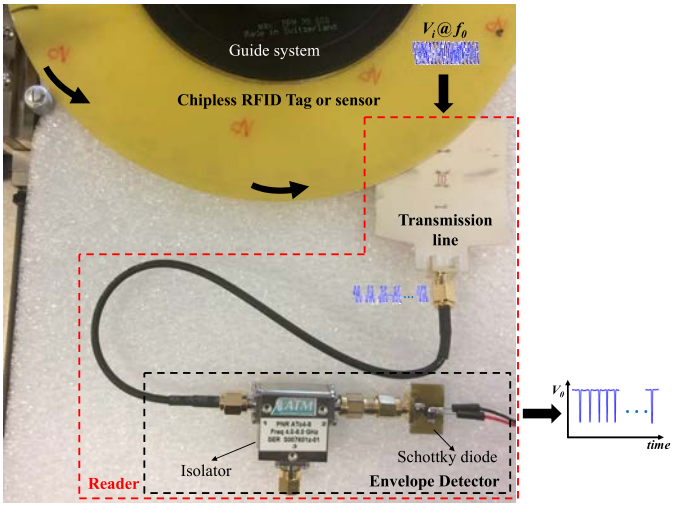

Fig. 8. Photograph of the experimental setup.

results. If a pair of notches is visible, typically these two notches are very close one each other as compared to the time distance between pairs of adjacent notches. Therefore, in this later case T_m is the time distance between pairs of adjacent notches (corresponding each pair of notches to a different S-SRR cross above the S-SRR of the line). By measuring T_m it follows that the angular velocity is given [29]

$$\omega_r = \frac{d\theta}{dt} = \lim_{\Delta t \to 0} \frac{\Delta\theta}{\Delta t} = \frac{\theta_m}{T_m} = \frac{2\pi / PPR}{T_m} \tag{1}$$

where θ is the angular position, t is time, θ_m is the angular period and *PPR* is equal to the number of resonant elements in the rotor.

The photograph of the experimental setup for angular velocity measurements can be seen in Fig. 8. The circulator employed to implement the isolator is the *ATM ATc4-8*. The envelope detector uses the *Avago HSMS-2860* Schottky diode and the *N2795A Active probe* (which acts as lowpass filter with $R = 1\text{M}\Omega$ and $C = 1$ pF), connected to an oscilloscope (the *Agilent MSO-X-3104A*) in order to visualize the envelope

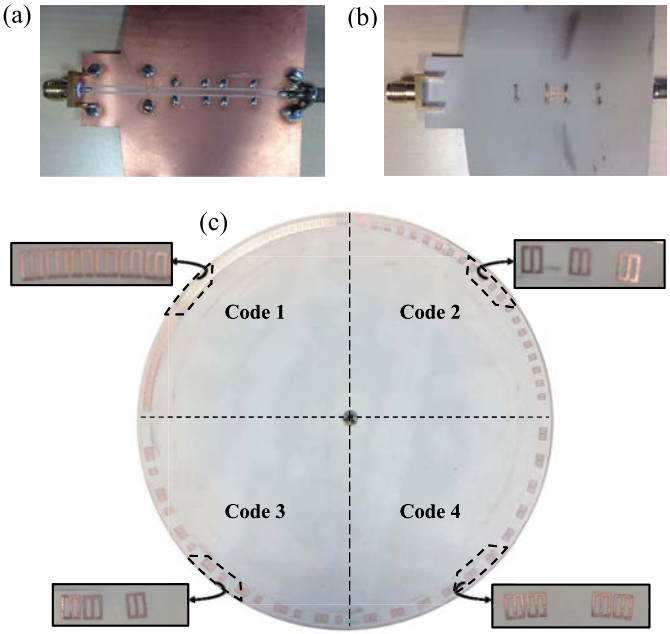

Fig. 9. Photograph of the transmission line reader, including CPW (a) and the S-SRR (b), and the fabricated encoders (c).

function. The carrier signal is generated by means of the *Agilent E4438C* function generator, whereas the displacement and velocity of the rotor is controlled by the *STM 23Q-3AN* stepper motor. The S-SRR loaded line has been re-designed and re-fabricated since the guiding system is not necessary [see Fig. 9(a) and (b)]. Nevertheless, it is important to vertically align the S-SRR of the line (stator) with those of the rotor, and this is achieved through stator motion in three dimensions, allowable by the experimental setup. Vertical motion is necessary to properly adjust the gap distance to the required value, i.e., 0.25 mm, or as much close as possible to it.

For chipless RFID tags, given a number of bits (and hence resonator positions), the S-SRR chain is typically linear. However, in the proof-of-concept presented here, circularly-shaped chipless tags are considered. The reason is that by considering circular S-SRR chains, the experimental set-up for angular velocity measurements can be used for tag reading as well. In this paper, four 40-bit circularly-shaped chipless tags have been fabricated and located at the four quadrants of the rotor [Fig. 9(c)]. By injecting a carrier signal with frequency $f_c = 4$ GHz at the input port of the CPW transmission line, it has been possible to obtain the envelope function corresponding to the different 40-bit encoders. The results are depicted in Fig. 10 together with the tag ID codes. The angular velocity of the rotor has been set to 3.5 rpm.

It can be appreciated in Fig. 10 that the ID codes of the four 40-bit chipless tags are correctly provided by the proposed reading system. The different notch depths are due to the fact that it is very difficult in practice to ensure a uniform gap separation between the S-SRR of the line and those of the tags (the in-house rotor system experiences some precession movement). Nevertheless, tag reading has been demonstrated and validated. It is worth mentioning that these four 40-bit encoders can be also seen as a single 160-bit chipless RFID

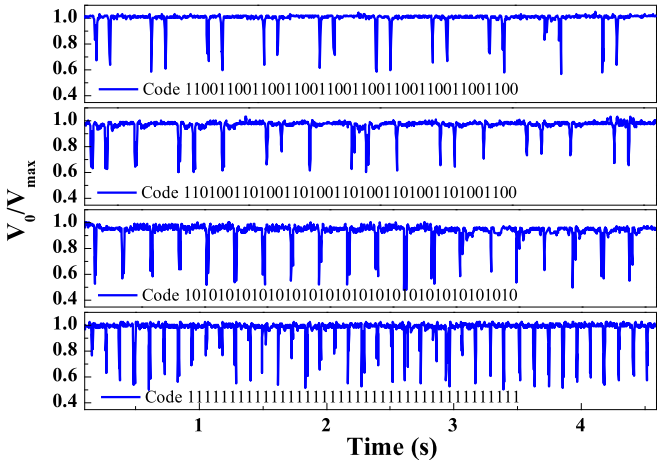

Fig. 10. Measured normalized envelope for four 40-bit fabricated chipless tags with the indicated ID codes.

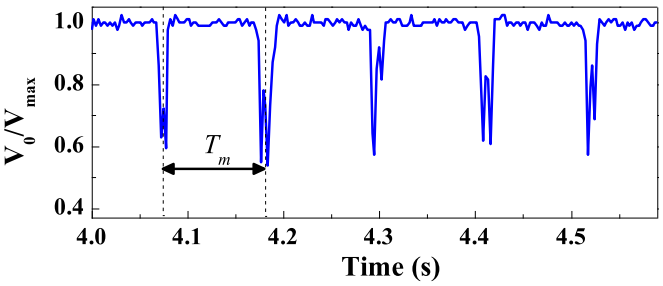

Fig. 11. Measured normalized envelope for a nominal 3.51 rpm speed.

tag with ID code composed by the cascade of the individual ID codes. Thus, the number of bits achievable with these approach, based on sequential bit reading by means of a harmonic signal, is only limited by the area occupied by the tag. In the proposed chipless tags, the information capacity per area unit is as high as 7 bit/cm^2.

For angular velocity measurements, S-SRRs at all the predefined, and equidistant, positions must be etched (or printed). Note that this is equivalent to a 160-bit encoder with all bits set to the logic state '1'. By using this rotor, quasi-instantaneous velocities can be measured, and changes of angular velocity within a cycle, manifested through variations in the time distance between adjacent notches (or pair of notches), can be detected. Indeed, the proposed system is also useful for angle measurement, and angle resolution is given by the number of resonant elements. For this main reason, and also to be able to detect changes in quasi-instantaneous angular velocities, it is convenient to enhance the number of S-SRR in the rotor as much as possible. However, for constant angular velocity measurements, S-SRR chains with small number of resonators or with absence of resonant elements at certain positions can be used. Indeed, the results given in Fig. 10 are useful to determine the angular velocity of the stepped motor (which is constant). Specifically, from the time distance between adjacent notch pairs for the 40-bit encoder with all bits set to '1' (see details in Fig. 11), the angular velocity is found to be 3.51 rpm, i.e., in good agreement with the nominal

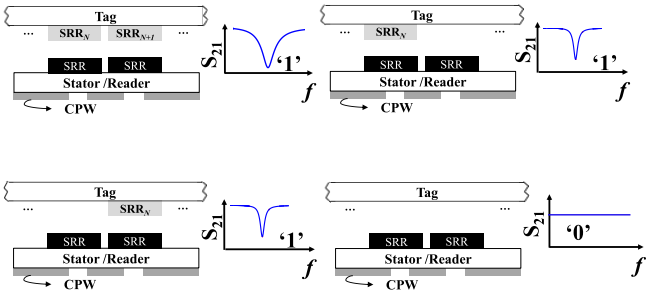

Fig. 12. The four different combinations of SRR pairs (tag) on top of the SRR-loaded CPW (reader).

value (note that the tolerance values of typical step motors are in the vicinity of 1.5%).

V. Discussion

In [29] and [30], the reported angular velocity sensor was implemented by means of 300 SRRs etched in the rotor. This was achieved by designing the resonant elements with a rectangular shape. The electrical size of a single S-SRR is not much smaller than the one of the SRR. Therefore, it follows that by using square shaped S-SRRs, it is not possible to accommodate as many resonant elements in the rotor perimeter as in the case of rectangular SRRs (obviously assuming that the resonance frequency is also comparable). In other words, the number of resonant elements per unit length (in the longitudinal direction of the resonator chain) is smaller in this work, as compared to [29] and [30]. In this regard, rectangular SRRs are a good option to optimize the number of pulses in angular velocity sensors.

However, SRRs are not the optimum resonant elements for chipless RFID tags to be read with SRR-loaded CPW transmission lines as those reported in [29] and [30], and used as stators. Each logic state is given by a pair of SRRs, rather than one. The reason is that by considering the distance between the slots of the CPW as the period of the SRR chain (in order to maximize the number of resonant elements), it follows that a pair of adjacent SRRs (if they are present in the assigned positions) lie on top of the slots of the CPW transmission line simultaneously. Consequently, a pair of adjacent predefined SRR positions (with presence or absence of resonant elements) cannot be considered as independent bits in chipless RFID encoders based on the SRR chain structure reported in [29] and [30]. Note that, according to Fig. 12, the four different combinations of SRR pairs (tag) on top of the SRR-loaded CPW (reader) either provide a single notch (a single SRR suffices) or an all-pass response, i.e., two logic states. Taking into account that the area occupied by a pair of rectangular SRRs in the rotor of [29] and [30] is 23 mm^2, and the area of the S-SRR used in this work is 9.9 mm^2, it follows that the density of information (number of bits per area unit) is more than twice in the present work, as compared to [29] and [30].

VI. Conclusions

In conclusion, a novel near-field chipless RFID system operating in time domain and based on sequential bit reading

has been proposed. The tags are a set of identical resonant elements (S-SRRs in this work) etched (or printed) on a dielectric substrate, and the presence or absence of such elements at predefined positions determines the logic state of the corresponding bit. Tag reading is carried out by near field coupling between a harmonically fed S-SRR-loaded CPW transmission line (reader) and the S-SRRs of the tag, which must be displaced, at constant velocity, above the CPW, in close proximity to it. By this means, the amplitude of the feeding signal is modulated, and the ID code is contained in the envelope function at the output port of the transmission line. Such envelope function can be inferred by means of an envelope detector. In the present paper, four circularly-shaped 40-bit encoders have been proposed, and the ID codes have been inferred by means of an experimental setup consisting of a stepped motor (providing circular motion to the tags) and the necessary electronics (to generate the harmonic carrier signal and to detect the envelope function). Interestingly, the same experimental set-up can be used for angular velocity measurements, where the rotation speed is determined from the time distance between adjacent notches in the envelope function. In this application, it is convenient to implement the S-SRR chain of the rotor with as many resonant elements as possible, since it has direct impact on angle resolution and on the capability to detect rotation speed variations within a cycle. However, in this work, constant angular velocities have been considered and the same encoders used as chipless RFID tags have been found to be suitable for the determination of angular velocities. Chipless RFID tags with unprecedented number of bits have been reported. Indeed, the four 40-bit tags used for validation of the approach can be seen as a single 160-bit tag, which is by far the chipless RFID tag with the largest number of bits reported so far. The information density is also very competitive (7 bit/cm^2). The proposed chipless RFID system can be envisaged for applications such as secure paper, where the reading distance can be sacrificed in favor of the number of bits. Specifically, corporate documents, ballots, exams, certificates, etc., with ID codes difficult to copy are some of the potential uses of the proposed chipless tags, providing counterfeiting functionality and a unique identification code, of great interest for security and authentication. In angular velocity sensors, the proposed system, based on S-SRRs, is an alternative to the sensors reported in [29] and [30], based on pairs of SRRs. In [30], by optimizing the frequency of the feeding signal, 1.200 pulses were achieved. Here, rather than optimizing the number of pulses, the idea was to demonstrate that the encoders can be used for angular velocity measurements. Indeed, for the measurement of constant, or average, rotation speeds, the rotor with four codes can be used for the determination of the rotation direction (clockwise or counterclockwise), provided the sequence of codes is not symmetric in some cases.

REFERENCES

[1] F. Martín, *Artificial Transmission Lines for RF and Microwave Applications*. Hoboken, NJ, USA: Wiley, 2015.

[2] R. Marques, F. Martín, and M. Sorolla, *Metamaterials with Negative Parameters: Theory, Design and Microwave Applications*. Hoboken, NJ, USA: Wiley, 2007.

[3] F. Martín, F. Falcone, J. Bonache, R. Marqués, and M. Sorolla, "Split ring resonator-based left-handed coplanar waveguide," *Appl. Phys. Lett.*, vol. 83, pp. 4652–4654, Nov. 2003.

[4] F. Falcone, T. Lopetegi, J. D. Baena, R. Marqués, F. Martín, and M. Sorolla, "Effective negative- stop-band microstrip lines based on complementary split ring resonators," *IEEE Microw. Wireless Compon. Lett.*, vol. 14, no. 6, pp. 280–282, Jun. 2004.

[5] J. D. Baena *et al.*, "Equivalent circuit models for split ring resonators and complementary split rings resonators coupled to planar transmission lines," *IEEE Trans. Microw. Theory Techn.*, vol. 53, no. 4, pp. 1451–1461, Apr. 2005.

[6] J. García-García *et al.*, "Microwave Filters with Improved Stop Band based on Sub-wavelength Resonators," *IEEE Trans. Microw. Theory Techn.*, vol. 53, no. 5, pp. 1997–2006, Jun. 2005.

[7] F. J. Herraiz-Martínez, G. Zamora, F. Paredes, F. Martín, and J. Bonache, "Multiband printed monopole antennas loaded with OCSRRs for PANs and WLANs," *IEEE Antennas Wireless Propag. Lett.*, vol. 10, pp. 1528–1531, 2011.

[8] F. J. Herraiz-Martínez, F. Paredes, G. Zamora, F. Martín, and J. Bonache, "Dual-band printed dipole antenna loaded with open complementary split-ring resonators (OCSRRs) for wireless applications," *Microw. Opt. Technol. Lett.*, vol. 54, pp. 1014–1017, Apr. 2012.

[9] J. Naqui, M. Durán-Sindreu, and F. Martín, "Novel sensors based on the symmetry properties of split ring resonators (SRRs)," *Sensors*, vol. 11, no. 8, pp. 7545–7553, 2011.

[10] C. Herrojo, J. Naqui, F. Paredes, and F. Martín, "Spectral Signature Barcodes based on S-shaped Split Ring Resonators (S-SRR)," *EPJ Appl. Metamater.*, vol. 3, pp. 1–6, Jun. 2016.

[11] C. Mandel, B. Kubina, M. Schüßler, and R. Jakoby, "Passive chipless wireless sensor for two-dimensional displacement measurement," in *Proc. 41st Eur. Microw. Conf.*, Manchester, U.K., 2011, pp. 79–82.

[12] M. Puentes, C. Weiss, M. Schüßler, and R. Jakoby, "Sensor array based on split ring resonators for analysis of organic tissues," in *IEEE MTT-S Int. Microw. Symp. Dig.*, Baltimore, MD, USA, Jun. 2011, pp. 1–4.

[13] M. S. Boybay and O. M. Ramahi, "Material characterization using complementary split-ring resonators," *IEEE Trans. Instrum. Meas.*, vol. 61, no. 11, pp. 3039–3046, Nov. 2012.

[14] C.-S. Lee and C.-L. Yang, "Complementary split-ring resonators for measuring dielectric constants and loss tangents," *IEEE Microw. Wireless Compon. Lett.*, vol. 24, no. 8, pp. 563–565, Aug. 2014.

[15] A. Ebrahimi, W. Withayachumnankul, S. Al-Sarawi, and D. Abbott, "High-sensitivity metamaterial-inspired sensor for microfluidic dielectric characterization," *IEEE Sensors J.*, vol. 14, no. 5, pp. 1345–1351, May 2014.

[16] C.-L. Yang, C.-S. Lee, K.-W. Chen, and K.-Z. Chen, "Noncontact measurement of complex permittivity and thickness by using planar resonators," *IEEE Trans. Microw. Theory Techn.*, vol. 64, no. 1, pp. 247–257, Jan. 2016.

[17] L. Su, J. Mata-Contreras, P. Vélez, and F. Martín, "Estimation of conductive losses in complementary split ring resonator (CSRR) loading an embedded microstrip line and applications," in *IEEE MTT-S Int. Microw. Symp. Dig.*, Honolulu, HI, USA, Jun. 2017.

[18] J. Naqui, *Symmetry Properties in Transmission Lines Loaded with Electrically Small Resonators: Circuit Modeling and Applications*. Springer, 2016.

[19] J. Naqui, M. Durín-Sindreu, and F. Martín, "Alignment and position sensors based on split ring resonators," *Sensors*, vol. 12, no. 9, pp. 11790–11797, Sep. 2012.

[20] A. K. Horestani, C. Fumeaux, S. F. Al-Sarawi, and D. Abbott, "Displacement sensor based on diamond-shaped tapered split ring resonator," *IEEE Sensors J.*, vol. 13, no. 4, pp. 1153–1160, Apr. 2013.

[21] A. K. Horestani, J. Naqui, D. Abbott, C. Fumeaux, and F. Martín, "Two-dimensional displacement and alignment sensor based on reflection coefficients of open microstrip lines loaded with split ring resonators," *Electron. Lett.*, vol. 50, no. 8, pp. 620–622, Apr. 2014.

[22] J. Naqui and F. Martin, "Transmission lines loaded with bisymmetric resonators and their application to angular displacement and velocity sensors," *IEEE Trans. Microw. Theory Techn.*, vol. 61, no. 12, pp. 4700–4713, Dec. 2013.

[23] J. Naqui and F. MartÃn, "Angular displacement and velocity sensors based on electric-LC (ELC) loaded microstrip lines," *IEEE Sensors J.*, vol. 14, no. 4, pp. 939–940, Apr. 2014.

[24] J. Naqui, J. Coromina, A. Karami-Horestani, C. Fumeaux, and F. Martín, "Angular displacement and velocity sensors based on coplanar waveguides (CPWs) loaded with S-shaped split ring resonators (S-SRR)," *Sensors*, vol. 15, pp. 9628–9650, Apr. 2015.

[25] J. Naqui, C. Damm, A. Wiens, R. Jakoby, L. Su, and F. Martín, "Transmission lines loaded with pairs of magnetically coupled stepped impedance resonators (SIRs): Modeling and application to microwave sensors," in *IEEE MTT-S Int. Microw. Symp. Dig.*, Tampa, FL, USA, Jun. 2014, pp. 1–4.
[26] J. Naqui, C. Damm, A. Wiens, R. Jakoby, L. Su, and F. Martín, "Transmission lines loaded with pairs of stepped impedance resonators: Modeling and application to differential permittivity measurements," *IEEE Trans. Microw. Theory Techn.*, vol. 64, no. 11, pp. 3864–3877, Nov. 2016.
[27] L. Su, J. Mata-Contreras, J. Naqui, and F. Martín, "Splitter/combiner microstrip sections loaded with pairs of complementary split ring resonators (CSRRs): Modeling and optimization for differential sensing applications," *IEEE Trans. Microw. Theory Techn.*, vol. 64, no. 12, pp. 4362–4370, Dec. 2016.
[28] L. Su, J. Mata-Contreras, J. Naqui, and F. Martín, "Configurations of splitter/combiner microstrip sections loaded with stepped impedance resonators (SIRs) for sensing applications," *Sensors*, vol. 16, no. 12, p. 2195, 2016, doi: 10.3390/s16122195.
[29] J. Naqui and F. Martín, "Application of broadside-coupled split ring resonator (BC-SRR) loaded transmission lines to the design of rotary encoders for space applications," in *IEEE MTT-S Int. Microw. Symp. Dig.*, San Francisco, CA, USA, May 2016, pp. 1–4.
[30] J. Mata-Contreras, C. Herrojo, and F. Martín, "Application of split ring resonator (SRR) loaded transmission lines to the design of angular displacement and velocity sensors for space applications," *IEEE Trans. Microw. Theory Techn.*, to be published, doi: 10.1109/TMTT.2017.2693981.
[31] C. S. Hartmann, "A global SAW ID tag with large data capacity," in *Proc. IEEE Ultrason. Symp.*, vol. 1, Oct. 2002, pp. 65–69.
[32] A. Chamarti and K. Varahramyan, "Transmission delay line based ID generation circuit for RFID applications," *IEEE Microw. Wireless Compon. Lett.*, vol. 16, no. 11, pp. 588–590, Nov. 2006.
[33] M. Schüßler, C. Damm, and R. Jakoby, "Periodically LC loaded lines for RFID backscatter applications," in *Proc. Metamater.*, Rome, Italy, Oct. 2007, pp. 103–106.
[34] N. Saldanha and D. C. Malocha, "Design Parameters for SAW multi-tone frequency coded reflectors," in *Proc. IEEE Ultrason. Symp.*, Oct. 2007, pp. 2087–2090.
[35] M. Schüßler, C. Damm, M. Maasch, and R. Jakoby, "Performance evaluation of left-handed delay lines for RFID backscatter applications," in *IEEE MTT-S Int. Microw. Symp. Dig.*, Jun. 2008, pp. 177–180.
[36] S. Harma, V. P. Plessky, C. S. Hartmann, and W. Steichen, "Z-path SAW RFID tag," *IEEE Trans. Ultrason., Ferroelectr., Freq. Control*, vol. 55, no. 1, pp. 208–213, Jan. 2008.
[37] T. Han, W. Wang, H. Wu, and Y. Shui, "Reflection and scattering characteristics of reflectors in SAW tags," *IEEE Trans. Ultrason., Ferroelectr., Freq. Control*, vol. 55, no. 6, pp. 1387–1390, Jun. 2008.
[38] S. Harma, V. P. Plessky, L. Xianyi, and P. Hartogh, "Feasibility of ultra-wideband SAW RFID tags meeting FCC rules," *IEEE Trans. Ultrason., Ferroelectr., Freq. Control*, vol. 56, pp. 812–820, 2012.
[39] F. J. Herraiz-Martínez, F. Paredes, G. Z. Gonzalez, F. Martín, and J. Bonache, "Printed magnetoinductive-wave (MIW) delay lines for chipless RFID applications," *IEEE Trans. Antennas Propag.*, vol. 60, no. 11, pp. 5075–5082, Nov. 2012.
[40] S. Tedjini, E. Perret, A. Vena, and D. Kaddout, "Mastering the electromagnetic signature of chipless RFID tags," in *Chipless and Conventional Radiofrequency Identification*. Hershey, PA, USA: IGI Global, 2012.
[41] I. Preradovic, I. Balbin, N. C. Karmakar, and G. F. Swiegers, "Multiresonator-based chipless RFID system for low-cost item tracking," *IEEE Trans. Microw. Theory Techn.*, vol. 57, no. 5, pp. 1411–1419, May 2009.
[42] S. Preradovic and N. C. Karmakar, "Design of chipless RFID tag for operation on flexible laminates," *IEEE Antennas Wireless Propag. Lett.*, vol. 9, pp. 207–210, 2010.
[43] O. Rance, R. Siragusa, P. Lemaître-Auger, and E. Perret, "Toward RCS magnitude level coding for chipless RFID," *IEEE Trans. Microw. Theory Techn.*, vol. 64, no. 7, pp. 2315–2325, Jul. 2016.
[44] J. McVay, A. Hoorfar, and N. Engheta, "Space-filling curve RFID tags," in *Proc. IEEE Radio Wireless Symp.*, Oct. 2006, pp. 199–202.
[45] I. Jalaly and D. Robertson, "Capacitively-tuned split microstrip resonators for RFID barcodes," in *Proc. Eur. Microw. Conf.*, Oct. 2005, pp. 4–7.
[46] H.-S. Jang, W.-G. Lim, K.-S. Oh, S.-M. Moon, and J.-W. Yu, "Design of low-cost chipless system using printable chipless tag with electromagnetic code," *IEEE Microw. Wireless Compon. Lett.*, vol. 20, no. 11, pp. 640–642, Nov. 2010.
[47] A. Vena, E. Perret, and S. Tedjini, "A fully printable chipless RFID tag with detuning correction technique," *IEEE Microw. Wireless Compon. Lett.*, vol. 22, no. 4, pp. 209–211, Apr. 2012.
[48] A. Vena, E. Perret, and S. Tedjini, "Design of compact and auto-compensated single-layer chipless RFID tag," *IEEE Trans. Microw. Theory Techn.*, vol. 60, no. 9, pp. 2913–2924, Sep. 2012.
[49] A. Vena, E. Perret, and S. Tedjini, "High-capacity chipless RFID tag insensitive to the polarization," *IEEE Trans. Antennas Propag.*, vol. 60, no. 10, pp. 4509–4515, Oct. 2012.
[50] C. Herrojo, J. Naqui, F. Paredes, and F. Martín, "Spectral signature barcodes implemented by multi-state multi-resonator circuits for chipless RFID tags," in *IEEE MTT-S Int. Microw. Symp. Dig.*, San Francisco, CA, USA, May 2016, pp. 1–4.
[51] C. Herrojo, F. Paredes, J. Mata-Contreras, S. Zuffanelli, and F. Martín, "Multistate multiresonator spectral signature barcodes implemented by means of S-shaped split ring resonators (S-SRRs)," *IEEE Trans. Microw. Theory Techn.*, to be published, doi: 10.1109/TMTT.2017.2672547.
[52] M. A. Islam and N. C. Karmakar, "A novel compact printable dual-polarized chipless RFID system," *IEEE Trans. Microw. Theory Techn.*, vol. 60, no. 7, pp. 2142–2151, Jul. 2012.
[53] A. Vena, E. Perret, and S. Tedjini, "Chipless RFID tag using hybrid coding technique," *IEEE Trans. Microw. Theory Techn.*, vol. 59, no. 12, pp. 3356–3364, Dec. 2011.
[54] A. Vena, E. Perret, and S. Tedjini, "A compact chipless RFID tag using polarization diversity for encoding and sensing," in *Proc. IEEE Int. Conf. RFID*, Jun. 2012, pp. 191–197.
[55] I. Balbin and N. C. Karmakar, "Phase-encoded chipless RFID transponder for large scale low cost applications," *IEEE Microw. Wireless. Compon. Lett.*, vol. 19, no. 8, pp. 509–511, Aug. 2009.
[56] S. Genovesi, F. Costa, A. Monorchio, and G. Manara, "Chipless RFID tag exploiting multifrequency delta-phase quantization encoding," *IEEE Antennas Wireless Propag. Lett.*, vol. 15, pp. 738–741, 2015.
[57] H. Chen *et al.*, "Left-handed materials composed of only S-shaped resonators," *Phys. Rev. E, Stat. Phys. Plasmas Fluids Relat. Interdiscip. Top.*, vol. 70, no. 5, pp. 1–4, Nov. 2004.
[58] H. Chen *et al.*, "Negative refraction of a combined double S-shaped metamaterial," *Appl. Phys. Lett.*, vol. 86, no. 15, p. 151909, 2005.
[59] H. Chen *et al.*, "Magnetic properties of S-shaped split ring resonators," *Prog. Electromagn. Res.*, vol. 51, pp. 231–247, 2005, doi: 10.2528/PIER04051201.

Cristian Herrojo was born in Badalona, Barcelona, Spain, in 1983. He received the Telecommunications Technical Engineering degree in electronic systems and Telecommunications Engineering degree from Universitat Autònoma de Barcelona, Barcelona, Spain, in 2010 and 2012, respectively, where he is currently pursuing the Ph.D. degree with a focus on the design of RF/microwave resonant structures applied to RFID tags without chip. He has a research grant from the FPI Program of the Education and Science Spanish Ministry.

Javier Mata-Contreras was born in Málaga, Spain, in 1976. He received the Ingeniería de Telecomunicación degree and the Ph.D. degree from the Universidad de Málaga, in 2000 and 2010, respectively. His Ph.D. dissertation was "Distributed Amplifiers and Mixers With Transmission Lines Based on Metamaterials." In 2000, he joined the UMA Department of Ingeniería de Comunicaciones, UMA, as an Assistant Professor. He is currently with CIMITEC and the Universitat Autònoma de Barcelona as a Visitant Professor. His research interests include active and passive microwave devices and active distributed circuits based on metamaterials, among others.

Ferran Paredes was born in Badalona, Barcelona, Spain, in 1983. He received the Telecommunications Engineering Diploma in electronics, the Telecommunications Engineering degree, and the Ph.D. degree in electronics engineering from the Universitat Autònoma de Barcelona, in 2004, 2006, and 2012, respectively. He was an Assistant Professor with the Universitat Autònoma de Barcelona from 2006 to 2008, where he is currently a Research Assistant. His research interests include metamaterial concepts, passive microwaves devices, antennas, and RFID.

Ferran Martín (M'04–SM'08–F'12) was born in Barakaldo, Spain, in 1965. He received the B.S. degree in physics and the Ph.D. degree from the Universitat Autònoma de Barcelona (UAB), Barcelona, Spain, in 1988 and 1992, respectively. From 1994 to 2006, he was an Associate Professor of Electronics with the Departament d'Enginyeria Electrònica, Universitat Autònoma de Barcelona, where he has been a Full Professor of Electronics, since 2007. In recent years, he has been involved in different research activities, including modeling and simulation of electron devices for high-frequency applications, millimeter wave, and THz generation systems, and the application of electromagnetic bandgaps to microwave and millimeter wave circuits. He is now very active in the field of metamaterials and their application to the miniaturization and optimization of microwave circuits and antennas. He is the Head of the Microwave Engineering, Metamaterials and Antennas Group (GEMMA Group), UAB, and the Director of CIMITEC, a Research Center on Metamaterials supported by TECNIO (Generalitat de Catalunya). He has organized several international events related to metamaterials, including Workshops at the IEEE International Microwave Symposium in 2005 and 2007 and the European Microwave Conference in 2009, and the Fifth International Congress on Advanced Electromagnetic Materials in Microwaves and Optics (Metamaterials 2011), where he has acted as a Chair of the Local Organizing Committee. He has acted as a Guest Editor for three Special Issues on Metamaterials in three International Journals. He has authored and co-authored over 500 technical conference, letter, journal papers, and book chapters, co-authored the book on Metamaterials entitled *Metamaterials with Negative Parameters: Theory, Design and Microwave Applications* (Wiley, 2008), authored the book *Artificial Transmission Lines for RF and Microwave Applications* (Wiley, 2015), and he has generated 16 Ph.D. degrees. He has filed several patents on metamaterials and has headed several Development Contracts.

Dr. Martín is a member of the IEEE Microwave Theory and Techniques Society. He is a Reviewer of the IEEE TRANSACTIONS ON MICROWAVE THEORY AND TECHNIQUES and the IEEE MICROWAVE AND WIRELESS COMPONENTS LETTERS, among many other journals, and he serves as a member of the Editorial Board of the *IET Microwaves, Antennas and Propagation* and the *International Journal of RF and Microwave Computer-Aided Engineering*. He is also a member of the Technical Committees of the European Microwave Conference and International Congress on Advanced Electromagnetic Materials in Microwaves and Optics (Metamaterials). Among his distinctions, he has received the 2006 Duran Farell Prize for Technological Research. He holds the Parc de Recerca UAB—Santander Technology Transfer Chair. He has been a recipient of two ICREA ACADEMIA Awards in 2008 and 2013. He is a Fellow of the IET since 2016.

Artículo MISM17

Near-Field Chipless-RFID Tags with Sequential Bit Reading Implemented in Plastic Substrates

C. Herrojo, J. Mata-Contreras, F. Paredes, A. Núñez,
E. Ramon, and F. Martín

Journal of Magnetism and Magnetic Materials xxx (2017) xxx–xxx

Contents lists available at ScienceDirect

Journal of Magnetism and Magnetic Materials

journal homepage: www.elsevier.com/locate/jmmm

Research articles

Near-field chipless-RFID tags with sequential bit reading implemented in plastic substrates

C. Herrojo [a], J. Mata-Contreras [a], F. Paredes [a], A. Núñez [b], E. Ramon [b], F. Martín [a,*]

[a] CIMITEC, Departament d'Enginyeria Electrònica, Universitat Autònoma de Barcelona, 08193 Bellaterra, Barcelona, Spain
[b] Institut de Microelectrònica de Barcelona, IMB-CNM (CSIC), Bellaterra, Spain

ARTICLE INFO

Article history:
Received 26 June 2017
Received in revised form 15 September 2017
Accepted 2 October 2017
Available online xxxx

ABSTRACT

Chipless radiofrequency identification (chipless-RFID) systems based on near-field coupling between the tag and the reader and sequential bit reading, with tags implemented on plastic substrates, are presented in this paper. In the proposed system, the tag is a set of identical resonant elements (S-shaped split ring resonators – S-SRRs), inkjet-printed on a plastic substrate (PEN), forming a resonator chain. The presence or absence of resonant elements at predefined and equidistant positions in the chain determines the logic state '1' and '0', respectively, associated with each resonant element. The reader is a coplanar waveguide (CPW) transmission line fed by a harmonic signal tuned to the resonance frequency of the resonant elements of the chain. Tag reading is achieved by displacing the chain of resonant elements above the CPW transmission line, in close proximity to it, so that near-field coupling between the CPW transmission line and the resonant elements of the tag results. By this means, the injected carrier signal is amplitude modulated, provided the transmission coefficient of the line varies with the presence or absence of resonant elements in the chain, and the identification (ID) code is contained in the envelope function. The functionality of the proposed system, with 10-bit tags occupying an area of 1.35 cm^2 (corresponding to an information density of 7.4 bit/cm^2), is demonstrated.

1. Introduction

Radiofrequency identification (RFID) is a wireless RF technology for the identification and tracking of items, consumer products, animals, vehicles, etc. [1]. A typical RFID system is composed by the tag, which contains a unique ID code stored in a silicon integrated circuit (IC), or chip, and the reader. In passive RFID systems operating in the ultra-high-frequency (UHF) band, the tag and the reader are equipped with antennas for communications purposes through the far-field, and the reader provides also the necessary energy to power-up the tag. These passive UHF-RFID tags are relatively cheap, at least as compared to active tags (typically operating at microwave frequencies), exhibit high data capacity, and do not need to be at short distance to the reader for interrogation purposes. Thus, UHF-RFID systems are by far superior to identification systems based on optical barcodes in terms of data storage capability, and reading distance (line-of-sight is not required and read ranges of several meters can be achieved with the activation energy of currently available tag chips). However, the cost of UHF-RFID tags, dictated by the presence of the chip, is of the order of several Eurocents, and this cost is too high for the penetration of the UHF-RFID technology in many applications where low-cost item products are involved.

To alleviate the cost of chiped tags, the chipless-RFID technology emerged several years ago [2–7]. In chipless-RFID tags, chips are replaced with printed encoders containing the ID code. Although the cost of these encoders can be potentially situated below the Eurocent barrier on account of the current cost of conductive inks, and future trends on the use of massive printing processes for tag fabrication (screen-printing, rotogravure, etc.), chipless tags have two main limitations, as compared to chip-based tags: (i) the data storage capability and (ii) the encoder size. Therefore the present challenges of researchers working on the topic of chipless-RFID are to reduce the size of the tags and to increase the number of bits as much as possible.

Chipless-RFID systems are based on two main approaches: (i) time domain based systems [8–17] and (ii) frequency domain based systems [2,3,18–37]. In chipless-RFID systems based on the former approach, tag reading is carried out through time domain reflectometry (TDR). TDR-based tags exhibit fast responses in comparison to frequency domain based tags. However, in TDR-based tags the tag ID is generated by the echoes of a pulsed signal caused by discontinuities or impedance mismatches in a delay line. In

* Corresponding author.
E-mail address: Ferran.Martin@uab.es (F. Martín).

https://doi.org/10.1016/j.jmmm.2017.10.005
0304-8853/

order to avoid overlapping of the reflected pulses, either large delay lines or very narrow pulses are needed. Hence, TDR-based tags exhibit a limited bit encoding capability. In frequency domain based chipless-RFID systems, encoders are implemented by means of resonant elements tuned at predefined frequencies. Such frequencies are distributed within a certain frequency band, and hence tag reading requires a multi-frequency interrogation signal covering the spectral bandwidth. Encoding is achieved by the presence or absence of abrupt spectral features in the amplitude, phase or group delay responses. In frequency domain based tags, each resonant element typically corresponds to 1 bit of information. However, tags based on multi-state resonators have been recently demonstrated [35–37] (in such tags, up to 2 bits per resonant element are achieved by resonator rotation). Finally, some chipless-RFID systems, designated as hybrid systems, use more than one domain (e.g. time, frequency, phase, polarization, etc.) simultaneously, in order to increase the number of bits per resonant element [28,31–34].

Despite numerous efforts to increase the number of bits in the previous approaches, the reported chipless-RFID tags are far from the data capacity of chiped tags. The main limitation in frequency domain and hybrid based tags is the spectral bandwidth required to accommodate a large number of bits. This is related to the achievable information density per frequency (DPF), which is typically small due to the bandwidth occupied by each resonant element.

In [38], a novel time domain approach for the implementation of chipless-RFID systems, which potentially allows for unprecedented data capacities, was reported. In this approach, the tags are implemented by means of chains of identical resonators, all tuned to the same frequency. Encoding is achieved by the presence or absence of resonant elements at predefined and equidistant positions in the chain, and tag reading is carried out through near-field coupling. Namely, a transmission line is fed by a harmonic signal tuned to the resonance frequency of the tag resonators. By displacing the tag over the transmission line, in close proximity to it, magnetic coupling between the line and the tag arises provided a resonator lies on top of the line. Thus, line-to-resonator coupling is modulated by tag motion, and such modulation is controlled by the tag ID. Such coupling modulation, in turn, modulates the transmission coefficient of the line and, consequently, the output signal is amplitude modulated as well. Therefore, the ID code is contained in the envelope function, and a simple envelope detector suffices for tag reading. Note that the spectral bandwidth is null (all the resonators are tuned to the same frequency) and hence the information DPF is virtually infinite. Hence, the number of bits is only limited by the area occupied by the resonators chain. In this paper, our aim is to demonstrate the functionality of this novel chipless-RFID approach with inkjet-printed tags on plastic substrates. This approach is of special interest in applications where the read distances can be sacrificed in favor of data capacity, such as security and authentication, where, typically, a large number of bits is necessary (e.g. secure paper in corporate documents, certificates, ballots, exams, etc.).

2. Principle of the proposed chipless-RFID system

The principle of operation of the proposed system is depicted in Fig. 1 [38]. The reader consists of a CPW transmission line fed by a harmonic signal, plus an envelope detector, preceded by a circulator, at the output port. The tags are implemented by means of S-SRR resonators (Fig. 2(a)) [39]. Such resonant elements are excited when they are situated on top of the CPW transmission line (in close proximity to it) as depicted in the figure, by virtue of the counter magnetic fields generated by the feeding signal [40]. However, in order to prevent from the coupling between the line and multiple resonant elements simultaneously, or between the resonant elements of the tag, an S-SRR has been etched in the back substrate side of the CPW transmission line, rotated 180° with regard to the S-SRRs of the tag chain (Fig. 2(b)). By this means, the resonance frequency of the pair of perfectly aligned S-SRRs (forming a broadside-coupled S-SRR) is smaller than the resonance frequency of a single S-SRR (4.4 GHz), and the above-cited couplings are prevented [41]. Indeed, the harmonic feeding signal is tuned to the fundamental resonance frequency of the broadside coupled S-SRR, f_0.

Each time an S-SRR of the tag lies on top of the S-SRR of the line (logic state '1'), line-to-resonator coupling is maximized, and the transmission coefficient of the line at f_0 as well as the amplitude of the output signal is minimized. Conversely, if the S-SRR is not present in one of the predefined positions in the chain (logic state '0'), the modulus of the transmission coefficient is roughly 1, and the amplitude of the output signal is identical to the one of the input signal. Thus, tag motion effectively modulates the amplitude of the output signal, according to the ID code of the tag. Therefore, by extracting the envelope function, the ID code can be inferred. To this end, an envelope detector, implemented by means of a diode and low-pass filter, is used. Since the diode is a highly non-linear device, a circulator configured as an isolator is cascaded between the output port of the line and the envelope detector. By this means, unwanted mismatching reflections from the diode are avoided.

A key advantage of this approach, based on near-field coupling for tag reading, is the fact that the tag merely consists of a chain of resonant elements. Antennas are not needed, simplifying tag design, size, and cost. Alignment between the tag chain and the S-SRR of the line is required, but some tolerance is acceptable since the transmission coefficient of the line at the frequency of the broadside coupled S-SRR, f_0, is also significantly reduced when the S-SRR of the line and tag are not perfectly aligned. The air

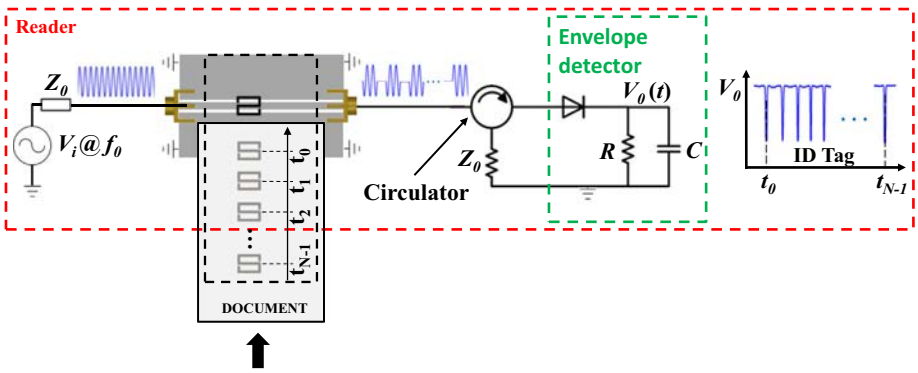

Fig. 1. Illustration of the working principle of the proposed chipless-RFID system.

Please cite this article in press as: C. Herrojo et al., Near-field chipless-RFID tags with sequential bit reading implemented in plastic substrates, Journal of Magnetism and Magnetic Materials (2017), https://doi.org/10.1016/j.jmmm.2017.10.005

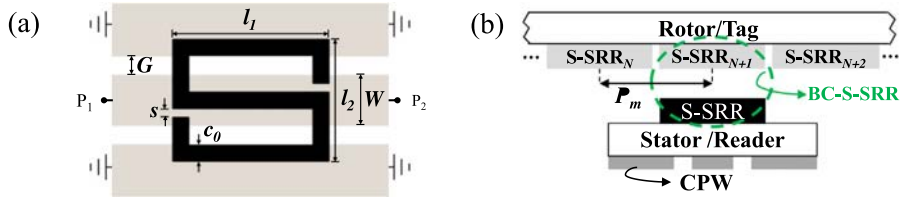

Fig. 2. S-SRR on top of a CPW (a) and cross sectional view of the S-SRR-loaded CPW and tag (b). Relevant dimensions are indicated.

gap distance between the tag and the line has also influence on coupling modulation, since it varies the resonance frequency of the broadside coupled S-SRR, where maximum coupling arises. In practice, the frequency of the feeding signal should be set to a value slightly above f_0, the frequency of the broadside coupled S-SRR corresponding to the nominal air gap separation, since it is difficult to precisely control the air gap and to guarantee the invariability of it during tag motion. Note that if the frequency of the feeding signal is smaller than the resonance frequency of the broadside coupled S-SRR corresponding to a certain air gap separation, larger than the nominal, false readings may arise.

3. Substrate and ink characterization

In this paper, tags based on a chain of S-SRRs printed by inkjet on a plastic substrate are presented for the first time. The Polyethylene naphtalate (PEN) film (*Dupont Teijin Q65FA*) with thickness h = 125 μm was employed as flexible substrate. The dielectric constant and loss tangent of this material have been inferred by means of a split cylinder resonator (model *Agilent 85072A*). The resulting values have been found to be ε_r = 3.36 and tan δ = 0.0042. Such loss tangent value is relatively small, not very far from the typical values of low-loss microwave substrates.

The used inkjet printer is the *Ceradrop Ceraprinter X-Serie*, and two layers of *DuPont™ PE410* conductive ink (with conductivity 7.28 × 10^6 S/m) have been printed in order to achieve a measured thickness of 3.3–3.5 μm.

4. Reader and tag design and fabrication

The CPW transmission line of the reader has been fabricated on the low-loss *Rogers RO3010* substrate with dielectric constant ε_r = 10.2, loss tangent tan δ = 0.0022 and thickness h = 0.635 mm. Both the CPW layout and the pattern of the S-SRR of the line have been

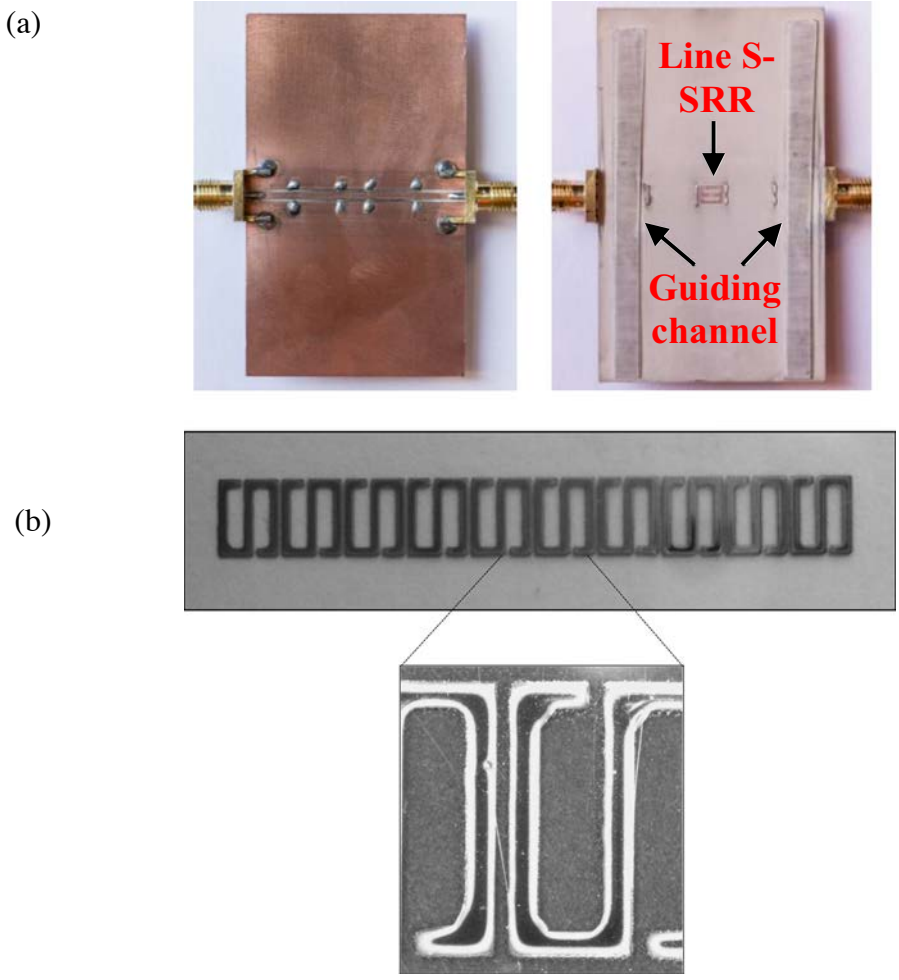

Fig. 3. Photograph of the fabricated S-SRR-loaded CPW used for reading purposes (a) and photograph of the fabricated 10-bit chipless-RFID tags (with code '1111111111') (b).

Please cite this article in press as: C. Herrojo et al., Near-field chipless-RFID tags with sequential bit reading implemented in plastic substrates, Journal of Magnetism and Magnetic Materials (2017), https://doi.org/10.1016/j.jmmm.2017.10.005

achieved by means of a drilling machine (*LPKF H100*). The metal layer is copper with a thickness of 35 μm. The dimensions of the S-SRR, in reference to Fig. 2 are l_1 = 3.8 mm, l_2 = 2.96 mm, c_0 = 0.4 mm and s = 0.2 mm. With these dimensions, the resonance frequency of the broadside coupled S-SRR resulting by printing an identical S-SRR on the above cited plastic substrate, and by considering an air gap of 0.25 mm, is found to be f_0 = 4 GHz. The photograph of the fabricated S-SRR-loaded CPW is shown in Fig. 3(a).

In the tag, S-SRRs with dimensions identical to those of the S-SRR of the line must be used for coding purposes. The distance between adjacent S-SRRs (in case they are present in two adjacent predefined positions) is 0.2 mm, resulting in a chain period of 3.16 mm. This S-SRR separation is enough to avoid overlapping between adjacent resonant elements after the printing process. The photograph of the fabricated tag, with all bits set to '1', is depicted in Fig. 3(b).

With regard to the additional elements necessary for a reading operation, the harmonic feeding signal is generated by means of the *Agilent E4438C* function generator. The envelope detector uses the *Avago HSMS-2860* Schottky diode and the *N2795A* active probe (which acts as low-pass filter with R = 1 MΩ and C = 1 pF), connected to an oscilloscope (the *Agilent MSO-X-3104A*) in order to visualize the envelope function. Finally, the circulator is the *ATM ATc4-8*, operative in the frequency region of interest. The photograph of the experimental set-up is shown in Fig. 4.

5. Results and discussion

The measured normalized envelope function corresponding to the tag of Fig. 3(b) is depicted in Fig. 5. Ten dips, corresponding to the ten S-SRRs, can be perfectly appreciated. Hence, the proposed chipless RFID system is validated by considering plastic substrates and resonant elements printed on it.

A detailed view of Fig. 5 indicates that in some cases a double dip, rather than a single dip, associated with the presence of a resonant element ('1' logic state) arises. This is due to the fact that, in practice, it is very difficult to maintain the gap distance to the same value during tag motion. If the frequency of the feeding (carrier) signal is slightly above the frequency of the broadside coupled S-SRR (variable with the air gap), then two dips per resonant element are expected, as discussed in [42]. Nevertheless, the tag ID can be

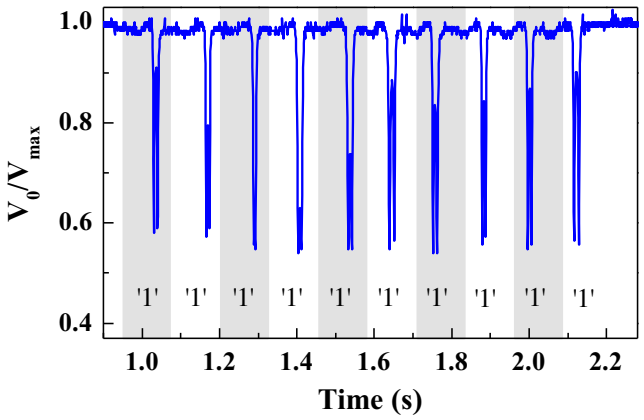

Fig. 5. Measured normalized envelope for the 10-bit chipless RFID tag of Fig. 3 (b).

perfectly read provided the normalized amplitude of the envelope function is situated below a certain threshold (e.g. 0.8) when the resonant element associated with a certain bit is present in the tag.

Let us now discuss another important aspect, i.e., the possibility to program the ID code. To reduce fabrication costs, it is convenient to fabricate all identical tags, i.e., with all bits set to '1', and, in a later stage (writing operation), detune the necessary resonators to implement the required ID code. Detuning means to physical alter the resonators in order to shift their resonance frequency beyond the region of interest. By this means, a logic '0' state is associated to a detuned resonant element, equivalent to its absence in a predefined position of the chain. In practice, detuning can be achieved by cutting the resonant elements. Alternatively, by short-circuiting the terminals of the S-SRR one also expects a significant displacement of their resonance frequency. In this work, we have cut alternating S-SRRs in the tag of Fig. 3(b), corresponding to the ID code '1010101010'. The photograph of the programmed tag is depicted in Fig. 6, and its measured normalized envelope function is depicted in Fig. 7. The obtained envelope demonstrates that such programming approach works, on account of the obtained ID code. Beyond the proof-of-concept presented here, in a real scenario, detuning by means of laser ablation (cut-

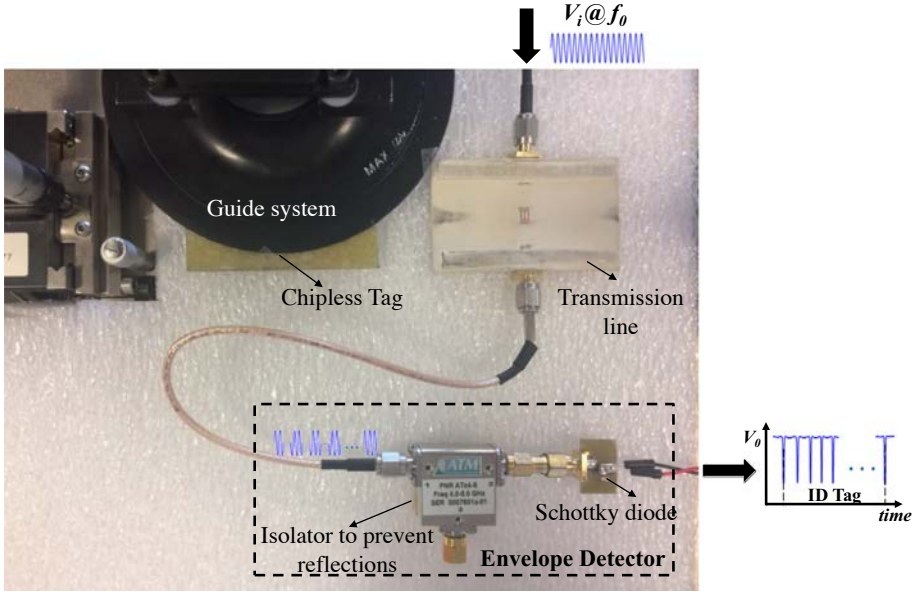

Fig. 4. Experimental set-up.

Please cite this article in press as: C. Herrojo et al., Near-field chipless-RFID tags with sequential bit reading implemented in plastic substrates, Journal of Magnetism and Magnetic Materials (2017), https://doi.org/10.1016/j.jmmm.2017.10.005

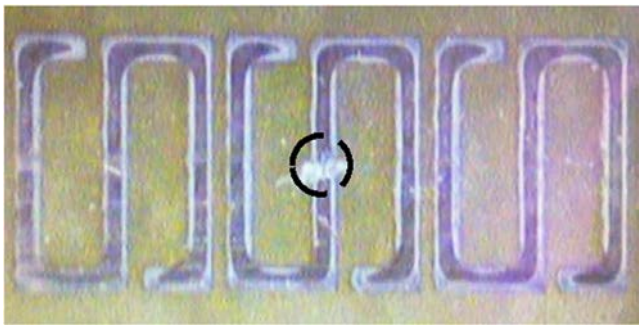

Fig. 6. Photograph of the programmed 10-bit tag, with alternating detuned S-SRRs.

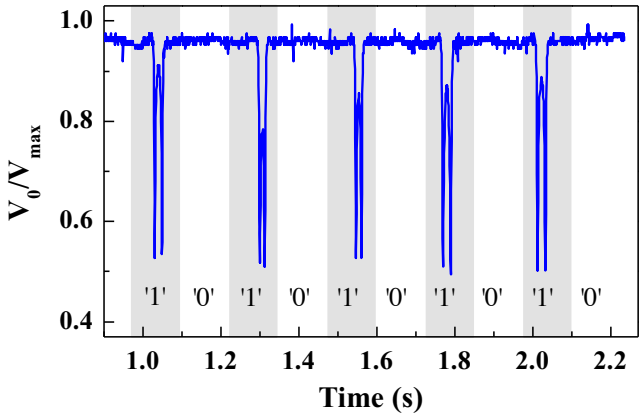

Fig. 7. Measured normalized envelope for the 10-bit chipless RFID tag of Fig. 6.

ting the resonant elements) or by means of inkjet printing (short-circuiting the terminals of the S-SRR) can be envisaged.

6. Conclusions

In conclusion, a chipless-RFID system based on near-field coupling between the tag and the reader and sequential bit reading has been validated by inkjet-printing the tags on a plastic substrate (PEN). Specifically, a 10-bit tag has been fabricated by using S-SRRs as resonant elements. By displacing the tag over the S-SRR-loaded CPW transmission line (active part of the reader) fed by a conveniently tuned harmonic signal, it has been demonstrated that the amplitude of the output signal is efficiently modulated according to the ID code of the tag. The experimental set-up implemented to extract the envelope function has revealed that the ID code is correctly obtained in the considered 10-bit chipless-RFID tags. The information density per area in the designed tags is 7.4 bit/cm^2. In the proposed system, the number of bits is only limited by the area occupied by the printed encoders (chain of resonant elements). Therefore, it is possible to obtain a number of bits comparable to that of chiped tags (96 bits, according to the EPC Class 1 Generation 2 Protocol), since 96 bits only require a S-SRR tag chain with 30.0 cm in length. This length is comparable with the dimensions of standard documents, and hence this approach can be useful for secure paper applications (e.g. for identification and authentication purposes). For such applications, the tags implemented on PEN can be conveniently laminated to embed them in paper substrates. Nevertheless, the next step in this research activity is to directly print the proposed chipless-RFID tags on conveniently functionalized paper. The possibility to program the tags by detuning the resonant elements has been also discussed, and a proof-of-concept, where the '0' state has been achieved by cutting the corresponding resonant elements, has been carried out.

Acknowledgements

This work was supported by MINECO-Spain (projects TEC2013-40600-R, TEC2016-75650-R and RTC-2014-2550-7), *Generalitat de Catalunya* (project 2014SGR-157), *Institució Catalana de Recerca i Estudis Avançats* (who awarded F. Martín), and by FEDER funds. C. Herrojo acknowledges MINECO for supporting his research activity through the FPI grant BES-2014-068164.

References

[1] J. Landt, The history of RFID, IEEE Potentials 24 (2005) 8–11.
[2] S. Preradovic, N.C. Karmakar, Chipless RFID: bar code of the future, IEEE Microw. Mag. 11 (2010) 87–97.
[3] S. Preradovic, N.C. Karmakar, Multiresonator-Based Chipless RFID: Barcode of the Future, Springer, 2011.
[4] N.C. Karmakar R. Koswatta P. Kalansuriya R. E-Azim Chipless RFID Reader Architecture Artech House 2013
[5] E. Perret, Radio Frequency Identification and Sensors: From RFID to Chipless RFID, John Wiley, New York, 2014.
[6] R. Rezaiesarlak, M. Manteghi, Chipless RFID: Design Procedure and Detection Techniques, Springer, 2015.
[7] N.C. Karmakar, M. Zomorrodi, C. Divarathne, Advanced Chipless RFID, John Wiley, Hoboken, NJ, 2016.
[8] C.S. Hartmann, A global SAW ID tag with large data capacity, in: Proceedings of IEEE Ultrasonics Symposium, October 2002, vol. 1, pp. 65–69.
[9] A. Chamarti, K. Varahramyan, Transmission delay line based ID generation circuit for RFID applications, IEEE Microw. Wirel. Compon. Lett. 16 (2006) 588–590.
[10] M. Schüßler, C. Damm, R. Jakoby, Periodically LC loaded lines for RFID backscatter applications, in: Proceedings of Metamaterials 2007, October, Rome, Italy, pp. 103–106.
[11] N. Saldanha, D.C. Malocha, Design parameters for SAW multi-tone frequency coded reflectors, in: 2007 IEEE Ultrasonics Symposium, 2007, pp. 2087–2090.
[12] M. Schüßler, C. Damm, M. Maasch, R. Jakoby, Performance evaluation of left-handed delay lines for RFID backscatter applications, in: Proceedings of the IEEE MTT-S International Microwave Symposium, 2008, pp. 177–180.
[13] S. Harma, V.P. Plessky, C.S. Hartmann, W. Steichen, "Z-path SAW RFID tag, IEEE Trans. Ultrason. Ferroelectric Freq. Control 55 (2008) 208–213.
[14] H. Tao, W. Weibiao, W. Haodong, S. Yongan, Reflection and scattering characteristics of reflectors in SAW tags, IEEE Trans. Ultrason. Ferroelectric Freq. Control 55 (2008) 1387–1390.
[15] S. Harma, V.P. Plessky, L. Xianyi, P. Hartogh, Feasibility of ultra-wideband SAW RFID tags meeting FCC rules, IEEE Trans. Ultrason. Ferroelectric Freq. Control 56 (2012) 812–820.
[16] F.J. Herraiz-Martínez, F. Paredes, G. Zamora, F. Martín, J. Bonache, Printed magnetoinductive-wave (MIW) delay lines for chipless RFID applications, IEEE Trans. Antennas Propag. 60 (2012) 5075–5082.
[17] S. Tedjini, E. Perret, A. Vena, D. Kaddout, Mastering the electromagnetic signature of chipless RFID tags, Chipless and Conventional Radiofrequency Identification, IGI Global, 2012.
[18] S. Preradovic, I. Balbin, N.C. Karmakar, G.F. Swiegers, Multiresonator-based chipless RFID system for low-cost item tracking, IEEE Trans. Microw. Theory Tech. 57 (2009) 1411–1419.
[19] S. Preradovic, N.C. Karmakar, Design of chipless RFID tag for operation on flexible laminates, IEEE Antennas Wirel. Propag. Lett. 9 (2010) 207–210.
[20] O. Rance, R. Siragusa, P. Lemaître-Auger, E. Perret, Toward RCS magnitude level coding for chipless RFID, IEEE Trans. Microw. Theory Tech. 64 (Jul. 2016) 2315–2325.
[21] J. McVay, A. Hoorfar, N. Engheta, Space-filling curve RFID tags, in: Proceedings of 2006 IEEE Radio Wireless Symposium, pp. 199–202.
[22] I. Jalaly, D. Robertson, Capacitively-tuned split microstrip resonators for RFID barcodes, in: Proceedings of European Microwave Conference, October, vol. 2, 2005, pp. 4–7.
[23] H.-S. Jang, W.-G. Lim, K.-S. Oh, S.-M. Moon, J.-W. Yu, Design of low-cost chipless system using printable chipless tag with electromagnetic code, IEEE Microw. Wirel. Compon. Lett. 20 (2010) 640–642.
[24] A. Vena, E. Perret, S. Tedjini, A fully printable chipless RFID tag with detuning correction technique, IEEE Microw. Wirel. Compon. Lett. 22 (4) (2012) 209–211.
[25] A. Vena, E. Perret, S. Tedjini, Design of compact and auto-compensated single-layer chipless RFID tag, IEEE Trans. Microw. Theory Tech. 60 (9) (Sept. 2012) 2913–2924.
[26] A. Vena, E. Perret, S. Tedjini, High-capacity chipless RFID tag insensitive to the polarization, IEEE Trans. Antennas Propag. 60 (10) (2012) 4509–4515.
[27] M.M. Khan, F.A. Tahir, M.F. Farooqui, A. Shamim, H.M. Cheema, 3.56-bits/cm^2 compact inkjet printed and application specific chipless RFID tag, IEEE Antennas Wirel. Propag. Lett. 15 (2016) 1109–1112.

[28] M.A. Islam, N.C. Karmakar, A novel compact printable dual-polarized chipless RFID system, IEEE Trans. Microw. Theory Tech. 60 (2012) 2142–2151.
[29] R. Rezaiesarlak, M. Manteghi, Complex-natural-resonance-based design of chipless RFID tag for high-density data, IEEE Trans. Antennas Propag. 62 (Feb. 2014) 898–904.
[30] M. Svanda, J. Machac, M. Polivka, J. Havlicek, A comparison of two ways to reducing the mutual coupling of chipless RFID tag scatterers, in: Proceedings of 21st International Conference on Microwave, Radar and Wireless Communications (MIKON), May, 2016, pp. 1–4.
[31] A. Vena, E. Perret, S. Tedjini, Chipless RFID tag using hybrid coding technique, IEEE Trans. Microw. Theory Tech. 59 (Dec. 2011) 3356–3364.
[32] A. Vena, E. Perret, S. Tedjini, A compact chipless RFID tag using polarization diversity for encoding and sensing, in: 2012 IEEE International Conference on RFID, 2012, pp. 191–197.
[33] I. Balbin, N.C. Karmakar, Phase-encoded chipless RFID transponder for large scale low cost applications, IEEE Microw. Wirel. Compon. Lett. 19 (2009) 509–511.
[34] S. Genovesi, F. Costa, A. Monorchio, G. Manara, Chipless RFID tag exploiting multifrequency delta-phase quantization encoding, IEEE Antennas Wirel. Propag. Lett. 15 (2015) 738–741.
[35] C. Herrojo, J. Naqui, F. Paredes, F. Martín, Spectral signature barcodes based on S-shaped Split Ring Resonators (S-SRR), EPJ Appl. Metamater. 3 (2016) 1–6.
[36] C. Herrojo, J. Naqui, F. Paredes, F. Martín, Spectral signature barcodes implemented by multi-state multi-resonator circuits for chipless RFID tags, in: IEEE MTT-S International Microwave Symposium (IMS'16), San Francisco, May, 2016.
[37] C. Herrojo, F. Paredes, J. Mata-Contreras, S. Zuffanelli, F. Martín, Multi-state multi-resonator spectral signature barcodes implemented by means of S-shaped Split Ring Resonators (S-SRR), IEEE Trans. Microw. Theory Tech. 65 (7) (2017) 2341–2352.
[38] C. Herrojo, J. Mata-Contreras, F. Paredes, F. Martín, Near-field chipless RFID encoders with sequential bit reading and high data capacity, in: IEEE MTT-S International Microwave Symposium (IMS'17), June, Honolulu, Hawaii, 2017.
[39] H. Chen, L. Ran, J. Huangfu, X. Zhang, K. Chen, T.M. Grzegorczyk, J.A. Kong, Left-handed materials composed of only S-shaped resonators, Phys. Rev. E 70 (5) (2004) 057605.
[40] J. Naqui, J. Coromina, A. Karami-Horestani, C. Fumeaux, F. Martín, Angular displacement and velocity sensors based on coplanar waveguides (CPWs) loaded with S-shaped split ring resonator (S-SRR), Sensors 15 (2015) 9628–9650.
[41] J. Mata-Contreras, C. Herrojo, F. Martín, Application of split ring resonator (SRR) loaded transmission lines to the design of angular displacement and velocity sensors for space applications, IEEE Trans. Microw. Theory Tech. (2017), https://doi.org/10.1109/TMTT.2017.2693981.
[42] C. Herrojo, J. Mata-Contreras, F. Paredes, F. Martín, Microwave encoders for chipless RFID and angular velocity sensors based on S-shaped split ring resonators (S-SRRs), IEEE Sens. J. 17 (15) (2017) 4805–4813.

Please cite this article in press as: C. Herrojo et al., Near-field chipless-RFID tags with sequential bit reading implemented in plastic substrates, Journal of Magnetism and Magnetic Materials (2017), https://doi.org/10.1016/j.jmmm.2017.10.005

Artículo EPJ17

High Data Density and Capacity in Chipless Radiofrequency Identification (Chipless-RFID) Tags Based on Double-chains of S-Shaped Split Ring Resonators (S-SRRs)

C. Herrojo, J. Mata-Contreras, F. Paredes and F. Martín

EPJ Appl. Metamat. 2017, **4**, 8

DOI: 10.1051/epjam/2017008

EPJ Applied Metamaterials

Available online at:
epjam.edp-open.org

RESEARCH ARTICLE OPEN ACCESS

High data density and capacity in chipless radiofrequency identification (chipless-RFID) tags based on double-chains of S-shaped split ring resonators (S-SRRs)

Cristian Herrojo, Javier Mata-Contreras, Ferran Paredes, and Ferran Martín*

CIMITEC, Departament d'Enginyeria Electrònica, Universitat Autònoma de Barcelona, 08193 Bellaterra, Spain

Received: 24 July 2017 / Received in final form: 7 October 2017 / Accepted: 10 October 2017

Abstract. The data density per surface (DPS) is a figure of merit in chipless radiofrequency identification (chipless-RFID) tags. In this paper, it is demonstrated that chipless-RFID tags with high DPS can be implemented by using double-chains of S-shaped split ring resonators (S-SRRs). Tag reading is achieved by near-field coupling between the tag and the reader, a CPW transmission line fed by a harmonic signal tuned to the resonance frequency of the S-SRRs. By transversally displacing the tag over the CPW, the transmission coefficient of the line is modulated by tag motion. This effectively modulates the amplitude of the injected (carrier) signal at the output port of the line, and the identification (ID) code, determined by the presence or absence of S-SRRs at predefined and equidistant positions in the chains, is contained in the envelope function. The DPS is determined by S-SRR dimensions and by the distance between S-SRRs in the chains. However, by using two chains of S-SRRs, the number of bits per unit length that can be accommodated is very high. This chipless-RFID system is of special interest in applications where the reading distance can be sacrificed in favor of data capacity (e.g., security and authentication). Encoding of corporate documents, ballots, exams, etc., by directly printing the proposed tags on the item product to prevent counterfeiting is envisaged.

Keywords: chipless RFID / coplanar waveguide / split ring resonators / high data capacity / security applications

1 Introduction

Transmission lines loaded with split ring resonators (SRRs) and with other electrically small resonators [1–5] have been used in numerous microwave applications, including filters [6,7], enhanced bandwidth components [8], multiband components [9–12], microwave sensors [13–30] and chipless radiofrequency identification (chipless-RFID) tags [31,32], among others. Concerning chipless RFID tags, the interest in this work, transmission lines loaded with multiple resonant elements, each tuned to a different frequency, have been proposed as multi-resonant frequency domain based tags [31–44]. In such chipless-RFID systems, the interrogation signal is a multi-frequency sweeping signal covering the spectral bandwidth of the resonant elements, and the ID code is inferred from the dips present in the frequency response (retransmission based tags) [31–37] or in the radar cross section response (backscattered tags) [38–44], caused by the resonant elements. Therefore, the presence or absence of dips at predefined frequencies (each one corresponding to a different bit) is associated with the logic state '1' or '0'. In general, the data capacity of these frequency-domain based tags is limited due to the required spectral bandwidth necessary to accommodate a large number of bits. Multi-state multi-resonator tags, where more than one bit of information is associated to each resonant element, have been proposed to increase the density of bits per frequency and per surface [36,37]. Another strategy consists of using more than one domain (hybrid tags) [45–49], e.g., encoders based on frequency position and polarization diversity [47], or encoders where frequency domain is combined with phase deviation [46].

Despite the efforts to increase the number of bits with the previous frequency-domain and hybrid chipless-RFID systems, the reported tags do not exhibit the data capacity of chiped tags. Another approach, based on time domain, was recently reported by the authors [50,51]. Within this approach, tags consist of a chain of identical resonant elements etched or printed on a dielectric substrate. The presence or absence of resonant elements at predefined and equidistant positions determines the logic state '1' or '0', and the number of bits is only limited by the area occupied by the tag, since the spectral bandwidth is virtually null in these tags. Therefore, high data capacity can be achieved

* e-mail: Ferran.Martin@uab.cat

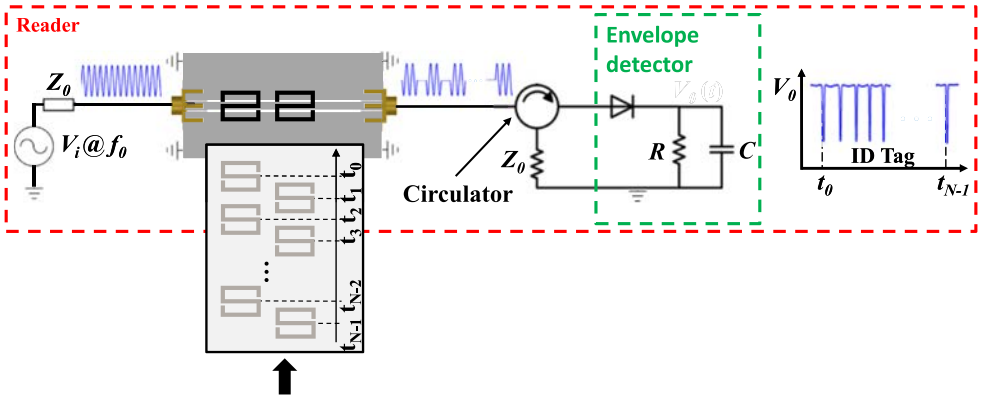

Fig. 1. Illustration showing the working principle of the proposed chipless-RFID system. A double chain of S-SRRs can be appreciated in the tag, according to the strategy to increase the data capacity per unit length proposed in the paper.

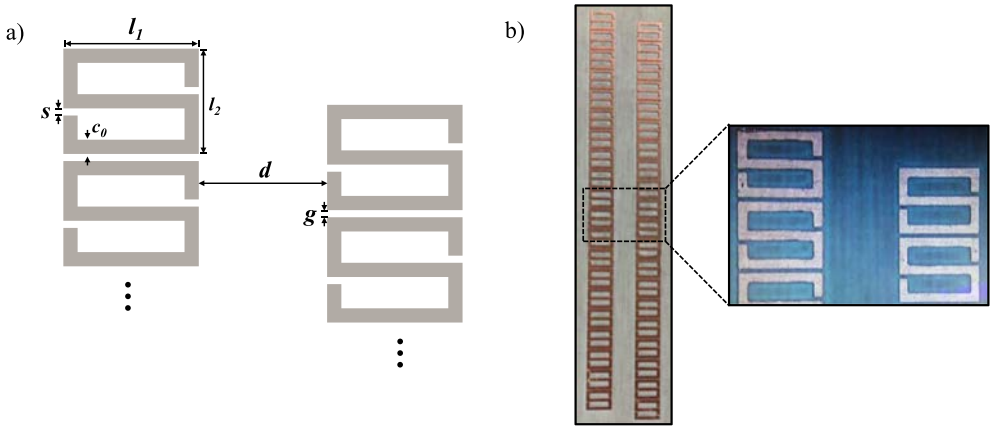

Fig. 2. Layout (zoom) of the double chain of S-SRRs (a) and photograph of the fabricated 40-bit chipless RFID tag (b). S-SRR dimensions are (in mm) $l_1 = 3.8$, $l_2 = 2.96$, $c_0 = 0.4$, $s = 0.2$, $g = 0.2$ and $d = 3.6$.

with this novel time-domain chipless-RFID systems. Nevertheless, in order to reduce the space occupied by the tags as much as possible, it is important to optimize the data density per surface (DPS), accommodating the largest possible number of resonant elements in a certain area.

In [50,51], the resonant elements are S-shaped split ring resonators S-SRRs. Tag reading proceeds sequentially through tag motion, by transversally displacing the tag over a coplanar waveguide transmission line fed by a harmonic signal tuned to the resonance frequency of the S-SRRs. By this means, the transmission coefficient of the line is modulated through near-field coupling between the line and the resonant elements. That is, each time an S-SRRs is aligned with the line axis, line-to-resonator coupling is maximized and the transmission coefficient is consequently minimized. This variable coupling, dictated by the presence or absence of resonant elements in the chain as the tag is displaced, effectively modulates the amplitude of the feeding (carrier) signal at the output port of the line, and the identification (ID) code is contained in the envelope function of the amplitude modulated (AM) signal. By using a simple envelope detector, the tag ID can thus be inferred. Figure 1 illustrates the working principle of this time-domain chipless RFID system based on near-field coupling.

In [51], 40-bit tags, occupying an area of 5.34 cm^2 and a chain length of 14 cm, were demonstrated. In this paper, we have doubled the number of bits, without significantly increasing the tag length (the critical dimension) by using a double-chain of resonant elements. The strategy to implement the double chain and the necessary modifications of the CPW transmission line (reader) are reported in this paper. The proposed system is validated by reading several fabricated tags with our experimental setup, and the ID code is obtained by visualizing the envelope function in an oscilloscope.

2 Tag and reader design and fabrication

Concerning the tags, they are based on the resonant elements used in [50,51], i.e., S-SRRs [52–54]. However, a double chain of S-SRRs is considered in this paper, with a relative displacement between S-SRR chains of half a chain period. The dimensions of the S-SRRs are those considered in [50,51]. A detail of the layout of the double S-SRR chain is depicted in Figure 2(a), whereas Figure 2(b) shows the picture of the 40-bit fabricated encoder with all the resonant elements present. The considered substrate for

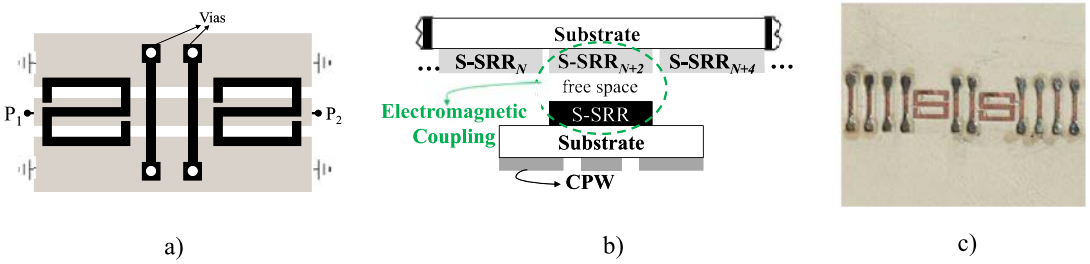

Fig. 3. Layout (a), cross sectional view including the tag (b) and photograph (c) of the designed and fabricated S-SRR-loaded CPW acting as active part of the reader. In (c) only the backside of the CPW is shown.

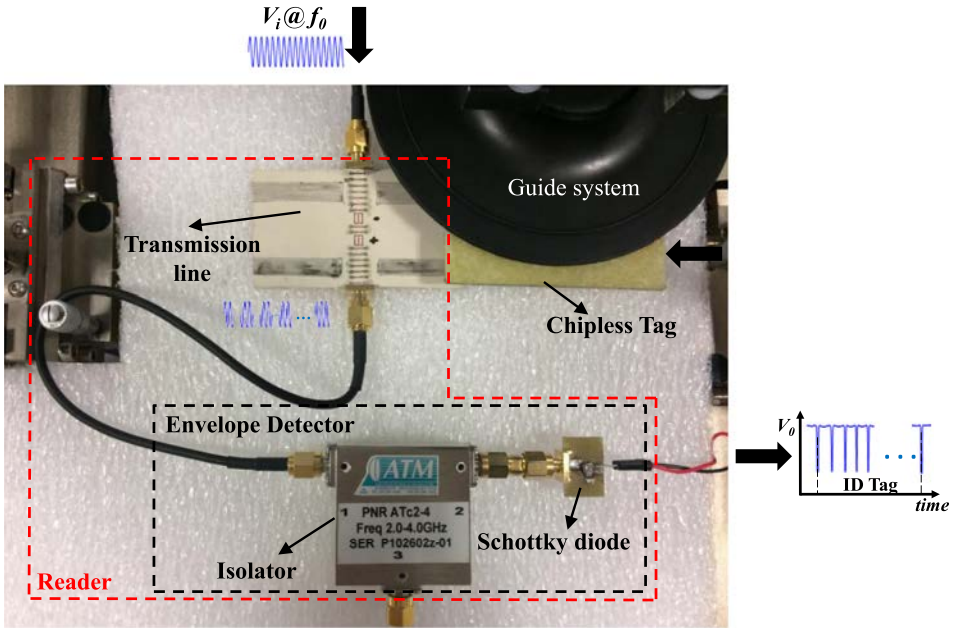

Fig. 4. Photograph of the experimental set-up.

tag implementation is the *Rogers RO4003C* with thickness $h = 203\,\mu$m, dielectric constant $\varepsilon_r = 3.55$ and tan $\delta = 0.0021$.

Let us now consider the design of the CPW transmission line of the reader. In [50,51], a S-SRR identical to those of the tag was etched in the back substrate side of the CPW, a 50 Ω line. The purpose of this resonant element etched in the reader side is to prevent from the appearance of inter-resonator coupling in the tag chain (through magnetoinductive waves [55–60]) as well as multiple couplings between the line and the S-SRRs of the chain [30]. The key aspect is that when one of the S-SRRs of the tag chain is perfectly aligned with the S-SRR of the reader, both particles can be viewed as a single particle, the broadside coupled S-SRR (BC-S-SRR), with smaller fundamental resonance. Thus, by tuning the frequency of the carrier feeding signal to the frequency of the BC-S-SRR, or slightly higher, the above-cited extra couplings are avoided. The reason is that the resonance frequency of the individual S-SRR is substantially higher.

If two chains of S-SRRs are considered in the tag (with a relative displacement of half a unit cell), this means that, consequently, two S-SRRs must be etched in the backside of the CPW transmission line. The distance between the S-SRRs in the CPW must be identical to the transverse distance between the S-SRR chains. Through this approach, if a S-SRR is etched in a certain predefined position, either in the outer or inner tag chain, the corresponding '1' state will be detected, since the coupling with the line is ensured. Figure 3 shows the layout, cross sectional view and photograph of the proposed and fabricated S-SRR-loaded CPW. The structure has been fabricated in the *Rogers RO3010* with thickness $h = 0.635$ mm, dielectric constant $\varepsilon_r = 10.2$.

3 Experimental set-up and validation

The photograph of the complete system is depicted in Figure 4. The frequency of the carrier signal is set to $f_c = 4$ GHz, which is the one corresponding to the BC-S-SRR by considering an air gap of 0.25 mm. By varying the air gap distance, the resonance frequency of the BC-S-SRR, f_0, obviously changes. If the carrier frequency is chosen as $f_c = f_0$ for a certain gap distance, and the air gap increases significantly, it may give rise to reading errors. The reason is that f_0 increases, and hence the modulation index decreases. Nevertheless, some tolerance exists since the

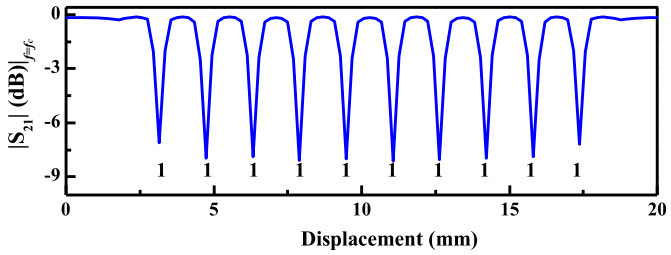

Fig. 5. Transmission coefficient at f_c, as the linear 10-bit tag is displaced above the S-SRR-loaded CPW transmission line, inferred from electromagnetic simulation using *Keysight Momentum*, by considering an aig gap of 0.25 mm.

notch, centered at f_0, exhibits certain bandwidth. Moreover, we can fine tune the carrier frequency in order to match it to the resonance frequency of the BC-SRR.

Before the experimental validation (to be discussed next), we have obtained the transmission coefficient at f_c through electromagnetic simulation, by considering a linearly shaped double S-SRR chain with all the SRRs present at the predefined positions (specifically, we have considered five S-SRRs in either chain, corresponding to a 10-bit encoder with ID code '1111111111'). The simulated response, obtained by displacing the tag over the S-SRR loaded CPW and depicted in Figure 5, reveals that the tag functionality is achieved.

In practice, the carrier signal is generated by means of the *Agilent E44338C* function generator. The output port of the S-SRR-loaded CPW is connected to an isolator (implemented with the *ATM ATc4-8* circulator) in order to prevent from mismatching reflections caused by the diode, an *Avago HSMS-2860* device. Such diode is the essential part of the envelope detector, used for rectification purposes. Filtering is achieved by means of the *N2795A* active probe (with resistance $R = 1\,\mathrm{M\Omega}$ and capacitance $C = 1\,\mathrm{pF}$), connected to the *Agilent MSO-X-3104A* oscilloscope in order to visualize the envelope function providing the ID code.

Reading of three different encoders has been carried out by means of the proposed set-up. The envelope function of the 40-bit encoder with all resonators present at the predefined positions (code 1 of Fig. 6) has been modified to achieve codes 2 and 3 of Figure 6. Specifically, we have cut some resonators, making them inoperative (i.e., equivalent to their absence, or '0' logic state) and hence programming the ID code corresponding to codes 2 and 3 of Figure 6. A drilling machine has been used to cut the required resonant elements along their symmetry plane. The data density per surface of the proposed tags is $\mathrm{DPS} = 5.53\,\mathrm{bit/cm^2}$, and the number of bits per unit length is 5.7 bit/cm. Since tag reading proceeds sequentially, necessarily the longitudinal dimension of the proposed tags is much larger than the transverse dimension, the later being independent on the number of bits and given by the transverse size of the double S-SRR chain. Therefore, the critical aspect, provided a large number of bits is required, is the number of bits per unit length. With the resulting density of bits per unit length,

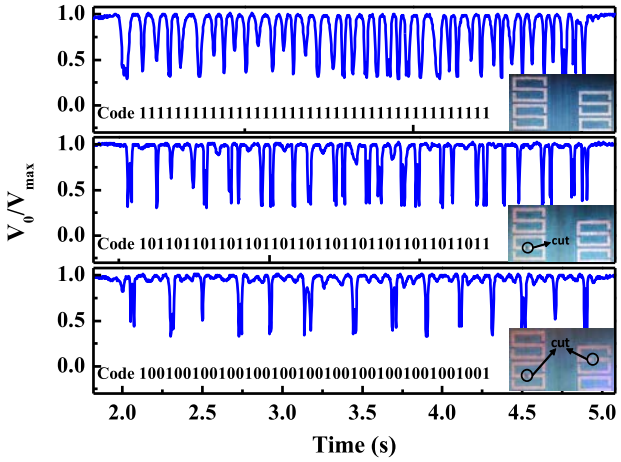

Fig. 6. Envelope functions of the 40-bit tags with the indicated codes.

it is possible to encode standard European documents (of size 29.7 cm × 21.0 cm) with 170 bits printed along the longer paper side.

4 Conclusions

In conclusion, a chipless-RFID system based on near-field and sequential bit reading, with tags implemented by double chains of S-SRRs, has been proposed. As compared to previous S-SRR based tags implemented with single chains of SRRs, the reported tags exhibit roughly twice the data density per unit length (i.e., 5.7 bit/cm). The strategy to accommodate such high bit density in the tags, as well as the modifications in the reader (S-SRR-loaded CPW), necessary to properly read the tags, has been discussed.

The possibility to program the tags by detuning the resonant elements has been also demonstrated, and a proof-of-concept, where the '0' state has been achieved by cutting the corresponding resonant elements, has been carried out. The reported high data capacity chipless-RFID system is contactless but needs proximity between the tag and the reader. It is thus of special interest in applications where a large number of bits is necessary, and read distance can be sacrificed. Encoding of secure documents, e.g., to avoid counterfeiting, is one of the envisaged applications. Work is in progress to implement the proposed tags in plastic and paper substrates.

This work was supported by MINECO-Spain (projects TEC2013-40600-R and TEC2016-75650-R), by *Generalitat de Catalunya* (project 2014SGR-157), by *Institució Catalana de Recerca i Estudis Avançats* (who awarded Ferran Martín), and by FEDER funds.

References

1. F. Martin, Artificial Transmission Lines for RF and Microwave Applications (John Wiley, Hoboken, NJ, USA, 2015)
2. R. Marques, F. Martín, M. Sorolla, Metamaterials with Negative Parameters: Theory, Design and Microwave Applications (John Wiley, Hoboken, NJ, USA, 2007)

3. F. Martín, F. Falcone, J. Bonache, R. Marqués, M. Sorolla, Split ring resonator based left handed coplanar waveguide, Appl. Phys. Lett. **83**, 4652 (2003)
4. F. Falcone, T. Lopetegi, J.D. Baena, R. Marqués, F. Martín, M. Sorolla, Effective negative-ε stop-band microstrip lines based on complementary split ring resonators, IEEE Microw, Wireless Compon. Lett. **14**, 280 (2004)
5. J.D. Baena, J. Bonache, F. Martín, R. Marqués, F. Falcone, T. Lopetegi, M.A.G. Laso, J. García, I. Gil, M. Flores-Portillo, M. Sorolla, Equivalent circuit models for split ring resonators and complementary split rings resonators coupled to planar transmission lines, IEEE Trans. Microw. Theory Techn. **53**, 1451 (2005)
6. J. Bonache, F. Martín, I. Gil, J. García-García, R. Marqués, M. Sorolla, Microstrip bandpass filters with wide bandwidth and compact dimensions, Microw. Opt. Technol. Lett. **46**, 343 (2005)
7. J. Bonache, I. Gil, J. García-García, F. Martín, Novel microstrip band pass filters based on complementary split rings resonators, IEEE Trans. Microw. Theory Techn. **54**, 265 (2006)
8. G. Sisó, J. Bonache, M. Gil, F. Martín, Application of resonant-type metamaterial transmission lines to the design of enhanced bandwidth components with compact dimensions, Microw. Opt. Technol. Lett. **50**, 127 (2008)
9. J. Bonache, G. Sisó, M. Gil, A. Iniesta, J. García-Rincón, F. Martín, Application of composite right/left handed (CRLH) transmission lines based on complementary split ring resonators (CSRRs) to the design of dual band microwave components, IEEE Microw. Wireless Compon. Lett. **18**, 524 (2008)
10. M. Durán-Sindreu, A. Vélez, F. Aznar, G. Sisó, J. Bonache, F. Martín, Application of open split ring resonators and open complementary split ring resonators to the synthesis of artificial transmission lines and microwave passive components, IEEE Trans. Microw. Theory Techn. **57**, 3395 (2009)
11. F.J. Herraiz-Martínez, G. Zamora, F. Paredes, F. Martín, J. Bonache, Multiband printed monopole antennas loaded with open complementary split ring resonators for PANs and WLANs, IEEE Ant. Wirel. Propag. Lett. **10**, 1528 (2011)
12. F.J. Herraiz-Martínez, F. Paredes, G. Zamora, F. Martín, J. Bonache, Dual-band printed dipole antenna loaded with open complementary split-ring resonators (OCSRRs) for wireless applications, Microw. Opt. Technol. Lett. **54**, 1014 (2012)
13. J. Naqui, M. Durán-Sindreu, F. Martín, Novel sensors based on the symmetry properties of split ring resonators (SRRs), Sensors **11**, 7545 (2011)
14. C. Mandel, B. Kubina, M. Schüßler, R. Jakoby, Passive chipless wireless sensor for two-dimensional displacement measurement, in: Proceedings of 41st European Microwave Conference, Manchester, UK, 2011, pp. 79–82
15. M. Puentes, C. Weiss, M. Schüßler, R. Jakoby, Sensor array based on split ring resonators for analysis of organic tissues, IEEE MTT-S Int. Microwave Symp. Dig., Baltimore, Maryland, June 2011
16. M.S. Boybay, O.M. Ramahi, Material characterization using complementary split-ring resonators, IEEE Trans. Instrum. Meas. **61**, 3039 (2012)
17. C.-S. Lee, C.-L. Yang, Complementary split-ring resonators for measuring dielectric constants and loss tangents, IEEE Microw. Wireless Compon. Lett. **24**, 563 (2014)
18. A. Ebrahimi, W. Withayachumnankul, S. Al-Sarawi, D. Abbott, High-sensitivity metamaterial-inspired sensor for microfluidic dielectric characterization, IEEE Sens. J. **14**, 1345 (2014)
19. C.-L. Yang, C.-S. Lee, K.-W. Chen, K.-Z. Chen, Noncontact measurement of complex permittivity and thickness by using planar resonators, IEEE Trans. Microw. Theor. Technol. **64**, 247 (2016)
20. L. Su, J. Mata-Contreras, P. Vélez, F. Martín, Estimation of conductive losses in complementary split ring resonator (CSRR) loading an embedded microstrip line and applications, in: IEEE MTT-S Int. Microw. Symp. (IMS'17), Honolulu, Hawaii, June 2017
21. J. Naqui, M. Durán-Sindreu, F. Martín, Alignment and position sensors based on split ring resonators, Sensors **12**, 11790 (2012)
22. A. Karami-Horestani, C. Fumeaux, S.F. Al-Sarawi, D. Abbott, Displacement sensor based on diamond-shaped tapered split ring resonator, IEEE Sens. J. **13**, 1153 (2013)
23. A.K. Horestani, J. Naqui, D. Abbott, C. Fumeaux, F. Martín, Two-dimensional displacement and alignment sensor based on reflection coefficients of open microstrip lines loaded with split ring resonators, Electron. Lett. **50**, 620 (2014)
24. J. Naqui, F. Martín, Transmission lines loaded with bisymmetric resonators and their application to angular displacement and velocity sensors, IEEE Trans. Microw. Theor. Technol. **61**, 4700 (2013)
25. J. Naqui, F. Martín, Angular displacement and velocity sensors based on electric-LC (ELC) loaded microstrip lines, IEEE Sens. J. **14**, 939 (2014)
26. J. Naqui, J. Coromina, A. Karami-Horestani, C. Fumeaux, F. Martín, Angular displacement and velocity sensors based on coplanar waveguides (CPWs) loaded with S-shaped split ring resonator (S-SRR), Sensors **15**, 9628 (2015)
27. L. Su, J. Mata-Contreras, J. Naqui, F. Martín, Splitter/combiner microstrip sections loaded with pairs of complementary split ring resonators (CSRRs): modeling and optimization for differential sensing applications, IEEE Trans. Microw. Theor. Technnol. **64**, 4362 (2016)
28. L. Su, J. Mata-Contreras, J. Naqui, F. Martín, Configurations of splitter/combiner microstrip sections loaded with stepped impedance resonators (SIRs) for sensing applications, Sensors **16**, 2195 (2016), doi:10.3390/s16122195
29. J. Naqui, F. Martín, Application of broadside-coupled split ring resonator (BC-SRR) loaded transmission lines to the design of rotary encoders for space applications, IEEE MTT-S Int. Microw. Symp. (IMS'16), San Francisco, 2016
30. J. Mata-Contreras, C. Herrojo, F. Martín, Application of split ring resonator (SRR) loaded transmission lines to the design of angular displacement and velocity sensors for space applications, IEEE Trans. Microw. Theory Techn. (to be published)
31. S. Preradovic, N.C. Karmakar, Chipless RFID: bar code of the future, IEEE Microw. Mag. **11**, 87 (2010)
32. S. Preradovic, N.C. Karmakar, Multiresonator-based chipless RFID: barcode of the future (Springer, 2011)
33. S. Preradovic, I. Balbin, N.C. Karmakar, G.F. Swiegers, Multiresonator-based chipless RFID system for low-cost item tracking, IEEE Trans. Microw. Theor. Technol. **57**, 1411 (2009)

34. S. Preradovic, N.C. Karmakar, Design of chipless RFID tag for operation on flexible laminates, IEEE Anten. Wirel. Propag. Lett. **9**, 207 (2010)
35. C. Herrojo, J. Naqui, F. Paredes, F. Martín, Spectral signature barcodes based on s-shaped split ring resonators (S-SRR), EPJ Appl. Metamater. **3**, 1 (2016)
36. C. Herrojo, J. Naqui, F. Paredes, F. Martín, Spectral signature barcodes implemented by multi-state multi-resonator circuits for chipless RFID tags, in: IEEE MTT-S International Microwave Symposium (IMS'16), San Francisco, 2016
37. C. Herrojo, F. Paredes, J. Mata-Contreras, S. Zuffanelli, F. Martín, Multi-state multi-resonator spectral signature barcodes implemented by means of S-shaped Split Ring Resonators (S-SRR), IEEE Trans. Microw. Theor. Technol. **65**, 2341 (2017)
38. O. Rance, R. Siragusa, P. Lemaître-Auger, E. Perret, Toward RCS magnitude level coding for chipless RFID, IEEE Trans. Microw. Theor. Technol. **64**, 2315 (2016)
39. J. McVay, A. Hoorfar, N. Engheta, Space-filling curve RFID tags, in: Proceedings of 2006 IEEE Radio Wireless Symposium, 2006, pp. 199–202
40. I. Jalaly, D. Robertson, Capacitively-tuned split microstrip resonators for RFID barcodes, in: Proceedings of European Microwave Conference, 2005, pp. 4–7
41. H.-S. Jang, W.-G. Lim, K.-S. Oh, S.-M. Moon, J.-W. Yu, Design of low-cost chipless system using printable chipless tag with electromagnetic code, IEEE Microw. Wireless Compon. Lett. **20**, 640 (2010)
42. A. Vena, E. Perret, S. Tedjini, A fully printable chipless RFID tag with detuning correction technique, IEEE Microw. Wirel. Compon. Lett. **22**, 209 (2012)
43. A. Vena, E. Perret, S. Tedjini, Design of compact and auto-compensated single-layer chipless RFID tag, IEEE Trans. Microw. Theor. Technol. **60**, 2913 (2012)
44. A. Vena, E. Perret, S. Tedjini, High-capacity chipless RFID tag insensitive to the polarization, IEEE Trans. Ant. Propag. **60**, 4509 (2012)
45. M.A. Islam, N.C. Karmakar, A novel compact printable dual-polarized chipless RFID system, IEEE Trans. Microw. Theor. Technol. **60**, 2142 (2012)
46. A. Vena, E. Perret, S. Tedjini, Chipless RFID tag using hybrid coding technique, IEEE Trans. Microw. Theor. Technol. **59**, 3356 (2011)
47. A. Vena, E. Perret, S. Tedjini, A compact chipless RFID tag using polarization diversity for encoding and sensing, in: 2012 IEEE Int. Conf. RFID, 2012, pp. 191–197
48. I. Balbin, N.C. Karmakar, Phase-encoded chipless RFID transponder for large scale low cost applications, IEEE Microw. Wirel. Comp. Lett. **19**, 509 (2009)
49. S. Genovesi, F. Costa, A. Monorchio, G. Manara, Chipless RFID tag exploiting multifrequency delta-phase quantization encoding, IEEE Ant. Wirel. Propag. Lett. **15**, 738 (2015)
50. C. Herrojo, J. Mata-Contreras, F. Paredes, F. Martín, Near-Field chipless RFID encoders with sequential bit reading and high data capacity, in: IEEE MTT-S Int. Microw. Symp. (IMS'17), Honolulu, Hawaii, 2017
51. C. Herrojo, J. Mata-Contreras, F. Paredes, F. Martín, Chipless RFID tags based on metamaterial concepts, in: The 11th International Congress on Engineered Material Platforms for Novel Wave Phenomena (Metamaterials), 2017
52. H. Chen, L. Ran, J. Huangfu, X. Zhang, K. Chen, T.M. Grzegorczyk, J.A. Kong, Left-handed materials composed of only S-shaped resonators, Phys. Rev. E. **70**, 1 (2004)
53. H. Chen, L. Ran, J. Huangfu, X. Zhang, K. Chen, T.M. Grzegorczyk, J.A. Kong, Negative refraction of a combined double S-shaped metamaterial, Appl. Phys. Lett. **86**, 151909 (2005)
54. H. Chen, L.-X. Ran, H.-F. Jiang Tao, X.-M. Zhang, K.-S. Cheng, T.M. Grzegorczyk, J.A. Kong, Magnetic properties of S-shaped split ring resonators, Prog. Electromagn. Res. **51**, 231 (2005)
55. E. Shamonina, V.A. Kalinin, K.H. Ringhofer, L. Solymar, Magneto-inductive waveguide, Electron. Lett. **38**, 371 (2002)
56. E. Shamonina, V.A. Kalinin, K.H. Ringhofer, L. Solymar, Magneto-inductive waves in one, two and three dimensions, J. Appl. Phys. **92**, 6252 (2002)
57. M.C.K. Wiltshire, E. Shamonina, I.R. Young, L. Solymar, Dispersion characteristics of magneto-inductive waves: comparison between theory and experiment, Electron. Lett. **39**, 215 (2003)
58. E. Shamonina, L. Solymar, Properties of magnetically coupled metamaterial elements, J. Magn. Magn. Mat. **300**, 38 (2006)
59. R.R.A. Syms, E. Shamonina, V. Kalinin, L. Solymar, A theory of metamaterials based on periodically loaded transmission lines: interaction between magnetoinductive and electromagnetic waves, J. Appl. Phys. **97**, 064909 (2005)
60. M.J. Freire, R. Marqués, F. Medina, M.A.G. Laso, F. Martin, Planar magnetoinductive wave transducers: theory and applications, Appl. Phys. Lett. **85**, 4439 (2004)

Cite this article as: Cristian Herrojo, Javier Mata-Contreras, Ferran Paredes, Ferran Martín, High data density and capacity in chipless radiofrequency identification (chipless-RFID) tags based on double-chains of S-shaped split ring resonators (S-SRRs), EPJ Appl. Metamat. 2017, **4**, 8

Artículo TMTT17

Near-Field Chipless-RFID System with High Data Capacity for Security and Authentication Applications

C. Herrojo, J. Mata-Contreras, A. Núñez, F. Paredes,
E. Ramon and F. Martín

Near-Field Chipless-RFID System With High Data Capacity for Security and Authentication Applications

Cristian Herrojo, *Graduate Student Member, IEEE*, Javier Mata-Contreras, Alba Núñez, Ferran Paredes, *Associate Member, IEEE*, Eloi Ramon, and Ferran Martín, *Fellow, IEEE*

***Abstract*— A high data capacity chipless radio frequency identification (chipless-RFID) system, useful for security and authentication applications, is presented in this paper. Reading is based on the near-field coupling between the tag, a chain of identical split-ring resonators (SRRs) printed on a (typically flexible) dielectric substrate (e.g., liquid crystal polymer, plastic, and paper), and the reader. Encoding is achieved by the presence or absence of SRRs at predefined (equidistant) positions in the chain, and tag identification (ID) is based on sequential bit reading. Namely, the tag must be longitudinally displaced, at short distance, over the reader, a microstrip line loaded with an SRR and fed by a harmonic signal. By this means, the harmonic signal is amplitude modulated, and the (ID) code is contained in the envelope function, which can be obtained by means of an envelope detector. With this system, tag reading requires proximity with the reader, but this is not an issue in many applications within the domain of security and authentication (e.g., secure paper for corporate documents and certificates). Several circularly shaped 40-bit encoders (implemented in a commercial microwave substrate), and the corresponding reader, are designed and fabricated as proof-of-concept demonstrators. Strategies for programming the tags and a first proof-of-concept chipless-RFID tag fabricated on plastic substrate through inkjet printing are included in this paper.**

***Index Terms*— Chipless radio frequency identification (chipless-RFID), microstrip technology, split ring resonators (SRRs).**

I. Introduction

CHIPLESS radio frequency identification (chipless-RFID) is an alternative to chipped-RFID systems for the identification (ID), tracking, and/or authentication of objects and items, where the silicon integrated circuit (IC) is replaced with a printable passive encoder [1]–[6]. Such encoder contains a unique signature that can be identified by means of an RF (or microwave) interrogation signal in frequency, time, or hybrid domains. The main advantage of chipless-RFID over RFID systems based on tags equipped with microchips is the low cost of the encoders, which can be fabricated by means of (additive) printing techniques, such as screen printing, rotogravure, flexography or inkjet, or, obviously, by means of photoetching. However, size and data capacity (crucial aspects of any ID system) of printable encoders reported to date are not competitive with the negligible dimensions and high memory storage capacity of silicon ICs.

Many efforts have been made in recent years to alleviate the previous limitations of chipless-RFID tags. There are two main approaches for data encoding in chipless RFID: time-domain reflectometry (TDR) [7]–[16] and spectral signature [1], [2], [17]–[36]. TDR-based tags exhibit fast responses as compared to frequency-domain tags, but their bit encoding capability is limited since tag ID is generated by the echoes of a pulsed signal (caused by discontinuities or impedance mismatches), and either large delay lines or very narrow pulses are needed to avoid overlapping of the reflected pulses. Therefore, most efforts to increase the data storage capacity have been focused on the frequency-domain-based tags. In this case, encoders are based on resonant elements tuned at predefined frequencies covering a certain spectral bandwidth. Encoding is achieved by the presence or absence of abrupt spectral features in the amplitude, phase, or group delay responses, and tag reading requires a multifrequency interrogation signal covering the whole spectral bandwidth of interest.

Spectral signature barcodes (as they are usually designated to point out the similarity with optical barcodes) can be of two main types: retransmission-based [17], [18] and backscattered-based [19], [25] tags. The former consists of a transmission line loaded with resonant elements (or with resonant elements coupled to it) and two cross-polarized antennas, one for reception and one for transmission, so that interference between the interrogation signal and the retransmitted encoded signal is minimized. By contrast, in backscattered tags, the resonant elements act as receiving and transmitting antennas and provide the spectral signature through the radar cross-sectional peaks. Typically, backscattered chipless tags are more compact since antennas are not required.

Manuscript received June 20, 2017; revised September 6, 2017 and October 14, 2017; accepted October 20, 2017. Date of publication November 14, 2017; date of current version December 12, 2017. This work was supported in part by MINECO-Spain under Project TEC2013-40600-R, Project TEC2016-75650-R, and Project RTC-2014-2550-7, in part by the Generalitat de Catalunya under Project 2014SGR-157, in part by the Institució Catalana de Recerca i Estudis Avançats (who awarded F. Martín), and in part by FEDER funds. The work of C. Herrojo was supported by MINECO through the FPI under Grant BES-2014-068164. This paper is an expanded version of [41], presented at the IEEE MTT-S International Microwave Symposium Conference. *(Corresponding author: Cristian Herrojo.)*

C. Herrojo, J. Mata-Contreras, F. Paredes, and F. Martín are with GEMMA/CIMITEC, Departament d'Enginyeria Electrònica, Universitat Autònoma de Barcelona, 08193 Barcelona, Spain (e-mail: cristian.herrojo@uab.cat; Ferran.Martin@uab.es).

A. Núñez and E. Ramon are with the Institut de Microelectrònica de Barcelona, IMB-CNM (CSIC), 08193 Barcelona, Spain.

Color versions of one or more of the figures in this paper are available online at http://ieeexplore.ieee.org.

Digital Object Identifier 10.1109/TMTT.2017.2768029

In frequency-domain-based tags, the number of bits is typically given by the number of resonant elements. Strategies to enhance the number of bits without an increase in the number of resonators (and hence bandwidth and size) include multistate multiresonator tags [34]–[36] and hybrid tags [27], [30]–[33]. The former exploits the fact that more than two states can be achieved by a single resonant element. Particularly, in retransmission-based tags the multistate functionality can be obtained through the controllability of the attenuation level of notches (amplitude response) achieved by rotation [35], [36]. Hybrid tags are multidomain tags where more than one domain (e.g., time, frequency, phase, and polarization) are used simultaneously in order to achieve more than one bit of information per resonant element. Examples of hybrid tags include encoders based on frequency position and polarization diversity [31], and encoders where the frequency domain is combined with phase deviation [30].

In spite of the recent efforts to increase the number of bits, mainly focused on increasing the spectral efficiency (bits/gigahertz), the reported chipless-RFID tags are far from the data capacity of chipped tags. In [36], it was shown that by sacrificing reading distance, and by using the concept of near-field (inductive) coupling between the tag and the reader, an information density per frequency of 16 bit/GHz can be achieved. In such multistate multiresonator tags, implemented by S-shaped split ring resonator (S-SRRs), a resonant particle introduced in [37]–[39], and used in several applications (e.g., sensors [40]), the resonant elements are etched in a different dielectric layer than the transmission line, a coplanar waveguide (CPW) acting as reader (front end). Tag reading requires proper alignment and contact between the tag and the transmission line (reader), which is not necessarily an issue in certain applications such as security and authentication, as reported in [36]. However, it is difficult in practice to increase the information density per surface and frequency by means of these tags since it is not possible to increase the number of states per resonator beyond four (as in [36]).

In this paper, a different and unconventional approach, first reported in [41], to significantly enhance the number of bits of chipless tags is used for the implementation of 40-bit chipless tags. The approach is based on sequential bit reading, and it is achieved by displacing the tag, a chain of identical resonators, over a transmission line (reader) fed by a harmonic signal. The presence or absence of resonant elements at predefined equidistant positions in the resonator chain modulates the input (carrier) signal, so that the ID code is present in the envelope of the modulated signal. Note that the interrogation signal is simply a harmonic signal. In these new chipless RFID tags, the information is given by the presence or absence of resonant elements at predefined positions. Equivalently, the ID code, obtained from the envelope function in the time domain, is given by the presence or absence of notches at predefined times. Conceptually, the working principle for tag reading in these chipless-RFID tags is similar to the one of the angular velocity sensors reported in [42] and [43].

The main innovation of the proposed system comes in the form of a reduced form factor of the tags by cutting out antennas, not using spectral features, and using sequential bit reading through motion of the tag over the reader. As compared to the work in [41], we report here a chipless RFID system where the reader is a microstrip line loaded with an SRR [44], [45] and the resonator chain uses the same resonant elements but rotated 180°. The implementation of the active part of the reader in the microstrip technology is important for backside isolation. Moreover, vias are not necessary. An important difference as compared to the chipless-RFID system proposed in [41] concerns the fact that the SRR-loaded line (reader) reported here is configured as a bandpass filter with a deep notch above the passband. The harmonic feeding signal is tuned to the frequency of maximum transmission. However, the system is designed in such a way that when an SRR of the tag lies on top of the SRR of the reader, the frequency response experiences a shift and the carrier frequency is strongly attenuated due to the shift in the transmission zero position. With this strategy, the dynamic range, or modulation index, is enhanced, as compared to [41]. We report 40-bit chipless RFID tags, which are circularly shaped for proper reading through a step motor used previously by Naqui and Martín [42] and Mata-Contreras *et al*. [43] for angular velocity measurements.

This paper is organized as follows. The working principle is succinctly summarized in Section II. The layout of the reader and the topology of the resonant elements are presented in Section III. The lumped-element equivalent circuit model of the structure and the method to extract the parameters are also included in this section. In Section IV, an exhaustive analysis of the proposed system, useful to determine the convenient carrier frequency of the feeding signal, is carried out. The effects of the air gap separation and lateral misalignments are also discussed in this section. The experimental setup for tag reading, as well as the fabricated tags, a set of four 40-bit tags implemented in the four quadrants of a circularly shaped narrow and flexible dielectric layer, is presented in Section V. The envelopes inferred from tag reading, corresponding to different chipless tags, and providing the ID codes, are also provided in Section V. Section VI is devoted to a discussion on different strategies for programmable tags based on resonator detuning, and it is demonstrated that by mechanically cutting the resonators along their symmetry plane, detuning, and consequently tag reconfigurability, is achieved. In this section, it is also demonstrated that the proposed chipless-RFID system works by printing the tags on plastic substrates of interest in many applications including security and authentication. Finally, the main conclusions are highlighted in Section VII.

II. Working Principle

The working principle of the proposed chipless-RFID system is based on the near-field coupling between the tag, a chain of identical resonant elements (SRRs), and the active part of the reader, an SRR-loaded microstrip line configured as bandpass filter. The SRR of the line is identical to the SRRs of the tags, but rotated 180°. The ID code is inferred sequentially and by proximity; namely, the SRR chain of the tag must be longitudinally (i.e., in the direction of the line axis) displaced

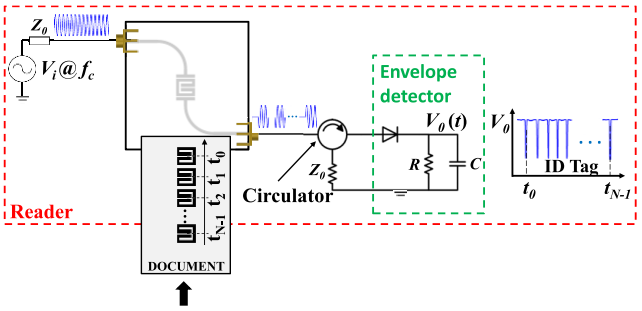

Fig. 1. Sketch of the proposed chipless-RFID system, consisting of the tag (set of resonators printed or etched on a substrate) and the reader (within the dashed rectangle), constituted by the harmonic generator, the SRR-loaded transmission line, the circulator, and the envelope detector.

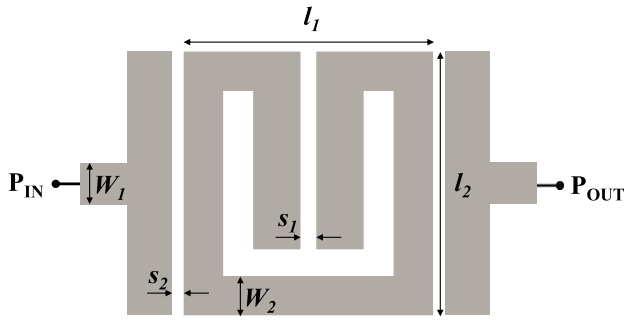

Fig. 2. Topology of the reader. Dimensions are (in mm): $l_1 = 3.16$, $l_2 = 3.35$, $s_1 = 0.2$, $s_2 = 0.2$, $W_1 = 0.56$, and $W_2 = 0.5$. The distance between adjacent SRRs (it they are present) in the tag chain is 0.2 mm.

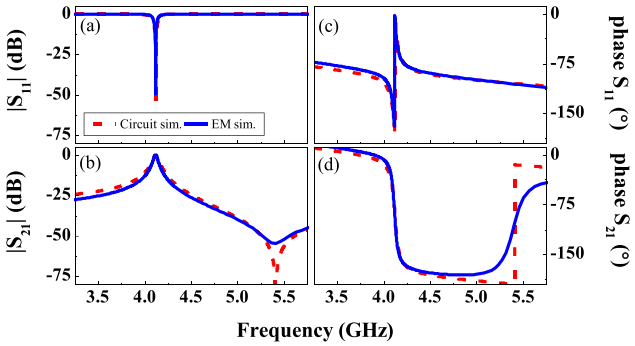

Fig. 3. Frequency response of the structure of Fig. 2 inferred from lossless electromagnetic and circuit simulation. (a) Magnitude of S_{11}. (b) Magnitude of S_{21}. (c) Phase of S_{11}. (d) Phase of S_{21}. The extracted parameters of the lumped element equivalent circuit (in reference to Fig. 4) are: $L_r = 27.1$ nH, $C_r = 0.03$ pF, $C_g = 0.05$ pF, and $C_p = 0.76$ pF.

above the position of the SRR of the line. The distance between the line SRR and the SRR chain (air gap separation) must be small, in order to favor the coupling between the SRR of the line and those of the chain.

Through tag motion, the frequency response of the SRR-loaded line varies substantially provided the coupling between the line and tag SRRs is efficiently modulated. To this end, small distances (air gap) are necessary. Moreover, the relative 180° orientation between the SRR of the line and those of the tag chain is necessary, since such orientation enhances the coupling in the optimum position (i.e., the one with perfectly aligned line and tag SRRs) [46], [47]. By contrast, when the tag chain is located with the intermediate positions between two adjacent SRRs just on top of the center of the line SRR, the coupling is negligible. Tag motion results in shifts in the frequency response which are intimately related to the coupling level for the vertically aligned SRRs. The consequence of these shifts is the modulation of the transmission coefficient of the SRR-loaded line with tag motion. If a harmonic (carrier) signal tuned to a certain frequency is injected to the input port of the SRR-loaded line, the signal at the output port is modulated by tag motion, and the ID code is contained in the envelope of the modulated signal. The sketch of the proposed chipless RFID system is depicted in Fig. 1.

In the proposed chipless-RFID tags, the logic "1" and "0" states are given by the presence or absence of SRRs at predefined and equidistant positions in the chain. To enhance sensitivity, it is convenient to choose the carrier frequency exhibiting the maximum excursion (variation) of the transmission coefficient with tag motion. Through this choice, the modulation index is optimized, and the logic states can be better discerned in a reading operation. This aspect will be discussed in Section IV. Nevertheless, the SRR-loaded microstrip structure acting as bandpass filter provides a large excursion between maximum and minimum transmission, and this represents a clear advantage as compared to the system proposed in [41].

III. Reader and Tag Topologies and Lumped-Element Equivalent Circuit Model

The active part of the reader, a microstrip line loaded with an SRR, is depicted in Fig. 2. The SRR is folded in order to reduce its electrical size. As mentioned before, the SRRs of the tag chain are identical, but rotated 180° (hence the topology is not repeated). In view of Fig. 2, it follows that the structure exhibits a bandpass behavior, and filter bandwidth is related to the width of the slot between the resonant element and the access lines, s_2. The frequency response of the structure of Fig. 2, inferred from the full-wave electromagnetic simulation (using *Keysight Momentum*), is depicted in Fig. 3. (The parameters of the *Rogers RO3010* substrate, with thickness $h = 0.635$ mm, dielectric constant $\varepsilon_r = 10.2$, and loss tangent $\tan\delta = 0.0022$, have been considered.) The transmission coefficient exhibits a transmission zero, given by the intrinsic resonance frequency of the SRRs, and a pole (or reflection zero), where all the injected power is transmitted to the output port (neglecting the effect of losses). This response is very useful for our purposes, due to the large insertion loss at the transmission zero frequency (with direct impact on the modulation index of the output signal in a reading operation, as will be later shown).

The structure of Fig. 2 can be described by the lumped-element π-circuit model depicted in Fig. 4. The parallel resonant tank L_r–C_r accounts for the SRR, whereas C_g and C_p take into account the effect of the slots and the capacitance to ground. (Losses are not considered in the model since the main aim is to justify the presence of the transmission zero.) In order to validate this model, the four reactive parameters must

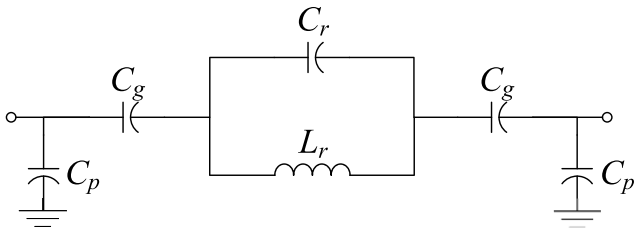

Fig. 4. Lumped element equivalent circuit model of the SRR-loaded microstrip line of Fig. 2.

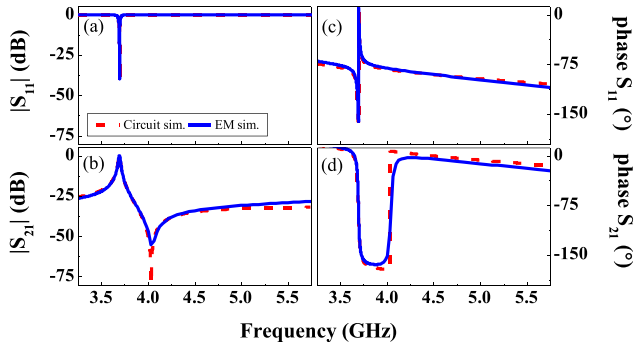

Fig. 5. Frequency response of the structure of Fig. 2 with tag cover as explained in the text, inferred from lossless electromagnetic and circuit simulation. (a) Magnitude of S_{11}. (b) Magnitude of S_{21}. (c) Phase of S_{11}. (d) Phase of S_{21}. The extracted parameters of the lumped element equivalent circuit are: $L_r = 11.9$ nH, $C_r = 0.13$ pF, $C_g = 0.05$ pF, and $C_p = 0.87$ pF.

be extracted. To this end, a procedure similar to those reported in [47]–[49] in reference to another type of resonator loaded lines is considered. Note that four conditions are necessary to unequivocally determine the four model parameters. The first condition is the transmission zero frequency, where the parallel resonant tank opens

$$f_z = \frac{1}{2\pi\sqrt{L_r C_r}}. \tag{1}$$

A second condition involving the elements of the series branch is the frequency where such branch shorts, i.e., it exhibits a null reactance. Such frequency, obtained by forcing the reactance of the resonant tank L_r–C_r plus the capacitance C_g to be zero, is

$$f_s = \frac{1}{\pi\sqrt{2L_r(C_g + 2C_r)}}. \tag{2}$$

Note that this frequency can be inferred from the reflection coefficient S_{11} represented in the Smith chart, since at that frequency the trace of S_{11} intersects the unit conductance circle. From the value of the parallel reactance, directly given by the Smith chart, the shunt capacitance values (C_p) are derived (third condition). Finally, at the reflection zero frequency f_r or frequency with maximum transmission, the iterative impedance, given by

$$Z_0(\omega) = \sqrt{\frac{Z_s(\omega)Z_p(\omega)/2}{1 + (Z_s(\omega)/2Z_p(\omega))}} \tag{3}$$

must be the reference impedance of the ports (50 Ω). This is the fourth and last condition, necessary to determine the elements of the circuit model. In (3), Z_s and Z_p are the impedance of the series and shunt branch of the π-circuit.

Application of the previous parameter extraction procedure gives the reactive parameters indicated in Fig. 3, where the circuit simulation of the frequency response (obtained by means of *Keysight ADS*) is also depicted. The good agreement between the lossless electromagnetic and circuit simulation validates the proposed circuit model of the SRR-loaded microstrip line (some discrepancies in the vicinity of f_z are due to radiation, not accounted for by the circuit model). Note that the considered lossless model is of interest as long as such model predicts the position of the reflection and transmission zero frequencies, relevant to this paper. In coherence with the lossless model, parameter extraction has been carried out from the lossless electromagnetic simulation. Parameter extraction from the measured results is also possible, but the inclusion of resistors in the model should be considered (as in [48]). Nevertheless, our purpose has been to provide a lossless model in order to gain insight into the design of the proposed near-field chipless systems.

The frequency response depicted in Fig. 3 corresponds to the SRR-loaded microstrip line without tag loading, i.e., surrounded by air. Let us now consider that the structure is loaded with the tag, and particularly for a tag position corresponding to perfectly aligned SRRs. For this position, referred to as reference position (REF), the pair of vertically aligned SRRs forms the so-called broadside-coupled SRR (BC-SRR) [46], [47]. This composite particle is characterized by a strong electric coupling between the individual SRRs, provided the air gap separation between them is small enough. The consequence is a significant decrease of the fundamental resonance frequency of the composite particle (BC-SRR), resulting in an overall shift of the transmission coefficient toward lower frequencies. By considering that the air gap separation is 265 μm (this value will be justified later), that the SRR of the tag is etched on the *Rogers RO4003C* substrate with thickness $h = 0.204$ mm, dielectric constant $\varepsilon_r = 3.55$, and loss tangent $\tan\delta = 0.0021$, and that this narrow substrate is attached to *FR4* (with thickness $h = 1.6$ mm, dielectric constant $\varepsilon_r = 4.7$, and loss tangent $\tan\delta = 0.014$) for mechanical stability, the resulting frequency response (inferred from electromagnetic simulation) is the one depicted in Fig. 5. Note that if the tag is attached to a different material, its effects can be taken into account at simulation and design level. Nevertheless, some tolerance exists in the material used to provide mechanical stability, due to the large excursion of the transmission coefficient experienced by tag motion. The circuit simulation with extracted parameters is also depicted in Fig. 5. (The parameters are indicated in the caption of Fig. 5.) Again, a good agreement between the lossless circuit and electromagnetic simulation is obtained. Interestingly, C_g and C_p have not experienced a significant variation as compared to the structure without tag cover, as expected. The main variation corresponds to the capacitance of the resonant element (BC-SRR), which has experienced an increase of roughly four times due to the broadside (face-to-face) capacitance between the metal strips of the particle.

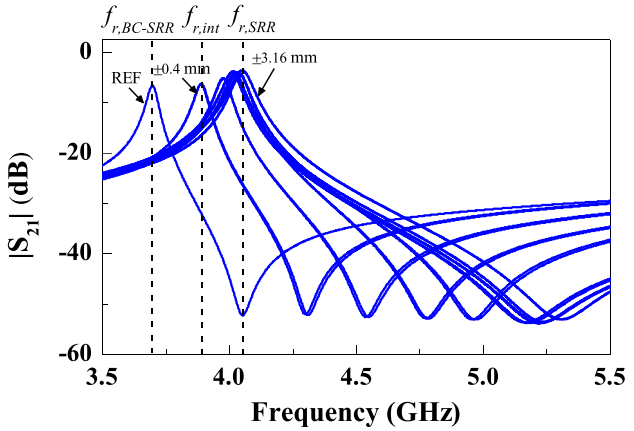

Fig. 6. Transmission coefficient (magnitude) of the SRR-loaded line of Fig. 2 with tag cover, for different relative positions between the SRR of the line and the SRR of the tag. Relevant frequencies, discussed in the text, are indicated. These results have been inferred by electromagnetic simulation.

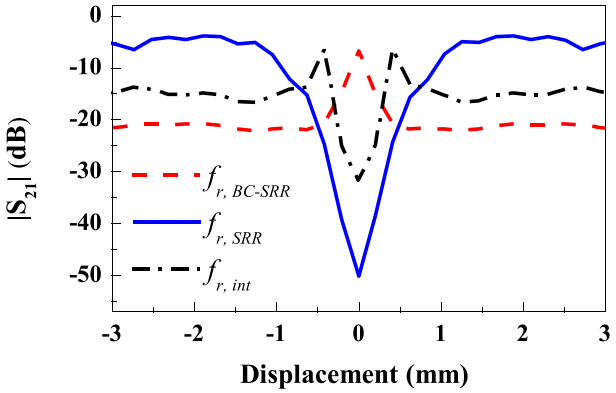

Fig. 7. Variation of the transmission coefficient as a function of the relative displacement for the indicated frequencies. These results have been inferred by electromagnetic simulation.

IV. Analysis and Optimization

The frequency response of the tag loaded structure for different relative positions between the SRR of the tag and the one of the line is depicted in Fig. 6. (Tag displacement is in the direction of the line axis.) In this case, losses have been considered since the maximum and minimum values of the transmission coefficient are important. The considered air gap separation is the one in reference to the response of Fig. 5 (i.e., 265 μm). As anticipated before, departure from the REF position modifies (shifts up) the transmission and reflection zero frequencies. Fig. 7 depicts the variation of the transmission coefficient as a function of the relative displacement for specific frequencies (indicated in the figure). One of these frequencies is the reflection zero frequency for the case of perfectly aligned SRRs (forming the BC-SRR). Let us designate this frequency as $f_{r,\mathrm{BC-SRR}}$. The transmission coefficient for this frequency is a maximum for the REF position. Departure from this position reduces the transmission coefficient, but it saturates to roughly -22 dB for a relatively small displacement. We have also depicted the variation of the transmission coefficient for the reflection zero frequency of the structure with completely misaligned SRRs. Note that this frequency is similar, but not identical, to the reflection zero

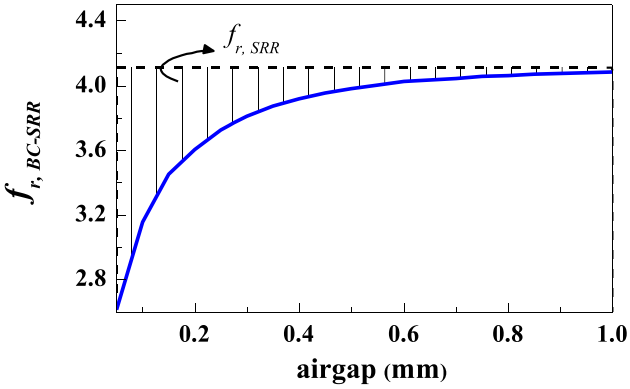

Fig. 8. Variation of $f_{r,\mathrm{BC-SRR}}$ with the air gap separation. These results have been inferred by electromagnetic simulation.

frequency of the structure without tag loading. The reason is that the presence of the tag substrate slightly modifies the resonance frequency of the SRR of the line. Nevertheless, this frequency is not influenced by the SRR of the tag, and hence it can be called $f_{r,\mathrm{SRR}}$ (to point out that this frequency is only given by the SRR of the line). For $f_{r,\mathrm{SRR}}$, the excursion (dynamic range) experienced by the transmission coefficient is close to 45 dB, i.e., -50 dB for the REF position, and roughly -5 dB for displacements above 1 mm. Finally, we have considered an intermediate frequency, called $f_{r,\mathrm{int}}$, corresponding to the reflection zero frequency for a displacement of 0.4 mm. In this case, the transmission coefficient as a function of the displacement exhibits a deep notch for the REF position, a maximum for a displacement of 0.4 mm, as expected, and then the transmission coefficient saturates to -15 dB as the relative displacement increases.

In view of Fig. 7, it is convenient to set the frequency of the feeding signal, or carrier frequency, to $f_c = f_{r,\mathrm{SRR}}$. The reason is that for this frequency, the maximum dynamic range is obtained. Nevertheless, by choosing the carrier frequency between $f_{r,\mathrm{BC-SRR}}$ and $f_{r,\mathrm{SRR}}$, the variation of the transmission coefficient is significant, and the value of the maximum transmission coefficient is close to the ideal value of 0 dB. Note that by setting f_c to values above $f_{r,\mathrm{SRR}}$ the dynamic range is also considerable, but the value of maximum transmission progressively decreases as f_c increases, a situation that must be avoided to prevent deterioration of the modulation index. Thus, according to this analysis, the frequency of the feeding signal (carrier frequency) must satisfy $f_{r,\mathrm{BC-SRR}} < f_c < f_{r,\mathrm{SRR}}$, but, preferably, it must be as close as possible to $f_{r,\mathrm{SRR}}$. This window for f_c is interesting from a practical viewpoint, since it is difficult to exactly predict the position of the optimum frequency, $f_{r,\mathrm{SRR}}$. This analysis reveals that the proposed system is not very sensitive to frequency drifts, this being a relevant aspect.

One important parameter notably influencing the behavior/performance of the proposed chipless RFID system is the air gap distance. As the gap increases, the SRR-loaded line is more insensitive to the presence of the tag, since the coupling between the SRR of the line and the SRR of the tag decreases. By increasing the air gap, $f_{r,\mathrm{BC-SRR}}$ increases, whereas $f_{r,\mathrm{SRR}}$ remains constant. Fig. 8 depicts the variation

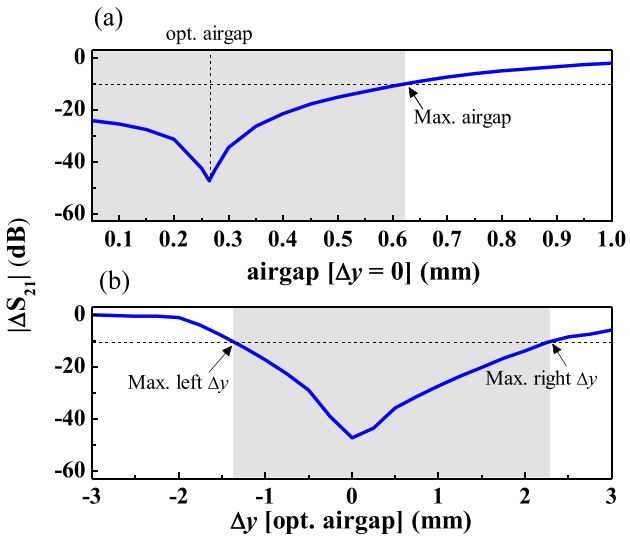

Fig. 9. Tolerance analysis for vertical and lateral displacement of the tag on the maximum variation of the transmission coefficient. (a) Effects of air gap variation. (b) Effects of lateral shift. The mechanical system used to provide relative motion between tag and reader must guarantee lateral and vertical misalignments within the indicated tolerance limits. These results have been inferred by electromagnetic simulation.

of $f_{r,\mathrm{BC-SRR}}$ with the air gap. It can be seen that the window for f_c decreases as the air gap increases. Nevertheless, the window is significant up to reasonable gap distances.

Let us now consider that the carrier frequency is set to the optimum frequency, $f_c = f_{r,\mathrm{SRR}}$, and let us represent the excursion experienced by the transmission coefficient with the air gap when the SRRs of the line and tag are perfectly aligned. The result, depicted in Fig. 9(a), reveals that there is an optimum gap spacing, 265 μm, providing the maximum variation of the transmission coefficient. The particularity of this gap separation is that, for perfectly aligned SRRs, the transmission zero frequency exactly coincides with the reflection zero frequency of the structure without tag on top of it, i.e., $f_{r,\mathrm{SRR}}$, which is in turn the carrier frequency. It should be highlighted, however, that this optimum gap space has been calculated for a particular carrier frequency, i.e., $f_c = f_{r,\mathrm{SRR}}$. If the carrier frequency is slightly below $f_{r,\mathrm{SRR}}$, then it is necessary to decrease the gap in order to allocate the transmission zero, for the perfectly aligned SRRs, at the position of the carrier frequency. Thus, the optimum gap separation depends on the carrier frequency, but such optimum gap separation increases with f_c. Since f_c should not be chosen to be higher than $f_{r,\mathrm{SRR}}$, it follows that $f_{r,\mathrm{SRR}}$ is the optimum carrier frequency, provided the optimum gap distance is the largest one within the interval. Nevertheless, small variations of f_c in the vicinity of $f_{r,\mathrm{SRR}}$ (with the gap set to the optimum value at $f_{r,\mathrm{SRR}}$) do also give significant excursions in the transmission coefficient.

In order to analyze the tolerance against lateral shifts of the tag with regard to the line axis, Fig. 9(b) depicts the maximum variation of the transmission coefficient for the optimum frequency $f_{r,\mathrm{SRR}}$ and the optimum gap separation at this frequency (265 μm). As can be seen, laterally shifting the tag degrades the excursion of the transmission coefficient.

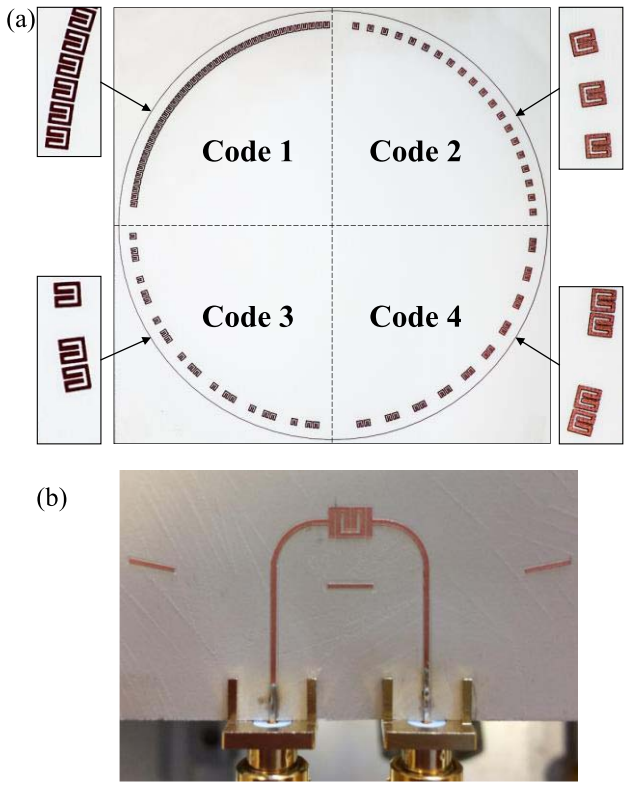

Fig. 10. Photograph of the fabricated (a) 40-bit chipless-RFID tags and (b) active part of the reader.

However, by considering a tolerance limit of −10 dB for a reliable reading operation, it follows that lateral shifts between −1.3 and +2.3 mm are within the allowable limits for misalignment in the transverse direction. These values are very reasonable on account of the considered SRR dimensions. It is worth mentioning that the tolerance interval is not symmetric. The reason is the lack of symmetry of the structure with regard to the line axis. However, due to the symmetry with regard to the midplane between the input and the output port for perfectly aligned SRRs, it follows that tag displacement in the positive or negative direction, from the REF position, along the line axis is undistinguishable. For this reason, the curves of Fig. 7 exhibit perfect symmetry.

V. Fabricated Tags, Experimental Setup, and Results

The in-house system for the measurement of the tag response is based on a step motor that provides angular motion to a rotor. For this reason, the fabricated chipless-RFID tags have been implemented as circular chains of SRRs. In particular, we have considered four different 40-bit tags based on the SRRs considered in the previous sections (see the dimensions in Fig. 2) and implemented on a narrow substrate attached to *FR4* for mechanical stability (see Section III in reference to Fig. 5). Such tags are allocated in the four quadrants of a circle [see Fig. 10(a)]. However, the whole structure can be viewed as a single 160-bit tag as well. The photograph of the SRR-loaded line (active part of the reader) is depicted in Fig. 10(b). Note that the 50 Ω access lines

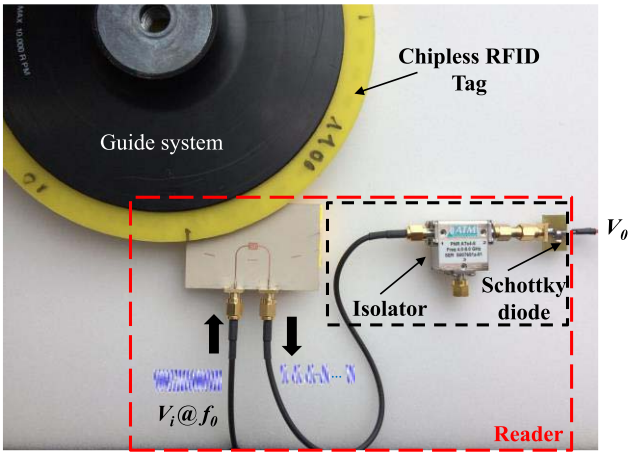

Fig. 11. Experimental setup used for tag reading.

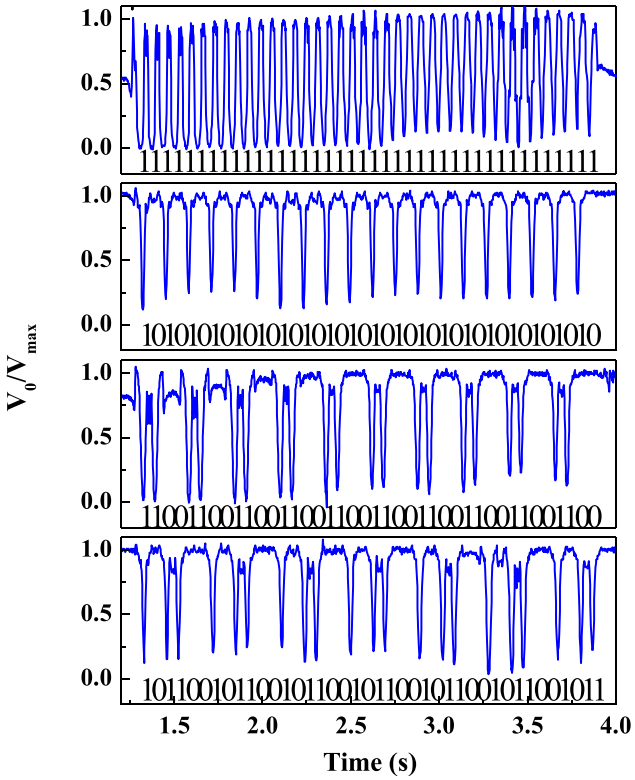

Fig. 12. Measured normalized envelope for the 40-bit fabricated tags. The depth of the dips, corresponding to the logic state "1," is significantly larger as compared to the system in [41].

have been bent to avoid mechanical friction between the port connectors and the tag during tag motion.

The photograph of the experimental setup is shown in Fig. 11. The *Agilent E4438C* function generator has been used to feed the SRR-loaded line through a harmonic signal tuned to $f_c = f_{r,\mathrm{SRR}} = 4$ GHz. This frequency provides reasonable SRR size and it is compatible with our measurement equipment, and system components. The envelope detector has been implemented by means of a Shottky diode (*Avago HSMS-2860*) and a low-pass filter. In practice, the low-pass filter functionality has been achieved by means of an active probe (*N2795A*), with resistance $R = 1$ MΩ and capacitance $C = 1$ pF, connected to an oscilloscope. Such oscilloscope (the *Agilent MSO-X-3104A*) is used to visualize the envelope function, providing the tag ID code. In order to avoid unwanted reflections from the Schottky diode (a highly nonlinear device), a circulator (model *ATM ATc4-8*), configured as an isolator, has been cascaded between the output port of the SRR-loaded line and the Shottky diode, similar to the system in [41]. Finally, the step motor *STM 23Q-3AN* is used to provide angular motion to the tags. The response of the four fabricated chipless tags is depicted in Fig. 12, where the ID codes are indicated. The logic states "1" and "0" are given by the presence and absence, respectively, of SRRs at the predefined positions, as mentioned before. The angular velocity of the step motor has been set to 5.33 r/min. It can be seen that the notches in the time response perfectly correlate with the logic state "1." The significant dip depth indicates that the reader is very sensitive for the detection of the logic state "1" and hence it is a robust system for tag ID. Thus, the results presented in Fig. 12 validate the proposed approach for the determination of the tag ID codes. The area of each 40-bit tag is as small as 4.75 cm^2 (corresponding to a density of 8.4 $\mathrm{bit/cm}^2$). Note that by increasing the number of bits of the tags, the time required to read a tag also increases. However, in practice, the tag reading speed may be large since the carrier frequency (4 GHz) is very large as compared to the rhythm of SRR crossing above the reader, imposed by any reasonable, but large, shifting speed of the tag. Tag displacement speed does not have any influence on system performance, since, as mentioned, any reasonable speed is necessarily small as compared to the carrier frequency. Nevertheless, in a real scenario, tag speed is actually limited by the sampling time of the data acquisition system, which must be significantly smaller than that of the temporal width of the dips.

VI. Discussion

An important aspect of chipless-RFID systems, with direct impact on cost, concerns the possibility of implementing programmable tags. As we have previously discussed, the presence or absence of resonant elements at the predefined tag positions determines the logic state of each bit. Note, however, that this approach is not optimum from the point of view of overall costs. In a real scenario, where tags are implemented by printing processes using conductive inks, the cost of the necessary ink for tag fabrication is small (calculated in the range of less than one eurocent) as compared to the price of typical RFID chips. However, each ID code requires a specific layout, and this may represent a significant cost burden, especially if high-quality massive printing processes are required for tag fabrication (e.g., rotogravure).

An alternative approach, of special interest if thousands of high data capacity tags are necessary, is to fabricate all-identical tags with all the resonators printed at the predefined positions (representing an optimum cost solution). Tag encoding (programming) can then be done in a later (low cost) stage by making inoperative those resonant elements with

Fig. 13. Photograph of the detuned SRR.

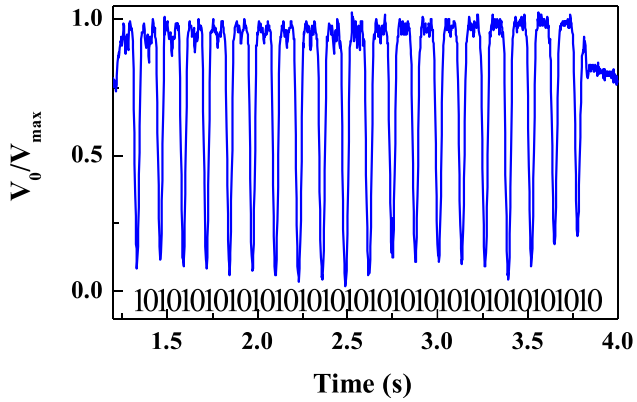

Fig. 14. Measured normalized envelope for the 40-bit programmed tag.

required "0" state. In this context, inoperative resonators means detuned resonators, i.e., with fundamental resonance significantly shifted. Resonator detuning can be achieved, e.g., by short-circuiting the resonant elements (an approach proposed in [17] for frequency-domain multiresonator spectral signature barcodes) or by physically cutting the resonant elements. In a real scenario, short-circuiting can be achieved by inkjet printing (requiring a minimum quantity of ink and sintering at room temperature), whereas resonator cutting can be achieved, for instance, by laser ablation.

In this paper, a proof-of-concept to demonstrate the programmable capability of the proposed chipless-RFID tags has been carried out. To this end, the 40-bit encoder with all resonators present at the predefined positions (code 1 of Fig. 10) has been modified (programmed). Specifically, we have cut alternate resonators, making them inoperative and hence programming the ID code corresponding to code 2 of Fig. 10. A drilling machine has been used to cut the required resonant elements along their symmetry plane. (The photograph of one of such detuned resonators is depicted in Fig. 13.) The measured normalized envelope function corresponding to this programmed tag is depicted in Fig. 14, where it can be appreciated that the 40-bit ID code is given by alternating states "1" and "0," as expected.

The functionality of the proposed chipless-RFID system has been demonstrated by tags implemented in a commercial (narrow) low-loss microwave substrate. However, the interest in a real application devoted to security and/or authentication is the implementation of these chipless-RFID tags on low-cost plastic or paper substrates through standard printing processes (e.g., rotogravure, and screen printing), and, eventually, programming in a later stage, as discussed

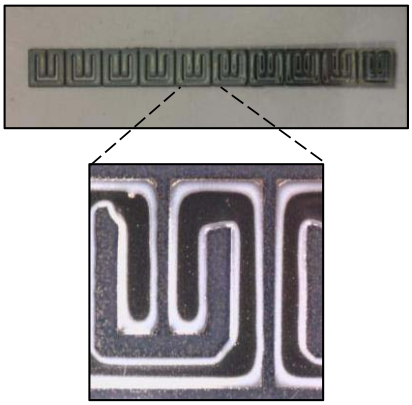

Fig. 15. Photograph of the 10-bit printed chipless tag implemented on PEN substrate.

before. Note that in applications such as secure paper (e.g., for anticounterfeiting of corporate documents, certificates, and ballots), the ideal solution is to directly print the tags on the tagged item (paper). Alternatively, a plastic substrate, with intermediate electromagnetic properties between commercial low-loss microwave substrates and paper, located in a specific region of the tagged item, can be considered for tag printing.

As a first proof-of-concept toward this direction, we have fabricated, by inkjet printing, a 10-bit tag with all bits set to "1" (all resonators present and functional) on the Polyethilene naphthalate (PEN) film (*Dupont Teijin Q65FA*) (Fig. 15). The used inkjet printer is the *Ceradrop CeraPrinter X-Serie*, and two layers of *DuPontPE410* conductive ink (with a measured conductivity of 7.28 S/m $\times 10^6$ S/m) have been printed in order to achieve a measured thickness of 3.3–3.5 μm. The considered substrate (PEN) has a measured thickness, dielectric constant, and loss tangent of $h = 0.125$ mm, $\varepsilon_r = 3.36$, and $\tan\delta = 0.0042$, respectively. For tag reading, the tag has been attached to the *FR4* substrate to provide mechanical stability.

Since the SRR chain is linear (see Fig. 15), rather than using the step motor, we have linearly displaced the tag over the SRR of the line (reader) through our available positioning system, which allows for manual linear motion in two dimensions (x, y). Apart from that, the setup for tag reading (i.e., for obtaining the envelope function) is identical to that described in Section V. The measured envelope function corresponding to the tag of Fig. 15 is depicted in Fig. 16. Ten dips, corresponding to the ten SRRs, can be perfectly appreciated. (The lower depth of the 2 s dip is due to fabrication related tolerances; nevertheless the ID code can be perfectly identified.) Hence, the proposed chipless RFID system is validated by considering plastic substrates and resonant elements printed on it.

We would like also to highlight that the proposed chipless-RFID system is conceived by taking into account that the relative speed between the tag and the reader should be constant. However, different (constant) velocities can be considered, preferably high in order to reduce the time needed for tag reading. In order to know such velocity, necessary for tag reading, one possibility is to add a pair of symbols (SRRs) at the beginning of the chain. The time distance between these

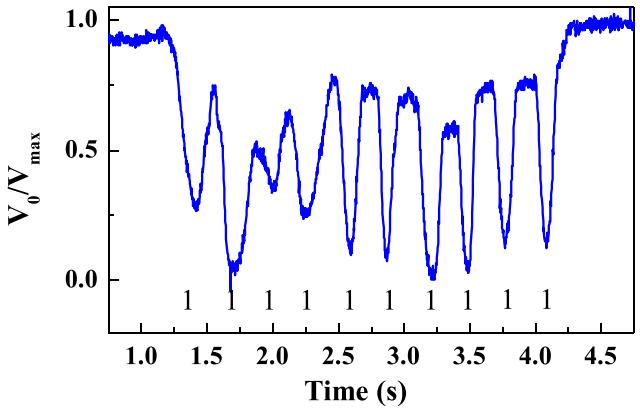

Fig. 16. Measured normalized envelope for the 10-bit programmed tag.

pair of symbols, read as logic "1," determine the time positions where tag must be read.

As previously mentioned, the main advantage of chipless RFID over RFID systems with tags equipped with chips is the lower cost of the chipless tags. In many applications involving thousands or millions of tags, or in order to tag low-cost items, chipless RFID is fully justified even at the expense of potentially higher cost in the reader side (in our case due to the mechanical elements needed to provide tag motion). Nevertheless, concerning the electronics of the reader of the proposed system, it is relatively low cost. Note that in a real scenario, the function generator should be replaced by a harmonic oscillator, and the information contained in the tag can be inferred by means of a low-cost postprocessing unit (out of the scope of this paper). Potential applications of the proposed near-field chipless-RFID system in the field of security and authentication include authentication and ID of corporate documents, ballots, exams, certificates, etc.

VII. Conclusion

In conclusion, we have presented a chipless-RFID system based on the near-field coupling and sequential bit reading that constitutes an improvement as compared to the first version reported in [41]. The tags are simply a set of identical resonant elements (SRRs) etched or printed on a dielectric substrate forming a chain, and the presence or absence of resonant elements at predefined positions in the chain determines the logic state. Reading is achieved by proximity between the tag and the reader, an SRR-loaded microstrip line fed by a harmonic signal (carrier). Specifically, it has been demonstrated that by displacing the tag (SRR chain) above the SRR of the line, the transmission coefficient is efficiently modulated, and this modulation is dictated by the presence/absence of SRRs in chain. The result is that the amplitude of the carrier signal is modulated at the output port of the microstrip line, and the ID code is contained in the envelope function. The main advantages of the proposed approach as compared to chipless RFID system proposed in [41] are as follows.

1) Vias are not required, since a microstrip line, rather than a CPW, is used as active part of the reader.
2) Backside isolation in the reader is guaranteed by the presence of the ground plane in the back substrate side.
3) The modulation index is high due to the high excursion of the transmission coefficient with the relative position between the tag and the SRR-loaded line.

Moreover, it has been found that the system is tolerant to air gap variations (distance between the tag and the SRR of the reader) up to 0.6 mm, and to lateral tag shifts up to 1.3 mm, which are very reasonable values on account of the dimensions of the tag SRRs. The number of bits of the proposed system is only limited by the space occupied by the tag chain, since tag reading simply requires a harmonic (single-tone continuous wave) signal. The achieved density of bits per area is as high as 8.4 bit/cm^2. Therefore, high data capacity (at the expense of reading by proximity), useful in applications such as security and authentication, is achievable. Particularly, applications in secure paper, where the tag ID can be directly printed on a paper substrate, and reading can be merely achieved by a mechanical system able to provide tag motion above the reader (plus the necessary electronics), are envisaged.

References

[1] S. Preradovic and N. C. Karmakar, "Chipless RFID: Bar code of the future," *IEEE Microw. Mag.*, vol. 11, no. 7, pp. 87–97, Dec. 2010.
[2] S. Preradovic and N. C. Karmakar, *Multiresonator-Based Chipless RFID: Barcode of the Future*. New York, NY, USA: Springer-Verlag, 2011.
[3] N. C. Karmakar, R. Koswatta, P. Kalansuriya, and R. E-Azim, *Chipless RFID Reader Architecture*. Norwood, MA, USA: Artech House, 2013.
[4] E. Perret, *Radio Frequency Identification and Sensors: From RFID to Chipless RFID*. New York, NY, USA: Wiley, 2014.
[5] R. Rezaiesarlak and M. Manteghi, *Chipless RFID: Design Procedure and Detection Techniques*. Springer, 2015.
[6] N. C. Karmakar, M. Zomorrodi, and C. Divarathne, *Advanced Chipless RFID*. Hoboken, NJ, USA: Wiley, 2016.
[7] C. S. Hartmann, "A global SAW ID tag with large data capacity," in *Proc. IEEE Ultrason. Symp.*, vol. 1. Oct. 2002, pp. 65–69.
[8] A. Chamarti and K. Varahramyan, "Transmission delay line based ID generation circuit for RFID applications," *IEEE Microw. Wireless Compon. Lett.*, vol. 16, no. 11, pp. 588–590, Nov. 2006.
[9] M. Schüßler, C. Damm, and R. Jakoby, "Periodically LC loaded lines for RFID backscatter applications," in *Proc. Metamater.*, Rome, Italy, Oct. 2007, pp. 103–106.
[10] N. Saldanha and D. C. Malocha, "Design Parameters for SAW multi-tone frequency coded reflectors," in *Proc. IEEE Ultrason. Symp.*, Oct. 2007, pp. 2087–2090.
[11] M. Schüßler, C. Damm, M. Maasch, and R. Jakoby, "Performance evaluation of left-handed delay lines for RFID backscatter applications," in *IEEE MTT-S Int. Microw. Symp. Dig.*, Jun. 2008, pp. 177–180.
[12] S. Harma, V. P. Plessky, C. S. Hartmann, and W. Steichen, "Z-path SAW RFID tag," *IEEE Trans. Ultrason., Ferroelect., Freq. Control*, vol. 55, no. 1, pp. 208–213, Jan. 2008.
[13] T. Han, W. Wang, H. Wu, and Y. Shui, "Reflection and scattering characteristics of reflectors in SAW tags," *IEEE Trans. Ultrason., Ferroelect., Freq. Control*, vol. 55, no. 6, pp. 1387–1390, Jun. 2008.
[14] S. Harma, V. P. Plessky, X. Li, and P. Hartogh, "Feasibility of ultra-wideband SAW RFID tags meeting FCC rules," *IEEE Trans. Ultrason., Ferroelect., Freq. Control*, vol. 56, no. 4, pp. 812–820, Apr. 2012.
[15] F. J. Herraiz-Martinez, F. Paredes, G. Z. Gonzalez, F. Martin, and J. Bonache, "Printed magnetoinductive-wave (MIW) delay lines for chipless RFID applications," *IEEE Trans. Antennas Propag.*, vol. 60, no. 11, pp. 5075–5082, Nov. 2012.
[16] S. Tedjini, E. Perret, A. Vena, and D. Kaddout, "Mastering the electromagnetic signature of chipless RFID tags," in *Chipless and Conventional Radiofrequency Identification*. IGI Global, 2012.
[17] I. Preradovic, I. Balbin, N. C. Karmakar, and G. F. Swiegers, "Multiresonator-based chipless RFID system for low-cost item tracking," *IEEE Trans. Microw. Theory Techn.*, vol. 57, no. 5, pp. 1411–1419, May 2009.
[18] S. Preradovic and N. C. Karmakar, "Design of chipless RFID tag for operation on flexible laminates," *IEEE Antennas Wireless Propag. Lett.*, vol. 9, pp. 207–210, 2010.

[19] O. Rance, R. Siragusa, P. Lemaître-Auger, and E. Perret, "Toward RCS magnitude level coding for chipless RFID," *IEEE Trans. Microw. Theory Techn.*, vol. 64, no. 7, pp. 2315–2325, Jul. 2016.
[20] J. McVay, A. Hoorfar, and N. Engheta, "Space-filling curve RFID tags," in *Proc. IEEE Radio Wireless Symp.*, Oct. 2006, pp. 199–202.
[21] I. Jalaly and D. Robertson, "Capacitively-tuned split microstrip resonators for RFID barcodes," in *Proc. Eur. Microw. Conf.*, vol. 2. Oct. 2005, pp. 4–7.
[22] H.-S. Jang, W.-G. Lim, K.-S. Oh, S.-M. Moon, and J.-W. Yu, "Design of low-cost chipless system using printable chipless tag with electromagnetic code," *IEEE Microw. Wireless Compon. Lett.*, vol. 20, no. 11, pp. 640–642, Nov. 2010.
[23] A. Vena, E. Perret, and S. Tedjini, "A fully printable chipless RFID tag with detuning correction technique," *IEEE Microw. Wireless Compon. Lett.*, vol. 22, no. 4, pp. 209–211, Apr. 2012.
[24] A. Vena, E. Perret, and S. Tedjini, "Design of compact and auto-compensated single-layer chipless RFID tag," *IEEE Trans. Microw. Theory Techn.*, vol. 60, no. 9, pp. 2913–2924, Sep. 2012.
[25] A. Vena, E. Perret, and S. Tedjini, "High-capacity chipless RFID tag insensitive to the polarization," *IEEE Trans. Antennas Propag.*, vol. 60, no. 10, pp. 4509–4515, Oct. 2012.
[26] M. M. Khan, F. A. Tahir, M. F. Farooqui, A. Shamim, and H. M. Cheema, "3.56-bits/cm^2 compact inkjet printed and application specific chipless RFID tag," *IEEE Antennas Wireless Propag. Lett.*, vol. 15, pp. 1109–1112, 2016.
[27] M. A. Islam and N. C. Karmakar, "A novel compact printable dual-polarized chipless RFID system," *IEEE Trans. Microw. Theory Techn.*, vol. 60, no. 7, pp. 2142–2151, Jul. 2012.
[28] R. Rezaiesarlak and M. Manteghi, "Complex-natural-resonance-based design of chipless RFID tag for high-density data," *IEEE Trans. Antennas Propag.*, vol. 62, no. 2, pp. 898–904, Feb. 2014.
[29] M. Svanda, J. Machac, M. Polivka, and J. Havlicek, "A comparison of two ways to reducing the mutual coupling of chipless RFID tag scatterers," in *Proc. 21st Int. Conf. Microw., Radar Wireless Commun. (MIKON)*, May 2016, pp. 1–4.
[30] A. Vena, E. Perret, and S. Tedjini, "Chipless RFID tag using hybrid coding technique," *IEEE Trans. Microw. Theory Techn.*, vol. 59, no. 12, pp. 3356–3364, Dec. 2011.
[31] A. Vena, E. Perret, and S. Tedjini, "A compact chipless RFID tag using polarization diversity for encoding and sensing," in *Proc. IEEE Int. Conf. RFID*, Apr. 2012, pp. 191–197.
[32] I. Balbin and N. C. Karmakar, "Phase-encoded chipless RFID transponder for large-scale low-cost applications," *IEEE Microw. Wireless Compon. Lett.*, vol. 19, no. 8, pp. 509–511, Aug. 2009.
[33] S. Genovesi, F. Costa, A. Monorchio, and G. Manara, "Chipless RFID tag exploiting multifrequency delta-phase quantization encoding," *IEEE Antennas Wireless, Propag. Lett.*, vol. 15, pp. 738–741, 2015.
[34] C. Herrojo, J. Naqui, F. Paredes, and F. Martín, "Spectral signature barcodes based on S-shaped split ring resonators (S-SRRs)," *EPJ Appl. Metamater.*, vol. 3, pp. 1–6, Jun. 2016.
[35] C. Herrojo, J. Naqui, F. Paredes, and F. Martín, "Spectral signature barcodes implemented by multi-state multi-resonator circuits for chipless RFID tags," in *IEEE MTT-S Int. Microw. Symp. Dig.*, San Francisco, CA, USA, May 2016, pp. 1–4.
[36] C. Herrojo, F. Paredes, J. Mata-Contreras, S. Zuffanelli, and F. Martín, "Multistate multiresonator spectral signature barcodes implemented by means of S-shaped split ring resonators (S-SRRs)," *IEEE Trans. Microw. Theory Techn.*, vol. 65, no. 7, pp. 2341–2352, Jul. 2017.
[37] H. Chen *et al.*, "Left-handed materials composed of only S-shaped resonators," *Phys. Rev. E, Stat. Phys. Plasmas Fluids Relat. Interdiscip. Top.*, vol. 70, no. 5, p. 057605, Nov. 2004.
[38] H. Chen, L. Ran, J. Huangfu, X. Zhang, and K. Chen, "Negative refraction of a combined double S-shaped metamaterial," *Appl. Phys. Lett.*, vol. 86, no. 15, p. 151909, 2005.
[39] H. Chen *et al.*, "Magnetic properties of S-shaped split ring resonators," *Prog. Electromagn. Res.*, vol. 51, pp. 231–247, 2005, doi: 10.2528/PIER04051201.
[40] J. Naqui, J. Coromina, A. Karami-Horestani, C. Fumeaux, and F. Martín, "Angular displacement and velocity sensors based on coplanar waveguides (CPWs) loaded with S-shaped split ring resonators (S-SRR)," *Sensors*, vol. 15, no. 5, pp. 9628–9650, 2015.
[41] C. Herrojo, J. Mata-Contreras, F. Paredes, and F. Martín, "Near-Field chipless RFID encoders with sequential bit reading and high data capacity," in *IEEE MTT-S Int. Microw. Symp. Dig.*, Honolulu, HI, USA, Jun. 2017, pp. 1564–1567.
[42] J. Naqui and F. Martín, "Application of broadside-coupled split ring resonator (BC-SRR) loaded transmission lines to the design of rotary encoders for space applications," in *IEEE MTT-S Int. Microw. Symp. Dig.*, San Francisco, CA, USA, May 2016, pp. 1–4.
[43] J. Mata-Contreras, C. Herrojo, and F. Martín, "Application of split ring resonator (SRR) loaded transmission lines to the design of angular displacement and velocity sensors for space applications," *IEEE Trans. Microw. Theory Techn.*, vol. 65, no. 11, pp. 4450–4460, Nov. 2017, doi: 10.1109/TMTT.2017.2693981.
[44] J. B. Pendry, A. J. Holden, D. J. Robbins, and W. J. Stewart, "Magnetism from conductors and enhanced nonlinear phenomena," *IEEE Trans. Microw. Theory Techn.*, vol. 47, no. 11, pp. 2075–2084, Nov. 1999.
[45] F. Martín, F. Falcone, J. Bonache, R. Marqués, and M. Sorolla, "Split ring resonator-based left-handed coplanar waveguide," *Appl. Phys. Lett.*, vol. 83, no. 22, pp. 4652–4654, Dec. 2003.
[46] R. Marqués, F. Medina, and R. Rafii-El-Idrissi, "Role of bianisotropy in negative permeability and left-handed metamaterials," *Phys. Rev. B, Condens. Matter*, vol. 65, p. 144441, Apr. 2002.
[47] F. Martin, *Artificial Transmission Lines for RF and Microwave Applications*. Hoboken, NJ, USA: Wiley, 2015.
[48] J. Bonache, M. Gil, I. Gil, J. Garcia-García, and F. Martín, "On the electrical characteristics of complementary metamaterial resonators," *IEEE Microw. Wireless Compon. Lett.*, vol. 16, no. 10, pp. 543–545, Oct. 2006.
[49] F. Aznar *et al.*, "Characterization of miniaturized metamaterial resonators coupled to planar transmission lines through parameter extraction," *J. Appl. Phys.*, vol. 104, no. 11, pp. 114501-1–114501-8, Dec. 2008.

Cristian Herrojo (GS'16) was born in Barcelona, Spain, in 1983. He received the Telecommunications Technical Engineering degree in electronic systems and Telecommunications Engineering degree in 2010 and 2012, respectively. He is currently pursuing the Ph.D. degree (with a focus on the design of RF/microwave resonant structures applied to RFID tags (radio frequency identification) without chip).

Javier Mata-Contreras was born in Málaga, Spain, in 1976. He received the Ingeniería de Telecomunicación and Ph.D. degrees from the Universidad de Málaga (UMA), Málaga, in 2000 and 2010, respectively. His Ph.D. dissertation was entitled "Distributed Amplifiers and Mixers with Transmission Lines based on Metamaterials."

In 2000, he joined the Department of Ingeniería de Comunicaciones, UMA, as an Assistant Professor. He is currently a Visitant Professor with CIMITEC and the Universitat Autònoma de Barcelona, Barcelona, Spain. His current research interests include active and passive microwave devices and active distributed circuits based on metamaterials.

Alba Núñez was born in Madrid, Spain, in 1991. She received the Physics Science degree and master's degree in advanced materials and nanophysics from the Universidad Complutense de Madrid, Madrid, in 2014 and 2015, respectively.

In 2016, she joined the Printed Electronic Group, Institute of Microelectronics of Barcelona IMB-CNM (CSIC), Barcelona, Spain. She is currently a Research Technician with a specialization in the fabrication of inkjet printed devices.

Ferran Paredes (A'15) was born in Barcelona, Spain, in 1983. He received the Telecommunications Engineering Diploma degree in electronics, Telecommunications Engineering degree, and Ph.D. degree in electronics engineering from the Universitat Autònoma de Barcelona, Barcelona, in 2004, 2006, and 2012, respectively.

From 2006 to 2008, he was an Assistant Professor with the Universitat Autònoma de Barcelona, where he is currently a Research Assistant. His current research interests include metamaterial concepts, passive microwaves devices, antennas, and RFID.

Eloi Ramon received the bachelor's degree in telecom engineering from the Polytechnic University of Catalonia, Barcelona, Spain, the master's degree in microelectronics and nanoelectronics engineering, and the Ph.D. degree in inkjet printed devices and circuits from the Autonomous University of Barcelona (UAB), Barcelona.

Since 1999, he has been an Associate Professor with the Electronic Department, UAB, where he is currently teaching Telecom and CS BsC and MA. In 2014, he joined IMB-CNM (CSIC), Barcelona, as a Printed Microelectronics Researcher and the Group Leader of the printed electronics research and development line. He has participated in more than 55 industrial and research projects. He has co-authored more than 40 papers and 50 conference presentations. His current research interests include printed and organic devices for electronic systems, radio-frequency, and biomedical applications, with a large focus on the application of inkjet printing technologies for functional devices manufacturing.

Dr. Ramon currently serves as a Reviewer and a Scientific Expert for different journals and public funding agencies.

Ferran Martín (M'04–SM'08–F'12) was born in Barakaldo, Vizcaya, Spain, in 1965. He received the B.S. degree in physics and Ph.D. degree from the Universitat Autònoma de Barcelona (UAB), Barcelona, Spain, in 1988 and 1992, respectively.

From 1994 to 2006, he was an Associate Professor of electronics with the Departament d'Enginyeria Electrònica, Universitat Autònoma de Barcelona, where he has been a Full Professor of electronics since 2007. He has been involved in different research activities, including modeling and simulation of electron devices for high-frequency applications, millimeter wave, terahertz generation systems, and the application of electromagnetic bandgaps to microwave and millimeter-wave circuits. His current research interests include metamaterials and their application to the miniaturization and optimization of microwave circuits and antennas. He is currently the Head of the Microwave Engineering, Metamaterials and Antennas Group (GEMMA Group), UAB, and the Director of CIMITEC. He has authored or co-authored over 500 technical conference, letter, journal papers, and book chapters. He also co-authored *Metamaterials with Negative Parameters: Theory, Design and Microwave Applications* (Wiley, 2008) and authored *Artificial Transmission Lines for RF and Microwave Applications* (Wiley, 2015). He has generated 17 Ph.D. students. He has filed several patents on metamaterials and has headed several development contracts.

Prof. Martín is a member of the IEEE Microwave Theory and Techniques Society. He is also a member of the Technical Committees of the European Microwave Conference and International Congress on Advanced Electromagnetic Materials in Microwaves and Optics (Metamaterials). He has been a Fellow of the IET since 2016. He was a recipient of two ICREA ACADEMIA awards in 2008 and 2013. He has organized several international events related to metamaterials, including workshops at the IEEE International Microwave Symposium in 2005 and 2007, respectively, the European Microwave Conference in 2009, and the Fifth International Congress on Advanced Electromagnetic Materials in Microwaves and Optics (Metamaterials 2011), where he was a Chair of the Local Organizing Committee. He was a Guest Editor of three Special Issues on Metamaterials in three international journals. He is a reviewer for the IEEE TRANSACTIONS ON MICROWAVE THEORY AND TECHNIQUES and IEEE MICROWAVE AND WIRELESS COMPONENTS LETTERS, among many other journals, and he serves as a member of the Editorial Board of the *IET Microwaves, Antennas and Propagation* and the *International Journal of RF and Microwave Computer-Aided Engineering*. He was the recipient of the 2006 Duran Farell Prize for Technological Research and holds the Parc de Recerca UAB—Santander Technology Transfer Chair.

Artículo MWCL18

Near-Field Chipless-RFID System with Erasable/Programmable 40-bit Tags Inkjet Printed on Paper Substrates

C. Herrojo, J. Mata-Contreras, F. Paredes, A. Núñez,
E. Ramon and F. Martín

Near-Field Chipless-RFID System With Erasable/Programmable 40-bit Tags Inkjet Printed on Paper Substrates

Cristian Herrojo, *Graduate Student Member, IEEE*, Javier Mata-Contreras, Ferran Paredes, *Member, IEEE*, Alba Núñez, Eloi Ramon, and Ferran Martín, *Fellow, IEEE*

***Abstract*— In this letter, a chipless radio frequency identification (chipless-RFID) system with erasable/programmable 40-bit tags inkjet printed on paper substrates, where tag reading proceeds sequentially through near-field coupling, is presented for the first time. The tags consist of a linear chain of identical split ring resonators (SRRs) printed at predefined and equidistant positions on a paper substrate, and each resonant element provides a bit of information. Tag programming is achieved by cutting certain resonant elements, providing the logic state "0" to the corresponding bit. Conversely, tags can be erased (all bits set to "1") by short circuiting those previously cut resonant elements through inkjet. An important feature of the proposed system is the fact that tag reading is possible either with the SRR chain faced up or faced down (with regard to the reader). To this end, two pairs of header bits (resonators), with different sequences, have been added at the beginning and at the end of the tag identification chain. Moreover, tag data storage capacity (number of bits) is only limited by the space occupied by the linear chain. The implementation of tags on paper substrates demonstrates the potential of the proposed chipless-RFID system in secure paper applications, where the necessary proximity between the reader and the tag, inherent to near-field reading, is not an issue.**

***Index Terms*— Chipless-radio frequency identification (RFID), microstrip, secure paper, split ring resonator (SRR).**

I. Introduction

CHIPLESS-RADIO frequency identification (RFID) is a wireless technology used for identification (ID), tracking, sensing, and authentication/security applications. In the field of authentication and security, one promising scenario for chipless-RFID is secure paper. Within this particular application, equipping documents (e.g., banknotes, certificates, exams, ballots, official documents, etc.,) with a planar ID code is envisaged as a means to fight against counterfeiting. The main general advantage of chipless-RFID over chipped-RFID systems is the absence of silicon integrated circuits, or chips, which are replaced with printed encoders in chipless-RFID tags. Such encoders can be fabricated by means of printing techniques, such as screen printing, rotogravure, flexography, or inkjet, and represent a low-cost solution as compared to conventional chipped tags. However, chipless-RFID tags present two main limitations: 1) data capacity and 2) tag size.

Many efforts have been carried out in recent years to partially alleviate the previous limitations of chipless-RFID systems. In frequency-domain-based chipless-RFID systems [1]–[3], encoders with multiple resonant elements, each one tuned to a different frequency, are used for coding. In such systems, the ID code is given by the presence/absence of abrupt spectral characteristics in the amplitude, phase, or group delay response of the tags, and each resonant element provides a bit of information. Thus, in order to increase the data density, and hence reduce tag size, hybrid techniques, where more than one domain is used simultaneously, have been reported [4]–[7]. Nevertheless, these hybrid approaches are still far from providing the data storage capability of UHF-RFID chipped tags. Moreover, the spectral bandwidth required to accommodate a significant number of bits is very high, and this is not compatible with the implementation of low-cost readers. Alternatively, in the so-called time-domain-based chipless-RFID systems, the ID code is determined from the echoes generated by a set of reflectors printed on a transmission line (the interrogation signal being a narrow pulse in time domain) [8]. Within such approach, the number of bits is limited by the need to avoid overlapping between reflected pulses.

In this letter, a different time-domain approach based on near-field and sequential bit reading, first reported in [9] and [10], is used for reading new 40-bit chipless-RFID tags inkjet printed on paper substrates. The working principle of the proposed system is depicted Fig. 1. The tags consist of a linear chain of identical equidistant resonators, either tuned (i.e., functional, hence providing the logic state "1") or detuned ("0"). The interrogation signal is a harmonic (carrier) signal tuned to the resonance frequency of the set of resonators, and the ID code is obtained from the envelope of the amplitude-modulated (AM) signal generated by tag motion. That is, tag reading proceeds through near-field coupling, by displacing the tag over the reader, a transmission line fed by the harmonic (carrier) signal. The

Manuscript received December 22, 2017; accepted January 31, 2018. Date of publication February 21, 2018; date of current version March 9, 2018. This work was supported in part by MINECO-Spain under Project TEC2013-40600-R, Project TEC2016-75650-R, and Project RTC-2014-2550-7, in part by the Institució Catalana de Recerca i Estudis Avançats (who awarded Ferran Martín), and in part by FEDER funds. The work of C. Herrojo was supported by MINECO through the FPI under Grant BES-2014-068164. *(Corresponding author: Cristian Herrojo.)*

C. Herrojo, F. Paredes, and F. Martín are with CIMITEC/GEMMA, Departament d'Enginyeria Electrònica, Universitat Autònoma de Barcelona. 08193 Barcelona, Spain (e-mail: cristian.herrojo@uab.cat).

A. Núñez and E. Ramon are with the CNM, Institut de Microelectrònica de Barcelona (CSIC), 08193 Barcelona, Spain.

J. Mata-Contreras is with the Departamento de Ingeniería de Comunicaciones, Escuela Técnica Superior de Ingeniería de Telecomunicación, Universidad de Málaga, 29071 Málaga, Spain.

Color versions of one or more of the figures in this paper are available online at http://ieeexplore.ieee.org.

Digital Object Identifier 10.1109/LMWC.2018.2802718

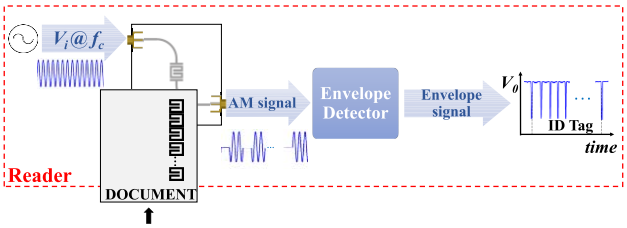

Fig. 1. Illustration of the working principle of the proposed chipless-RFID system. In a reading operation, the tag is displaced at short distance over the reader through a mechanical guiding system providing tag/reader alignment.

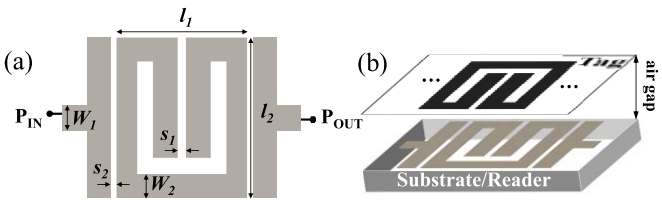

Fig. 2. (a) Layout of the active part of the reader. (b) 3-D view of the loaded reader with one of the SRRs of the tag aligned with the SRR of the reader. Dimensions are: $l_1 = 3.16$ mm, $l_2 = 3.35$ mm, $s_1 = 0.2$ mm, $s_2 = 0.2$ mm, $W_1 = 0.56$ mm, and $W_2 = 0.5$ mm. The distance between adjacent SRRs in the tag chain is 0.2 mm.

presence or absence of functional (tuned) resonators at the predefined positions determines the ID code of the tag, as long as signal transmission (and hence the output amplitude) is related to line-to-resonator coupling. (Variable with tag motion and only manifested when a tuned resonator is on top of the transmission line.)

II. Reader and Programmable/Erasable Tags

The active part of the reader is a microstrip line loaded with a split ring resonator (SRR) [Fig. 2(a)], and it is implemented on the *Rogers RO3010* substrate with thickness $h = 1.27$ mm and dielectric constant $\varepsilon_r = 10.2$. The magnitude of the transmission coefficient (S_{21}) of this structure (unloaded reader) exhibits a passband behavior with a transmission zero, as depicted in Fig. 3. Such response shifts down when the active part of the reader is loaded with the tag (see also Fig. 3), and the displacement level depends on the coupling between the tag and the reader. Indeed, the coupling (and the frequency shift) is maximum when one of the SRRs of the tag is just on top of the SRR of the reader, with perfect alignment and opposite orientation, i.e., rotated 180° [see Fig. 2(b)].

Therefore, by setting the frequency of the feeding signal to f_c (the resonance frequency of the unloaded reader), the excursion of the amplitude of the envelope function at the output port is expected to be high.

The tags are linear chains of identical SRRs, where each SRR provides a bit of information. Such tags can be either programmed, by cutting the resonant elements associated with the logic state "0" (making them inoperative), or erased, by short circuiting the cut SRRs through inkjet (thus adding conductive ink in order to set the corresponding bit to "1"). This approach is different from [9] and [10], where encoding was achieved by the presence/absence of resonant elements at the predefined and equidistant positions in the tag. The main advantage of tag programming/erasing is the possibility of massive manufacturing of all-identical tags, thus reducing fabrication costs. Once

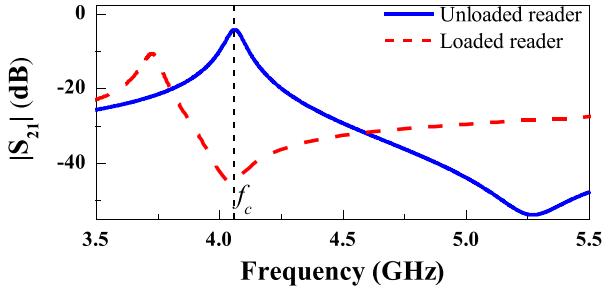

Fig. 3. Magnitude of the transmission coefficient (S_{21}) of the unloaded reader and reader loaded with the tag with one of the SRRs perfectly aligned with the SRR of the line, considering an air gap of 0.25 mm. These results have been inferred by electromagnetic simulation, using *Keysight Momentum*.

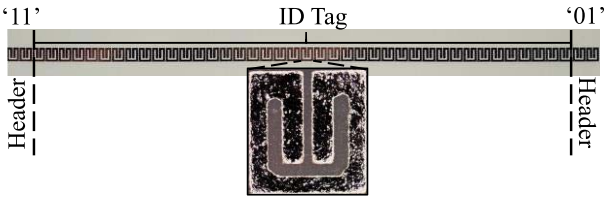

Fig. 4. Photograph of the fabricated 40-bit tag with all bits set to the logic state "1."

fabricated, tags can be programmed in a later stage, and erased and re-programmed as many times as needed.

III. Orientation-Independent Tag Reading

Another relevant aspect of the proposed tags is the fact that tag reading is independent of their orientation with regard to the reader, i.e., tag reading is either possible by displacing the tag over the reader with the resonator chain printed on the top (face up) or the bottom (face down) side of the tag substrate. To this end, two pair of bits (header bits) have been added at the beginning (sequence "11") and at the end (sequence "10") of the tag code, as depicted in the fabricated tag of Fig. 4. Such tag, with all ID bits set to "1" (all resonators functional), has been inkjet printed on paper substrate. The dielectric constant and loss tangent of this letter, with thickness $h = 215$ μm, have been inferred by means of a split cylinder resonator (model *Agilent 85072A*). The resulting values have been found to be $\varepsilon_r = 3.11$ and $\tan\delta = 0.039$. The used inkjet printer is *Ceradrop Ceraprinter X-Serie*, and one layer of *Dupont PE410* conductive ink (with conductivity 7.28×10^6 S/m) has been printed in order to achieve a measured thickness of 2.6 μm.

As mentioned before, to achieve maximum coupling between the SRR of the reader and the SRRs of the tag (thus achieving a high modulation index in the output signal), the relative orientation of both resonant elements must be 180°. Therefore, tag guiding over the reader must be carried out in the form specified in Fig. 2(b), either with the tag SRRs faced up or down. These two scenarios are distinguished by the fact that tags are read the following inverse sequences, which justifies the need of header bits. In a real-scenario, the tags must be printed at the edge of the paper, as illustrated in Fig. 1. Hence, the two un-readable tag orientations, with reader and tag SRRs identically oriented, are automatically avoided.

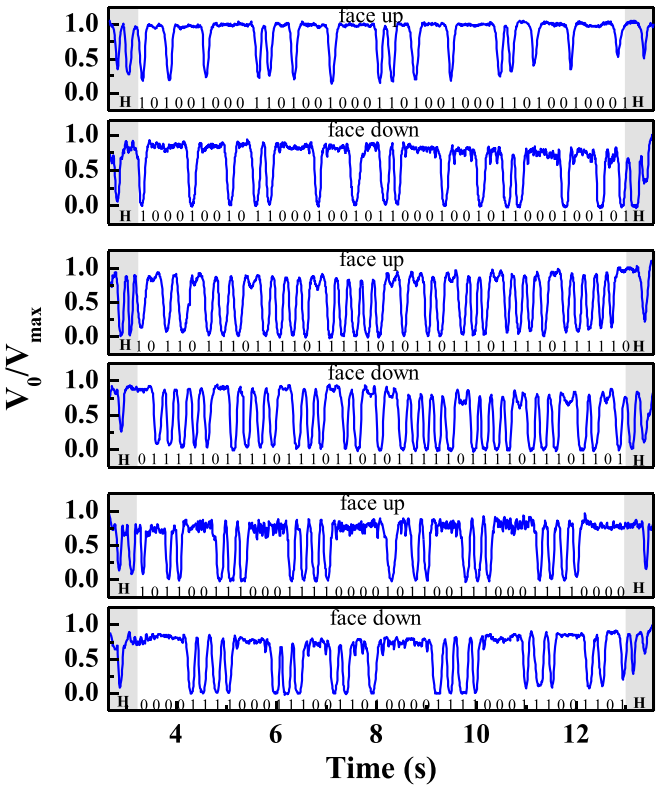

Fig. 5. Measured normalized envelope for the 40-bit programmed tags with the indicated codes.

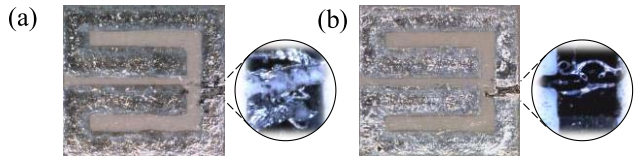

Fig. 6. Zoomed-in view of a (a) programmed (cut) SRR and (b) erased (short-circuited) SRR, the latter achieved by adding conductive ink.

IV. Experimental Validation

The response of three generated 40-bit tags (see Fig. 5), programmed by cutting several resonant elements [Fig. 6(a) shows a zoomed-in view of an SRR cut], with faced up and faced down orientation have been measured in order to validate the proposed chipless-RFID system, with programmable/erasable tags and orientation-independent near-field tag reading. Note that the header bits (the first two bits of the tag) provide the information relative to tag positioning, with sequences "11" and "10" corresponding to face-up and face-down orientations, respectively. Such responses have been obtained by means of the experimental setup available in our laboratory. The carrier signal (with frequency $f_c = 4$ GHz) is generated by means of the *Agilent E44338C* signal generator and the *Agilent MSO-X-3104A* oscilloscope is used for tag readout. The envelope of the AM signal at the output of the transmission line is extracted by means of an isolator (*ATM ATc4-8*), used to prevent reflections, and a Schottky diode (*Avago HSMS-2860*), acting as envelope detector.

In addition, the measured response depicted in Fig. 7 demonstrates that the tags can be erased by short circuiting

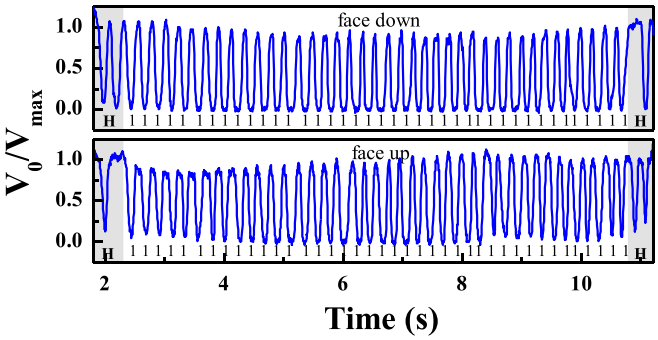

Fig. 7. Measured normalized envelope for the 40-bit erased tag.

those resonant elements previously cut [see Fig. 6(b)]. Although tag erasing in chipless-RFID systems is unusual, this may be useful either for further tag reprogramming, or for correcting errors generated during tag encoding.

V. Conclusion

In conclusion, a chipless-RFID system based on near-field coupling and sequential bit reading has been validated by reading several codes generated by programming and erasing a single 40-bit tag inkjet printed on a paper substrate. Such tags exhibit two important features: 1) they can be programmed and erased and 2) tags can be read either faced up or down with regard to the reader. The former aspect is relevant in applications requiring thousands of tags, since a single mask at fabrication level (for the implementation of all-identical tags) is required (hence saving costs), and leaving tag encoding (programming) to a later stage (custom level).

References

[1] I. Preradovic, I. Balbin, N. C. Karmakar, and G. F. Swiegers, "Multiresonator-based chipless RFID system for low-cost item tracking," *IEEE Trans. Microw. Theory Techn.*, vol. 57, no. 5, pp. 1411–1419, May 2009.

[2] S. Preradovic and N. C. Karmakar, "Design of chipless RFID tag for operation on flexible laminates," *IEEE Antennas Wireless Propag. Lett.*, vol. 9, pp. 207–210, 2010.

[3] A. Vena, E. Perret, and S. Tedjini, "High-capacity chipless RFID tag insensitive to the polarization," *IEEE Trans. Antennas Propag.*, vol. 60, no. 10, pp. 4509–4515, Oct. 2012.

[4] S. Genovesi, F. Costa, A. Monorchio, and G. Manara, "Chipless RFID tag exploiting multifrequency delta-phase quantization encoding," *IEEE Antennas Wireless Propag. Lett.*, vol. 15, pp. 738–741, 2015.

[5] A. Vena, E. Perret, and S. Tedjini, "Chipless RFID tag using hybrid coding technique," *IEEE Trans. Microw. Theory Techn.*, vol. 59, no. 12, pp. 3356–3364, Dec. 2011.

[6] A. El-Awamry, M. Khaliel, A. Fawky, M. El-Hadidy, and T. Kaiser, "Novel notch modulation algorithm for enhancing the chipless RFID tags coding capacity," in *Proc. IEEE Int. Conf. RFID*, San Diego, CA, USA, Apr. 2015, pp. 25–31.

[7] C. Herrojo, F. Paredes, J. Mata-Contreras, S. Zuffanelli, and F. Martín, "Multistate multiresonator spectral signature barcodes implemented by means of S-shaped split ring resonators (S-SRRs)," *IEEE Trans. Microw. Theory Techn.*, vol. 65, no. 7, pp. 2341–2352, Jul. 2017.

[8] F. J. Herraiz-Martinez, F. Paredes, G. Z. Gonzalez, F. Martin, and J. Bonache, "Printed magnetoinductive-wave (MIW) delay lines for chipless RFID applications," *IEEE Trans. Antennas Propag.*, vol. 60, no. 11, pp. 5075–5082, Nov. 2012.

[9] C. Herrojo, J. Mata-Contreras, F. Paredes, and F. Martín, "Near-field chipless RFID encoders with sequential bit reading and high data capacity," in *IEEE MTT-S Int. Microw. Symp. Dig.*, Honolulu, HI, USA, Jun. 2017, pp. 1564–1567.

[10] C. Herrojo, J. Mata-Contreras, A. Núñez, F. Paredes, E. Ramon, and F. Martín, "Near-field chipless-RFID system with high data capacity for security and authentication applications," *IEEE Trans. Microw. Theory Techn.*, vol. 65, no. 12, pp. 5298–5308, Dec. 2017.

Artículos No Fundamentales de la Tesis*

* Los artículos de congresos[(c)] no pueden formar parte fundamental de la tesis por compendio de publicaciones, tal y como dice la normativa del doctorado en Ingeniería Electrónica y de Telecomunicación de la Universitat Autònoma de Barcelona. Sin embargo, en esta tesis se han incluido como complementación. Asimismo, incluidos en la lista, artículos pendientes de aceptación.

Artículo del Congreso IMS16

Spectral Signature Barcodes Implemented by Multi-state Multi-resonator Circuits for Chipless RFID Tags

C. Herrojo, J. Naqui, F. Paredes and F. Martín

Spectral Signature Barcodes Implemented by Multi-State Multi-Resonator Circuits for Chipless RFID Tags

Cristian Herrojo, Jordi Naqui, Ferran Paredes and Ferran Martín

CIMITEC, Departament d'Enginyeria Electrònica, Universitat Autònoma de Barcelona, 08193 Bellaterra, Spain. (e-mail: cristian.herrojo@uab.cat)

Abstract — This paper presents the first spectral signature barcodes, operative at the S frequency band, implemented by means of multi-state resonators, each one able to provide more than 1-bit of information using a single frequency. The barcodes consist of a coplanar waveguide transmission line loaded with S-shaped split ring resonators (S-SRR), which are etched in the back substrate side. The S-SRRs are electrically small, hence providing compact size to the barcode. Moreover, and most important, each S-SRR provides three or four logic states for the tri-state and the four-state multi-resonator based barcode, respectively. This multi-state functionality is achieved by rotating the S-SRRs. By this means, the coupling level between the line and the resonator is controlled, and the notch depth in the transmission coefficient at the S-SRR resonance can thus be set to intermediate levels between the maximum and minimum rejection. This is a clear improvement as compared to previous bi-state (1-bit) resonator based barcodes, where the logic states '0' and '1' are achieved by the presence or absence of notch. This work also represents a progress as compared to other approaches of multi-state resonators that exploit their two first resonance frequencies (hence allowing for size reduction but not for an improvement of data capacity in a given bandwidth). As illustrative example, a tri-state resonator based barcode with 10 resonators (giving 3^{10} = 59.049 different codes, or more than 15 bits) and 1 GHz spectral bandwidth is designed and fabricated. An approach to achieve four states (2-bits) per resonator is also discussed.

Index Terms — RFID tags, radiofrequency bar codes, coplanar transmission line (CPW).

I. Introduction

Radiofrequency identification (RFID) is a wireless technology that uses radio waves to identify and communicate objects or items with an interrogator, or reader [1]. To this end, the objects are equipped with an RFID tag that typically contains a small antenna (for communication purposes) and an integrated circuit, or microchip, which stores information relative to the object. UHF-RFID tags are usually designed to exhibit long read ranges (several meters), and line-of-sight for identification is not required. However, these tags suffer from one important limitation that prevents from the further deployment of this technology, namely, their cost. This is mainly caused by the fabrication and assembly of the microchip. One route to palliate fabrication costs of the tags is to replace the microchip with a passive encoder. As long as these encoders are based on planar structures, tag fabrication can be carried out by means of printed techniques, or with other low cost fabrication techniques for planar circuits. Obviously, the penalty associated to cost reduction in these chipless tags (as they are usually known) is twofold: (i) size increase, and (ii) loss of data storage capacity. Within this framework, the battle horse in chipless tags is to reduce as much as possible the size of the encoders and increase as much as possible the number of bits.

There are two main approaches for the implementation of chipless tags [2]: those based on time domain, and those based on frequency domain. The former approach uses reflectors in a waveguiding structure [3], and tag ID is obtained from the echoes produced by the tag. This approach needs a relatively small spectral bandwidth, but the number of achievable bits is very limited as well. Improved bit capacity is obtained in frequency domain based chipless tags, where typically multiple resonators loading a transmission line, and tuned at different frequencies, are used [4], [5]. In multi-resonator chipless tags, the spectral signature is determined by a set of notches in the transmission coefficient. Thus, each bit of information is typically related to a resonant element, and the logic state '0' or '1' is determined by the absence or presence, respectively, of notch at the resonance frequency of the resonator.

In order to reduce size and increase the data capacity (number of bits) per GHz (a figure of merit), we propose a new approach of multi-resonator chipless tags, where we use circular S-shaped split ring resonators (S-SRRs) that provide more than two logic states per resonant element. S-SRRs are electrically very small, hence being beneficial in terms of size. On the other hand, the logic states are determined by the level of attenuation of the notch, which is controlled by the coupling level that results by S-SRR rotation. Following this approach, we have designed and implemented a 15-bit encoder at S-band based on 10 tri-state resonant elements with a size of 860 mm^2 and spectral bandwidth of 1 GHz. The strategy to implement barcodes with 2-bits per resonant element is also discussed.

II. S-SRRs: Topology and Design Requirements

The proposed spectral signature barcodes are based on S-SRR-loaded coplanar waveguides (CPWs). A detail of one of such resonators loading the line is shown in Fig. 1. Since the working principle to achieve three or four states per resonator is the control of line-to-resonator coupling by rotation, we have chosen a circular S-shaped topology. By this means, the dependence of the notch depth (in dB) to the rotation angle is

978-1-5090-0698-4/16/$31.00 ©2016 IEEE

quite linear, and this is convenient in order to obtain clearly discernible levels for the different states. The working principle is as follows. If the S-SRR orientation is the one depicted in Fig. 2(a), the counter magnetic fields generated by the line excite the particle, generating a notch in the transmission coefficient at the fundamental resonance. By contrast, by rotating the particle 90° [Fig. 2(b)], the net axial magnetic field in either half of the resonator is negligible, resulting in very soft line-to-resonator coupling and hence very small attenuation at resonance. Between these two extremes [Fig. 2(c)], the attenuation level (or notch depth) depends on the rotation angle. Thus, different (i.e., more than two) logic states per resonator can be achieved by considering different S-SRR orientations.

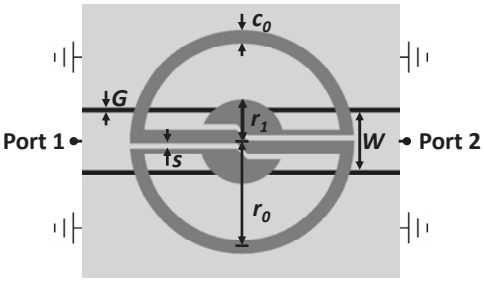

Fig. 1. Typical topology of a CPW loaded with an S-SRR (etched in the back substrate) side and relevant dimensions.

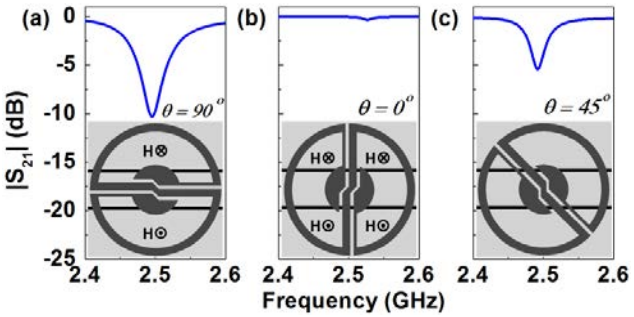

Fig. 2. Working principle of the multi-state resonator. (a) maximum coupling, (b) minimum coupling; (c) intermediate coupling.

An important aspect is the invariability of the notch frequency with the rotation angle (this avoids overlapping with the resonance frequency of adjacent resonators). It has been found that these resonators do not present significant variation of their resonance frequency with the rotation angle [6], and hence are useful for that purpose. Nevertheless, the angles (related to each state) should be chosen by taking into account not only the notch depths they produce, but also the resulting notch frequencies (which must be as close as possible).

These resonators are electrically smaller than SRRs or electric LC (ELC) resonators [6], this being an important aspect in terms of miniaturization. Another important aspect is the notch depth and bandwidth corresponding to maximum coupling state. In this regard, a tradeoff is necessary since a deep notch allows for the definition of intermediate states with wide guards between the corresponding thresholds, but this goes against bandwidth reduction. In this work, the aim is to consider resonators with resonance frequencies separated 100 MHz at S-band. The topology of the resonators has been optimized in order to simultaneously achieve more than 10 dB attenuation and less than 50 MHz bandwidth at half maximum (of attenuation). To this end, it has been necessary to maximize/minimize the capacitance/inductance of the S-SRR [6], resulting in the topology of Fig. 1 for the S-SRR tuned at 2.5 GHz.

Fig. 3(a) depicts the simulated response (including losses) of the structure of Fig. 1 for different rotation angles, and Fig. 3(b) shows the variation of the notch depth (in dB) as well as the variation of the notch frequency. The notch frequency variation is lower than 15 MHz and the results of Fig. 3 indicate that for 45° and 90° orientations the notch frequencies only differ in 3 MHz, and the notch depths (in dB) are related by a factor of 2. Hence 0°, 45° and 90° are the preferred orientations for the implementation of a tri-state single frequency resonator.

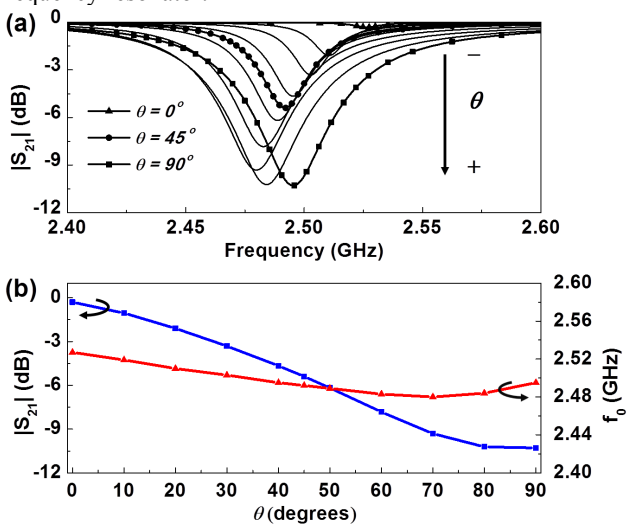

Fig. 3. (a) Simulated frequency response of the S-SRR-loaded CPW of Fig. 1 for different angular orientations; (b) Variation of the notch depth and frequency with the rotation angle. The simulations have been carried out with *Keysight Momentum*. The considered substrate is the *Rogers RO4003C* with thickness h = 0.81 mm, dielectric constant $\varepsilon_r = 3.55$ and $\tan\delta = 0.0021$. S-SRR dimensions (in reference to Fig. 1) are: $r_1 = 1.3$ mm, $r_0 = 3.4$ mm, $s = 0.2$ mm, $c_0 = 0.5$ mm. Line dimensions are: $W = 2.1$ mm, $G = 0.2$ mm corresponding to a 50 Ω transmission line.

III. Design of the Tri-State 10-Resonator Barcode

In order to implement a 10-resonator barcode, we have simply scaled up or down the length of the circumference of the S-SRR of Fig. 1, leaving the other geometrical parameters unaltered. S-SRR lengths have been optimized in order to achieve resonance frequencies distant 100 MHz, between 2.1 GHz and 3.0 GHz. The layouts and frequency responses of three encoders with the indicated (arbitrary) codes are

depicted in Fig. 4. The three responses are compared to the one with all the resonators rotated 90° (maximum coupling), corresponding to the sequence '11111111111'. Note that the intermediate state (45°) is designated by 'X'. As can be appreciated, the difference in the notch depth for states 'X' and '1' for an individual S-SRR is significant, regardless of the configuration of the neighbor S-SRRs.

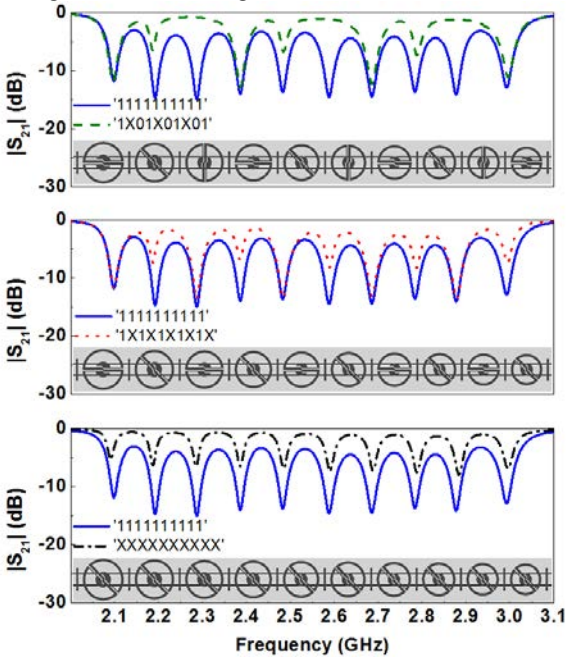

Fig. 4. Layout and frequency response (simulated) of the spectral signature barcodes with the indicated codes.

IV. Experimental Results

The encoders of Fig. 4 have been fabricated by means of a photo-mask etching technique (this includes the encoder with all the resonators rotated 90°). The measured responses (S_{21}) are depicted in Fig. 5. Note that by setting the thresholds at −5 dB and −10 dB, the three different states are perfectly distinguishable in the responses. The number of different codes that can be generated with these encoders is 3^{10} = 59.049 (i.e., above the number of codes corresponding to 15 bits, or 2^{15} = 32.768). Size is competitive (i.e., 95 mm × 9 mm), and the information density measured as the number of bits per unit frequency (> 15 bits/GHz) is high as well.

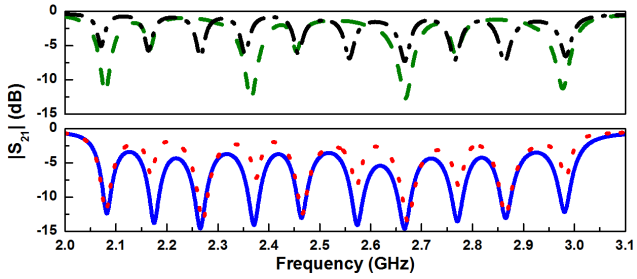

Fig. 5. Measured frequency responses corresponding to the codes of Fig. 4.

V. Discussion

Increasing the number of states per resonant element (e.g. four) is possible, but this requires further dynamic range (stronger notch depth for the maximum coupling state), and this means wider bandwidth as well. By modifying the topology of the resonant elements, the dynamic range has been enhanced. A preliminary result of a 4-bit barcode with two resonators and resonance frequencies separated 125 MHz is depicted in Fig. 6. The simulated frequency responses of the indicated states reveal that the different states can be distinguished. Thus, it is possible to further increase the information density (> 16 bit/GHz) by using four-state resonators.

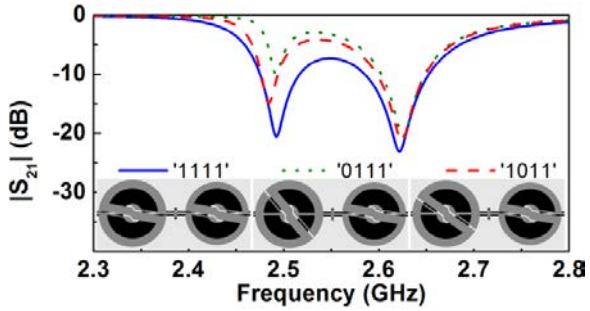

Fig. 6. Layout and frequency response (simulated) of the four-state 2-resonators spectral signature barcodes with the indicated codes.

VI. Conclusion

It has been shown that it is possible to enhance the information density (number of bits per unit frequency) in frequency domain radiofrequency barcodes by considering multi-state resonators operating each one at a single frequency. This is different from other approaches [7] that use dual-band multi-state resonators, hence occupying higher spectral bandwidth for the same data capacity.

Acknowledgement

This work has been supported by MINECO (Spain) under project TEC2013-40600-R and FEDER Funds. Thanks are also given to AGAUR-Generalitat de Catalunya for partially funding this research activity through the project 2014SGR-157. Ferran Martín is in debt to ICREA for supporting his work. Cristian Herrojo has been granted by MINECO with a FPI grant (ref. BES-2014-068164) and has collaborated with project RTC-2014-2550-7, also supported by MINECO.

References

[1] V.D. Hunt, A. Puglia, M. Puglia, *RFID: A Guide to Radiofrequency Identification*, John Wiley, New York, 2007.

[2] S. Preradovic and N. C. Karmakar, "Chipless RFID: Bar Code of the Future," *IEEE Microwave Magazine*, vol. 11, pp. 87-97, 2010.

[3] A. Chamarti and K. Varahramyan, "Transmission delay line based ID generation circuit for RFID applications," *IEEE Microw. Wireless Compon. Lett.*, vol. 16, pp. 588-590, 2006.
[4] S. Preradovic, I. Balbin, N. C. Karmakar, and G. F. Swiegers, "Multiresonator-based chipless RFID system for low-cost item tracking," *IEEE Trans. Microw. Theory Techn.*, vol. 57, pp. 1411-1419, 2009.
[5] S. Preradovic and N. C. Karmakar, "Design of chipless RFID tag for operation on flexible laminates," *IEEE Anten. Wireless Propag. Lett.*, vol. 9, pp. 207-210, 2010.
[6] J. Naqui, J. Coromina, A. Karami-Horestani, C. Fumeaux, and F. Martín, "Angular displacement and velocity sensors based on coplanar waveguides (CPWs) loaded with S-shaped split ring resonator (S-SRR)", *Sensors*, vol. 15, pp. 9628-9650, 2015.
[7] M. S. Bhuiyan, A.K.M Azad, N. Karmakar, "Dual-band modified complementary split ring resonator (MCSRR) based multi-resonator circuit for chipless RFID tag", *2013 IEEE Eight International Conference on Intelligent Sensors, Sensor Networks and Information Processing*, Melbourne, VIC, April 2013, pp. 277-281.

978-1-5090-0698-4/16/$31.00 ©2016 IEEE

Artículo del Congreso IMS17

Near-Field Chipless RFID Encoders with Sequential Bit Reading and High Data Capacity

C. Herrojo, J. Mata-Contreras, F. Paredes and F. Martín

Near-Field Chipless RFID Encoders with Sequential Bit Reading and High Data Capacity

Cristian Herrojo, Javier Mata-Contreras, Ferran Paredes and Ferran Martín

CIMITEC, Departament d'Enginyeria Electrònica, Universitat Autònoma de Barcelona, 08193 Bellaterra, Spain.
(e-mail: cristian.herrojo@uab.cat)

Abstract — This paper presents a novel and unconventional approach for the implementation of chipless RFID systems with high data capacity, suitable for authentication and security applications. Contrarily to previous time-domain or frequency-domain chipless RFID tags, where encoding is achieved either by generating defects (reflectors) in a transmission line (producing echoes in an input pulsed signal), or by etching multiple resonators (each tuned to a different frequency) in a dielectric substrate (providing a unique spectral signature), respectively, the chipless tags proposed in this paper consist of a set of identical resonators conveniently aligned and etched (or printed) on a dielectric layer (e.g., liquid crystal polymer, paper, etc). The resonators are located at predefined equidistant positions in such a way that the presence or absence of resonators in such positions corresponds to the '1' or '0' logic states, respectively. The reader is simply a coplanar waveguide (CPW) transmission line fed by a harmonic signal tuned to the frequency of the resonant elements. In a reading operation, the tag must be mechanically guided and transversally displaced over the CPW, so that the resonant elements modulate the amplitude of the feeding harmonic signal (through electromagnetic coupling) as they cross the axis of the CPW transmission line. This sequential bit reading alleviates the spectral bandwidth limitations of previous multi-resonator chipless RFID tags since the resonators are all identical in the proposed encoders. Therefore, the data capacity (number of bits) can be substantially enhanced since it is only limited by the area occupied by the resonant elements. The necessary close proximity between the tag and the reader is not an issue in certain applications such as authentication and security (e.g., secure paper), where the reading distances can be sacrificed in favor of a high number of bits. The design of 10-bit encoders based on this approach, and implemented by means of S-shaped split ring resonators (S-SRRs) etched on a flexible microwave substrate, is reported. The area of the encoders is as small as 1.35 cm^2. The number of bits can be significantly increased by simply adding further S-SRRs to the codes. Thus, high data capacity can be achieved without penalizing the complexity of the reader.

Index Terms — Chipless RFID, coplanar waveguide, split ring resonators.

I. Introduction

One of the drawbacks of radiofrequency identification (RFID) technology is the high cost of chip-based tags. Although such tags exhibit very high data capacity (due to the presence of the silicon integrated circuit 0IC), in certain applications (e.g., identification and tracking of low-cost items) the price of chip-based tags is prohibitive. In other applications related to authentication and security, where counterfeiting, fraud and unauthorized copying of valuable documents are key issues, low-cost encoders fully integrated with the tagging items are required. Chipless RFID technology alleviates the previous cost requirements since tags are equipped with printed encoders replacing the silicon ICs. Such tags can be implemented in flexible substrates (e.g., LCP, paper, etc.). Alternatively, the printed encoders can be integrated with the tagging item as part of it, in order to provide unique ID signatures, of interest in authentication and security applications (banknotes, certificates, official and corporate documents, exams, ballots, etc).

Chipless RFID tags can be categorized as time-domain [1]-[3] or frequency-domain based tags [4]-[6]. In time-domain chipless RFID tags, the code is determined from the echoes of a pulsed signal produced by a set of reflectors printed on a slow-wave transmission line. By contrast, a set of resonators, each one tuned to a different frequency and printed on a dielectric substrate, provides the so-called spectral signature in frequency-domain chipless tags. One limitation of this multi-resonator approach is the spectral bandwidth required to accommodate a significant number of bits. Strategies such as polarization diversity [7] or multi-state resonators (where up to four logic stages, i.e., two bits, per resonant element have been demonstrated) [8], [9] have been recently reported. Although a relatively high data density per frequency (DPF) and density per surface (DPS) is achieved by means of these approaches, it is not possible to implement tags with the required number of bits that many applications demand.

In this paper, we propose a novel approach for the implementation of chipless RFID tags. Such tags are similar to optical encoders, and consist of a set of identical resonators aligned and printed on a dielectric layer. Encoding is achieved by the presence or the absence of resonant elements at predefined equidistant positions. Since the spectral bandwidth of such tags is virtually null, the achievable number of bits is merely limited by the area occupied by the codes.

II. Working principle of the proposed chipless RFID systems

Reading of the proposed chipless RFID tags is based on electromagnetic coupling between the tag and the reader, a coplanar waveguide (CPW) transmission line fed by a harmonic signal tuned at the resonance frequency of the set of resonators. Note that with the proposed approach, the reading distance is limited to the sub-millimeter scale in order to guarantee line-to resonator coupling. Different to previous multi-resonator/transmission-line based chipless tags, where the resonant elements and transmission line are etched or

978-1-5090-6360-4/17/$31.00 ©2017 IEEE

printed on the same substrate and communication with the reader is achieved by means of cross polarized antennas (which are essential part of the tag, as well), in this work tag reading is by near-field coupling. As depicted in Fig. 1, in a reading operation the tags must be forced to transversally move above the transmission line in close proximity to it, so that electromagnetic coupling between the line and the resonators is possible. Each time a resonator lies on top of the line, the coupling prevents signal to be transmitted through the line, effectively modulating the injected harmonic signal. Thus, the ID signature is obtained by reading the amplitude of the envelope (output) signal, inferred from an envelope detector. The required proximity between the reader (transmission line) and the tag (set of resonators) is not necessarily an issue in certain applications such as those indicated earlier (authentication and security). The main advantage of the approach is the fact that the number of bits is not limited by bandwidth constraints, as occurs in multi-resonator based chipless tags. Indeed, in applications such as secure paper (e.g., to avoid counterfeiting or copying of corporate or official documents), it is potentially possible to print the tag resonators along one of the edges, opening the path to the design of chipless RFID tags with unprecedented data capacity.

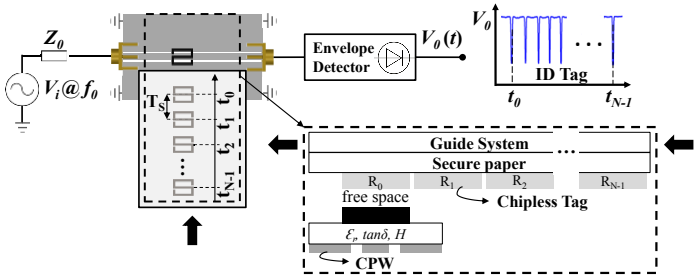

Fig. 1. Illustration of the working principle of the proposed chipless RFID system. The cross sectional view is depicted in the inset. The black arrows indicate tag motion in a reading operation.

III. TAG AND READER DESIGN, FABRICATION AND CHARACTERIZATION

In the proof-of-concept developed in this work, we have implemented the encoders on the *Rogers RO4003C* substrate with thickness h = 203 μm and dielectric constant η_r = 3.55, through a drilling machine. The resonant elements are square S-shaped split ring resonators (S-SRRs), formerly used in [9] for the implementation of multi-resonator chipless tags. Such resonant elements [see the typical topology in Fig. 2(a)] are electrically small and can be properly excited by the counter magnetic field lines generated in the slots of the CPW (reader) when such particles are aligned and oriented as depicted in Fig. 2(a).

In order to optimize the area occupied by the S-SRRs, it is necessary to minimize its separation as much as possible. This results in inter-resonator coupling and simultaneous coupling

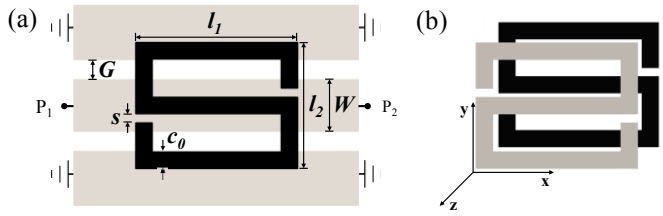

Fig. 2. Square S-shaped SRR coupled to a CPW transmission line (a) and 3D view of the broadside coupled S-SRR (BC-S-SRR) (b).

between the line and several S-SRRs, consequently appearing multiple transmission zeros located at positions difficult to predict a priori. To solve this problem, we have etched an identical S-SRR in the back substrate side of the CPW transmission line, but oppositely oriented [see Fig. 2(b)]. By this means, the resonance frequency of the structure that results when the S-SRR of the line and one of the S-SRRs of the tag chain are just one on top of the other (giving rise to the broad-side coupled S-SRR, BC-S-SRR), is significantly smaller, thereby preventing coupling with the neighbor S-SRRs. This means that the frequency of the harmonic feeding signal must be actually tuned to the frequency of the BC-S-SRR.

The CPW transmission line and the S-SRR of the reader have been etched on opposite sides of a *Rogers RO3010* substrate with thickness h = 635 μm and dielectric constant η_r = 10.2. The bottom and top photographs of this line (a 50 Ω line) are depicted in Figs. 3(a) and (b). Such figure includes the photograph of a 10-bit tag [Fig. 3(c)] with all the resonators present (i.e., all states corresponding to the logic '1'). To characterize such tag-reader system, we have generated a guiding channel in the top side of the CPW, as shown in Fig. 3(b). Moreover, the tag has been attached to a rigid substrate (with thickness h = 1.6 mm and dielectric constant η_r = 4.7) for mechanical stability. Figure 4 depicts the measured frequency response for different positions of the tag in the vicinity of the reference position (corresponding to a perfect alignment between the S-SRR of the reader and one of the S-SRRs of the tag). It can be seen that when the tag is not situated in the reference position, the attenuation at the reference frequency (the notch frequency of the BC-S-SRR) severely decreases.

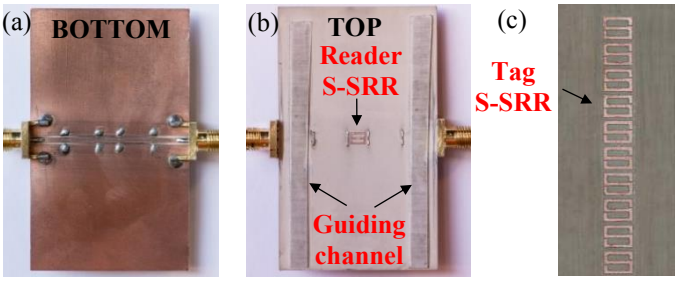

Fig. 3. Transmission line reader, including the CPW (a) and the S-SRR (b), and photograph of the fabricated encoder (c). CPW dimensions, in ref. to Fig. 2(a), are (in mm) W = 1.2 and G = 0.48; S-SRR dimensions are (in mm) l_1 = 3.8, l_2 = 2.96, c_0 = 0.4 and s = 0.2.

978-1-5090-6360-4/17/$31.00 ©2017 IEEE

We have also completely displaced the fabricated tag above the CPW, as it is required in a reading operation, and we have recorded the attenuation at the reference frequency. The result, depicted in Fig. 5, reveals the presence of 10 attenuation peaks, corresponding to the ten S-SRRs of the considered tag.

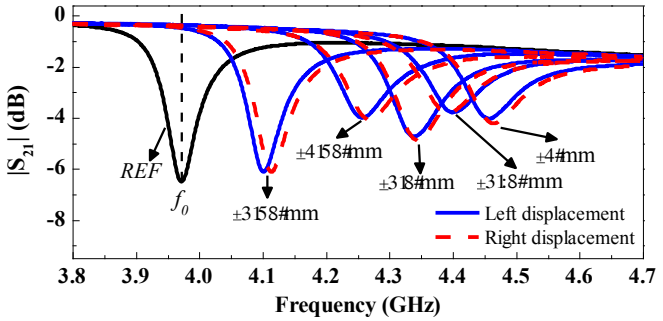

Fig. 4 Measured frequency response of the tag-CPW for different relative positions of the tag in the vicinity of the reference position.

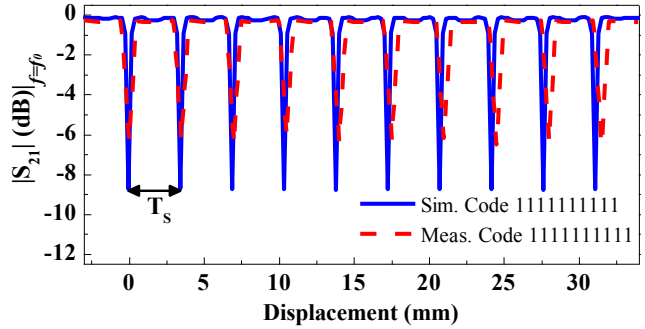

Fig. 5. Attenuation of the tag-CPW at the reference frequency as the tag moves completely (transversally) above the CPW.

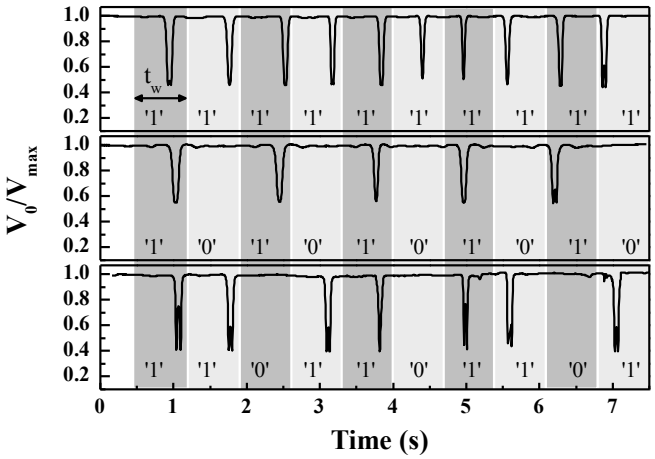

Fig. 6. Measured normalized envelope for 3 fabricated encoders with the indicated codes. The minima are not exactly at same positions within the readout windows since the in-house guiding system does not guarantee uniform displacement velocity of the tag.

IV. Experimental Setup and Tag Reading Operation

The proof-of-concept of the chipless RFID system of Fig. 1 is implemented as follows. The harmonic signal is generated by means of the *Agilent E44338C* signal generator, whereas an oscilloscope (*Agilent MSO-X-3104A*) is used for tag readout. The envelope of the modulated signal at the output of the CPW is extracted by means of an isolator (*ATM ATc4-8*), used to prevent reflections, and a Schottky diode (*Avago HSMS-2860*), acting as envelope detector. With this experimental setup, the ID signatures of three fabricated encoders have been obtained. To this end, the time-varying envelope variation within temporal windows of predefined time (t_w) is recorded, providing the ID code, as illustrated in Fig. 6.

V. Conclusions

In summary, a novel approach for the implementation of chipless RFID systems, based on near-field coupling between the tag and the reader and sequential bit reading, has been proposed. The encoders consist of a chain of S-SRRs etched (or printed) on a dielectric (flexible) substrate, whereas the active part of the reader is a CPW transmission line, also loaded with a S-SRR. As proof-of-concept demonstrators, we have fabricated and characterized three 1.35cm^2 10-bit encoders. The obtained results point out the potential of the approach for achieving chipless RFID encoders with unprecedented data capacity, useful in applications such as authentication or security, where the reading distance can be sacrificed in favor of the number of bits.

Acknowledgement

This work was supported by MINECO-Spain (projects TEC2013-40600-R and RTC-2014-2550-7), *Generalitat de Catalunya* (project 2014SGR-157), *Institució Catalana de Recerca i Estudis Avançats* (who awarded F. Martín), and by FEDER funds. C. Herrojo acknowledges MINECO for supporting his research activity through the FPI grant BES-2014-068164.

References

[1] C. S. Hartmann, "A global SAW ID tag with large data capacity," in *Proc. of IEEE Ultrasonics Symposium*, Oct. 2002, vol. 1, pp. 65–69.

[2] M. Schüßler, C. Damm, M. Maasch, and R. Jakoby, "Performance evaluation of left-handed delay lines for RFID backscatter applications," in Proc. of the *IEEE MTT-S International Microwave Symposium 2008*, pp. 177-180.

[3] F.J. Herraiz-Martínez, F. Paredes, G. Zamora, F. Martín, and J. Bonache, "Printed magnetoinductive-wave (MIW) delay lines for chipless RFID applications", *IEEE Trans. Ant. Propag.*, vol. 60, pp. 5075-5082, Nov. 2012.

[4] S. Preradovic, I. Balbin, N. C. Karmakar, and G. F. Swiegers, "Multiresonator-based chipless RFID system for low-cost item tracking," *IEEE Trans. Microw. Theory Techn.*, vol. 57, pp. 1411-1419, 2009.

[5] S. Preradovic and N. C. Karmakar, "Design of chipless RFID tag for operation on flexible laminates," *IEEE Anten. Wireless Propag. Lett.*, vol. 9, pp. 207-210, 2010.

[6] S. Preradovic and N. C. Karmakar, *Multiresonator-based Chipless RFID: Barcode of the Future*, Springer, 2012.

978-1-5090-6360-4/17/$31.00 ©2017 IEEE

[7] A. Vena, E. Perret, S. Tedjini, "A compact chipless RFID tag using polarization diversity for encoding and sensing", *2012 IEEE International Conference on RFID (RFID)*, Orlando (FL), Apr. 2012.
[8] M. S. Bhuiyan, A.K.M Azad, N. Karmakar, "Dual-band modified complementary split ring resonator (MCSRR) based multi-resonator circuit for chipless RFID tag", *2013 IEEE Eight International Conference on Intelligent Sensors, Sensor Networks and Information Processing*, Melbourne, VIC, Apr. 2013, pp. 277-281.
[9] C. Herrojo, J. Naqui, F. Paredes, F. Martín, "Spectral signature barcodes implemented by multi-state multi-resonator circuits for chipless RFID tags", *IEEE MTT-S International Microwave Symposium* (IMS'16), San Francisco, May 2016.
[10] J. Naqui, J. Coromina, A. Karami-Horestani, C. Fumeaux, and F. Martín, "Angular displacement and velocity sensors based on coplanar waveguides (CPWs) loaded with S-shaped split ring resonator (S-SRR)", *Sensors*, vol. 15, pp. 9628-9650, 2015.

978-1-5090-6360-4/17/$31.00 ©2017 IEEE

Artículo del Congreso EuMC18

Erasable/Programmable Chipless-RFID Tags with Orientation-Independent Sequential Bit Reading

C. Herrojo, M. Moras, F. Paredes, J. Mata-Contreras, A. Núñez, E. Ramon and F. Martín

Erasable/Programmable Chipless-RFID Tags with Orientation-Independent Sequential Bit Reading

Cristian Herrojo[1], Miquel Moras[2], Ferran Paredes[1], Javier Mata-Contreras[1], Alba Núñez[2], Eloi Ramon[2] and Ferran Martín[1]

[1]CIMITEC, Departament d'Enginyeria Electrònica, Universitat Autònoma de Barcelona, 08193 Bellaterra, Spain

[2]Institut de Microelectrònica de Barcelona, IMB-CNM (CSIC), 08193, Bellaterra, Spain

e-mail: cristian.herrojo@uab.cat

***Abstract* — This paper presents erasable/programmable chipless radiofrequency identification (chipless-RFID) tags that can be read by proximity (through near-field coupling to the reader) and sequentially in time domain. The tags consist of a linear chain of identical resonant elements printed at predefined and equidistant positions on a dielectric substrate, and each resonant element provides a bit of information. The tags can be programmed by cutting (detuning) those resonators with bit set to the '0' logic state, whereas tags can be erased (all bits set to '1') by simply short-circuiting those resonant elements previously detuned, thus recovering their functionality. The reader is a transmission line loaded with a resonant element identical to those of the tag chain and fed by a harmonic signal (interrogation signal). Such signal must be tuned to a frequency in the vicinity of the fundamental resonance frequency of the resonant elements, and tag reading proceeds by displacing the tag chain over the line axis, in close proximity to it, through a guiding system. The main relevant aspect of the proposed tags is the fact that by adding a pair of header bits (resonators), with different code, at both sides of the tag chain, it is possible to read the tags regardless of their relative orientation to the reader. Namely, it is demonstrated that tag reading is either possible by displacing the tag over the reader with the resonator chain printed on the top or the bottom face of the tag substrate. This is an important practical aspect for the potential use of this chipless-RFID system in secure paper applications, since the user does not need to know how to introduce the tag in the guiding system (i.e., face-up or face-down). System validation is reported by considering tags implemented in low-loss commercial microwave substrates, and also printed on ordinary (low-cost) din A4 paper.**

***Keywords* — Chipless-RFID, microstrip, split ring resonators.**

I. INTRODUCTION

Chipless-RFID is a wireless technology used for identification, tracking, sensing and security, among other applications. It is an alternative to chipped-RFID, where the silicon integrated circuit (or chip) is replaced with a printed encoder. Thus, chipless tags are cheaper than chipped ones, but their storage capability and dimensions cannot, in general, compete against the data information capacity and size of tags equipped with chips. Moreover, the read distances in chipless-RFID systems are usually significantly smaller than those achievable in passive UHF-RFID systems with chipped tags.

Most chipless-RFID systems proposed to date consider tags with multiple resonant elements tuned to different frequencies [1]-[4]. Tag reading in such systems requires an interrogation signal covering the whole spectral bandwidth occupied by the resonant elements, and the identification (ID) code is given by singularities contained in the magnitude or phase response of the tags. Since each resonant element exhibits a finite bandwidth, it follows that ultra wide spectral bandwidths (not compatible with simple and low-cost readers) are necessary to accommodate a large number of bits. Therefore, the data capacity in these frequency-domain chipless-RFID systems is limited. To alleviate this drawback, chipless-RFID systems exploiting two domains simultaneously (hybrid systems) have been reported. Hybrid coding is used to increase the data density per bandwidth, and examples include frequency/phase deviation [5], frequency/notch bandwidth [6], frequency/notch magnitude [7] and frequency/peak magnitude [8], among others. Nevertheless, even with hybrid coding, it is not possible to implement robust chipless-RFID systems with the (large) number of bits that many applications require.

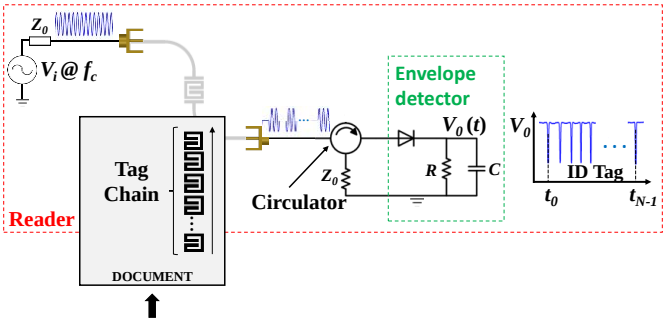

Fig. 1. Sketch of the chipless-RFID system, consisting of the tag (set of resonators printed or etched on a substrate) and the reader (within the dashed rectangle), constituted by the harmonic generator, the SRR-loaded transmission line, the circulator (used to avoid reflections from the diode), and the envelope detector.

Recently, a chipless-RFID system in time domain, based on near-field and sequential bit reading has been proposed [9], [10]. The working principle is different than the one of chipless-RFID systems based on time domain reflectometry (TDR) [11], [12], where the ID code is contained in the echoes generated by the tag (a delay line with reflectors) to a pulsed (interrogation) signal.

In this work, the interrogation signal is a harmonic (single tone) signal, and the ID code is contained in the envelope of the amplitude modulated signal generated by the tag, a linear

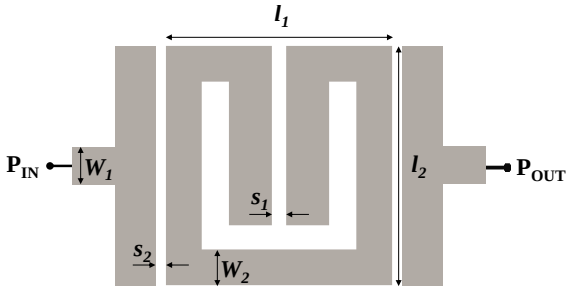

Fig. 2. Layout of the active part of the reader, implemented on the Rogers RO3010 substrate with thickness h = 1.27 mm and dielectric constant ε_r = 10.2. Dimensions are (in mm): l_1 = 3.16, l_2 = 3.35, s_1 = 0.2, s_2 = 0.2, W_1 = 0.56, and W_2 = 0.5. The distance between adjacent SRRs in the tag chain is 0.2 mm.

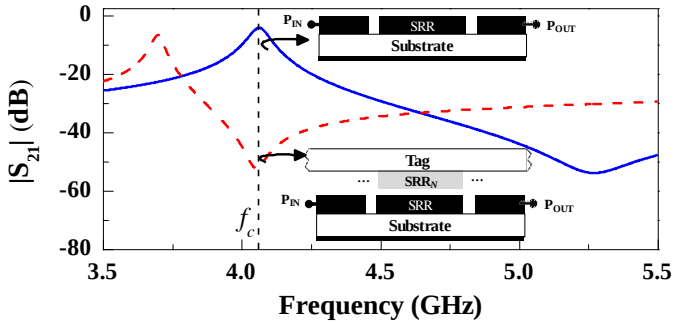

Fig. 3. Frequency response of the unloaded reader and reader loaded with the tag with one of the SRRs perfectly aligned with the reader SRR, considering an air gap (vertical distance between the tag and the reader) of 0.25 mm.

chain of identical resonant elements (see Fig. 1). Tag reading proceeds through near-field coupling by displacing the tag over the reader, a transmission line fed by the above-mentioned harmonic (carrier) signal. The presence or absence of functional resonators determines the ID code of the tag, and such code is inferred from the envelope function at the output port of the line as long as the transmission coefficient of the line (and hence the amplitude at the output port) is modulated by the coupling between the line (reader) and the functional resonators.

The main originality of the work concerns tag programming and erasing. Hence, in a real scenario, identical tags with all-functional resonators can be massively fabricated (e.g. by low-cost R2R printing technologies), avoiding the use of specifics masks for the different codes. Moreover, it is shown that by introducing header bits in the tags, it is possible to read them independently on whether such tags are displaced over the reader either face-up or face-down.

II. Reader and Programmable/Erasable Tags with Header Bits

The active part of the reader is a microstrip line loaded with a split ring resonator (SRR) in bandpass configuration (Fig. 2). The response of this structure without tag on top of it (Fig. 3) exhibits a pass band and a transmission zero. However, when the tag (with the SRRs rotated 180º with regard to the SRR of the line), is on top of the line, and one of the functional SRRs of the tag chain is perfectly aligned with the one of the line, inter-resonator coupling is maximized, and the frequency response is significantly shifted towards lower frequencies (see Fig. 3). As can be seen, the transmission coefficient at the band pass frequency of the unloaded reader experiences a significant variation (decrease) with tag motion. Consequently, by choosing this frequency as the carrier frequency, f_c, of the feeding (interrogation) signal, the excursion of the amplitude of the envelope function (or modulation index) at the output port will be high, as desired to properly read the ID codes.

As mentioned before, the tags are constituted by a linear chain of resonators, identical to the one of the reader. In [9], [10], the presence or absence of resonant elements at predefined (and equidistant) positions in the chain was used for coding purposes. In this work, coding is achieved by altering (cutting) certain resonant elements, i.e., those associated to the logic state '0'. By this means, resonators are detuned, and they are no longer functional, not being able to modulate the amplitude of the feeding signal. The main advantage of this approach is the fact that tags can be programmed after being manufactured, thus reducing fabrications costs (provided a single mask is needed for the massive fabrication of identical tags, with all resonators being present and functional). Although in a real scenario, resonator detuning can be achieved, e.g., by laser ablation, in this work, resonator etching is considered for that purpose, as proof-of-concept.

Although the need to erase (or re-write) the tags in chipless-RFID systems is unusual, it is possible to do so by short-circuiting the resonant elements (recovering their functionality). To this end, additive inkjet printing can be used. However, in this work, we have simply added soldering tin to the detuned resonators, as will be shown in the next section.

In order to ensure the functionality of the chipless-RFID system regardless of the relative orientation of the tags with regard to the reader (face-up or down), the solution is to add header bits at the beginning and end of the tag chain. Particularly, we have added two pairs of header bits to 10-bit tags, as illustrated in the fabricated tag of Fig. 4, with all bits set to '1' (all resonant elements being functional). Such tag has been implemented on the *Rogers RO4003C* substrate with thickness h = 254 μm and dielectric constant ε_r = 3.55. According to this, it is clear that the first two (header) bits of the sequence (either '11' or '10') determine tag orientation, and hence the ID code can be correctly inferred. It is worth mentioning (for clarification purposes) that since the SRRs of the tag and the SRR of the reader must be oppositely oriented, there are only two possible combinations for tag guiding over the reader, i.e., face up or down, in both cases with the tag SRRs conveniently oriented. The two additional combinations, that is, face up or down and tag SRRs with identical orientation to the reader cannot be read. Nevertheless, in secure paper applications, it is reasonable to print the tags in one of the paper edges. Therefore, these additional (not readable) tag orientations are automatically excluded. Alternatively, two oppositely-oriented independent reader front-ends, each one positioned at the extremes of the guiding channel, can be considered in order to account for all orientations.

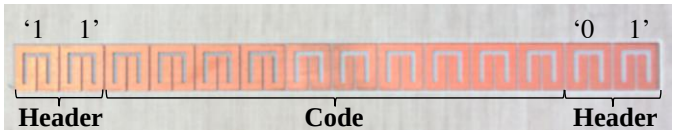

Fig. 4. Photograph of the fabricated tag with all bits set to ‘1’.

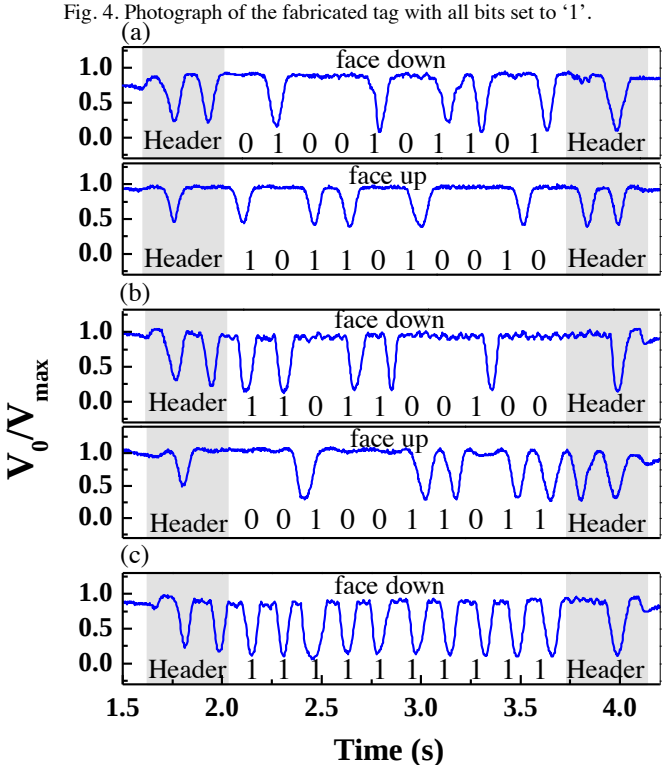

Fig. 5. Envelope functions of the tags with the indicated codes.

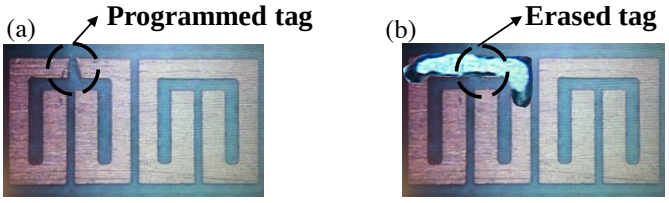

Fig. 6. Detail of a detuned (programmed) SRR (a) and SRR with soldering tin (erased) for functionalization (b).

III. CHIPLESS-RFID SYSTEM VALIDATION

To validate the ideas proposed in this work, we have generated several codes (tag programming) by cutting certain resonant elements. The functionality of the required detuned (cut) resonators can be recovered by adding soldering tin on the corresponding SRRs. The responses of the generated codes (with up and down faced tags) are depicted in Figs. 5(a) and 5(b). Such responses have been obtained by means of the experimental set-up available in our laboratory (reported in [10]), which allows for linear displacement (guiding) of the tags over the reader. The carrier frequency has been set to $f_c = 4$ GHz and the envelope functions have been visualized by means of an oscilloscope (after obtaining them through an envelope detector preceded by an isolator). It can be appreciated that the first two header bits are either ‘11’ or ‘10’ corresponding to the face up and down orientation, respectively, of the tag.

Finally, we have recovered the functionality of all the resonant elements, and the resulting code (only faced down) is depicted in Fig. 5(c). Figure 6 shows the detail (zoom) of the tag with cut SRRs and the same tag after recovering the functionality of the resonant elements. In view of the responses of Fig. 5, the functionality of the proposed chipless-RFID system, with erasable/programmable tags and orientation-independent tag reading, is validated. It is important to emphasize that tags can be programmed (after erasing) as many times as required, with the unique limit of its mechanical stability. Namely, multiple programming/erasing cycles may give rise to tag degradation. Nevertheless, in typical applications, tags should be programmed only once, in order to provide the unique ID code after being fabricated. In rare occasions, erasing and reprogramming should be required, but this is a possibility that can be exploited if needed.

To further validate the functionality of the system and to demonstrate the potential for application in secure paper, we have printed a 40-bit tag (plus the header bits) on ordinary (and low-cost) paper (din A4) by means of inkjet printing, using the *Ceradrop Ceraprinter X-Serie* inkjet printer and one layer of *Dupont™ PE410* conductive ink (with measured thickness and conductivity of 2.6 μm and 7.28x10^6 S/m, respectively). The photograph of the tag, with all bits set to ‘1’, can be seen in Fig. 7. We have obtained the response of such tag, but in this second validation example by using a modified (adapted) printer as guiding system of the tag over the reader. Moreover, as compared to the first experimental set-up used to obtain the responses of Fig. 5, in this second case we have replaced the isolator and envelope detector implemented by discrete components with an integrated circuit (*Analog Devices ADL5511*) able to provide the envelope function, followed by a data acquisition target (*National Instruments myRIO*) connected to a computer. The whole experimental set-up is shown in Fig. 8, whereas the response of the tag (faced up and down) can be seen in Fig. 9(a). We have then programmed the tag with the code indicated in Fig. 9(b). The corresponding envelope function, inferred from this novel set-up for tag reading, is also depicted in Fig. 9(b). With these results, it is clearly pointed out that this system is useful for document encoding, by printing the ID codes directly on it. The fact that the functionality is validated by using ordinary din A4 paper, the possibility to write and erase the tags, and the capability of tag reading with tag faced up or down are important aspects for the application of this system in a real scenario.

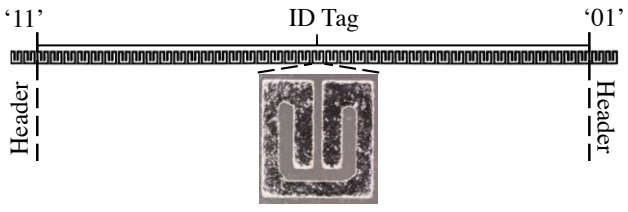

Fig. 7. Photograph of the tag with all bits set to ‘1’ printed on din A4 paper.

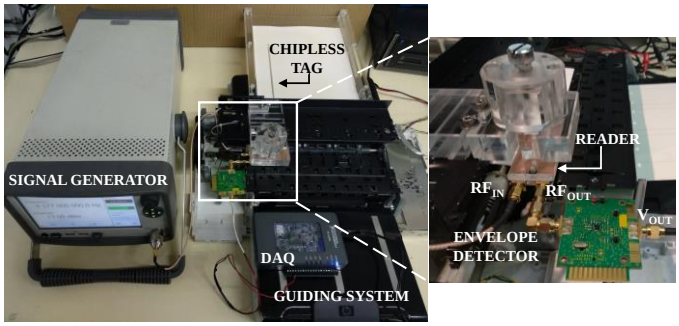

Fig. 8. Photograph of the experimental set-up used for obtaining the tag responses (envelope functions) in those tags printed on din A4 paper.

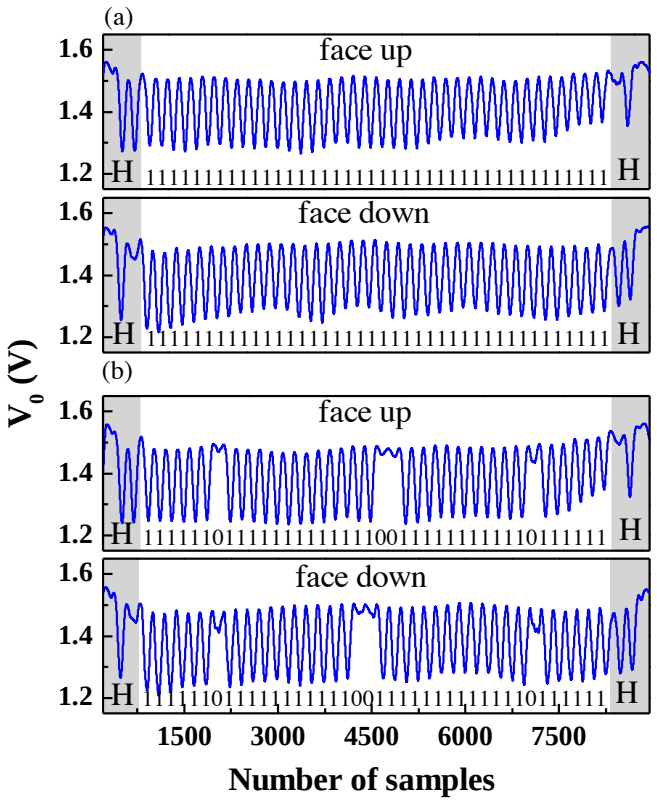

Fig. 9. Envelope functions of the inkjet-printed tags with the indicated codes. Since the envelope function has been inferred from a data acquisition system in this second validation experimental set-up, the abscise axis is the number of samples, rather than the time.

IV. Conclusions

In summary, it has been demonstrated that chipless-RFID tags with orientation-independent sequential bit reading (through electromagnetic coupling with the reader) can be implemented. It has been also shown that such tags can be easily programmed and erased. This is a fundamental aspect for the future application of these chipless-RFID systems in secure paper applications, where, foreseeable, all-identical tags can be massively printed on the paper documents under consideration (hence reducing costs), and the unique ID signature (used to provide authentication and security) generated in a later stage. We have first validated the system by considering 10-bit tags implemented on commercially available microwave substrates, and then by printing 40-bit tags on ordinary (din A4) paper. This latter validation is fundamental since it points out that the system works without the need to consider special (high cost) papers or tag substrates, consequently demonstrating the versatility of the proposed chipless-RFID system. To our knowledge, this is the first time that a chipless-RFID system with erasable/programmable 40-bit tags printed on ordinary paper is reported. Moreover, the number of bits can be increased by simply adding more resonant elements in the chain, either cascaded or in other configurations (under present study).

Acknowledgement

This work was supported by MINECO-Spain (projects TEC2013-40600-R, TEC2016-75650-R and RTC-2014-2550-7), *Generalitat de Catalunya* (project 2014SGR-157), *Institució Catalana de Recerca i Estudis Avançats* (who awarded F. Martín), and by FEDER funds. C. Herrojo acknowledges MINECO for supporting his research activity through the FPI grant BES-2014-068164.

References

[1] S. Preradovic, I. Balbin, N. C. Karmakar, and G. F. Swiegers, "Multiresonator-based chipless RFID system for low-cost item tracking," *IEEE Trans. Microw. Theory Techn.*, vol. 57, pp. 1411-1419, 2009.

[2] S. Preradovic and N. C. Karmakar, "Design of chipless RFID tag for operation on flexible laminates," *IEEE Anten. Wireless Propag. Lett.*, vol. 9, pp. 207-210, 2010.

[3] A. Vena, E. Perret, and S. Tedjini, "High-capacity chipless RFID tag insensitive to the polarization", *IEEE Trans. Ant. Propag.*, vol. 60, pp. 4509-4515, Oct. 2012.

[4] S. Genovesi, F. Costa, A. Monorchio, G. Manara, "Chipless RFID tag exploiting multifrequency delta-phase quantization encoding", *IEEE Ant. Wireless, Propag. Lett.*, vol. 15, pp. 738-741, 2015.

[5] A. Vena, E. Perret, S. Tedjini, "Chipless RFID tag using hybrid coding technique," *IEEE Trans. Microw. Theory Techn.*, vol. 59, pp. 3356-3364, Dec. 2011.

[6] A. El-Awamry *et al.*, "Novel notch modulation algorithm for enhancing the chipless RFID tags coding capacity" *2015 IEEE International Conference on RFID* (RFID), pp. 25-31, San Diego, CA, Apr. 2015.

[7] C. Herrojo, F. Paredes, J. Mata-Contreras, S. Zuffanelli and F. Martín, "Multi-state multi-resonator spectral signature barcodes implemented by means of S-shaped Split Ring Resonators (S-SRR)", *IEEE Trans. Microw. Theory Techn.*, vol. 65, pp. 2341-2352, Jul. 2017.

[8] O. Rance, R. Siragusa, P. Lemaître-Auger, E. Perret, "Toward RCS magnitude level coding for chipless RFID," *IEEE Trans. Microw. Theory Techn.*, vol. 64, pp. 2315-2325, Jul. 2016.

[9] C. Herrojo, J. Mata-Contreras, F. Paredes, F. Martín, "Near-Field chipless RFID encoders with sequential bit reading and high data capacity", *IEEE MTT-S Int. Microw. Symp.* (IMS'17), Honolulu, Hawaii, June 2017.

[10] C. Herrojo, J. Mata-Contreras, A. Núñez, F. Paredes, E. Ramón, and F. Martín, "Near-field chipless-RFID system with high data capacity for security and authentication applications", *IEEE Trans. Microw. Theory Techn.*, vol. 65, pp. 5298-5308, Dec. 2017.

[11] M. Schüßler, C. Damm, M. Maasch, and R. Jakoby, "Performance evaluation of left-handed delay lines for RFID backscatter applications," in Proc. of the *IEEE MTT-S International Microwave Symposium 2008*, pp. 177-180.

[12] F.J. Herraiz-Martínez, F. Paredes, G. Zamora, F. Martín, and J. Bonache, "Printed magnetoinductive-wave (MIW) delay lines for chipless RFID applications", *IEEE Trans. Ant. Propag.*, vol. 60, pp. 5075-5082, Nov. 2012.

Artículo TECH18

Very Low-cost 80-bit Chipless-RFID Tags Inkjet Printed on Ordinary Paper

C. Herrojo, M. Moras, F. Paredes, A. Núñez, E. Ramon,
J. Mata-Contreras and F. Martín

technologies

MDPI

Article

Very low-cost 80-bit chipless-RFID tags inkjet printed on ordinary paper

Cristian Herrojo [1,*], Miquel Moras [2], Ferran Paredes [1], Alba Núñez [2], Eloi Ramon [2], Javier Mata-Contreras [3], Ferran Martín [1]

[1] CIMITEC, Departament d'Enginyeria Electrònica, Universitat Autònoma de Barcelona, 08193 Bellaterra, Spain; Ferran.Martin@uab.es
[2] Institut de Microelectrònica de Barcelona, IMB-CNM (CSIC), 08193 Bellaterra, Spain.
[3] Departamento de Ingeniería de Comunicaciones, Universidad de Málaga, 29016 Málaga, Spain
* Correspondence: cristian.herrojo@uab.cat; Tel.: +34 93 581 35 22

Received: date; Accepted: date; Published: date

Abstract: A time-domain chipless-RFID system with 80-bit tags inkjet-printed on ordinary DIN A4 paper is reported in this work. The tags, consisting of a linear chain of resonant elements (with as many resonators as number of identification bits plus header bits), are read sequentially and by proximity (through near-field coupling). To this end, a transmission line fed by a harmonic (interrogation) signal tuned to the resonance frequency of the tag resonators (or close to it), is used as reader. Thus, in a reader operation, the tag chain is mechanically displaced over the transmission line, so that coupling between the line and the functional resonant elements of the tag chain is favored. The logic states '1' and '0' are determined by the functionality and non-functionality (resonator detuning), respectively, of the resonant elements of the chain. Through near-field coupling, the transmission coefficient of the line is modulated and, consequently, the output signal is amplitude modulated (AM), being the identification code contained in the envelope function. As long as the tags are inkjet-printed on ordinary DIN A4 paper, their cost is very small. Moreover, tags can be programmed and erased, so that all-identical tags can be massively fabricated (and then programmed in a latter stage), further reducing fabrications costs. The reported prototype tags, with 80 bits of information plus 4 header bits, point out the potential of this approach, of particular interest in secure paper applications.

Keywords: Chipless-RFID; inkjet printing; microwave encoders; time-domain signature barcodes.

1. Introduction

Chipless radiofrequency identification (chipless-RFID) has emerged in the last fifteen years as an alternative to RFID systems with tags equipped with silicon integrated circuits (IC), or chips [1-6]. State-of-the-art chipless-RFID systems cannot compete against chipped-RFID in terms of data storage capacity, size and read distances [7,8]. However, one clear limitation of chipped tags is their cost, related to the presence of the silicon chip, and thereby alleviated in chipless-RFID tags. Thus, chipless-RFID systems are of special interest in applications where the tagged items are low-cost.

Many efforts have been dedicated in recent years to improve the data storage capability of chipless-RFID systems and to reduce the size of the ID encoders, typically consisting of a metallic pattern printed on a flexible dielectric substrate (including plastic or paper, among others). There are two main approaches for the implementation of chipless-RFID systems: (i) time-domain systems [9-14], and (ii) frequency-domain systems [1,2,15-30]. In time-domain systems, the typical operation principle is time-domain reflectometry (TDR). The ID code is contained in the echoes generated by a delay line with scatters (encoder) in response to a pulsed (interrogation) signal. Unless SAW

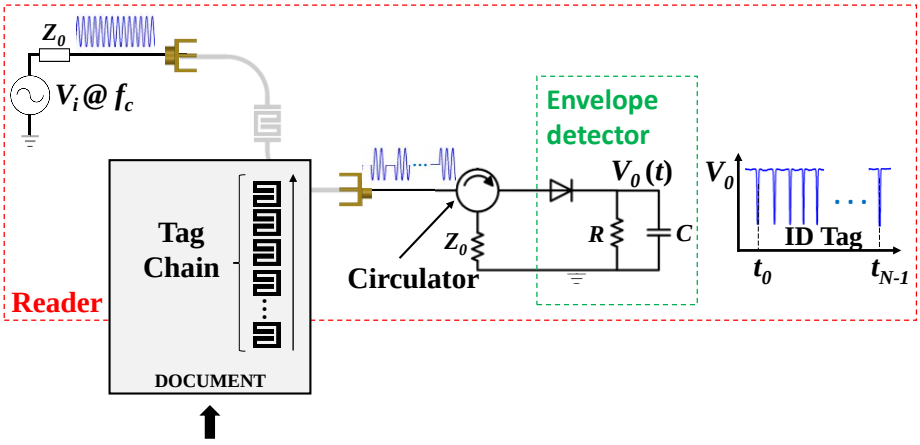

Figure 1. Sketch of the operating principle of the time-domain chipless-RFID system based on near-field and sequential bit reading.

technology is considered [31-35], TDR-based tags implemented by either etching or printing the encoders on a planar substrate exhibit a very limited data storage capability [10,13]. In frequency-domain, 35-bit tags have been reported by loading a transmission line with spiral resonators [1,15]. In such frequency-domain tags, also called spectral signature barcodes, the ID code is given by the singularities present in the radar-cross section (RCS) response (backscattered tags) [22] or in the magnitude or phase of the retransmitted response (retransmission based tags) [15,16,23]. Typically, as many resonators as number of bits are necessary, each resonator being tuned to a different frequency. Therefore, the spectral bandwidth of such frequency-domain tags increases with the number of bits, and a very wide multi-frequency (sweeping) interrogation signal is required for tag reading, provided such number of bits (or resonators) is significant. This makes the reader more expensive, preventing the implementation of chipless-RFID systems with a number of bits close to the one of the standard EPC global of chipped UHF-RFID (96 bits).

In order to increase the data density per frequency, and per area unit, hybrid tags, exploiting several domains simultaneously, have been reported [36-49]. Examples include tags where frequency position is combined with phase deviation [36], or with polarization diversity [37], or with notch bandwidth [48], and tags where the frequency is combined with the peak [41],[42] or notch [43],[44] magnitude, among others [38]-[40],[45]-[47],[49]. In all these cases, more than one bit per resonant element is achieved. Nevertheless, the data storage capability of these hybrid tags is also limited.

Recently, the authors have presented a novel time-domain approach for chipless-RFID systems, where the number of bits can be dramatically increased [50-55]. In this paper, we demonstrate the functionality of this system by reading 80-bit tags (plus header bits) inkjet-printed on ordinary din A4 paper. This represents a milestone in terms of number of bits and cost. Such low cost arises from the fact that a single layer of conducive ink suffices for the fabrication of readable tags, and ordinary paper is extremely cheap. Moreover, all-identical tags can be massively manufactured, and then programmed in a later stage, further reducing fabrication costs.

2. The chipless-RFID system: operating principle, reader and tag

2.1. Operating principle

The operating principle of the time-domain chipless-RFID system based on near-field and sequential bit reading, first reported in [50], is succinctly reviewed in this paper for coherence and completeness. The tag consists of a linear chain of identical resonant elements printed, or etched, at predefined and equidistant positions on a dielectric substrate (typically a flexible substrate, such as plastic, paper, etc.). The ID code is given by the functionality or non-functionality of the resonant

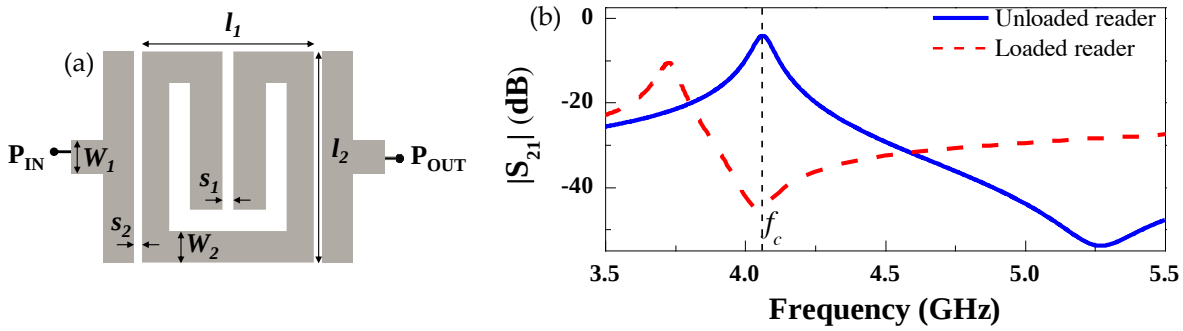

Figure 2. Layout of the SRR-loaded microstrip line of the reader (a), and transmission coefficients with and without oppositely oriented SRR on top of it (b). Dimensions are (in mm): l_1 = 3.16, l_2 = 3.35, s_1 = 0.2, s_2 = 0.2, W_1 = 0.56, and W_2 = 0.5. The considered air gap is 0.25 mm. The substrate of the line is the *Rogers RO3010* with thickness h = 0.635 mm and dielectric constant ε_r = 10.2. The substrate of the tag is the *Rogers RO4003C* with thickness h = 0.204 mm and dielectric constant ε_r = 3.55. Figure extracted from [55]; printed with permission.

elements, where a resonator is not functional if it is detuned, namely, not resonating at its fundamental resonance frequency. Resonator detuning is achieved, e.g., by cutting it. For tag reading, an element able to detect the functionality of the resonant elements is required. For that purpose, a transmission line fed by a harmonic signal tuned to the resonance frequency of the tag resonators, or close to it, is adequate. Thus, by displacing the tag chain over the fed line, coupling between the line and the resonant elements is expected (as long as the resonant elements are functional and the distance between the line and the resonant elements is small). The effect is a variation of the transmission coefficient at the feeding frequency, due to near-field coupling, and consequently, amplitude of the output signal is modulated. Hence, the ID code is contained in the envelope function of the amplitude modulated (AM) signal, which can be inferred by means of an envelope detector. The working principle of this unconventional time-domain chipless-RFID system is illustrated in Fig. 1. As compared to frequency-domain chipless-RFID systems, the time-domain approach illustrated in Fig. 1 exhibits a relevant advantage: the interrogation signal is a harmonic (single tone) signal. Thus, the cost of the reader can be significantly reduced since a multi-frequency sweeping signal is not required. Indeed, the spectral bandwidth of the proposed tags is virtually null, since all the resonant elements of the tag are identical (i.e., tuned to the same frequency). The difference between these tags and spectral signature barcodes is that reading is based on frequency division multiplexing in spectral signature barcodes, whereas in the novel chipless-RFID systems proposed by us, time division multiplexing is used for tag reading.

2.2. The reader

As we have mentioned in the previous subsection, the active part of the reader is a transmission line fed by a harmonic signal. Particularly, the considered structure is a microstrip line loaded with a split ring resonator (SRR) in bandpass configuration, as depicted in Fig. 2 [54]. This structure exhibits two singular frequencies: (i) a reflection zero frequency (where the signal between the input and the output port is transmitted), and (ii) a transmission zero frequency. By this means, a large excursion of the transmission coefficient is achieved when a resonant element identical to the SRR of the line is aligned and oppositely oriented to it. The net effect is an overall displacement of the transmission coefficient to the left, as depicted in Fig. 2(b). By properly tuning resonator dimensions, and the vertical distance between the line and the oppositely oriented resonator (air gap), it is possible to optimize the variation of the transmission coefficient at the frequency of maximum transmission of the unloaded SRR-loaded line, f_c, as seen in Fig. 2(b). Thus, the tags will be implemented as chains of

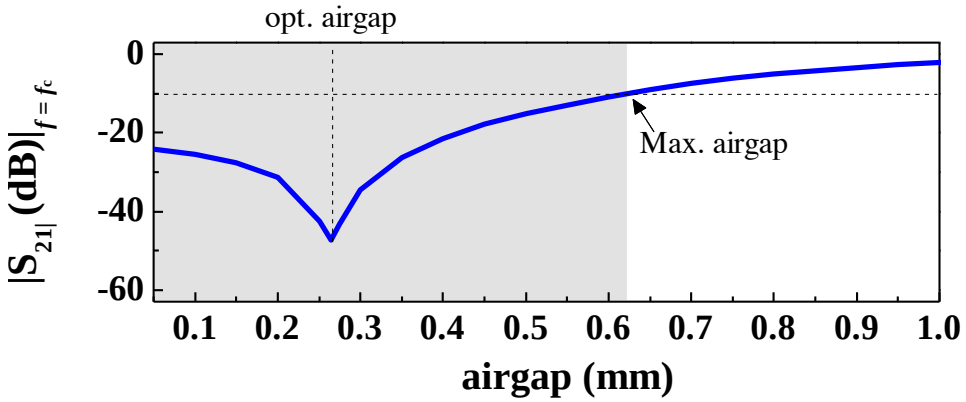

Figure 3. Transmission coefficient at f_c for different values of the air gap, corresponding to the reader loaded with perfectly alignedSRR. Figure extracted from [54]; printed with permission.

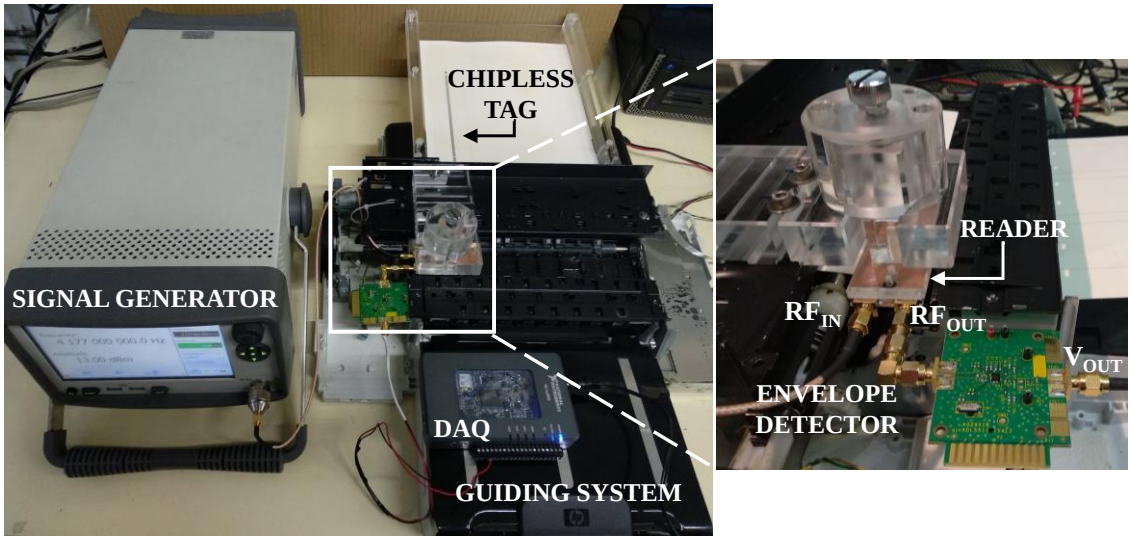

Figure 4. Photograph of the reader.

SRRs, printed on a different substrate, and tag reading will proceed by mechanically displacing the tag chain over the SRR of the line, with the SRRs of the tag oppositely oriented and aligned with regard to the SRR of the line. In practice, it is difficult to keep the air gap uniform, but some tolerance in the air gap distance is acceptable as long as the variation of the transmission coefficient at f_c is significant even when the air gap deviates from the optimum value (Fig. 3).

The reader consists not only of the SRR-loaded line, but also of the envelope detector plus the necessary electronics to generate the harmonic (interrogation) signal. In [50-55], the envelope detector was implemented by means of a Schotcky diode (*Avago HSMS-2860*), an active probe which acts as a low pass filter (with $R = 1$ MΩ and $C = 1$ pF) and an isolator to prevent reflections from the diode. In this work, an integrated circuit (*Analog Devices ADL5511*) able to provide the envelope function (hence reducing costs) is alternatively used. The envelope signal is then driven to a data acquisition card (*National Instruments myRIO*) connected to a computer, where the sampled data can be viewed. The harmonic feeding signal is generated by means of the *Agilent E44338C* function generator. An important part of the reader is the mechanical system needed to displace the tag over the transmission line of the reader, in close proximity to it. To this end, a printer has been adapted and equipped with an *adhoc* guiding channel in order to absorb the tag (printed encoder). Good alignment and uniform air gap distance between the tag chain and the resonator of the reader is achieved with this system. The photograph of the complete reader is depicted in Fig. 4, where the different reader parts are indicated.

Figure 5. Photograph of the fabricated 80-bit tag with all bits set to '1' and with header bits.

2.3. The tags

As we have previously mentioned, the tags consist of a linear chain of SRRs identical to the one of the reader line. To demonstrate the viability of the system with very low-cost tags, we have opted for using ordinary din A4 paper as tag substrate. Obviously, the response of the SRR-loaded line of the reader, in turn loaded with the tag, depends on the tag substrate, but this dependence is relatively soft, as long as tag substrates with similar thickness and dielectric constant are considered. Moreover, we have implemented the tags by inkjet-printing using the *Dupont™ PE410* conductive ink with measured conductivity of 7.28×10^6 S/m. One layer (with measured thickness of 2.6 μm) suffices, thereby optimizing tag cost. The number of resonant elements has been set to 80 for the ID code (corresponding to 80-bit tags), plus four SRRs for the header bits. Such header bits are needed since the tag can be displaced over the reader starting from the two extremes (corresponding to tag SRRs either faced up or down). The photograph of the fabricated tag with all ID bits set to the logic state '1' (i.e., with all resonators functional) is depicted in Fig. 5.

It is worth mentioning that tags can be programmed and erased after being fabricated. This is an important aspect since fabrication costs can be further reduced, provided all-identical tags can be massively manufactured (requiring only a single mask), and then programmed in a later stage (custom level). Tag programming can be achieved by cutting those resonators with logic state '0', hence detuning them. This can be done mechanically, or by means of other systems such as, e.g., laser ablation. Moreover, tag erasing can be achieved by simply short-circuiting those previously detuned SRRs (for instance, by means of inkjet-printing). Tag erasing (after programming) and reprogramming is unusual, but this possibility exists and means that a single tag can be recycled several times.

3. Results and discussion

To illustrate the potential of the proposed approach, we have obtained the ID code of the fabricated tag with all ID bits set to '1'. Figure 6(a) depicts the inferred code, with tag SRRs faced up and down. As can be seen, the code is correctly read regardless of the relative orientation between the tag and the reader. We have then programmed the tag by cutting certain resonant elements. Particularly, we have considered the sequence (for the ID code) '11111111101111111011111111111110011111111110001111111010111111111011111111111'. Tag reading in this case provides the responses shown in Fig. 6(b), with tag SRRs faced up and down, where it can be appreciated that the ID code is successfully obtained. Finally, we have erased the tag and reprogrammed it with the ID code '11111111111111111110101011111111111100100111111111111111101011111111111000, and the results derived from tag reading, depicted in Fig. 6(c), reveal that, again, the ID code is correctly inferred regardless of tag orientation. With these results, it is clearly pointed out that: (i) the number of achievable bits with this system is only limited by tag size; (ii) tag cost is very small as long as ordinary DIN A4 paper is used for tag substrate and a single layer of conductive ink suffices to correctly read the tags; (iii) tags can be programmed and erased as many times as needed. With these characteristics, the proposed chipless-RFID system can be of interest in applications devoted to secure paper, where, by printing the ID codes directly on the document of interest, it is equipped with a secure code, difficult to reproduce. Indeed, the codes can

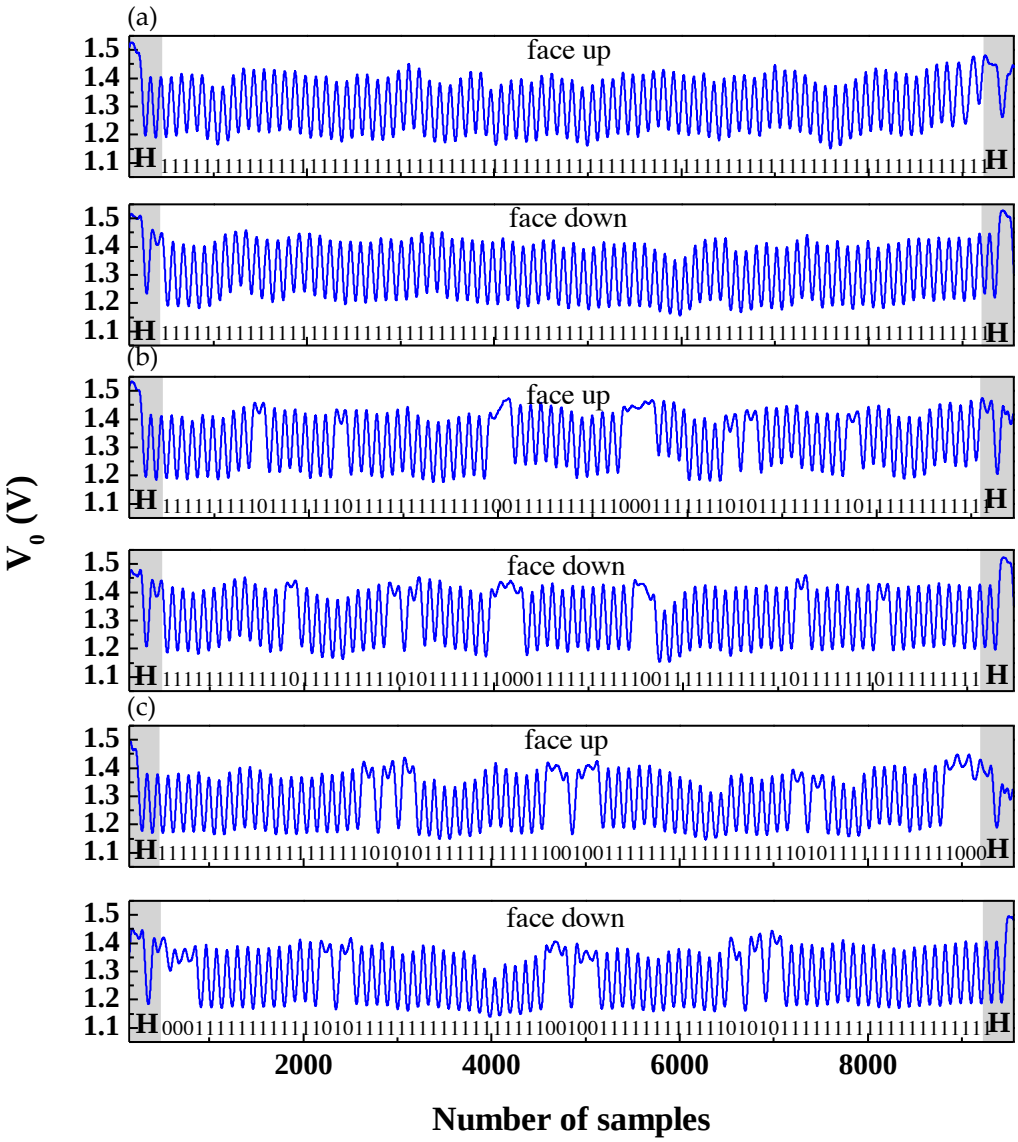

Figure 6. Measured envelope functions of the inkjet-printed 80-bit tag with the indicated codes. Since the envelope function has been inferred from a data acquisition system, the abscise axis is the number of samples.

be photocopied, but tag reading requires a sophisticated system of the type shown in Fig. 4. Moreover, it is possible to fabricate the tags through lamination, resulting in buried encoders difficult to reproduce. Banknotes, certificates, corporate documents, ballots, exams, medical recipes, etc. are different types of documents that can take benefit of the proposed encoding system, providing them further security against counterfeiting.

The future research direction will be to boost the number of resonant elements per unit length of the tag. Typically, in chipless-RFID systems one figure of merit is the density of information per area unit. In the proposed chipless-RFID system, however, the tags exhibit an extremely long shape factor, and, consequently, the interest is to accommodate the largest possible number of bits along the tag length (typically limited by the size of the document). Obviously, this can be achieved by increasing the resonance frequency of the SRRs (hence reducing its size), but this typically increases the cost of the associated electronics (harmonic signal generation, etc.). Therefore, the next challenge is to find novel resonator topologies, very short in the longitudinal direction of the tag chain, providing high sensitive tags that can be read through near-field coupling (sequentially) by means of a dedicated (*adhoc*) reader.

4. Conclusions

To conclude, 80-bit chipless-RFID tags inkjet printed on ordinary DIN A4 paper have been presented for the first time. These tags are of special interest for secure paper applications, where the encoders can be directly printed on the document of interest. Reading by proximity (through near-field), as required in the reported chipless-RFID system, is not an issue in such applications, where the small distance between the tag and the reader may provide certain level of confidence against spying, snooping or eavesdropping. Additional advantages of the system are the high number of achievable bits (only limited by tags size), the low-cost of the tags, and the possibility to program and erase the tags.

Acknowledgments: This work was supported in part by MINECO-Spain under Project TEC2016-75650-R, in part by Generalitat de Catalunya under project 2017SGR-1159, in part by the Institució Catalana de Recerca i Estudis Avançats (who awarded Ferran Martín), and in part by FEDER funds. Cristian Herrojo acknowledges MINECO for supporting his research activity through the FPI grant BES-2014-068164.

Author Contributions: C.H. and F.M. conceived the reported time-domain chipless-RFID approach; C.H., F.P. and J.M-C. designed the active part of the reader and the tags; M.M. developed the electronics necessary for tag reading; A.N. fabricated the tags; C.H., F.P, M.M and E.R. carried out the validation experiments; F.M wrote the paper in collaboration with all the authors.

Conflicts of Interest: The authors declare no conflict of interest. The founding sponsors had no role in the design of the study; in the collection, analyses, or interpretation of data; in the writing of the manuscript, and in the decision to publish the results.

References

1. Preradovic S.; Karmakar N. C. Chipless RFID: bar code of the future. *IEEE Microwave Magazine* **2010**, *11*, pp. 87-97.
2. Preradovic S.; Karmakar N. C. *Multiresonator-Based Chipless RFID: Barcode of the Future*; Springer: New York, USA, 2011.
3. Karmakar N.C.; Koswatta R.; Kalansuriya P.; E-Azim R.; *Chipless RFID Reader Architecture*; Artech House, 2013.
4. Perret E. *Radio Frequency Identification and Sensors: From RFID to Chipless RFID*; John Wiley: New York, USA, 2014.
5. Rezaiesarlak R.; Manteghi M. *Chipless RFID: Design Procedure and Detection Techniques*; Springer: New York, USA, 2015.
6. Karmakar N. C.; Zomorrodi M.; Divarathne C. *Advanced Chipless RFID*; John Wiley: Hoboken, NJ, USA, 2016.
7. Finkenzeller K.; *RFID Handbook: Radio-Frequency Identification Fundamentals and Applications*, 2nd Ed.; John Wikey: New York, USA, 2004.
8. Hunt V. D.; Puglia A.; Puglia M. *RFID: A Guide to Radio Frequency Identification*; John Wiley: New York, USA, 2007.
9. Chamarti A.; Varahramyan K. Transmission delay line based ID generation circuit for RFID applications. *IEEE Microw. Wireless Compon. Lett.* **2006**, *16*, pp. 588-590.
10. Schüßler M.; Damm C.; Jakoby R. Periodically LC loaded lines for RFID backscatter applications. In Proc. of Metamaterials 2007, Rome, Italy, October 2007; pp. 103-106.
11. Schüßler M.; Damm C.; Maasch M.; Jakoby R. Performance evaluation of left-handed delay lines for RFID backscatter applications. In Proc. of the IEEE MTT-S International Microwave Symposium, Atlanta, USA, June 2008; pp. 177-180.
12. Shao B.; Chen Q.; Amin Y.; Mendoza D. S.; Liu R.; Zheng L. R. An ultra-low-cost RFID tag with 1.67 Gbps data rate by ink-jet printing on paper substrate. In IEEE Asian Solid State-Circuits Conference, Beijing, China, November 2010; pp. 1–4.
13. Herraiz-Martínez F. J.; Paredes F.; Zamora G.; Martín F.; Bonache J. Printed magnetoinductive-wave (MIW) delay lines for chipless RFID applications. *IEEE Trans. Ant. Propag.* **2012**, *60*, pp. 5075-5082.
14. Tedjini S.; Perret E.; Vena A.; Kaddout D. Mastering the electromagnetic signature of chipless RFID tags. In *Chipless and Conventional Radiofrequency Identification: Systems for Ubiquitous Tagging*; IGI Global: Hershey, USA 2012.

15. Preradovic S.; Balbin I.; Karmakar N. C.; Swiegers G. F. Multiresonator-based chipless RFID system for low-cost item tracking. *IEEE Trans. Microw. Theory Techn.* **2009**, *57*, pp. 1411-1419.
16. Preradovic S.; Karmakar N. C. Design of chipless RFID tag for operation on flexible laminates. *IEEE Anten. Wireless Propag. Lett.* **2010**, *9*, pp. 207-210.
17. McVay J.; Hoorfar A.; Engheta N. Space-filling curve RFID tags. In Proc. of 2006 IEEE Radio and Wireless Symposium, San Diego, CA, USA, October 2006; pp. 199–202.
18. Jalaly I.; Robertson D. Capacitively-tuned split microstrip resonators for RFID barcodes. In Proc. of European Microwave Conference, Paris, France, October 2005; pp. 4–7.
19. Jang H.-S.; Lim W.-G.; Oh K.-S.; Moon S.-M.; Yu J.-W. Design of low-cost chipless system using printable chipless tag with electromagnetic code. *IEEE Microw. Wireless Compon. Lett.* **2010**, *20*, pp. 640-642.
20. Vena A.; Perret E.; Tedjini S. A fully printable chipless RFID tag with detuning correction technique. *IEEE Microw. Wireless Compon. Lett.* **2012**, *22*, pp. 209-211.
21. Vena A.; Perret E.; Tedjini S. Design of compact and auto-compensated single-layer chipless RFID tag. *IEEE Trans. Microw. Theory Techn*. **2012**, *60*, pp. 2913-2924.
22. Vena A.; Perret E.; Tedjini S. High-capacity chipless RFID tag insensitive to the polarization. *IEEE Trans. Ant. Propag.* **2012**, *60*, pp. 4509-4515.
23. Girbau D.; Lorenzo J.; Lazaro A.; Ferrater C.; Villarino R. Frequency-coded chipless RFID tag based on dual-band resonators. *IEEE Antennas Wireless Propag. Lett*. **2012**, *11*, pp. 126–128.
24. Khan M. M.; Tahir F. A.; Farooqui M. F.; Shamim A.; Cheema H. M. 3.56-bits/cm^2 compact inkjet printed and application specific chipless RFID tag. *IEEE Ant. Wireless Propag. Lett*. **2016**, *15*, pp. 1109-1112.
25. Rezaiesarlak R.; Manteghi M. Complex-natural-resonance-based design of chipless RFID tag for high-density data. *IEEE Trans. Ant. Propag.* **2014**, *62*, pp. 898-904.
26. Bhuiyan M. S.; Karmakar N.C. A spectrally efficient chipless RFID tag based on split-wheel resonator. In International Workshop on Antenna Technology: Small Antennas, Novel EM Structures, and Applications, Sydney, NSW, Australia, March 2014.
27. Nijas C.M.; Deepak U.; Vinesh P.V.; Sujith R.; Mridula S.; Vasudevan K.; Mohanan P. Low-cost multiple-bit encoded chipless RFID tag using stepped impedance resonator. *IEEE Trans. Antennas Propag*., **2014,** *62*, pp. 4762–4770.
28. Machac J.; Polivka M. Influence of mutual coupling on performance of small scatterers for chipless RFID tags. In 24th International Radioelektronika Conference, 2014.
29. Svanda M.; Machac J.; Polivka M.; Havlicek J. A comparison of two ways to reducing the mutual coupling of chipless RFID tag scatterers. In Proc. of 21st International Conference on Microwave, Radar and Wireless Communications (MIKON), Krakow, Poland, May 2016.
30. Herrojo C.; Naqui J.; Paredes F.; Martín F. Spectral Signature Barcodes based on S-shaped Split Ring Resonators (S-SRR). *EPJ Applied Metamaterials* **2016**, *3*, pp. 1-6.
31. Hartmann C. S. A global SAW ID tag with large data capacity. In Proc. of IEEE Ultrasonics Symposium, Munich, Germany, October 2002; pp. 65–69.
32. Saldanha N.; Malocha D.C. Design Parameters for SAW multi-tone frequency coded reflectors. In Proc. Of IEEE Ultrasonics Symposium, New York, USA, October 2007; pp. 2087-2090.
33. Harma S.; Plessky V.P.; Hartmann C.S.; Steichen W. Z-path SAW RFID tag. *IEEE Trans. Ultrasonics, Ferroelectric Freq. Control* **2008**, *55*, pp. 208-213.
34. Tao H.; Weibiao W.; Haodong W.; Yongan S. Reflection and scattering characteristics of reflectors in SAW tags. *IEEE Trans. Ultrasonics, Ferroelectric Freq. Control* **2008**, *55*, pp. 1387-1390.
35. Harma S.; Plessky V.P.; Xianyi L.; Hartogh P. Feasibility of ultra-wideband SAW RFID tags meeting FCC rules. *IEEE Trans. Ultrasonics, Ferroelectric Freq. Control* **2012**, *56*, pp. 812-820.
36. Vena A.; Perret E.; Tedjini S. Chipless RFID tag using hybrid coding technique. *IEEE Trans. Microw. Theory Techn.* **2011**, *59*, pp. 3356-3364.
37. Vena A.; Perret E.; Tedjini S. A compact chipless RFID tag using polarization diversity for encoding and sensing. 2012 IEEE International Conference on RFID, Orlando, FL, USA; pp. 191-197.
38. Islam M. A.; Karmakar N. C. A novel compact printable dual-polarized chipless RFID system. *IEEE Trans. Microw. Theory Techn.* **2012**, *60*, pp. 2142-2151.
39. Balbin I.; Karmakar N.C. Phase-encoded chipless RFID transponder for large scale low cost applications. *IEEE Microw. Wireless. Comp. Lett.* **2009**, *19*, pp. 509-511.
40. Genovesi S.; Costa F.; Monorchio A.; Manara G. Chipless RFID tag exploiting multifrequency delta-phase quantization encoding. *IEEE Ant. Wireless, Propag. Lett.* **2015**, *15*, pp. 738-741.

41. Rance O.; Siragusa R.; Lemaitre-Auger P.; Perret E. RCS magnitude coding for chipless RFID based on depolarizing tag. In IEEE MTT-S International Microwave Symposium, Phoenix, USA, May 2015.
42. Rance O.; Siragusa R.; Lemaître-Auger P.; Perret E. Toward RCS magnitude level coding for chipless RFID. *IEEE Trans. Microw. Theory Techn.* **2016**, *64*, pp. 2315-2325.
43. Herrojo C.; Naqui J.; Paredes F.; Martín F. Spectral signature barcodes implemented by multi-state multi-resonator circuits for chipless RFID tags. IEEE MTT-S International Microwave Symposium (IMS'16), San Francisco, USA, May 2016.
44. Herrojo C.; Paredes F.; Mata-Contreras J.; Zuffanelli S.; Martín F. Multi-state multi-resonator spectral signature barcodes implemented by means of S-shaped Split Ring Resonators (S-SRR). *IEEE Trans. Microw. Theory Techn.* **2017**, *65*, pp. 2341-2352.
45. Gupta S.; Nikfal B.; Caloz C. Chipless RFID system based on group delay engineered dispersive delay structures. *IEEE Antennas Wireless Propag. Lett*. **2011**, *10*, pp. 1366–1368.
46. Nair R.; Perret E.; Tedjini S. Chipless RFID based on group delay encoding. In IEEE International Conference on RFID-Technologies and Applications, Sitges, Spain, September 2011; pp. 214–218.
47. Feng C.; Zhang W.; Li L.; Han L.; Chen X.; Ma R. Angle-based chipless RFID tag With high capacity and insensitivity to polarization. *IEEE Trans. Antennas Propag*. **2015**, *63*; pp. 1789–1797.
48. El-Awamry A.; Khaliel M.; Fawky A.; El-Hadidy M.; Kaiser T. Novel notch modulation algorithm for enhancing the chipless RFID tags coding capacity. In 2015 IEEE International Conference on RFID, San Diego, CA, USA, April 2015; pp. 25–31.
49. Vena A.; Babar A. A.; Sydanheimo L.; Tentzeris M. M.; Ukkonen L. A novel near-transparent ASK-reconfigurable inkjet-printed chipless RFID tag. *IEEE Antennas Wireless Propag. Lett.* **2013**, *12*, pp. 753–756.
50. Herrojo C.; Mata-Contreras J.; Paredes F.; Martín F. Near-Field Chipless RFID Encoders with Sequential Bit Reading and High Data Capacity". IEEE MTT-S International Microwave Symposium (IMS'17), Honolulu, Hawaii, June 2017.
51. Herrojo C.; Mata-Contreras J.; Paredes F.; Martín F. Microwave encoders for chipless RFID and angular velocity sensors based on S-shaped split ring resonators (S-SRRs). *IEEE Sensors J*. **2017**, *17*, pp. 4805-4813.
52. Herrojo C.; Mata-Contreras J.; Paredes F.; Núñez A.; Ramon E.; Martín F. Near-field chipless-RFID tags with sequential bit reading implemented in plastic substrates. *Int. J. Magnetism. Magnetic Mat*. (in press).
53. Herrojo C.; Mata-Contreras J.; Paredes F.; Martín F. High data density and capacity in chipless radiofrequency identification (chipless-RFID) tags based on double-chains of S-shaped split ring resonators (S-SRRs). *EPJ Appl. Metamat.* **2017**, *4*, article 8, 6 pages.
54. Herrojo C.; Mata-Contreras J.; Paredes F.; Núñez A.; Ramon E.; Martín F. Near-field chipless RFID system with high data capacity for security and authentication applications. *IEEE Trans. Microw. Theory Techn*. **2017**, *65*, pp. 5298-5308.
55. Herrojo C.; Mata-Contreras J.; Paredes F.; Núñez A.; Ramon E.; Martín F. Near-field chipless-RFID system with erasable/programmable 40-bit tags inkjet printed on paper substrates. *IEEE Microw. Wireless. Comp. Lett.* (accepted). DOI: 10.1109/LMWC.2018.2802718.

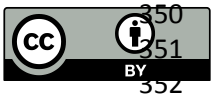

Artículo MAG18

Time-Domain Signature Chipless-RFID Tags: Near-field Chipless-RFID systems with high data capacity

C. Herrojo, M. Moras, F. Paredes, A. Núñez, J. Mata-Contreras, E. Ramon, and F. Martín

Time-Domain Signature Chipless-RFID tags

Near-field chipless-RFID systems with high data capacity

[1]Cristian Herrojo, [2]Miquel Moras, [1]Ferran Paredes, [2]Alba Núñez, [3]Javier Mata-Contreras, [2]Eloi Ramon, [1]Ferran Martín

[1]CIMITEC, Departament d'Enginyeria Electrònica
Universitat Autònoma de Barcelona, 08193 Bellaterra (Barcelona), Spain
Corresponding author: Ferran.Martin@uab.es

[2] Institut de Microelectrònica de Barcelona, IMB-CNM (CSIC), 08193 Bellaterra, Spain

[3]Departamento de Ingeniería de Comunicaciones, Universidad de Málaga, 29016 Málaga, Spain

Chipless radiofrequency identification (chipless-RFID) technology has emerged in the last years as an alternative to RFID systems with tags equipped with silicon integrated circuits (ICs), or chips [1]-[6]. The main advantage of chipless-RFID systems over their chipped counterparts is the lower cost of the tags, motivated by the fact that the identification (ID) code is contained in a printed planar encoder (implementable with conductive inks), rather than being stored in a silicon chip. Low-cost tags (desirably below the dollar-cent barrier) are necessary in many RFID applications involving tagged items or objects with moderate or low price, where chip-based tagging would represent a significant penalty in terms of overall costs. However, chipless-RFID systems present three main drawbacks, as compared to conventional (i.e., chip-based) RFID technology: (i) large tag size, (ii) limited data storage capacity, and (iii) shorter read-ranges. These negative aspects, and the fact that the materials (inks) and manufacturing processes (such as substrate functionalization, printing, etc.) needed for tag fabrication do not still represent a significant reduction in tag price (as compared, e.g., to the cost of passive UHF-RFID tags, of the order of several cents), have limited the penetration of chipless-RFID technology in the market. In this article, an overview of the recent advances to increase the data density of printed encoders, with direct impact on tag size and data capacity, is carried out. Moreover, a recent chipless-RFID concept, based on near-field and sequential bit reading, providing very high data storage capacity (only limited by tag size), is discussed in detail. It is also pointed out that these novel chipless-RFID systems, with tag reading by proximity, are of special interest for

security and authentication applications, where reading at short distance from the tag provides system confidence against external interferences, spying, or eavesdropping.

CHIPLESS RFID VERSUS CHIPPED RFID AND OPTICAL BARCODES

Radiofrequency identification (RFID) is a wireless technology mainly used for identification and tracking of objects, goods, beings, animals, persons, etc. [7],[8]. Most commercially available RFID systems use identification (ID) tags equipped with silicon integrated circuits (IC), or chips, which contain the information relative to the tagged item. As compared to optical bar codes or QR codes, RFID tags are able to store significantly much more information, being possible the identification of individual items. Moreover, RFID tags do not require direct line-of-sight with the reader, and reading distances of several meters are possible in far-field passive tags operating in the UHF band (UHF-RFID tags). Such distances can be extended up to dozens of meters in tags equipped with batteries (active tags), at the expense of higher tag cost and size. Despite the fact that passive UHF-RFID tags are relatively cheap (several cents of dollar), its use is prohibitive in many applications involving low-cost tagged items. Tag cost is dictated by the presence and placement of the IC (by contrast tag size is determined by the antenna, needed for communication purposes with the reader), and it is difficult to envision a future scenario (at least at short term) where the prices of chipped tags drop to 1 dollar-cent or below.

Within the previous context, chipless-RFID has emerged as an alternative technology to chip-based RFID to partially alleviate the high cost of silicon chips [1]-[6]. In chipless-RFID, the tags typically consist of a printed encoder and in some cases they are equipped with an antenna for communication with the reader. By replacing the microchips with such encoders, tag cost can be dramatically reduced, and reasonable predictions situate the cost of massively manufactured chipless-RFID tags below 1 cent [1]. Note that in chipless-RFID, tag price is dictated by the (progressively decreasing) cost of conductive inks, and by the printing fabrication processes (rotogravure, rotary or planar screen-printing, inkjet, etc.). The final cost is mainly determined by the amount of ink required by the encoder (in turn related with the data storage capability, or number of bits), and by the tag antenna, if it is present.

Indeed, chipless-RFID tags are situated between chip-based tags and optical barcodes (or QR codes) in terms of performance (i.e., read range), and cost. Table 1 provides a comparison between these ID technologies that includes performance, cost, size, and other aspects, relevant in certain applications. According to the table, current warhorses in chipless-RFID research are related to the improvement in tag storage capacity, size, and read range (important limitations, as anticipated before, as compared to chipped RFID). Progress in any of these aspects, combined with the advantageous characteristics (mainly tag cost, low power needed by the reader, and robustness against harsh environments), may push chipless-RFID technology towards its progressive penetration in the market.

Table 1. Comparison between chipless-RFID tags, chipped RFID tags, and optical ID codes.

	Optical ID codes	**Chipless RFID**	**Chipped RFID**
Cost	Ultra low	Low	Medium
Size	Very small	Large	Medium
Read range	Very small	Small/moderate	High
Data storage	Medium	Medium	High
Simultaneous reading	No	No	Yes
Reprogrammable	No	Yes (with limits)	Yes
Single band operation	Yes	No	Yes
Power level (reader)	---	Low	Moderate
Harsh environment	No	Yes (with limits)	No
Easy to copy	Yes	No	No

An important aspect highlighted in Table 1, related to tag costs, concerns the possibility to write and erase the tags, a feature which is not possible in optical barcodes or QR codes. By massively printing all-identical chipless tags, and programming them in a later stage, tag manufacturing costs can be reduced significantly, since a single mask is needed for that purpose. Tag programming (and erasing) is possible under certain circumstances, as will be discussed later, and it is a key factor for the potential success of chipless-RFID in future. However, it is not realistic to write/erase (reprogram) the ID code of the tags as many times as in chip-based tags. Moreover, it is not always possible to manufacture all-identical tags and then write the ID code in a later stage (e.g., if the code depends on the shape of the elements forming the encoder). For these main reasons, this aspect has been market as "Yes (with limits)" in Table 1.

Another important issue, very sensitive in applications devoted to security and authentication, is copying and plagiarism. Optical barcodes (or QR codes) can be simply photocopied, and the copy has exactly the same functionality as the original code. So, low-cost copying is possible in optical ID systems. By contrast, copying of RFID tags (both chipless and chipped) is possible, but more sophisticated (and hence high cost) systems are needed for that purpose. Particularly, chipless-RFID tags based on printed conductive inks can be reverse-engineered (unless the encoders are buried), and consequently can be reproduced. However, to this end, high-cost printers, conductive inks, and custom printing processes are required. On the other hand, although photocopied chipless-RFID tags contain, indeed, the ID code, tag reading cannot be achieved by means of a specific (dedicated) chipless-RFID reader (able to read the ink-based printed tags). Thus, counterfeiting of items or goods is prevented, unless high-cost systems are used for copying.

Other differences between the considered wireless ID technologies refer to the possibility of simultaneous tag reading (only possible in chip-based RFID systems), the required power level of the reader (moderate in chipped RFID systems, as long as a minimum power level is needed to activate the chip), and the bandwidth of the

interrogation signal (narrow, i.e., single-band, in optical ID codes and chipped RFID systems, but wide in chipless-RFID systems). Finally, concerning the possibility of tag operation in harsh environments, it should be mentioned that silicon ICs exhibit limited robustness against extreme ambient factors (temperature, humidity, radiation, etc). Therefore, chipless-RFID tags can be considered to be (in general) superior in this aspect, although the properties of conductive inks may be degraded if they are subjected to extreme conditions, as well. On the other hand, in certain environments subjected to pollution, the functionality of optical barcodes and QR codes may be limited, contrary to the superior robustness of radiofrequency systems against dirtiness.

CLASSIFICATION OF CHIPLESS-RFID SYSTEMS

A former detailed classification of chipless-RFID systems (or tags) was given in [1]. It is nowadays accepted that there are two main categories of printed chipless tags, i.e., time-domain based tags [9]-[14] and frequency-domain based tags [1],[2][15]-[30], and a third group, where several domains are exploited simultaneously (hybrid tags) [31]-[44]. Besides these types of tags, there is a recently reported approach for the implementation of chipless-RFID systems, where tags are read by proximity (through near-field) and sequentially [45]-[50]. This unconventional system exploits time-domain, but the working principle is different than the one of most chipless-RFID systems operating in time domain. The main advantage of this approach is the achievable number of bits, only limited by tag size. The ID code is contained in the amplitude modulated signal generated by the tags, which can be considered to be time-domain signature barcodes, in analogy to the frequency (or spectral) signature barcodes of frequency-domain based chipless-RFID tags [1]. Since these novel chipless-RFID systems are the main purpose of this article, we will study them separately in the next Section. So, let us succinctly review the cited approaches, in order to understand the potential of time-domain signature barcodes in terms of data capacity.

Time-domain based systems

The general working principle of time-domain based chipless-RFID systems is time domain reflectometry (TDR) –see Fig. 1. In these systems, the ID code is contained in the echoes generated by a delay line (with reflectors situated at certain positions corresponding to the specific ID code) to a pulsed interrogation signal. TDR based tags exhibit fast responses as compared to frequency-domain tags, but their bit encoding capability is limited, and either large delay lines or very narrow pulses are needed to avoid overlapping of the reflected pulses. Tags based on surface acoustic wave (SAW) technology [51]-[55] exhibit competitive performances, but at the expense of high cost, as long as a fully planar approach is not involved in this case (these tags need electro-acoustic transducers).

Frequency-domain (spectral signature) based systems

For the reasons explained before, most fully planar chipless-RFID tags are implemented on the basis of frequency-domain reading, rather than time-domain. Frequency-domain

based tags, also designated as spectral signature barcodes, consist of a set of resonant elements each one tuned to a different frequency. Typically, each resonant element provides a bit of information, and the corresponding logic state, '1' or '0', depends on whether the resonant element is functional or detuned (inoperative) at the fundamental frequency. Thus, tag reading proceeds by sending a multi-frequency interrogation signal (covering the spectral bandwidth) to the tag, and the ID code is given by the presence or absence of abrupt spectral features either in the amplitude, phase or group delay responses. Figure 2 illustrates the working principle of frequency-domain chipless-RFID systems, where two types of tags can be considered: (i) retransmission-based [15],[16], [23] and (ii) backscattered-based [22] tags. In the former, a transmission line is loaded with the encoding resonant elements, and it is equipped with two cross-polarized antennas for reception/transmission from/to the reader. In backscattered chipless tags, the resonant elements provide the spectral signature through the peaks in their radar cross section (RCS) response, and antennas are avoided, hence reducing the size of the tags.

Despite the fact that a considerable number of bits (35) has been reported in spectral signature chipless-RFID tags based on spiral resonators [15], see Fig. 3, the required spectral bandwidth for tag reading is very wide, and this represents a penalty in terms of reader costs in a real scenario, where the sweeping interrogation signal must be generated by means of a voltage-controlled oscillator (VCO). Therefore, strategies to increase the density of bits per frequency (DPF), exploiting more than one domain simultaneously, have been recently reported, giving rise to the so-called hybrid approach, to be discussed next.

Hybrid approach (enhancing the data density)

In hybrid tags, the main aim is to increase the number of bits by providing more than two logic states per resonant element, using simultaneously two independent parameters (or domains) for coding. By this means, the data density per frequency (DPF) and the data density per surface (DPS), two figures of merit in chipless tags, can be effectively improved. Various proposals of hybrid chipless-RFID tags can be found in the literature, including tags where frequency position is combined with phase deviation [31], or with polarization diversity [32], or with notch bandwidth [43], and tags where the frequency is combined with the peak [36],[37] or notch [38],[39] magnitude, among others [33]-[35],[40]-[42],[44].

Let us illustrate the potential of hybrid tags with two examples. In [31], Vena *et al*. achieved a coding capacity equivalent to 22.9 bits with only five resonant elements, by combining frequency position with phase deviation. For that purpose, the authors use C-shaped resonators, with resonance frequencies in the range 2.5 GHz – 7.5 GHz, printed on *FR4* substrate (Fig. 4). The principle is based on the RCS responses of these resonant elements, which exhibit a peak and a dip. The peak frequency essentially depends on the length of the resonant element, whereas the dip position is given by the ratio g/L, as defined in Fig. 4. Figure 5 depicts the four responses inferred from a single resonant

element, by slightly modifying its dimensions. For each resonance peak, there are two dips that provide different phase response. With this example, it is shown that a single resonant element suffices to implement at least two bits. Therefore, by allowing further variations in the dimensions, it is possible to enhance the coding capacity per resonant element (4.6 bits per resonant element in [31]).

Another possibility mentioned before and reported here as second illustrative example, exploits the magnitude level of the RCS of C-shaped resonant elements [37]. The tags are very similar to those of the previous example, but in this case the modulation in resonator dimensions is focused on varying the peak level of the RCS. Figure 6 depicts three different tags, together with the measured responses (RCS magnitude level) of the three first peaks. The potential to generate multiple states per resonant element can be appreciated. Within this approach, 3 bits per resonant element are achievable, according to the authors [37].

Although hybrid coding techniques provide enhanced data density per frequency, an intrinsic limitation is related to the fact that resonator bandwidth requirements increase as the number of bits per resonant element is forced to increase. In other words, to achieve dozens of bits (but still far from the data capacity of chipped tags), significant fractional bandwidths are needed. Note, for instance, that in [31] the fractional bandwidth occupied by the tags is as high as 100%, and only 22.9 bits are achieved, i.e., very far from the 96 bits of UHF-RFID tags, according to the electronic product code (EPC) tag data standard. Let us review in the next section a recently proposed approach, useful to dramatically increase the number of bits, where the interrogation signal is simply a harmonic (single-tone) signal. Tag reading by proximity (near-field) is a due, but this is not necessarily an issue in applications related to security and authentication, as will be discussed.

VERY HIGH DATA-STORAGE CAPACITY TAGS: TIME-DOMAIN SIGNATURE NEAR-FIELD CHIPLESS-RFID SYSTEMS

The first proposals of chipless-RFID systems based on frequency-domain were conceived on the basis of the presence or absence of resonant elements tuned at the predefined frequencies within the spectral bandwidth, or, equivalently, on the basis of the functionality or not (detuning) of such resonant elements [15],[16]. Within this approach, the tag ID code is “frequency distributed”, and this represents a penalty in terms of reader costs, as long as a wideband interrogation signal is required for tag reading. Alternatively, this scheme based on resonator presence/absence (or resonator functionality/detuning) can be implemented in time domain, by considering identical resonators (functional or detuned, depending on the logic state) that are read sequentially (i.e., at different time) [45]-[50]. To this end, the resonant elements forming the code must be simply grouped forming a chain, and its functionality (and hence the ID code) can be detected, e.g., through near-field, by displacing the resonator chain (the tag) over the active part of the reader, in close proximity to it. According to this strategy, the ID code is “time distributed”. Indeed, to be more precise, we should

say that both the frequency-domain encoders and these novel time-domain encoders contain the ID code distributed in space. However, tag reading proceeds by frequency sweeping in the former case, and by time-division multiplexing in the second case. Conceptually, both systems are very similar, but in the novel proposed chipless-RFID system, the required spectral bandwidth is virtually null, since a (single-tone) harmonic interrogation signal, tuned to the frequency of the resonators (or close to it), is required for tag reading, as will be shown. In parallelism to the designation of spectral (or frequency) signature barcodes to the frequency-domain chipless-RFID tags, we can call time-domain signature barcodes to these novel chipless tags based on chains of identical (functional or detuned) resonators.

In order to sequentially detect the functional and detuned resonators of the chain through near-field, as required in a reading operation, an element sensitive to electromagnetic coupling with the resonant elements of the tag, e.g., a transmission line, is needed. By feeding such line (active part of the reader) with a harmonic signal tuned to the frequency of the tag resonators (or close to it), the presence of functional resonators very close to the line will generate line-to-resonator coupling, which in turn will modify (decrease) the transmission coefficient. Consequently, by displacing the tag chain over the line (next to it), the amplitude of the feeding signal will be modulated at the output port of the line according to the presence or absence of functional resonators, and hence the ID code can be inferred from such amplitude-modulated (AM) signal. The interrogation signal is, thus, a single-tone (carrier) signal, the system works similar to an AM modulator, and the ID code is given by the envelope function, which can be obtained by means of an envelope detector. The working principle of this time-domain chipless-RFID system is illustrated in Fig. 7.

Let us now make some considerations with regard to the reader. By simply using a transmission line (microstrip, CPW, etc.) as sensitive element for tag reading through electromagnetic coupling (near-field), a fundamental limitation arises. Namely, in order to accommodate the largest possible number of bits per area unit, the distance between adjacent resonators in the tag must be reduced as much as possible (within the limits of the fabrication technology). Under these circumstances, both inter-resonator coupling in the tag chain (similar to the coupling that takes place in magneto-inductive wave transducers [56]) and multiple couplings between the line and several tag resonators (those closest to the line) cannot be avoided. However, these couplings obscure the detection of the functional and detuned resonators, hence limiting the readability of the system, as discussed in [45]. Therefore, a solution to prevent such undesired effects (couplings) must be introduced, in order to achieve a high information density per surface (a figure of merit) by minimizing inter-resonator distance.

The strategy to solve the previous problem is to introduce a resonant element (identical to those of the tag chain) in the transmission line of the reader, coupled to it (such solution was indeed first introduced in [57],[58], for the implementation of angular velocity sensors based on chains of resonant elements). This generates a transmission zero (or notch) in the transmission coefficient of the line. However, the frequency

position of this notch can be modulated by coupling the resonator of the line to an identical resonator. Thus, if the tag resonators chain is displaced in close proximity to the resonator of the line, and the feeding (carrier) signal is tuned to the frequency of the notch that results from the coupling between both resonators (the one of the line and the one of the chain, provided it is functional), the previous undesired multiple couplings are avoided. The reason is that such couplings occur at the frequency of the isolated resonators, different from the one of the coupled resonators, which is smaller.

The first tag prototypes based on this time-domain approach were implemented by means of S-shaped split ring resonators (S-SRRs), a particle first reported in [59]-[61], and later used in the design of angular velocity sensors [62]. Thus, the reader necessary to obtain the ID codes was based on an S-SRR loaded line, particularly a CPW (Fig. 8) [45]. This resonant element exhibits high magnetic coupling to the CPW at the fundamental resonance since the currents are antiparallel in each loop (one clockwise and the other one counterclockwise) at that frequency [62]. Therefore, the particle can be easily excited by the counter magnetic fields present at both slots of the CPW transmission line. By considering a gap distance between the S-SRR of the line and the one of tag of 0.25 mm, the fundamental resonance frequency of the coupled and perfectly aligned S-SRRs is found to be f_0 = 4 GHz (the considered substrates for the CPW and tag are indicated in the caption of Fig. 8). By tuning the feeding interrogation signal to that frequency, $f_c = f_0$, the excursion experienced by the transmission coefficient by tag motion is depicted in Fig. 9. The transmission coefficient is minimum (with measured –6 dB transmission) in the reference position (perfectly aligned S-SRRs) and it is maximum (close to 0 dB transmission) when the relative displacement between the S-SRRs of the line and tag is half a chain period. By varying the gap distance, inevitable in a real scenario, the response of Fig. 9 changes, but there is some tolerance in the excursion experienced by the measured transmission coefficient (6 dB in Fig. 9). This excursion has direct impact on the modulation index of the output signal. Therefore, it is a key parameter in these time-domain chipless-RFID systems.

In [46], the S-SRR based tag and reader system was validated by considering circularly-shaped 40-bit tags, whereas in [48] a double linear chain of S-SRRs was considered in order to reduce the length of the tags. In this later case, a pair of S-SRRs loading the CPW is needed, but the operation principle is exactly the same. Fig. 10 depicts the experimental set-up used to read the ID codes by means of an oscilloscope. Note that the diode of the envelope detector is preceded by an isolator (implemented by means of a circulator) in order to avoid unwanted reflections due to the high nonlinearity of the diode. The responses of different tags, with the indicated codes, are depicted in Fig. 11. It is worth mentioning that the different codes have been inferred by cutting certain resonators in a unique fabricated tag (shown in Fig. 10), hence detuning them and making them inoperative. Therefore, tag programming is demonstrated. It is also remarkable to highlight that the number of bits achievable with this approach is only limited by tag size, provided the mechanical system is able to displace the whole tag over the S-SRR-loaded line of the reader.

To provide further robustness to this type of chipless-RFID systems, it is convenient to expand the excursion experienced by the transmission coefficient at the frequency of the interrogation signal as much as possible. For that purpose, a reader based on a SRR-loaded microstrip line in bandpass configuration was proposed in [49] (Fig. 12). The singularity of this topology is the fact that it exhibits a pass band followed by a transmission zero. By loading this structure with a tag based on identical SRRs but oppositely oriented, i.e., rotated 180°, the transmission coefficient shifts to lower frequencies. Through a proper design, it is possible to match the transmission zero of the tag-loaded structure (with perfect alignment between the SRR of the reader and one SRR of the tag, REF position) to the frequency of maximum transmission of the unloaded reader, f_0, as Fig. 13 illustrates. This frequency, f_0, is roughly the same than the one corresponding to maximum transmission in the reader loaded with completely misaligned tag (i.e., with the tag displaced ±3.16 mm with regard to the REF position). By these means, a significant excursion of the transmission coefficient at f_c is achieved (roughly 45 dB), provided f_c is tuned to f_0. This excursion is much larger than the one of the previously discussed system, based on an S-SRR-loaded CPW reader. In [49], circularly-shaped 40-bit tags were implemented in low-loss commercial microwave substrates, and linear 10-bit tags were fabricated by inkjet printing in plastic substrate, i.e., polyethilene naphthalate (PEN) film (*Dupont Teijin Q65HA*). The functionality of the system to read both types of tags was demonstrated in [49].

The latest advances concerning these time-domain signature tags and chipless-RFID systems have been recently achieved by implementing programmable/erasable 40-bit tags with header bits on *PowerCoat*^{TM} *HD ultra smooth* paper substrate (with thickness $h = 215\ \mu$m and measured dielectric constant and loss factor of $\varepsilon_r = 3.11$ and $\tan\delta = 0.039$, respectively) [50]. The resonant elements of the tags were printed by inkjet, and the topology of such resonators is identical to the one of the SRRs of Fig. 12. Therefore, the same reader can be used to infer the ID codes, regardless of the specific substrate type and metallic layer (copper or conductive ink). The fabricated reader and tag (with all SRRs functional, i.e., all providing the logic state '1') are depicted in Fig. 14. The responses of this tag, with SRRs faced up or down (distinguished thanks to the header bits), after programming several codes, are depicted in Fig. 15. Tag programming was achieved by cutting certain resonators, providing the logic state '0'. Tag erasing can be achieved by short-circuiting previously cut resonators by adding conductive ink. This was done in [50], in order to recover the original ID code, and the resulting response (Fig. 16) exhibits the expected 40 dips of the ID code with all bits set to '1' (plus the additional dips corresponding to the header bits). Implementing these tags on paper substrate, indicates that secure paper is a canonical application of this time-domain chipless-RFID system, based on near-field and sequential bit reading. By printing a coded chain of resonant elements in the border of a certain document (e.g., an official or corporate document, certificate, ballot, exam, etc), security against counterfeiting is provided at low cost (note that in the tag of Fig. 14, a single layer of conductive ink, with thickness of roughly 2.5 μm, was printed). Moreover, the results of Fig. 15 and 16 demonstrate that tag programming and erasing is possible, further reducing fabrication

costs, as long as all identical tags can be massively fabricated (requiring only a single mask), and then programmed, e.g., by means of low cost printers, in a later stage (custom level).

In [50], the ID codes were visualized in an oscilloscope and the feeding signal was generated by means of a commercial function generator. Moreover, the relative motion between the tag and the reader was achieved by means of a mechanical guiding system (based on a step motor) providing either circular (for the circularly shaped tags) or linear (for the linear tags) displacement [Fig. 10(a)]. In the last proof-of-concept demonstrator, a printer was adapted and equipped with an *adhoc* guiding channel in order to absorb the tag (document with the printed encoder). This system guarantees good alignment and roughly constant air gap distance between the tag chain and the resonator of the reader, also conveniently placed and adapted to the modified printer. Moreover, the envelope detector, implemented by means of a diode, an active probe (with resistance and capacitance $R = 1$ MΩ and $C = 1$ pF, respectively) and an isolator, to prevent reflections from the diode, in the experimental setup shown in Fig. 10, is replaced with an integrated circuit (*Analog Devices ADL5511*) able to provide the envelope function (hence reducing costs). Such envelope signal is then driven to a data acquisition card (*National Instruments myRIO*) connected to a computer, where the sampled data can be viewed. The photograph of this experimental setup is depicted in Fig. 17. From the sampled data, the ID code can be easily inferred by means of a simple post-processing scheme, able to detect the notches. This setup has been used to read 80-bit (plus the header bits) chipless-RFID tags inkjet printed on ordinary (and low cost) DIN A4 paper. The photograph of the printed tag, with all bits set to '1' is depicted in Fig. 18. Reading such code with both tag orientations (faced up and down) has produced the responses depicted in Fig. 19(a). Then, tag programming has been done by cutting (detuning) some resonant elements, writing the '0' logic state in the corresponding resonator. The resulting code and responses are shown in Fig. 19(b), where the functionality and validity of the system can be appreciated. These latter results are important since the functionality of the system is demonstrated by considering chipless tags printed on ordinary and low-cost paper. Therefore, the reported time-domain signature barcodes may find application in many diverse scenarios involving the use of ordinary paper equipped with printed ID codes for identification and authentication purposes.

CONCLUSIONS

In this article, we have discussed several strategies for the implementation of chipless-RFID systems, including time-domain reflectometry (TDR), frequency-domain spectral signature barcodes, and several approaches where different domains are exploited simultaneously in order to increase the information density (or number of bits) per spectral bandwidth. Despite the fact that several systems where various bits of information per resonant element of the tag have been reported, an intrinsic limitation in the achievable number of bits is related to the bandwidth occupied by each resonator. Such bandwidth, wider as larger the data capacity of the resonant element is, cannot

exceed certain limits in order to avoid an excessive cost of the reader (which must generate a multi-frequency sweeping interrogation signal for tag reading). To solve the previous limitation, a time-domain chipless-RFID approach, where tags are read through near-field coupling (with sequential bit reading) by means of a harmonic interrogation signal, has been recently reported, and such approach has been reviewed in this article. Validation examples have been discussed and reported, including tag implementation in commercially available substrates and also on paper substrates, where the tags have been printed by inkjet. It has been pointed out that this novel and unconventional system is of special interest in applications involving secure paper, where tag reading by proximity may represent an added value in terms of confidence against gathering or spying.

ACKNOWLEDGMENTS

This work was supported by MINECO-Spain (projects TEC2016-75650-R, TEC2014-59679-C2-1-R and RTC-2014-2550-7), *Generalitat de Catalunya* (project 2017SGR-1159), *Institució Catalana de Recerca i Estudis Avançats* (who awarded F. Martín), and by FEDER funds. C. Herrojo acknowledges MINECO for supporting his research activity through the FPI grant BES-2014-068164.

References

1. S. Preradovic and N. C. Karmakar, "Chipless RFID: bar code of the future," *IEEE Microwave Magazine*, vol. 11, pp. 87-97, 2010.
2. S. Preradovic and N. C. Karmakar, *Multiresonator-Based Chipless RFID: Barcode of the Future*, Springer, 2011.
3. N.C. Karmakar, R. Koswatta, P. Kalansuriya, R. E-Azim, *Chipless RFID Reader Architecture*, Artech House, 2013.
4. E. Perret, *Radio Frequency Identification and Sensors: From RFID to Chipless RFID*, John Wiley, New York, 2014.
5. R. Rezaiesarlak, M. Manteghi, *Chipless RFID: Design Procedure and Detection Techniques*, Springer, 2015.
6. N. C. Karmakar, M. Zomorrodi, C. Divarathne, *Advanced Chipless RFID*, John Wiley, Hoboken, NJ, 2016.
7. K. Finkenzeller, *RFID Handbook: Radio-Frequency Identification Fundamentals and Applications*, 2nd Ed. New York, NY, USA: Wiley, 2004.
8. V. D. Hunt, A. Puglia, and M. Puglia, *RFID: A Guide to Radio Frequency Identification*, New York, NY, USA, Wiley, 2007.
9. A. Chamarti and K. Varahramyan, "Transmission delay line based ID generation circuit for RFID applications," *IEEE Microw. Wireless Compon. Lett.*, vol. 16, pp. 588-590, 2006.
10. M. Schüßler, C. Damm, and R. Jakoby, "Periodically LC loaded lines for RFID backscatter applications," in Proc. of *Metamaterials 2007*, Rome, Italy, October 2007, pp. 103-106.
11. M. Schüßler, C. Damm, M. Maasch, and R. Jakoby, "Performance evaluation of left-handed delay lines for RFID backscatter applications," in Proc. of the *IEEE MTT-S International Microwave Symposium 2008*, pp. 177-180.
12. B. Shao, Q. Chen, Y. Amin, D. S. Mendoza, R. Liu, and L.-R. Zheng, "An ultra-low-cost RFID tag with 1.67 Gbps data rate by ink-jet printing on paper substrate," in *IEEE Asian Solid State-Circuits Conf.*, 2010, pp. 1–4.
13. F.J. Herraiz-Martínez, F. Paredes, G. Zamora, F. Martín, and J. Bonache, "Printed magnetoinductive-wave (MIW) delay lines for chipless RFID applications", *IEEE Trans. Ant. Propag.*, vol. 60, pp. 5075-5082, Nov. 2012.
14. S. Tedjini, E. Perret, A. Vena, D. Kaddout, "Mastering the electromagnetic signature of chipless RFID tags", in *Chipless and Conventional Radiofrequency Identification*, ed. IGI Global, 2012.

15. S. Preradovic, I. Balbin, N. C. Karmakar, and G. F. Swiegers, "Multiresonator-based chipless RFID system for low-cost item tracking," *IEEE Trans. Microw. Theory Techn.*, vol. 57, pp. 1411-1419, 2009.
16. S. Preradovic and N. C. Karmakar, "Design of chipless RFID tag for operation on flexible laminates," *IEEE Anten. Wireless Propag. Lett.*, vol. 9, pp. 207-210, 2010.
17. J. McVay, A. Hoorfar, and N. Engheta, "Space-filling curve RFID tags," in Proc. of *2006 IEEE Radio Wireless Symp.*, pp. 199–202.
18. I. Jalaly and D. Robertson, "Capacitively-tuned split microstrip resonators for RFID barcodes," in Proc. of *European Microwave Conference*, October 2005, vol. 2, pp. 4–7.
19. H.-S. Jang, W.-G. Lim, K.-S. Oh, S.-M. Moon, and J.-W. Yu, "Design of low-cost chipless system using printable chipless tag with electromagnetic code", *IEEE Microw. Wireless Compon. Lett.*, vol. 20, pp. 640-642, 2010.
20. A. Vena, E. Perret, and S. Tedjini, "A fully printable chipless RFID tag with detuning correction technique", *IEEE Microw. Wireless Compon. Lett.*, vol. 22(4), pp. 209-211, 2012.
21. A. Vena, E. Perret, and S. Tedjini, "Design of compact and auto-compensated single-layer chipless RFID tag", *IEEE Trans. Microw. Theory Techn.*, vol. 60(9), pp. 2913-2924, Sep. 2012.
22. A. Vena, E. Perret, and S. Tedjini, "High-capacity chipless RFID tag insensitive to the polarization", *IEEE Trans. Ant. Propag.*, vol. 60(10), pp. 4509-4515, Oct. 2012.
23. D. Girbau, J. Lorenzo, A. Lazaro, C. Ferrater, and R. Villarino, "Frequency-coded chipless RFID tag based on dual-band resonators," *IEEE Ant. Wireless Propag. Lett.*, vol. 11, pp. 126–128, 2012.
24. M. M. Khan, F. A. Tahir, M. F. Farooqui, A. Shamim, H. M. Cheema, "3.56-bits/cm^2 compact inkjet printed and application specific chipless RFID tag," *IEEE Ant. Wireless Propag. Lett.*, vol. 15, pp. 1109-1112, 2016.
25. R. Rezaiesarlak and M. Manteghi, "Complex-natural-resonance-based design of chipless RFID tag for high-density data," *IEEE Trans. Ant. Propag.*, vol. 62, pp. 898-904, Feb. 2014.
26. M. S. Bhuiyan and N. Karmakar, "A spectrally efficient chipless RFID tag based on split-wheel resonator," in *Int. Antenna Technol. Workshop on Small Antennas, Novel EM Struct., Mater., Appl.*, 2014, pp. 1–4.
27. C. M. Nijas *et al.*, "Low-cost multiple-bit encoded chipless RFID tag using stepped impedance resonator," *IEEE Trans. Ant. Propag.*, vol. 62, no. 9, pp. 4762–4770, Sep. 2014.
28. J. Machac and M. Polivka, "Influence of mutual coupling on performance of small scatterers for chipless RFID tags," in *24th Int. Radioelektron. Conf.*, 2014, pp. 1–4.
29. M. Svanda, J. Machac, M. Polivka, J. Havlicek., "A comparison of two ways to reducing the mutual coupling of chipless RFID tag scatterers," in Proc. of *21st International Conference on Microwave, Radar and Wireless Communications (MIKON)*, May 2016, pp. 1-4.
30. C. Herrojo, J. Naqui, F. Paredes and F. Martín, "Spectral signature barcodes based on S-shaped Split ring resonators (S-SRR)", *EPJ Applied Metamaterials*, vol. 3, pp. 1-6, Jun. 2016.
31. A. Vena, E. Perret, S. Tedjini, "Chipless RFID tag using hybrid coding technique," *IEEE Trans. Microw. Theory Techn.*, vol. 59, pp. 3356-3364, Dec. 2011.
32. A. Vena, E. Perret, S. Tedjini, "A compact chipless RFID tag using polarization diversity for encoding and sensing", *2012 IEEE Int. Conf. RFID*, pp. 191-197, 2012.
33. M. A. Islam and N. C. Karmakar, "A novel compact printable dual-polarized chipless RFID system," *IEEE Trans. Microw. Theory Techn.*, vol. 60, pp. 2142-2151, Jul. 2012.
34. I. Balbin, N.C. Karmakar, "Phase-encoded chipless RFID transponder for large scale low cost applications", *IEEE Microw. Wireless. Compon. Lett.*, vol. 19, pp. 509-511, 2009.
35. S. Genovesi, F. Costa, A. Monorchio, G. Manara, "Chipless RFID tag exploiting multifrequency delta-phase quantization encoding", *IEEE Ant. Wireless Propag. Lett.*, vol. 15, pp. 738-741, 2015.
36. O. Rance, R. Siragusa, P. Lemaitre-Auger, and E. Perret, "RCS magnitude coding for chipless RFID based on depolarizing tag," in *IEEE MTT-S Int. Microw. Symp. Dig.*, 2015, pp. 1–4.
37. O. Rance, R. Siragusa, P. Lemaître-Auger, E. Perret, "Toward RCS magnitude level coding for chipless RFID," *IEEE Trans. Microw. Theory Techn.*, vol. 64, pp. 2315-2325, Jul. 2016.
38. C. Herrojo, J. Naqui, F. Paredes, F. Martín, "Spectral signature barcodes implemented by multi-state multi-resonator circuits for chipless RFID tags", *IEEE MTT-S International Microwave Symposium* (IMS'16), San Francisco, May 2016.
39. C. Herrojo, F. Paredes, J. Mata-Contreras, S. Zuffanelli and F. Martín, "Multi-state multi-resonator spectral signature barcodes implemented by means of S-shaped Split Ring Resonators (S-SRR)", *IEEE Trans. Microw. Theory Techn.*, vol. 65, no. 7, pp. 2341-2352, Jul. 2017.
40. S. Gupta, B. Nikfal, and C. Caloz, "Chipless RFID system based on group delay engineered dispersive delay structures," *IEEE Ant. Wireless Propag. Lett.*, vol. 10, pp. 1366–1368, 2011.

41. R. Nair, E. Perret, and S. Tedjini, "Chipless RFID based on group delay encoding," in *IEEE Int. RFID-Technol. Appl. Conf.*, 2011, pp. 214–218.
42. C. Feng, W. Zhang, L. Li, L. Han, X. Chen, and R. Ma, "Angle-based chipless RFID tag With high capacity and insensitivity to polarization," *IEEE Trans. Ant. Propag.*, vol. 63, no. 4, pp. 1789–1797, Apr. 2015.
43. A. El-Awamry, M. Khaliel, A. Fawky, M. El-Hadidy, and T. Kaiser, "Novel notch modulation algorithm for enhancing the chipless RFID tags coding capacity," in *IEEE Int. RFID Conf.*, 2015, pp. 25–31.
44. A. Vena, A. A. Babar, L. Sydanheimo, M. M. Tentzeris, and L. Ukkonen, "A novel near-transparent ASK-reconfigurable inkjet-printed chipless RFID tag," *IEEE Ant. Wireless Propag. Lett.*, vol. 12, pp. 753–756, 2013.
45. C. Herrojo, J. Mata-Contreras, F. Paredes, Ferran Martín, "Near-field chipless RFID encoders with sequential bit reading and high data capacity", *IEEE MTT-S Int. Microw. Symp.* (IMS'17), Honolulu, Hawaii, June 2017.
46. C. Herrojo, J. Mata-Contreras, F. Paredes, F. Martín, "Microwave encoders for chipless RFID and angular velocity sensors based on S-shaped split ring resonators (S-SRRs)", *IEEE Sensors J.*, vol. 17, pp. 4805-4813, Aug. 2017.
47. C. Herrojo, J. Mata-Contreras, F. Paredes, A. Núñez, E. Ramón, F. Martín, "Near-field chipless-RFID tags with sequential bit reading implemented in plastic substrates", *Int. J. Magnetism. Magnetic Mat.*, published online, https://doi.org/10.1016/j.jmmm.2017.10.005.
48. C. Herrojo, J. Mata-Contreras, F. Paredes, F. Martín, "High data density and capacity in chipless radiofrequency identification (chipless-RFID) tags based on double-chains of S-shaped split ring resonators (S-SRRs)", *EPJ Appl. Metamat.*, vol. 4, article 8, 6 pages, Oct. 2017.
49. C. Herrojo, J. Mata-Contreras, F. Paredes, Ferran Martín, "Near-field chipless RFID system with high data capacity for security and authentication applications", *IEEE Trans. Microw. Theory Techn.*, vol. 65 (12), pp. 5298-5308, Dec. 2017.
50. C. Herrojo, J. Mata-Contreras, F. Paredes, A. Núñez, E. Ramon, and F. Martín "Near-field chipless-RFID system with erasable/programmable 40-bit tags inkjet printed on paper substrates", *IEEE Microw. Wireless Compon. Lett.*, published online, DOI: 10.1109/LMWC.2018.2802718.
51. C. S. Hartmann, "A global SAW ID tag with large data capacity," in Proc. of *IEEE Ultrasonics Symposium*, October 2002, vol. 1, pp. 65–69.
52. N. Saldanha, D.C. Malocha, "Design Parameters for SAW multi-tone frequency coded reflectors" *2007 IEEE Ultrasonics Symp.*, pp. 2087-2090, 2007.
53. S. Harma, V.P. Plessky, C.S. Hartmann, W. Steichen, "Z-path SAW RFID tag" *IEEE Trans. Ultrasonics, Ferroelectric Freq. Control*, vol. 55, pp. 208-213, 2008.
54. H. Tao, W. Weibiao, W. Haodong, S. Yongan, "Reflection and scattering characteristics of reflectors in SAW tags", *IEEE Trans. Ultrasonics, Ferroelectric Freq. Control*, vol. 55, pp. 1387-1390, 2008.
55. S. Harma, V.P. Plessky, L. Xianyi, P. Hartogh, "Feasibility of ultra-wideband SAW RFID tags meeting FCC rules" *IEEE Trans. Ultrasonics, Ferroelectric Freq. Control*, vol. 56, pp. 812-820, 2012.
56. E. Shamonina, V.A. Kalinin, K.H. Ringhofer, and L. Solymar, "Magneto-inductive waveguide", *Electron. Lett.*, vol. 38, pp. 371–373, 2002.
57. J. Naqui, F. Martín, "Application of broadside-coupled split ring resonator (BC-SRR) loaded transmission lines to the design of rotary encoders for space applications", *IEEE MTT-S Int. Microw. Symp.* (IMS'16), San Francisco, May 2016.
58. J. Mata-Contreras, C. Herrojo, F. Martín, "Application of split ring resonator (SRR) loaded transmission lines to the design of angular displacement and velocity sensors for space applications", *IEEE Trans. Microw. Theory Techn.*, vol. 65, no. 11, pp. 4450-4460, Nov. 2017.
59. H. Chen, L. Ran, J. Huangfu, X. Zhang, K. Chen, T. M. Grzegorczyk, and J. A. Kong, "Left-handed materials composed of only S-shaped resonators," *Phys. Rev. E*, vol. 70, no. 5, p. 057605, Nov. 2004.
60. H. Chen, L. Ran, J. Huangfu, X. Zhang, K. Chen, T. M. Grzegorczyk, and J. A. Kong, "Negative refraction of a combined double S-shaped metamaterial," *Appl. Phys. Lett.*, vol. 86, no. 15, p. 151909, 2005.
61. H. Chen, L.-X. Ran, H.-F. Jiang Tao, X.-M. Zhang, K.-S. Cheng, T. M Grzegorczyk, and J. A. Kong, "Magnetic properties of S-shaped split ring resonators," *Prog. Electromagn. Res.*, vol. 51, pp. 231–247, 2005.
62. J. Naqui, J. Coromina, A. Karami-Horestani, C. Fumeaux, and F. Martín, "Angular displacement and velocity sensors based on coplanar waveguides (CPWs) loaded with S-shaped split ring resonator (S-SRR)", *Sensors*, vol. 15, pp. 9628-9650, 2015.

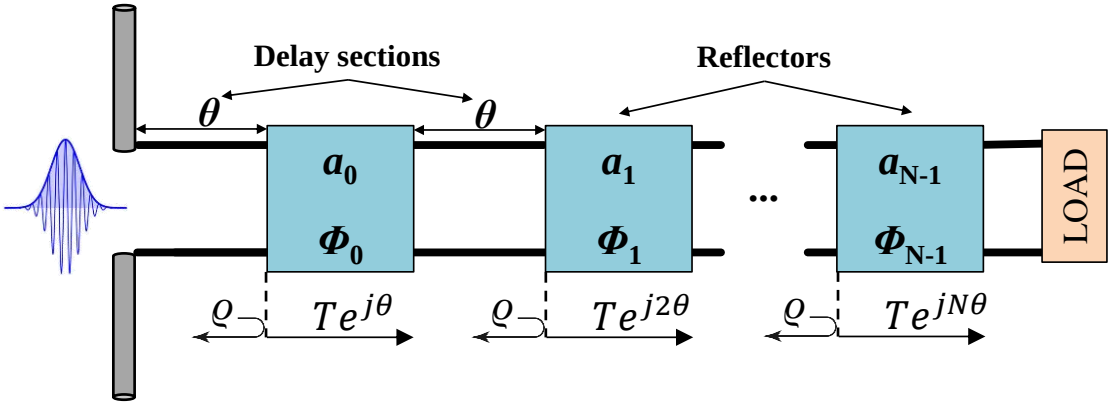

Figure 1. Working principle of chipless-RFID systems based on time-domain reflectometry (TDR).

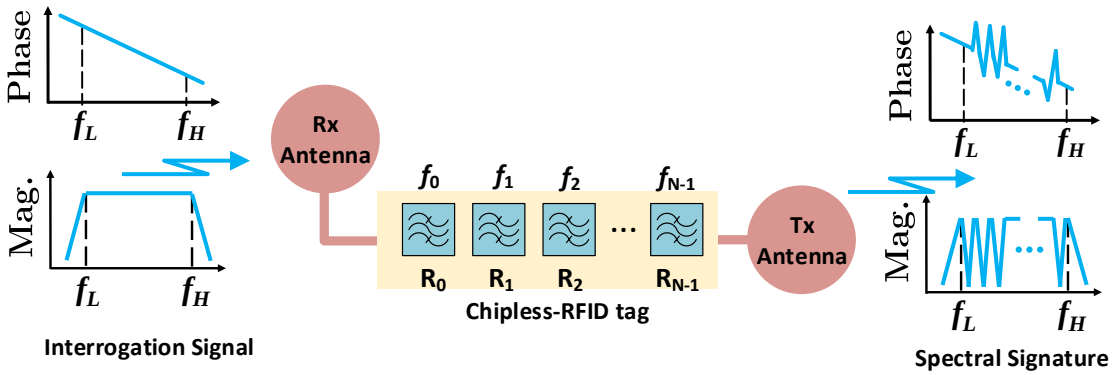

(a)

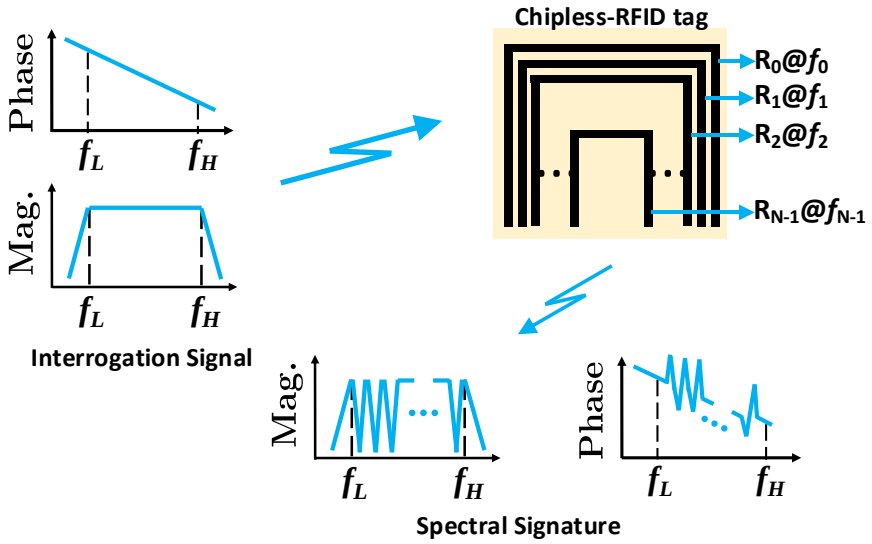

(b)

Figure 2. Working principle of retransmission (a) and backscattered (b) frequency-domain chipless-RFID systems.

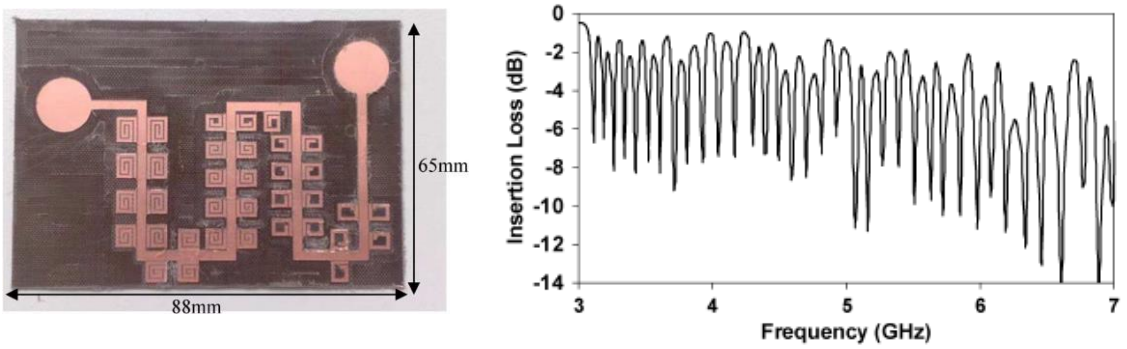

(a) (b)

Figure 3. Photograph (a) and measured response (b) of a 35-bit retransmission based chipless-RFID tag implemented by means of spiral resonators, where all bits are set to '1'. Reprinted with permission from [15]; copyright 2009 IEEE.

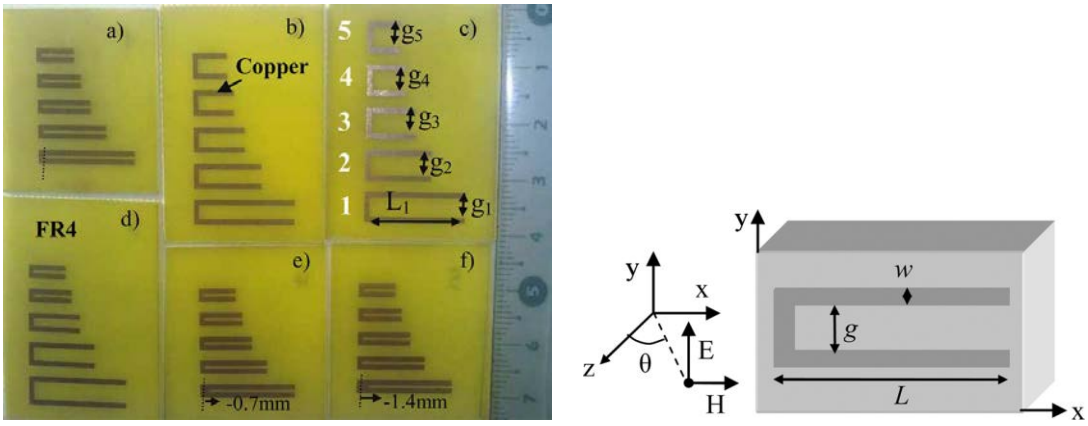

(a) (b)

Figure 4. Photograph of six chipless-RFID tags based on frequency position and phase deviation (a) and topology of the C-shaped resonant element with relevant dimensions and polarization indicated (b). Reprinted with permission from [31]; copyright 2011 IEEE.

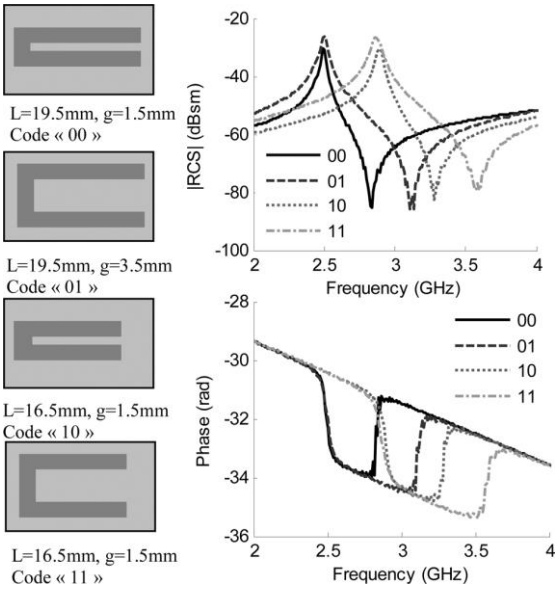

Figure 5. Responses achieved with a single C-shaped resonator (corresponding to two bits), inferred by varying the dimensions, as indicated. Reprinted with permission from [31]; copyright 2011 IEEE.

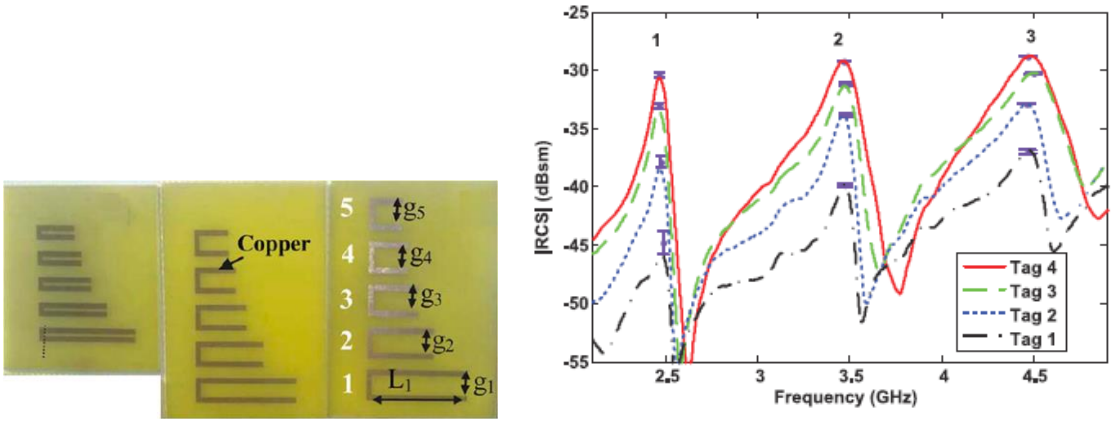

(a) (b)

Figure 6. Photograph of three chipless-RFID tags based on frequency position and RCS peak magnitude (a) and measured response (b). Reprinted with permission from [37]; copyright 2016 IEEE.

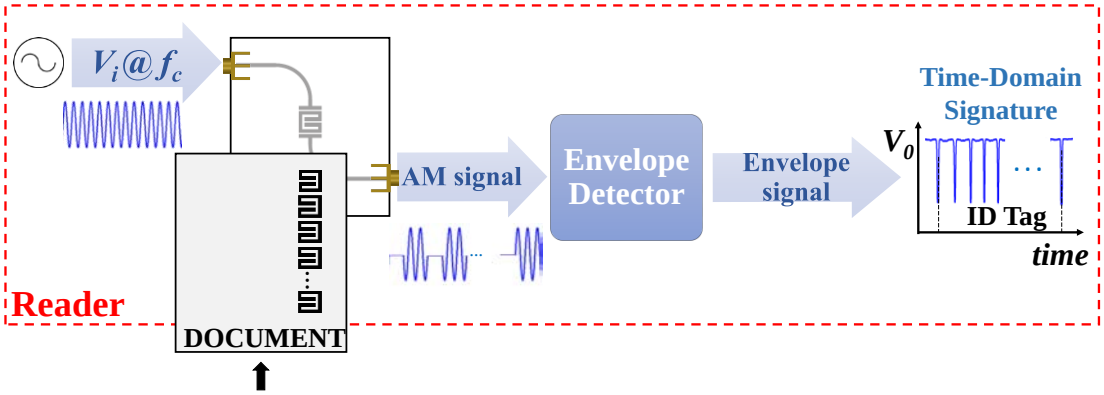

Figure 7. Working principle of time-domain chipless-RFID systems based on near-field coupling and sequential bit reading.

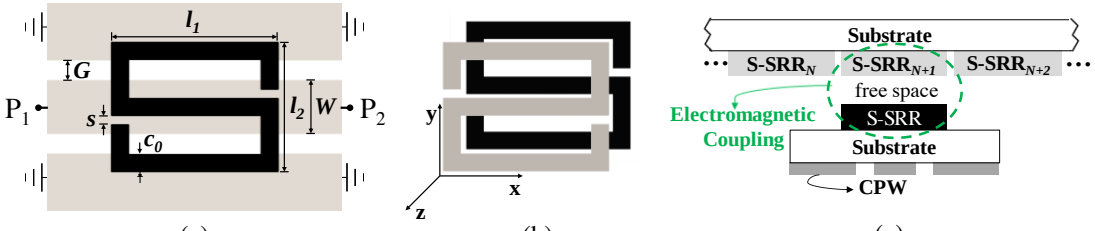

(a) (b) (c)

Figure 8. Layout of the square shaped S-SRR coupled to a CPW transmission line (a), 3D view of the broadside coupled S-SRR (BC-S-SRR) (b), and cross-sectional view of the S-SRR-loaded CPW (reader) with an S-SRR based chipless tag on top of it (c). Dimensions are (in mm) $W = 1.2$ and $G = 0.48$, $l_1 = 3.8$, $l_2 = 2.96$, $c_0 = 0.4$, $s = 0.2$. CPW transmission line and tag are separated by a 0.25 mm air gap. The distance between adjacent S-SRRs (if they are present) in the tag chain is 0.2 mm. For the CPW, the considered substrate is the *Rogers RO3010* with dielectric constant $\varepsilon_r = 10.2$ and thickness $h = 0.635$ mm. For the tag chain the considered substrate is the *Rogers RO4003C* with dielectric constant $\varepsilon_r = 3.55$ and thickness $h = 0.204$ mm.

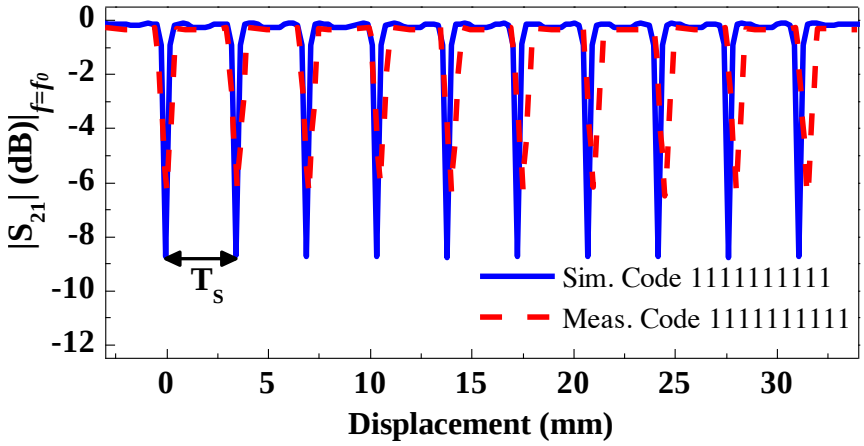

Figure 9. Measured and simulated (inferred from the electromagnetic simulator *Keysight Momentum*) magnitude of the transmission coefficient at f_c, as the linear 10-bit tag is displaced above the S-SRR-loaded CPW transmission line, by considering an air gap of 0.25 mm.

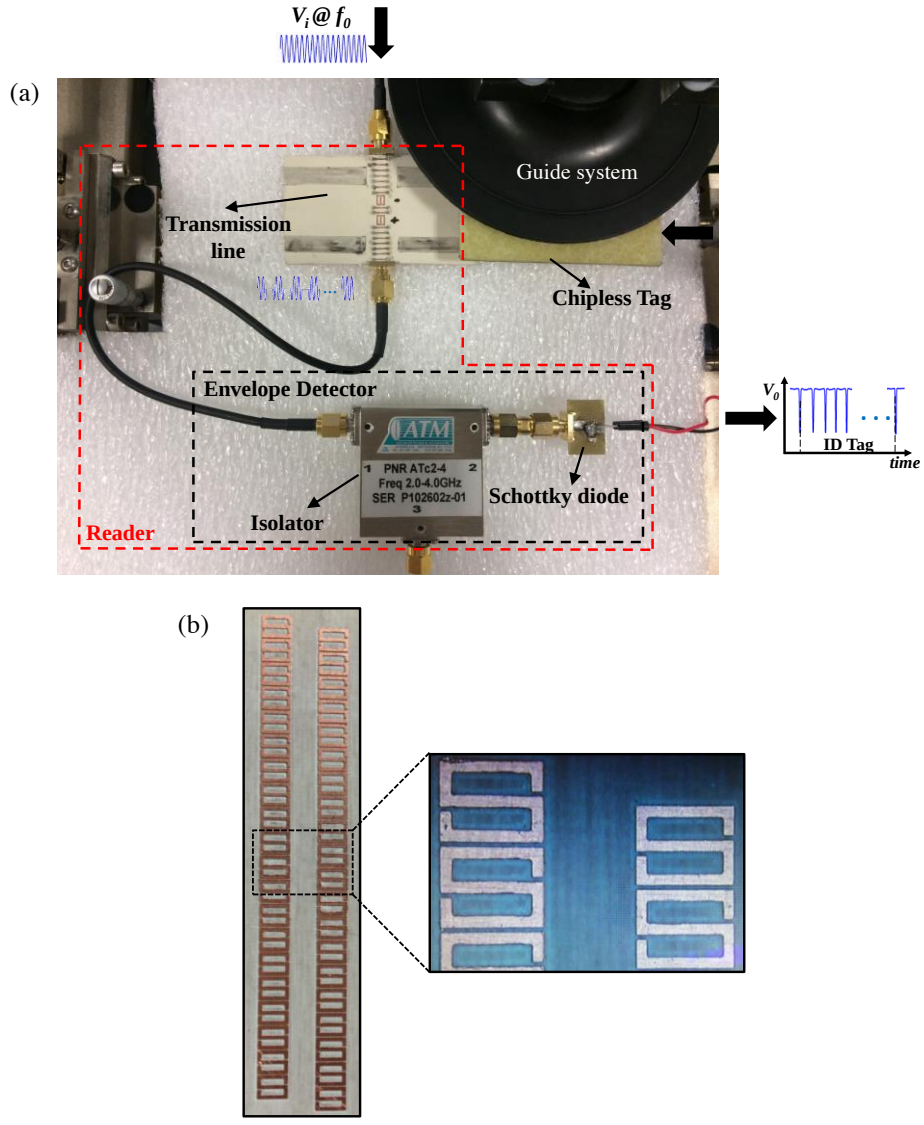

Figure 10. Photograph of the experimental set-up (a) and fabricated double-chain tag with all bits set to the logic state '1' (b). Reprinted with permission from [48]; copyright 2017 EDP Sciences.

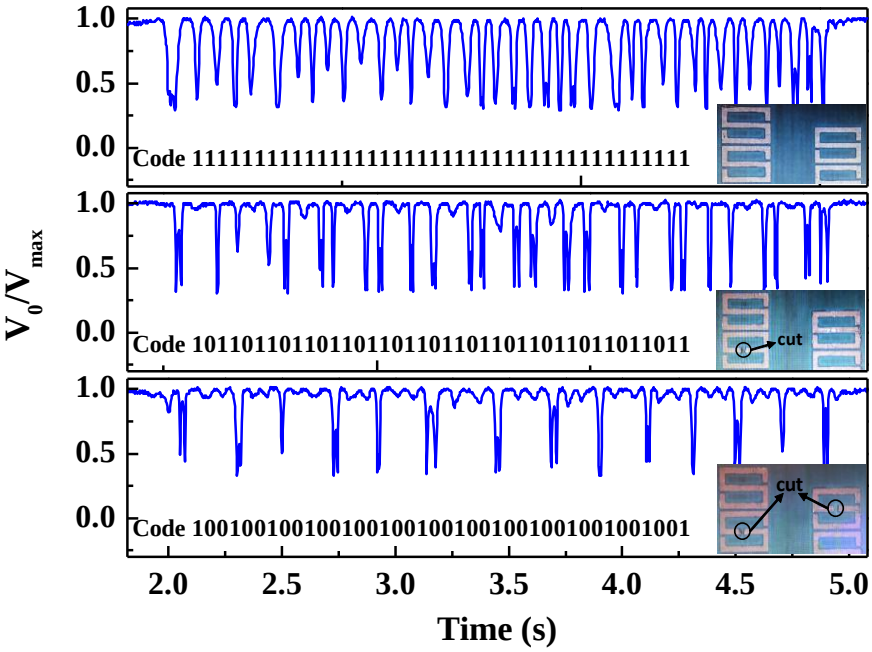

Figure 11. Measured normalized envelope of the 40-bit tags with the indicated codes. Reprinted with permission from [48]; copyright 2017 EDP Sciences.

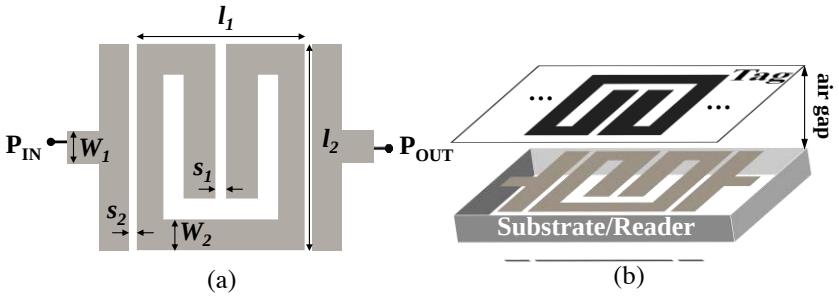

Figure 12. Layout of the topology of the reader based on a SRR-loaded microstrip line in bandpass configuration (a) and 3D view of the loaded reader with one of the SRRs of the tag perfectly aligned with the SRR of the reader (b). Dimensions are (in mm): $l_1 = 3.16$, $l_2 = 3.35$, $s_1 = 0.2$, $s_2 = 0.2$, $W_1 = 0.56$, and $W_2 = 0.5$. The distance between adjacent SRRs (if they are present) in the tag chain is 0.2 mm. For the reader, the considered substrate is the *Rogers RO3010* with dielectric constant $\varepsilon_r = 10.2$ and thickness $h = 0.635$ mm. For the tag chain the considered substrate is the *Rogers RO4003C* with dielectric constant $\varepsilon_r = 3.55$ and thickness $h = 0.204$ mm.

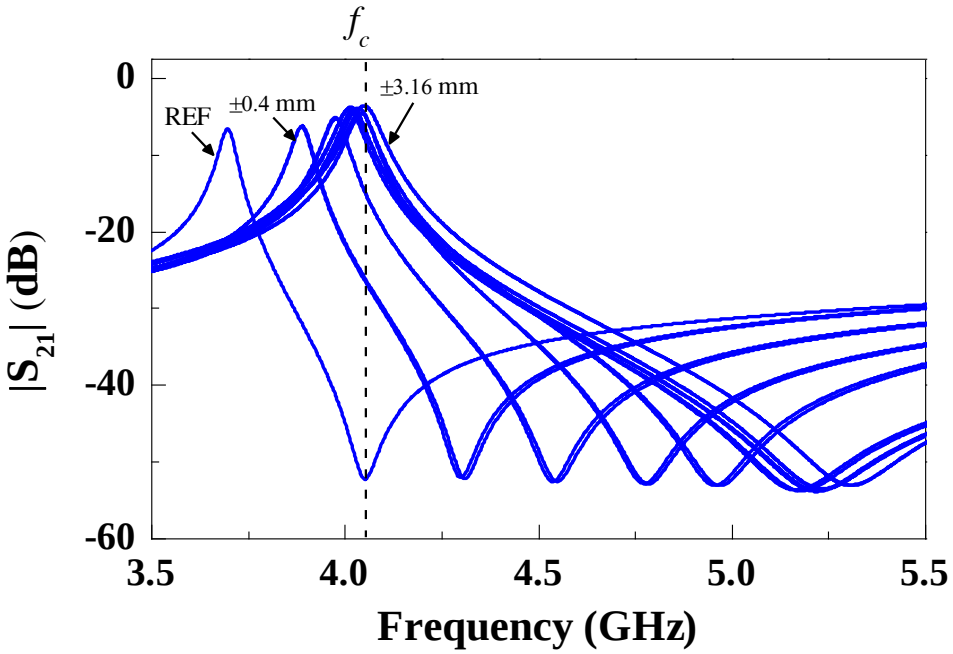

Figure 13. Transmission coefficient (magnitude) of the SRR-loaded line of Fig. 12 with tag cover, for different relative positions between the SRR of the line and the SRR of the tag. These results have been inferred by electromagnetic simulation using *Keysight Momentum*. Reprinted with permission from [49]; copyright 2017 IEEE.

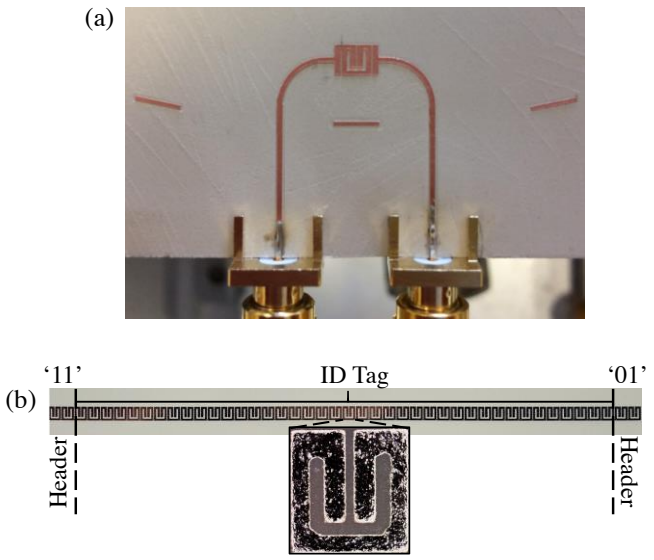

Figure 14. Photograph of the fabricated SRR-loaded microtrip line for tag reading (a) and 40-bit tag with header bits implemented on paper substrate (with all bits set to the logic state '1') (b).

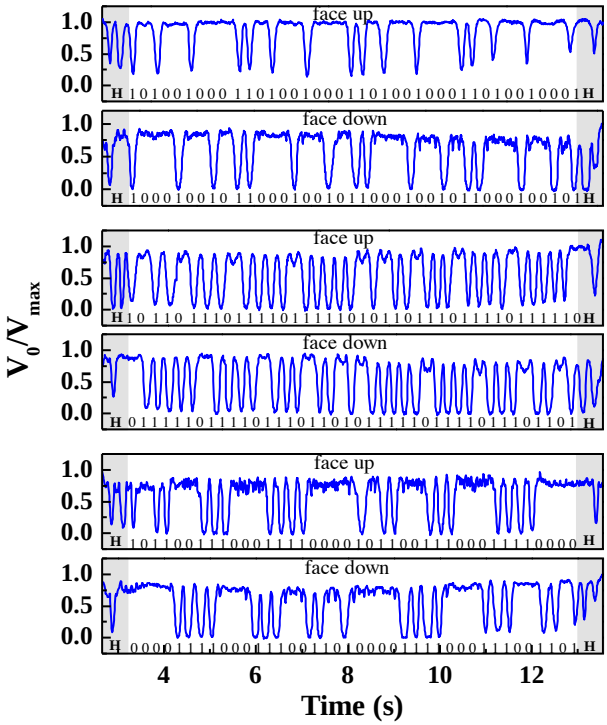

Figure 15. Measured normalized envelope for the 40-bit programmed tags with the indicated codes and with header bits. Reprinted with permission from [50]; copyright 2018 IEEE.

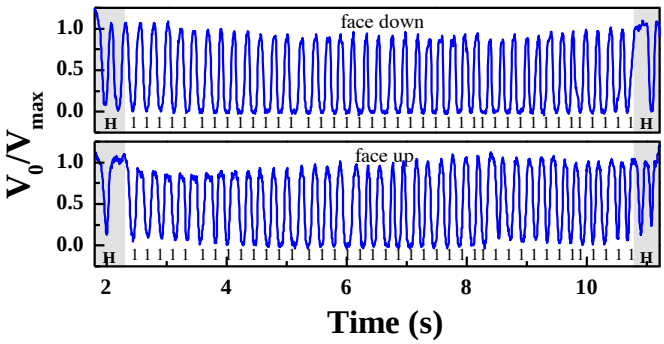

Figure 16. Measured normalized envelope for the 40-bit erased tag with header bits. Reprinted with permission from [50]; copyright 2018 IEEE.

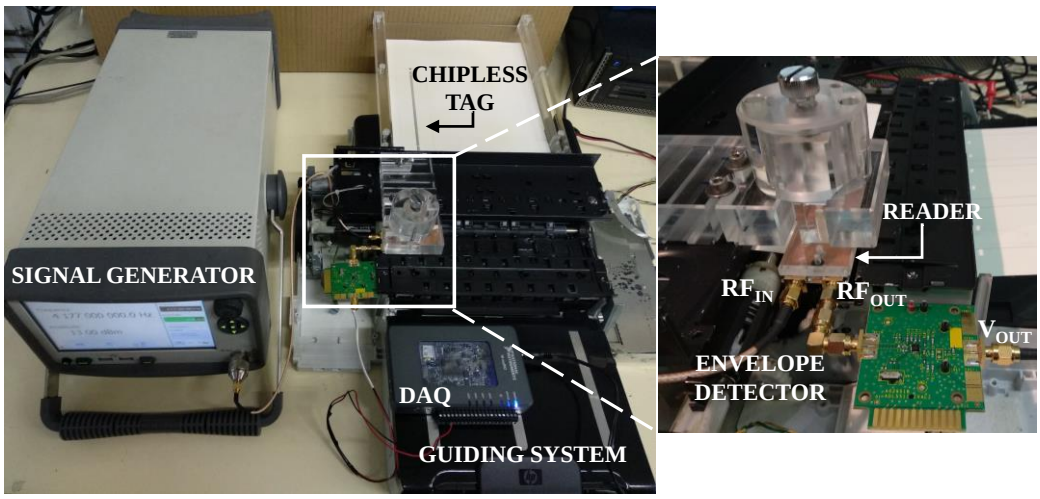

Figure 17. Photograph of the experimental set-up used for obtaining the tag responses (envelope functions) in those tags printed on DIN A4 paper.

Figure 18. Photograph of the 80-bit tag with header bits implemented on ordinary DIN A4 paper (with all bits set to the logic state '1').

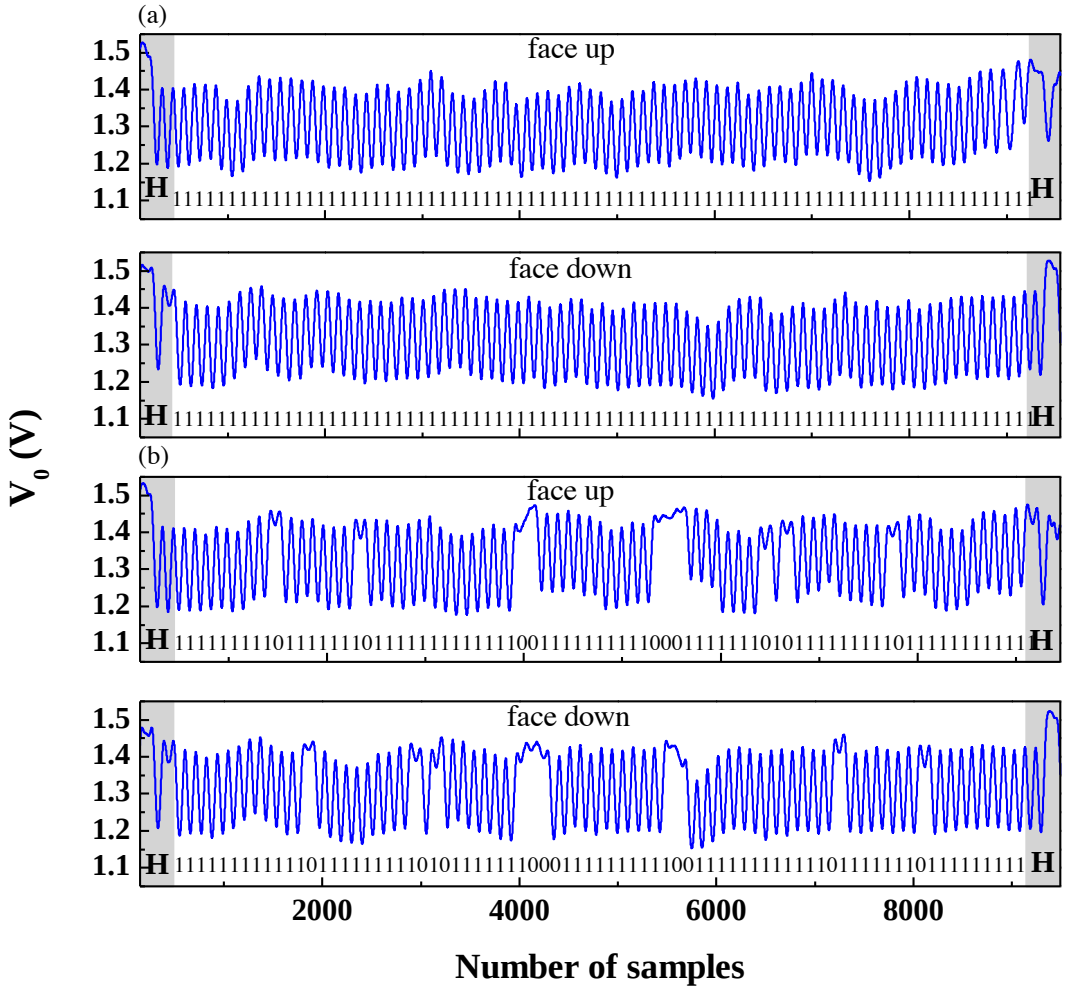

Figure 19. Measured envelope of the inkjet-printed (a) 80-bit tag with all bits set to the logic state '1' and (b) 80-bit programmed tag with the indicated code and with header bits. Since the envelope function has been inferred from a data acquisition system in this second validation experimental set-up, the abscise axis is the number of samples, rather than the time.

Artículo SENSORS18

Near-Field Chipless-RFID Sensing and Identification System with Switching Reading

F. Paredes, C. Herrojo, J. Mata-Contreras, and F. Martín

sensors

MDPI

Article

Near-Field Chipless-RFID Sensing and Identification System with Switching Reading

Ferran Paredes[1,*], Cristian Herrojo[1], Javier Mata-Contreras[1], Miquel Moras[2], Alba Núñez[2], Eloi Ramon[2] and Ferran Martín[1]

[1] GEMMA/CIMITEC, Departament d'Enginyeria Electrònica, Universitat Autònoma de Barcelona, 08193 Bellaterra, Spain. E-mail: Ferran.Martin@uab.es

[2] Institut de Microelectrònica de Barcelona, IMB-CNM (CSIC), 08193 Bellaterra, Spain

* Correspondence: Ferran.Paredes@uab.es; Tel.: +34 93 581 35 22

Academic Editor: name
Received: date; Accepted: date; Published: date

Abstract: A chipless radiofrequency identification (chipless-RFID) and sensing system, where tags are read by proximity (near-field) through a switch, is presented. The tags consist of a set of identical resonant elements (split ring resonators –SRRs), printed or etched at predefined and equidistant positions, forming a linear chain, and each SRR provides a bit of information. The logic state ('1' or '0') associated to each resonator depends on whether it is present or not in the predefined position. The reader is an array of power splitters used to feed a set of SRR-loaded transmission lines (in equal number to the number of resonant elements, or bits, of the tag). The feeding (interrogation) signal is a harmonic (single-tone) signal tuned to a frequency in the vicinity of the fundamental resonance of the SRRs. The set of SRR-loaded lines must be designed so that the corresponding SRRs are in perfect alignment with the SRRs of the tag, provided the tag is positioned on top of the reader. Thus, in a reading operation, as long as the tag is very close to the reader, the SRRs of the tag modify (decrease) the transmission coefficient of the corresponding reader line (through electromagnetic coupling between both SRRs), and the amplitude of the output signal is severely reduced. Therefore, the identification (ID) code of the tag is contained in the amplitudes of the output signals of the SRR-loaded lines, which can be inferred sequentially by means of a switching system. As compared to previous chipless-RFID systems based on near-field and sequential bit reading, in the proposed system the tags can be merely positioned on top of the reader, conveniently aligned, without the need to mechanically displace them across the reader. Since tag reading is only possible if the tag is very close to the reader, this system can be also used as proximity sensor including target identification. The proposed chipless-RFID and sensing approach is validated by reading a designed four-bit tag. For identification purposes, this system is of special interest in applications where a low number of bits suffices and tag reading by proximity is acceptable (or, even, convenient). Applications mostly related to secure paper, particularly involving a limited number of items (e.g., exams, ballots, etc.), in order to provide authenticity and avoid counterfeiting are envisaged. As proximity sensor, the system may be of interest to detect and distinguish different targets in applications such as smart packaging.

Keywords: chipless-RFID; split ring resonators (SRRs); microwave sensors.

1. Introduction

Radiofrequency identification (RFID) is a wireless technology useful in many applications, including identification, tracking, sensing and security, among others [1,2]. Typically, RFID tags are equipped with an antenna (for communication with the reader) and a silicon integrated circuit (IC),

or chip, where information is stored. Although chipped RFID tags are relatively inexpensive (typically several eurocents), in many applications this cost may represent a significant percentage of the item price, and this prevents from the full expansion of this technology in many sectors.

To alleviate this cost-related limitation of chipped-RFID, many efforts have been dedicated in the last decade to the so-called chipless-RFID, where chips are replaced with printed encoders [3-8]. Such encoders, typically implemented on plastic substrates by means of printing techniques, such as inkjet printing (or massive manufacturing processes, such as rotogravure, or screen-printing, etc.), using conductive inks, are low-cost as compared to silicon ICs. However, printed encoders occupy significant area (proportional to the number of bits) and their data storage capability is small as compared to the 96-bits of regulated passive UHF-RFID technology. Additionally, the read ranges in chipless-RFID are small as compared to those achievable in RFID systems with tags equipped with chips (several meters in passive UHF-RFID and dozens of meters in systems that use active tags). Therefore, many efforts have been focused in recent years to improve the data storage capacity and read distances of chipless-RFID systems.

There are two main approaches for the implementation of chipless-RFID systems: those based on the time domain [9-18], and those based on the frequency domain [3,4,19-40]. Most systems within the former approach are based on time domain reflectometry (TDR), where the ID code is given by the echoes generated by the tag (a delay line with reflectors at certain positions) to a narrow pulse (interrogation signal). Despite the fact that TDR tags implemented on surface acoustic wave (SAW) technology are competitive [9,12,14-16], such tags are not compatible with standard printing processes. On the other hand, attempts to implement TDR based tags on fully planar technology have been successful, but the achieved number of bits has been very limited [11,13,17].

Frequency-domain based chipless-RFID systems use printed tags consisting of a set of resonant elements, each tuned to a different frequency. In such tags, each resonator typically provides a bit of information, '1' or '0' depending on whether the resonator is functional or detuned, and the interrogation signal is a multi-frequency signal that must cover the whole spectral bandwidth occupied by the tag. The ID code is given by the presence or absence of singularities at the predefined frequencies of the different tag resonators, contained either in the transmission coefficient (retransmission based tags [19,20]) or in the radar cross section (backscattered tags [21,[27]). In these tags, the number of bits is limited by the achievable density of bits per frequency, which is related to the spectral bandwidth of each resonant element. The required frequency swept of the interrogation signal is proportional to the number of bits. Consequently, it is not possible to exceed certain limits with a simple and low-cost reader.

To partially alleviate the limited data storage capability of spectral signature barcodes (as such frequency-domain based tags are usually designated), hybrid encoding, i.e., exploiting several domains simultaneously, has been proposed. Examples include frequency/phase deviation [32], frequency/notch bandwidth [39], frequency/notch magnitude [38] and frequency/peak magnitude [40], among others. By this means, more than one bit of information per resonant element has been demonstrated, but the reported tags are far from the data storage capability of chipped tags.

In [41-46], a new approach for the implementation of chipless-RFID systems, based on near-field and sequential bit reading, was proposed. This is a time-domain approach, but, rather than in the echoes of a pulsed signal, the ID information is contained in the envelope of an amplitude modulated signal, generated by the tag when this is displaced over the reader, in close proximity to it. The tag is a set of identical resonators forming a linear chain. The resonant elements are etched at predefined and equidistant positions in the tag substrate, and the logic state '1' or '0' is determined by the functionality of the resonant element (similar to spectral signature barcodes). The reader is a transmission line fed by a harmonic (single tone) carrier signal tuned to a frequency in the vicinity of the resonance frequency of the tag resonators. Thus, by displacing the resonant elements of the tag sequentially over the transmission line, in close proximity to it, line-to-resonator coupling with those functional resonators of the tag arises, thereby modulating the transmission coefficient at the carrier frequency. Therefore, the amplitude of the carrier (feeding) signal is modulated, and the ID code is contained in the envelope function, which can be inferred from an envelope detector. The

functionality of this near-field chipless-RFID system has been validated by reading tags with 40 bits [45], and the robustness has been demonstrated by reading tags implemented on plastic substrates through conductive inks [42], and also on paper substrates [46].

The previous chipless-RFID system requires a mechanical guiding of the tag over the reader (for sequential tag reading). In this paper, we propose a new time-domain chipless-RFID sensing and identification system, conceptually similar to the previous one, where tag reading does not require tag motion. In this new system, the tags are identical to those of near-field chipless-RFID, i.e., linear chains of identical resonators (present or not at predefined and equidistant positions), but tag reading merely requires properly positioning the tag over the active part of the reader. Since tag reading requires proximity, the proposed system may be useful as proximity sensor with identification capability.

2. The proposed chipless-RFID sensing and identification system

The sketch of the proposed chipless-RFID sensing and identification system is depicted in Fig. 1. The interrogation signal, with frequency f_c, is injected to the input port of a microstrip line, which divides the signal in as many channels as number of bits in the considered tags (four in our case). In each channel, the sensing (reading) element is a transmission line loaded with a split ring resonator (SRR) in band pass configuration (i.e., the SRRs are coupled to the input and output access lines through gap capacitors, providing a band pass functionality). The tag is a linear chain of SRRs identical to those of the reader, but oppositely oriented in order to favor the coupling between tag and reader SRRs. By positioning the tag on top of the reader, in close proximity to it and with the SRRs of the tag face-to-face to those of the reader, the electromagnetic coupling between the SRRs of the lines and the functional SRRs of the tag modifies the transmission coefficient of the corresponding lines, effectively modifying (decreasing) the amplitude of the feeding signal at the output ports of such lines. Note that this modulation is only effective in those channel lines with functional SRR on top of it. Therefore, the ID code is contained in the amplitudes of the output signals of the different channels, with high and low level amplitude corresponding to the '0' and '1' logic states, respectively. It is important to highlight that the frequency of the feeding signal, f_c, must be selected in the band pass of the frequency response of the unloaded channel lines (i.e., without tag SRRs on top of them). The reason is that with this selection we obtain a significant decrease of the transmission coefficient at f_c when the SRR of the tag is situated on top of the SRR of the line. Consequently, a high amplitude contrast between the '0' and '1' logic states is obtained, as desired in order to have a reasonable tolerance margin against possible misalignments between the tag and the reader and to increase the vertical detection distance (typically up to 1 mm). It is worth mentioning that the tag can be contacted to the reader if the SRRs are etched in the opposite side of the substrate.

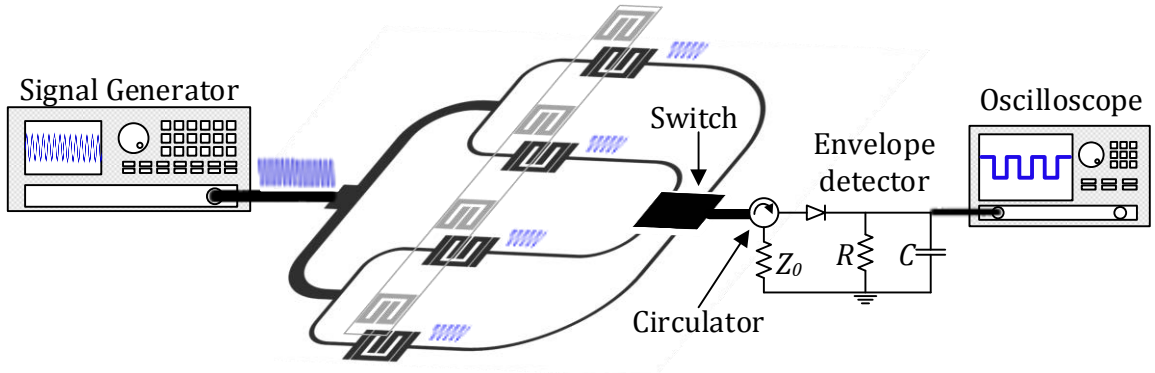

Figure 1. Sketch of the proposed chipless-RFID sensing and identification system. The envelope detector is preceded by a circulator (configured as an isolator) in order to avoid mismatching reflections from the diode (a highly nonlinear device).

For tag reading, a switch is considered, as shown in Fig. 1, in order to read the tag sequentially. The output port of the switch is connected to an envelope detector, which provides the amplitude of the output port of each channel line, and consequently the ID code of the tag. Such code can only be detected (read) if the tag is within the influence of the electromagnetic fields generated by the channel lines (i.e., a distance of the order of 1 mm). This means that the proposed system can be used as proximity detector, with identification functionality, that is, we can detect the presence of a target in a certain position (very close to the reader, or detector), and identify it.

The layout of the channel lines (all identical) is the similar to the one considered in [45,46] for the implementation of a near-field chipless-RFID system with sequential bit reading through tag motion (see Fig. 2a). Such layout has been optimized in order to obtain a selective bandpass response, with central frequency at 2.25 GHz (see Fig. 3). The considered substrate is the *Rogers RO3010* with dielectric constant ε_r = 10.2 and thickness h = 0.635 mm. By situating an oppositely oriented SRR on top of the line SRR, face-to-face to it, as the perspective view of Fig. 2(b) indicates, the electromagnetic coupling between both SRRs modifies the transmission coefficient. The simulated responses for different distances between line and tag SRRs (air gap) are also depicted in Fig. 3, where it can be appreciated that the transmission coefficient at f_c experiences a significant excursion up to roughly 1 mm separation. In the results of Fig. 3, the SRR of the tag is etched in the upper (top) side of the tag substrate (Fig. 2c). By etching the SRRs on the other (bottom) side of the tag substrate (Fig. 2d), the system is also functional. In this case, the read distance increases (Fig. 4), but it is not possible to contact the tag with the reader, as long as the tag and line SRRs are put in direct connection, i.e., short-circuited (an undesired situation).

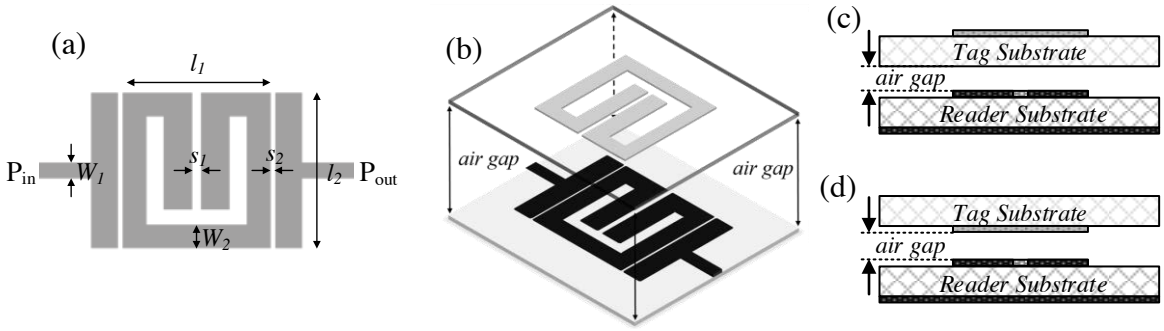

Figure 2. (a) Layout of the channel lines, consisting of a SRR-loaded microstrip line with SRR coupled to the input and output ports through capacitive gaps (relevant dimensions are indicated); (b) perspective view of the channel line with tag on top of it; (c) cross section view of the channel line with tag on top of it and tag SRRs etched on the top side of the substrate (further away from the reader); (d) section view of the channel line with tag on top of it and tag SRRs etched on the bottom substrate side (closer to the reader).

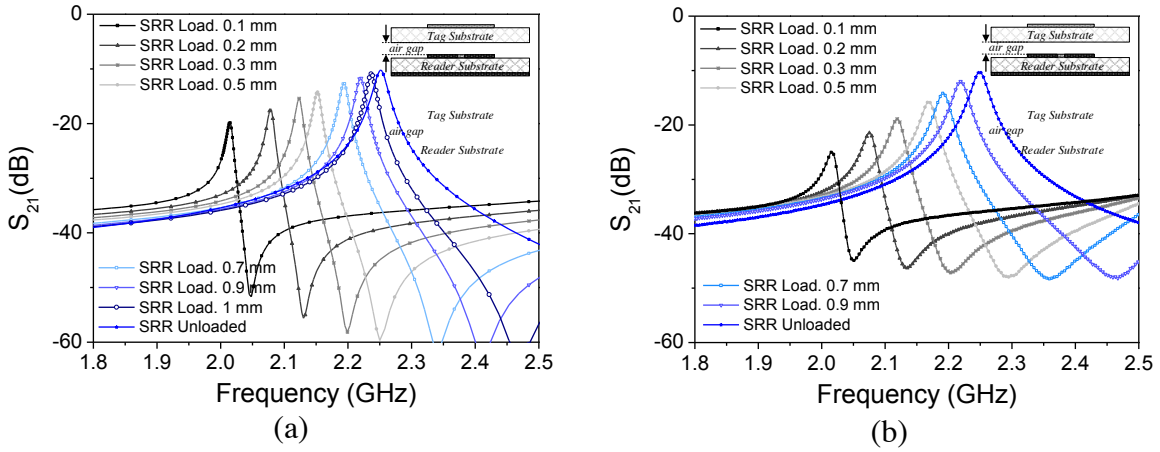

Figure 3. Frequency responses of the channel line without tag on top of it and with tag SRR (perfectly aligned) at different distances. The considered configuration is the one of Fig. 2(c); (a) Electromagnetic

simulation; (b) measurement. Dimensions are W_1 = 0.58 mm, W_2 = 0.87 mm, l_1 = 5.53 mm, l_2 = 5.86 mm, s_1 = 0.35 mm, s_2 = 0.2 mm. The considered tag substrate has dielectric constant of ε_r = 10.2 and thickness h = 0.63 mm.

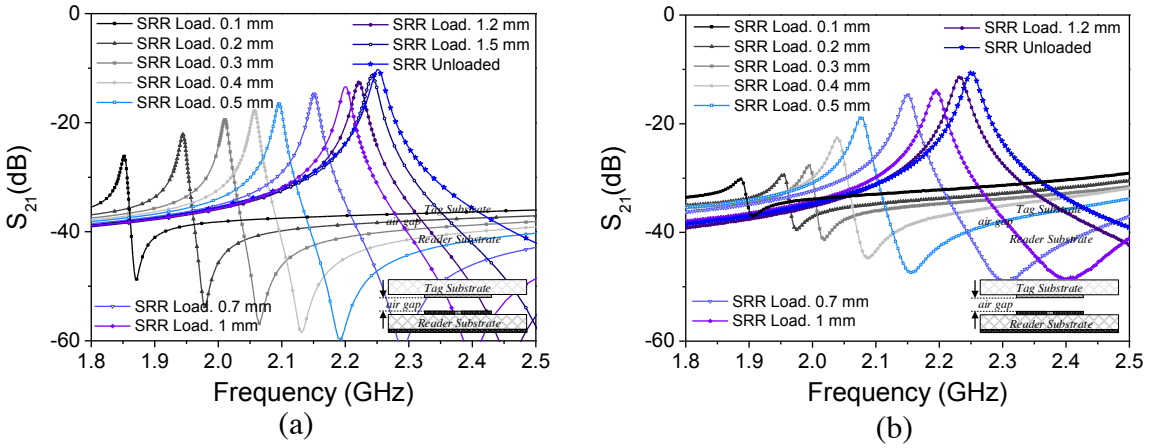

Figure 4. Frequency responses of the channel line without tag on top of it and with tag SRR (perfectly aligned) at different distances. The considered configuration is the one of Fig. 2(d); (a) Electromagnetic simulation; (b) measurement. Dimensions and tag substrate are those indicated in the caption of Fig. 3.

Let us now analyze the response of one of the SRR-loaded lines in the whole system, with a tag with all resonators functional on top of it (and faced up). The structure is depicted in Fig. 5(a), whereas the simulated responses, for different air gap distances, are shown in Fig. 5(b). Note that, in this case, the maximum transmission for each response is roughly 6 dB smaller (as compared to Fig. 3), corresponding to an output power level divided by four. This is an expected value on account of the power splitting of the T-junctions. Nevertheless, it is demonstrated that by tuning the feeding signal in the vicinity of the frequency of maximum transmission for the unloaded reader (2.25 GHz), the excursion experienced by the transmission coefficient is significant up to air gaps close to 1 mm, thanks to the presence of the transmission zero in the responses. Note that the optimum situation in terms of dynamic range is the one corresponding to an air gap of roughly 0.5 mm, since in this case the transmission zero is close to 2.25 GHz, and the excursion experienced by the transmission coefficient with and without tag SRR on top of the reader line is larger than 40 dB. The measured responses, depicted in Fig. 5(c), are in good agreement with the simulated ones. It is worth mentioning that the responses of Fig. 5 correspond to the transmission coefficient between the input and the output port 2. Nevertheless, similar responses are obtained for the transmission coefficients of the other output ports. To demonstrate this, Fig. 6 depicts the responses of the different transmission coefficients for the reader without tag, and with an all-functional SRRs tag, situated a distance (air gap) of 0.1 mm. As can be seen, the two sets of responses are very similar, indicating that the behavior of each channel is roughly the same.

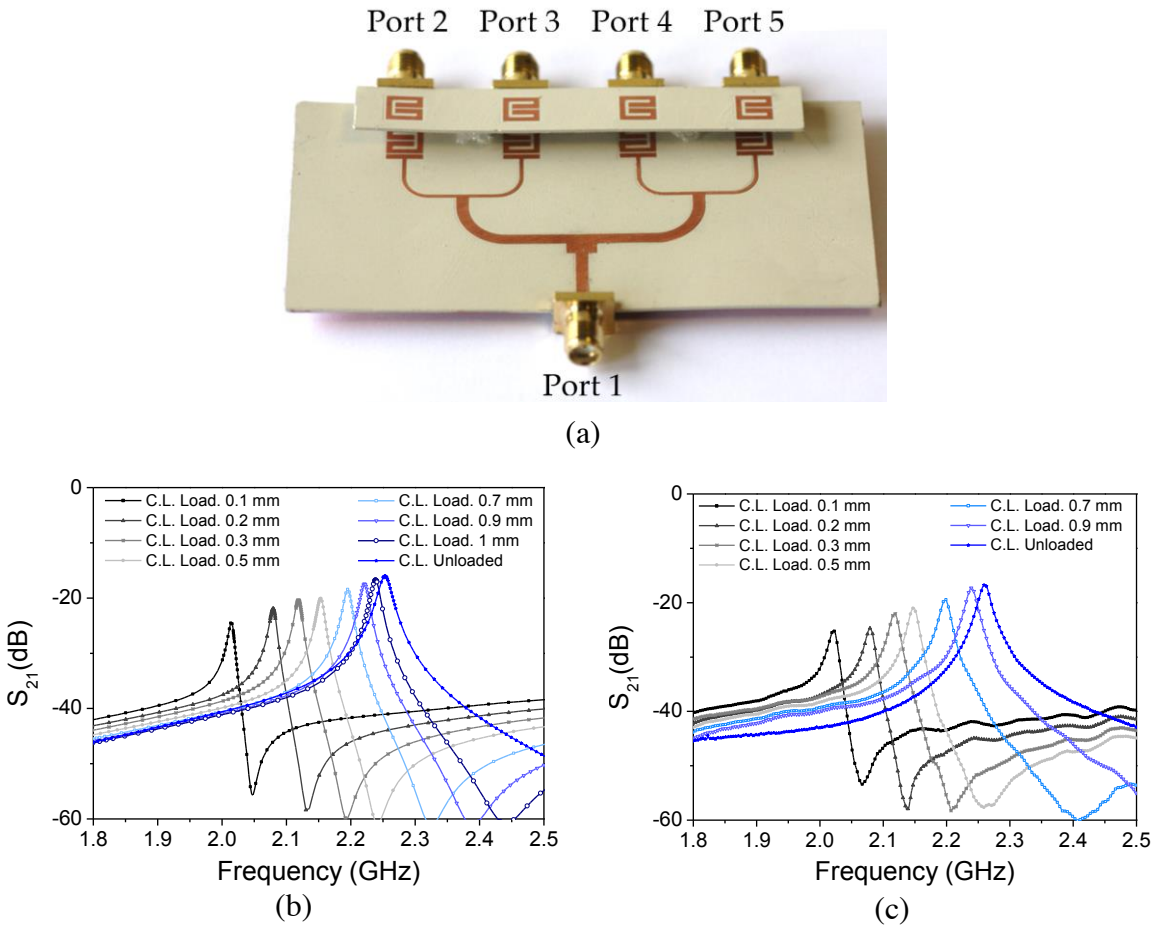

Figure 5. Frequency responses of the channel line without tag on top of it and with tag SRR (perfectly aligned) at different distances. The considered configuration is the one of Fig. 2(c). (a) Photograph of the prototype with tag on top and faced up; (b) Electromagnetic simulation; (c) Measurement.

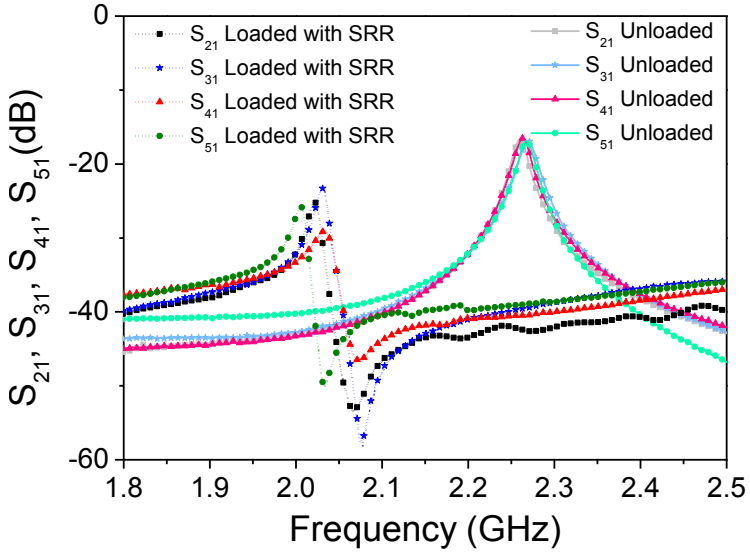

Figure 6. Transmission coefficient for the different channel lines with and without tag SRRs on top of them.

For tag reading, a switching scheme is considered, where each reader channel is sequentially selected, and the corresponding signal is driven to the output port of the switch, which is in turn connected to the input port of the envelope detector. The switch is based on the *Analog Devices HMC241AQS16E* integrated circuit. The photograph of the switch circuit is depicted in Fig. 7a. The switch requires two supply pins (VCC and GND, as well as pins A and B to select the switch input channels. In order to select the switch output ports automatically, as well as to manage the switching time, an *Atmel ATmega328P* microcontroller and the necessary electronic components, disposed in a printed circuit board (PCB), have been used (see Fig. 7b).

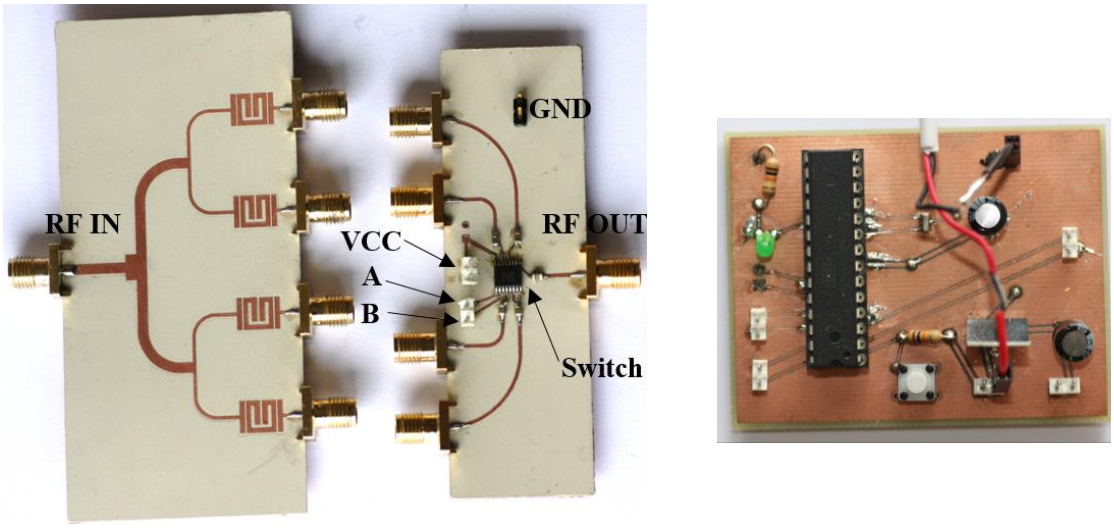

Figure 7. (a) Photograph of the power divider and switch; (b) Photograph of the control circuit. The switch is managed by means of the microcontroller, which is responsible for carrying out a sequential scanner of the channel lines as well as powering the switch.

3. System validation

The whole chipless setup, used for experimental validation, is shown in Fig 8. The *Agilent E44338C* signal generator is used to feed the power divider with a harmonic signal (whose amplitude is reduced 6 dB at each channel line of the power divider, for the reasons explained before). The switch, managed by a microcontroller and powered by an USB power tank, sequentially redirects the RF input channel lines to an RF output. To be able to discern the channel line position, the microcontroller has been programmed to wait 0.1 s between channels sweep, and the switch time has been configured to take 2 s at the first channel line and 1 s for the rest of the lines (see Fig. 9, where the gray vertical stripes indicate the 2 s time of the first channel). By this means, the initiation of the bit sequence is clearly identified. The switch RF output is connected to the envelope detector, which is indeed preceded by an isolator (implemented by means of the *L3 Narda-ATM ATc4-8* circulator), in order to prevent from unwanted reflections from the diode, a highly nonlinear device. The diode used to obtain the envelope function is the *Avago HSMS-2860*, whereas the necessary low-pass filter is implemented by means of the *Agilent N2795A* active probe (with resistance and capacitance $R = 1\ \text{M}\Omega$ and $C = 1\ \text{pF}$, respectively), connected to an oscilloscope (model *Agilent MSO-X-3104A*).

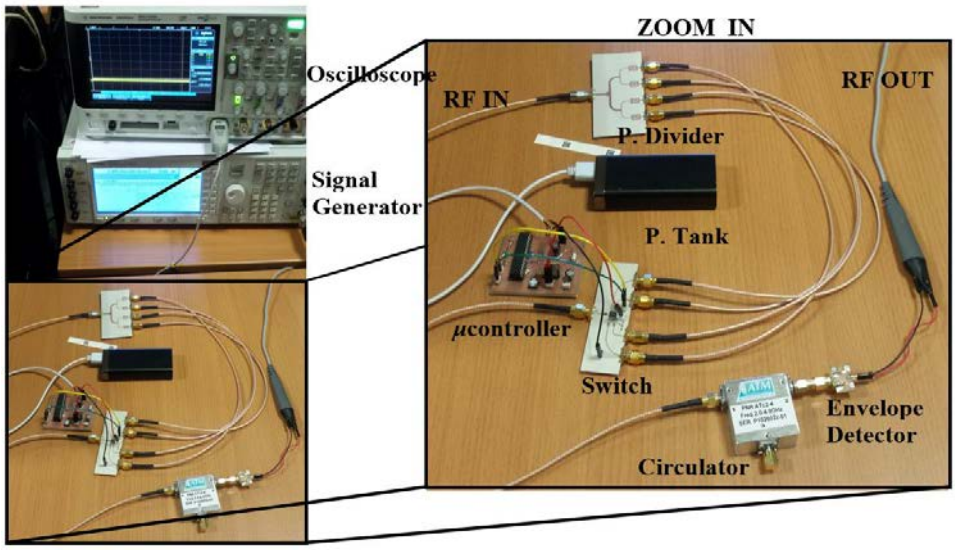

Figure 8. Photograph of the chipless setup, where all components are shown.

In order to validate the system, a chipless tag was fabricated by using one layer of *Dupont™ PE410* Ag conductive ink (thickness of 2.6 μm and conductivity of 7.28×10^6 S/m) inkjet printed on *PowerCoat™ HD ultra-smooth* paper dielectric constant ε_r = 3.1 and thickness h = 230 µm (the *Ceradrop Ceraprinter X-Serie* inkjet printer has been used). We have used paper as substrate and conductive ink for tag printing in order to be closer to a real scenario, where this kind of systems can be focused on applications where direct code printing on the item of interest is envisaged (e.g. smart packaging). Switching reading was first applied in absence of tag, equivalent to a tag without resonators (with code '0000'). From this response (see Fig. 9a), it is reasonable to set the threshold level to differentiate the two logic states to 0.2 V. Further tag readings, corresponding to different codes with SRRs faced up, are included in Fig. 9, and it can be seen that the obtained responses validate the proposed approach.

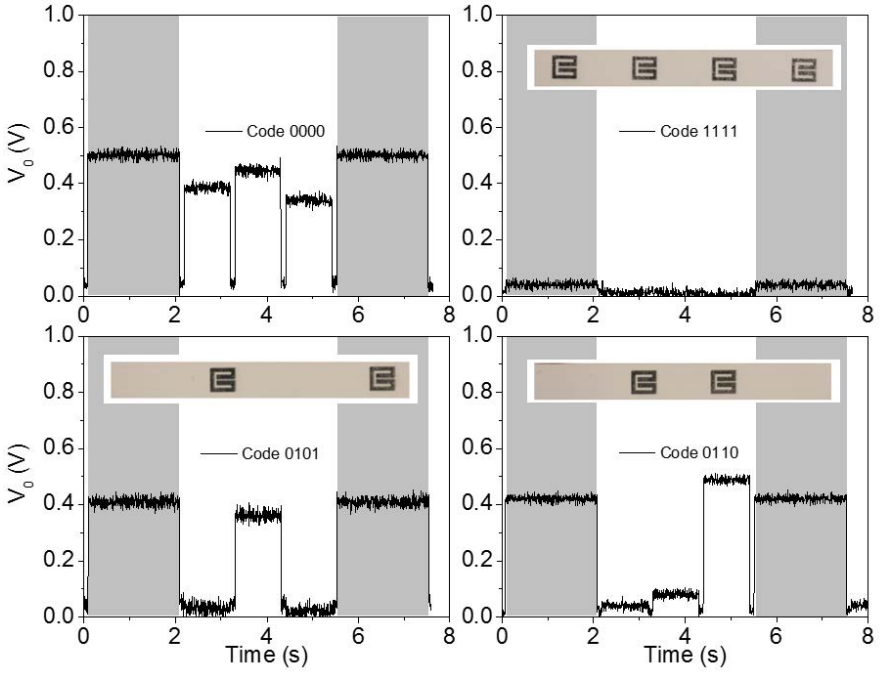

Figure 9. Envelope functions of the tags with the indicated codes. The considered codes are: (a) '0000'; (b) '1111'; (c) '0101'; (d) '0110'. These responses have been obtained by leaving the tag to rest on top of the reader lines. The gray vertical stripes show the first channel line, where the switch time has been configured to 2 s.

5. Conclusion

In conclusion, a novel chipless-RFID system, where the tags are read by proximity through near-field and the bits are sequentially inferred from a switch, has been proposed in this paper. The validity of the system has been demonstrated by considering 4-bit tags consisting of chains of SRRs inkjet printed on a paper substrate. As compared to previous chipless-RFID systems based on near-field coupling and sequential bit reading in time-domain, where the tags must be mechanically displaced over the reader for tag reading, in the system reported in this paper tag motion is not needed. Time division multiplexing is carried out by means of a switch, managed by a microcontroller, which sequentially provides the logic state of each bit. Such logic state is in turn provided by the amplitude of the signal present at the output port of each channel (or bit) line of the reader (inferred form an envelope detector). Since tag reading proceeds by proximity, the system is also useful as proximity sensor with identification capability.

Acknowledgments: This work was supported by MINECO-Spain (projects TEC2016-75650-R, TEC2014-59679-C2-1-R and RTC-2014-2550-7), Generalitat de Catalunya (project 2017SGR-1159), Institució Catalana de Recerca i Estudis Avançats (who awarded F. Martín), and by FEDER funds. C. Herrojo acknowledges MINECO for supporting his research activity through the FPI grant BES-2014-068164.

Author Contributions: "Ferran Paredes and Cristian Herrojo designed and carried out the experiments, as well as analyzed the data; Miquel Moras and Alba Núñez implemented PCBs and printed the ink resonators into paper-based tags, respectively; Javier Mata-Contreras performed the setup and contributed with his knowledge in sensors field; Eloi Ramon and Ferran Martín conceived the work and wrote the paper. Ferran Martín has been the director of the research.

Conflicts of Interest: The authors declare no conflict of interest. The founding sponsors had no role in the design of the study; in the collection, analyses, or interpretation of data; in the writing of the manuscript, and in the decision to publish the results.

References

1. Finkenzeller, K. *RFID Handbook: Fundamentals and Applications in Contactless Smart Cards, Radio-Frequency Identification and Near-Field Communication*, 3rd ed.; John Wiley: New York, USA, 2010; 9780470665121.
2. Hunt, V.D.; Puglia, A.; Puglia, M. *RFID: A Guide to Radiofrequency Identification*, 1st ed.; John Wiley: New York, USA, 2007; 9780470107645.
3. Preradovic, S.; Karmakar, N.C. Chipless RFID: bar code of the future, *IEEE Microw. Mag.* **2010**, 11, 87-97, 10.1109/MMM.2010.938571.
4. Preradovic, S.; Karmakar, N. C. *Multiresonator-Based Chipless RFID: Barcode of the Future*, 1st ed.; Springer: London, UK, 2011; 9781461420958.
5. Karmakar, N.C.; Koswatta, R.; Kalansuriya, P.; Azim, R.E. *Chipless RFID Reader Architecture*, 1st ed.; Artech House: Boston, USA, 2013; 9781608075614.
6. Perret, E. *Radio Frequency Identification and Sensors: From RFID to Chipless RFID*, 1st ed.; John Wiley: New York, USA, 2014; 9781848217669.
7. Rezaiesarlak R.; Manteghi, M. *Chipless RFID: Design Procedure and Detection Techniques*, Springer: London, UK, 2015; 9783319101699.
8. Karmakar, N. C.; Zomorrodi, M.; Divarathne, C. *Advanced Chipless RFID*, John Wiley: New York, USA, 2016; 9781119227311.
9. Hartmann, C. S. A global SAW ID tag with large data capacity. In Proceedings of IEEE Ultrasonics Symposium, Munich, Germany, October 2002; pp. 65–69.
10. Chamarti, A.; Varahramyan, K. Transmission delay line based ID generation circuit for RFID applications. *IEEE Microw. Wireless Compon. Lett*. **2006**, 16, 588-590, 10.1109/LMWC.2006.884897.
11. Schüßler, M.; Damm, C.; Jakoby, R. Periodically LC loaded lines for RFID backscatter applications. In Proceedings of Metamaterials 2007, Rome, Italy, October 2007; pp. 103-106.
12. Saldanha, N.; Malocha, D.C. Design Parameters for SAW multi-tone frequency coded reflectors. In Proceedings of IEEE Ultrasonics Symp., New York, USA, October 2007; pp. 2087-2090.
13. Schüßler, M.; Damm, C.; Maasch, M.; Jakoby, R. Performance evaluation of left-handed delay lines for RFID backscatter applications. In Proceedings of the IEEE MTT-S Intern. Microw. Symp., Atlanta, USA, June 2008; pp. 177-180.

14. Harma, S.; Plessky, V.P.; Hartmann, C.S.; Steichen, W. Z-path SAW RFID tag. *IEEE Trans. Ultrasonics, Ferroelectric Freq. Control* **2008**, 55, 208-213, 10.1109/TUFFC.2008.629.
15. Tao, H.; Weibiao, W.; Haodong, W.; Yongan, S. Reflection and scattering characteristics of reflectors in SAW tags. *IEEE Trans. Ultrasonics, Ferroelectric Freq. Control* **2008**, 55, 1387-1390, 10.1109/TUFFC.2008.802.
16. Harma, S.; Plessky, V.P.; Xianyi, L.; Hartogh, P. Feasibility of ultra-wideband SAW RFID tags meeting FCC rules. *IEEE Trans. Ultrasonics, Ferroelectric Freq. Control* **2012**, 56, 812-820, 10.1109/TUFFC.2009.1104.
17. Herraiz-Martínez, F.J.; Paredes, F.; Zamora, G.; Martín, F.; Bonache, J. Printed magnetoinductive-wave (MIW) delay lines for chipless RFID applications. *IEEE Trans. Ant. Propag.* **2012**, 60, 5075-5082, 10.1109/TAP.2012.2207681
18. Tedjini, S.; Perret, E.; Vena, A.; Kaddout, D. Mastering the electromagnetic signature of chipless RFID tags. In *Chipless and Conventional Radiofrequency Identification*, 1st ed.; IGI Global: Hershey, USA, 2012; 9781466616165.
19. Preradovic, S.; Balbin, I.; Karmakar, N. C.; Swiegers, G. F. Multiresonator-based chipless RFID system for low-cost item tracking. *IEEE Trans. Microw. Theory Techn*. **2009**, 57, 1411-1419, 10.1109/TMTT.2009.2017323.
20. Preradovic, S.; Karmakar, N. C. Design of chipless RFID tag for operation on flexible laminates. *IEEE Anten. Wireless Propag. Lett*. **2010**, 9, 207-210, 10.1109/LAWP.2010.2045872.
21. Rance, O.; Siragusa, R.; Lemaître-Auger, P.; Perret, E. Toward RCS magnitude level coding for chipless RFID. *IEEE Trans. Microw. Theory Techn*. **2016**, 64, 2315-2325, 10.1109/TMTT.2016.2562625.
22. McVay, J.; Hoorfar, A.; Engheta, N. Space-filling curve RFID tags. In Proceedings of the 2006 IEEE Radio Wireless Symp., San Diego, USA, January 2006; pp. 199-202.
23. Jalaly, I.; Robertson, D. Capacitively-tuned split microstrip resonators for RFID barcodes. In Proceedings of Europ. Microw. Conf., Paris, France, October 2005, pp. 4–7.
24. Jang, H.S.; Lim, W.G.; Oh, K.S.; Moon, S.M.; Yu, J.W. Design of low-cost chipless system using printable chipless tag with electromagnetic code. *IEEE Microw. Wireless Compon. Lett*. **2010**, 20, 640-642, 10.1109/LMWC.2010.2073692.
25. Vena, A.; Perret, E.; Tedjini, S. A fully printable chipless RFID tag with detuning correction technique. *IEEE Microw. Wireless Compon. Lett*. **2012**, 22, 209-211, 10.1109/LMWC.2012.2188785.
26. Vena, A.; Perret, E.; Tedjini, S. Design of compact and auto-compensated single-layer chipless RFID tag. *IEEE Trans. Microw. Theory Techn.* **2012**, 60, 2913-2924, 10.1109/TMTT.2012.2203927.
27. Vena, A.; Perret, E.; Tedjini, S. High-capacity chipless RFID tag insensitive to the polarization. *IEEE Trans. Ant. Propag*. **2012**, 60, 4509-4515, 10.1109/TAP.2012.2207347.
28. Khan, M.M.; Tahir, F.A.; Farooqui, M.F.; Shamim, A.; Cheema, H.M. 3.56-bits/cm2 compact inkjet printed and application specific chipless RFID tag. *IEEE Ant. Wireless Propag. Lett.* **2016**, 15, 1109-1112, 10.1109/LAWP.2015.2494864.
29. Islam, M.A.; Karmakar, N.C. A novel compact printable dual-polarized chipless RFID system. *IEEE Trans. Microw. Theory Techn*. **2012**, 60, 2142-2151, 10.1109/TMTT.2012.2195021.
30. Rezaiesarlak, R.; Manteghi, M. Complex-natural-resonance-based design of chipless RFID tag for high-density data, *IEEE Trans. Ant. Propag*. **2014**, 62, 898-904, 10.1109/TAP.2013.2290998.
31. Svanda, M.; Machac, J.; Polivka, M.; Havlicek, J. A comparison of two ways to reducing the mutual coupling of chipless RFID tag scatterers. In Proceedings of 21st Intern. Conf. Microw. Radar & Wireless Comm. (MIKON), Krakow, Poland, May 2016, pp. 1-4.
32. Vena, A.; Perret, E.; Tedjini, S. Chipless RFID tag using hybrid coding technique. *IEEE Trans. Microw. Theory Techn*. **2011**, 59, 3356-3364, 10.1109/TMTT.2011.2171001.
33. Vena, A.; Perret, E.; Tedjini, S.; A compact chipless RFID tag using polarization diversity for encoding and sensing. In Proceedings of IEEE Int. Conf. RFID, Orlando, USA, April 2012, pp. 191-197.
34. Balbin, I.; Karmakar, N.C. Phase-encoded chipless RFID transponder for large scale low cost applications. *IEEE Microw. Wireless. Comp. Lett*. **2009**, 19, 509-511, 10.1109/LMWC.2009.2024840.
35. Genovesi, S.; Costa, F.; Monorchio, A.; Manara, G. Chipless RFID tag exploiting multifrequency delta-phase quantization encoding. *IEEE Ant. Wireless, Propag. Lett.* **2015**, 15, 738-741, 10.1109/LAWP.2015.2471101.
36. Herrojo, C.; Naqui, J.; Paredes, F.; Martín, F. Spectral Signature Barcodes based on S-shaped Split Ring Resonators (S-SRR). *EPJ Appl. Metamat.* **2016**, 3, 1-6, https://doi.org/10.1051/epjam/2016002.

37. Herrojo, C.; Naqui, J.; Paredes, F.; Martín, F. Spectral signature barcodes implemented by multi-state multi-resonator circuits for chipless RFID tags. In Proceedings of the IEEE MTT-S Intern. Microw. Symp., San Francisco, USA, Mary 2016.
38. Herrojo, C.; Paredes, F.; Mata-Contreras, J.; Zuffanelli, S.; Martín, F. Multi-state multi-resonator spectral signature barcodes implemented by means of S-shaped Split Ring Resonators (S-SRR). *IEEE Trans. Microw. Theory Techn.* **2017**, 65, 2341-2352, 10.1109/TMTT.2017.2672547.
39. El-Awamry, A.; Khaliel, M.; Fawky, A.; El-Hadidy, M.; Kaiser, T. Novel notch modulation algorithm for enhancing the chipless RFID tags coding capacity. In Proceedings of IEEE Intern. Conf. RFID, San Diego, USA, April 2015, pp. 25-31.
40. Rance, O.; Siragusa, R.; Lemaître-Auger, P.; Perret, E. Toward RCS magnitude level coding for chipless RFID. *IEEE Trans. Microw. Theory Techn.* **2016**, 64, 2315-2325, 10.1109/TMTT.2016.2562625.
41. Herrojo, C.; Mata-Contreras, J.; Paredes, F.; Martín, F. Near-Field chipless RFID encoders with sequential bit reading and high data capacity. In Proceedings of the IEEE MTT-S Intern. Microw. Symp., Honolulu, USA, June 2017.
42. Herrojo, C.; Mata-Contreras, J.; Paredes, F.; Núñez, A.; Ramón, E.; Martín, F. Near-field chipless-RFID tags with sequential bit reading implemented in plastic substrates. *Intern. Journ. Magnetism & Magnetic Mat.* **2017**, https://doi.org/10.1016/j.jmmm.2017.10.005.
43. Herrojo, C.; Mata-Contreras, J.; Paredes, F.; Martín, F. Microwave encoders for chipless RFID and angular velocity sensors based on S-shaped split ring resonators (S-SRRs). *IEEE Sensors Journ*. **2017**, 17, 4805-4813, 10.1109/JSEN.2017.2715982.
44. Herrojo, C.; Mata-Contreras, J.; Paredes, F.; Martín, F. High data density and capacity in chipless radiofrequency identification (chipless-RFID) tags based on double-chains of S-shaped split ring resonators (S-SRRs). *EPJ Appl. Metamat.* **2017**, 4, 1-6, https://doi.org/10.1051/epjam/2017008.
45. Herrojo, C.; Mata-Contreras, J.; Paredes, F.; Martín, F. Near-field chipless RFID system with high data capacity for security and authentication applications. *IEEE Trans. Microw. Theory Tech.* **2017**, 65, 5298-5308, 10.1109/TMTT.2017.2768029.
46. Herrojo, C.; Mata-Contreras, J.; Paredes, F.; Núñez, A.; Ramon, E.; Martín, F. Near-field chipless-RFID system with erasable/programable 40-bit tags inkjet printed on paper substrates. *IEEE Microw. Wireless Comp.s Lett.* **2018**, 10.1109/LMWC.2018.2802718.

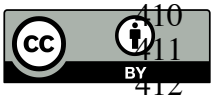

Publicaciones del Autor

Artículos en Revistas

1. C. Herrojo, J. Naqui, F. Paredes, and F. Martín, "Spectral signature barcodes based on s-shaped split ring resonators (S-SRRs)," *EPJ Appl. Metamat.*, vol. 3, pp. 1-6, Apr. 2016.

2. C. Herrojo, F. Paredes, J. Mata-Contreras, S. Zuffanelli, and F. Martín, "Multistate multiresonator spectral signature barcodes implemented by means of s-shaped split ring resonators (S-SRRs)," *IEEE Trans. Microw. Theory Tech.*, vol. 65, no. 7, pp. 2341-2352, Jul. 2017.

3. J. Mata-Contreras, C. Herrojo, and F. Martín, "Application of split ring resonator (SRR) loaded transmission lines to the design of angular displacement and velocity sensors for space applications," *IEEE IEEE Trans. Microw. Theory Tech.*, vol. 65, no. 11, pp. 4450-4460, Nov. 2017.

4. C. Herrojo, J. Mata-Contreras, F. Paredes, and F. Martín, "Microwave encoders for chipless RFID and angular velocity sensors based on s-shaped split ring resonators," *IEEE Sensors J.*, vol. 17, no. 15, pp. 4805-4813, Aug. 2017.

5. C. Herrojo, J. Mata-Contreras, F. Paredes, A. Núñez, E. Ramon, and F. Martín, "Near-field chipless-RFID tags with sequential bit reading implemented in plastic substrates," *J. Magn. Magn. Mater.*, Oct. 2017.

6. C. Herrojo, J. Mata-Contreras, F. Paredes, and F. Martín, "High data density and capacity in chipless radiofrequency identification (chipless-RFID) tags based on double-chains of S-shaped split ring resonators (S-SRRs)," *EPJ Appl. Metamat.*, vol. 4, pp. 1-8, Oct. 2017.

7. C. Herrojo, J. Mata-Contreras, A. Núñez, F. Paredes, E. Ramon, and F. Martín, "Near-field chipless-RFID system with high data capacity for security and authentication applications," *IEEE Trans. Microw. Theory Tech.*, vol. 65, no. 12, pp. 5298-5308, Dec. 2017.

8. C. Herrojo, J. Mata-Contreras, F. Paredes, A. Núñez, E. Ramon, and F. Martín, "Near-field chipless-RFID system with erasable/programmable 40-bit tags inkjet printed on paper substrates," *IEEE Microw. Compon. Lett.*, vol. 28, no. 3, pp. 272-274, Mar 2018.

9. J. Mata-Contreras, C. Herrojo, and F. Martín, "Detecting the rotation direction in contactless angular velocity sensors implemented with rotors loaded with multiple chains of resonators," *IEEE Trans. Microw. Theory Tech.* Enviado.

10. F. Paredes, C. Herrojo, M. Moras, J. Mata-Contreras, A. Núñez, E. Ramon, and F. Martín, "Near-field chipless-RFID sensing and identification system with switching reading," *Sensors*. Enviado.

11. C. Herrojo, M. Moras, F. Paredes, A. Núñez, J. Mata-Contreras, E. Ramon, and F. Martín, "Time-domain signature Chipless-RFID tags: near-field chipless-RFID systems with high data capacity," *IEEE Microw. Mag.* Enviado.

12. C. Herrojo, M. Moras, F. Paredes, J. Mata-Contreras, A. Núñez, E. Ramon, and F. Martín, "Very low-cost 80-bit chipless-RFID tags inkjet printed on ordinary paper," *Technologies*. Enviado.

Contribuciones en Congresos

1. C. Herrojo, J. Naqui, and F. Martín, "S-shaped split ring resonators (S-SRRs) for the design of spectral signature barcodes", in *International Workshop on Metamaterials-by-Design, Theory, Methods, and Applications to Communications and Sensing*, Paris, France, 3-4 Dec. 2015. Invited.

2. C. Herrojo, J. Naqui, F. Paredes, and F. Martín, "Spectral signature barcodes implemented by multi-state multi-resonator circuits for chipless RFID tags," in *2016 IEEE MTT-S International Microwave Symposium*, San Francisco, CA, May 2016, pp. 1-4.

3. C. Herrojo, J. Mata-Contreras, F. Paredes, and F. Martín, "Near-field chipless RFID tags for identification and authentication applications", in *Progress in Electromagnetic Research Symposium*, St Petersburg, Russia, May 2017. Invited.

4. C. Herrojo, J. Mata-Contreras, F. Paredes, and F. Martín, "Near-field chipless RFID encoders with sequential bit reading and high data capacity," in *2017 IEEE MTT-S International Microwave Symposium*, Honololu, HI, Jun. 2017, pp. 1564-1567.

5. C. Herrojo, J. Mata-Contreras, F. Paredes, A. Núñez, E. Ramon, and F. Martín, "Near-field chipless-RFID tags with sequential bit reading implemented in

plastic substrates", in *Moscow International Symposium on Magnetism*, Moscow, Russia, Jul. 2017. Invited.

6. C. Herrojo, J. Mata-Contreras, F. Paredes and F. Martín, "Chipless RFID tags based on metamaterial concepts," in *2017 11th International Congress on Engineered Materials Platforms for Novel Wave Phenomena (Metamaterials)*, Marseille, France, Aug. 2017, pp. 139-141. Invited.

7. F. Martín, C. Herrojo, P. Vélez, L. Su, J. Mata-Contreras, and F. Paredes, "Application of metamaterial concepts to sensors and chipless RFID," in *Journal of Physics: Conference Series*, Madrid, Spain, Dec. 2017. Invited.

8. J. Mata-Contreras, C.Herrojo, and F. Martín, "Electromagnetic rotary encoders based on split ring resonators (SRR) loaded microstrip lines," in *2018 IEEE MTT-S International Microwave Symposium*, Philadelphia, USA, Jun. 2018. Aceptado.

9. C. Herrojo, M. Moras, F. Paredes, J. Mata-Contreras, A. Núñez, E. Ramon, and F. Martín, "Erasable/programmable chipless-RFID tags with orientation-independent sequential bit reading," in *European Microwave Conference*, Madrid, Spain, Sep. 2018. Enviado.

10. C. Herrojo, J. Mata-Contreras, A. Núñez, F. Paredes, E. Ramon, and F. Martín, "Application of metamaterial concepts to chipless RFID," in *SPIE Photonics Europe*, Strasbourg, France, Apr. 2018. Enviado. Invited.

Contribuciones en Workshops

1. C. Herrojo, J. Mata-Contreras, F. Paredes, and F. Martín, "Chipless RFID systems, technology and applications," in "Chipless RFID systems with high datacapacity for security and authentication applications," *European Microwave Conference*, Nuremberg, Germany, Oct. 2017.

2. F. Martín, P. Vélez, C. Herrojo, Metamaterials, metasurfaces and applications," in "Novel sensors and chipless-RFID systems based on metamaterials and symmetry properties," in *European Microwave Conference*, Madrid, Spain, Sep. 2018. Aceptado.

3. F. Martín, C. Herrojo, E. Ramon, "Backscatter communications the next paradigm for IoT approaches" in "Near-field chipless-RFID systems with very high data capacity for secure paper applications," *European Microwave Conference*, Madrid, Spain, Sep. 2018. Aceptado.

Patentes

1. **Título:** *A Chipless RFID tag, a Chipless RFID system, and a method for encoding data on a Chipless RFID tag.*
   Inventores: Cristian Herrojo, Ferran Martín, Javier Mata Contreras y Ferran Paredes.
   Solicitante: Universitat Autònoma de Barcelona.
   Número de solicitud: GB1708720.6
   Fecha de solicitud: 1 de junio de 2017.